ENS DE LYON

THESE

pour l'obtention du grade de Docteur, délivré par

l'ECOLE NORMALE SUPERIEURE DE LYON

Ecole Doctorale N°340
BMIC - Biologie Moléculaire Intégrative et Cellulaire

Discipline : SCIENCES DE LA VIE ET DE LA SANTE (Aspects moléculaires et cellulaires de la biologie)

Soutenue publiquement le 26 septembre 2025, par :

Dominika LETKOVÁ

Rôle épigénétique du variant d'histone H3.3 dans l'établissement des rythmes circadiens des mammifères

Epigenetic role of H3.3 histone variant in establishment of mammalian circadian rhythms

---

Après avis de :

Urs ALBRECHT, Professeur, Université de Fribourg	Rapporteur
Armelle CORPET, Maîtresse de conférences HDR, Université Claude Bernard Lyon 1	Rapporteure

Devant le jury composé de :

Marie SÉMON, Professeure des universités, Ecole Normale Supérieure de Lyon	Présidente
Urs ALBRECHT, Professeur, Université de Fribourg	Rapporteur
Armelle CORPET, Maîtresse de conférences HDR, Université Claude Bernard Lyon 1	Rapporteure
Matthieu GÉRARD, Personnalité scientifique HDR, CEA	Examinateur
Aline PROBST, Directrice de recherche, Université Clermont Auvergne / CNRS	Examinatrice
Kiran PADMANABHAN, Chargé de recherche - HDR, Ecole Normale Supérieure de Lyon / INSERM	Directeur de thèse

“*It is important to make a dream of life and of a dream reality*.”

“*We must believe that we are gifted for something and that this thing must be attained*.”

- Marie Curie-Skłodowska

Table of contents

Acknowledgements **5**
Abstract **7**
Résumé **9**
List of figures **11**
List of tables **13**
List of abbreviations **14**
Introduction **17**
1. Circadian rhythms: from molecular mechanisms to physiology **17**
1.1 Circadian clocks: an important feature for organismal fitness and homeostasis 17
1.1.1 Discovery of circadian rhythms: from plants to mammals 17
1.1.2 Universal properties of circadian oscillators 19
1.2 Organization levels of circadian clocks in mammals 21
1.2.1 Suprachiasmatic nuclei: the master clock 21
1.2.2 Peripheral oscillators 22
1.2.3 Example of a mammalian peripheral clock: liver at the center of the interplay between circadian timing system and metabolism 22
1.3 Molecular mechanisms of mammalian circadian clocks 25
1.4 Circadian clock disruption in diseases 27
2. Chromatin dynamics and epigenetic signatures **29**
2.1 Chromatin organization: general overview 29
2.2 Epigenetic mechanisms establishing dynamic chromatin changes 31
2.2.1 Example of epigenetic signatures: post-translational modifications of histones 31
2.2.2 Chromatin remodelers of the SWI/SNF family 32
2.2.3 Histone variants: general overview 36
3. Interplay between chromatin dynamics and circadian clocks **40**
3.1 Crosstalk between circadian clocks and epigenome 40
3.1.1 Dynamics in histone marks and chromatin accessibility 40
3.1.2 H2A.Z histone variant chromatin state dynamics at clock *loci* 41
3.1.3 Circadian chromatin remodeling 42
4. H3.3 histone variant **44**
4.1 The H3 histone family: key modulators of chromatin states 44
4.2 The H3.3 histone variant 44
4.2.1 Specific deposition pathways of H3.3 variant 45
4.2.2 H3.3 as a key transcriptional regulator and beyond 45
4.2.3 Fragile H3.3/H2A.Z dual-variant nucleosomes 46
5. Research hypotheses and aims **48**

5.1 Scientific context and hypotheses 48
5.2 Mouse models and aims of the project 48
Materials and methods 50
Materials....50
1. Reagents, chemicals and products used in this work....50
Methods 53
1. Mouse models, genotyping and tissue collections 53
2. Nuclei isolation from murine livers 54
3. Native purification of H3.3A protein complexes for mass spectrometry analysis 56
4. LC-MS/MS analysis 59
5. Native immunoprecipitation and western-blotting....60
6. Native chromatin immunoprecipitation-sequencing....63
7. Data filtering, ChIP-Seq analysis and graphical representation 64
8. Cross-linked ChIP-qPCR....65
9. mRNA expression levels and RT-qPCR....68
10. Real-time bioluminescence monitoring assay of circadian oscillations in cultured cells 68
11. Subcellular protein tissue fractionation....69
12. MG132 treatment and subcellular protein fractionation....70
13. Reanalysis of published siRNA screens....70
Results....71
1. Characterization of liver-specific H3.3A protein complexes over time....71
1.1 Establishment of the purification method and encountered challenges....71
1.2 H3.3A day-time dependent assembly with BMAL1-CLOCK transcription factors 72
1.3 Identification of SWI/SNF PBAF chromatin remodelers as main H3.3A interactors 74
1.4 Circadian PBAF-BMAL1 complex assembles on dynamic H3.3 variant chromatin 74
2. Rhythmicity in H3.3A nucleosome occupancy....76
2.1 H3.3A variant generates 24h chromatin dynamics at clock *loci* 76
2.2 Impact of circadian clock disruption on H3.3A chromatin landscapes 76
3. Reorganization of chromatin remodelers upon circadian disruption....80
3.1 Loss of ARID2 leads to PBAF complex disassembly in the absence of PER 80
3.2 Remodeler 'switch' to cBAF/BRM complexes marks the clock-disrupted state in PerKO livers....81
4. Alterations in fragile H3.3A chromatin states and BMAL1 binding....85
4.1 BMAL1-CLOCK is recruited to fragile H3.3 nucleosomes during the active phase 85

4.2 Identification of two different subsets of H3K115ac-marked fragile nucleosomes 87
4.3 Fragile H3.3 chromatin in PerKO livers enhances BMAL1 E-box accessibility...87
4.4 BMAL1 turnover in the absence of circadian feedback....89
5. Impact on circadian clock function....91
5.1 Role of H3.3 in circadian clock function....91
5.2 Impact of specific PBAF/cBAF components on circadian rhythms....91
Discussion 94
Proposed model, open questions and perspectives 94
References 103
Supplementary materials 117
List of supplementary materials....117
Figure S1. Timeline of major early discoveries in the field of mammalian circadian research 118
Figure S2. Detailed model of the mammalian core-clock mechanism. 119
Figure S3. Differential enrichment of PBAF/cBAF components in H3.3A complexes in wild-type vs. PerKO livers. 120
Table S1. Mass spectrometry analysis of detected peptides of PBAF/cBAF components in H3.3A complexes in wild-type vs. PerKO livers. 121
Table S2. ChIP fragment length and Tapestation profiles. 125
Table S3. Primer sequences. 129
Quantification of immunoprecipitation experiments....130
Chapitres et résumés des chapitres en français 138
Articles 183
List of articles....183
Article 1. Mammalian PERIOD2 regulates H2A.Z incorporation in chromatin to orchestrate circadian negative feedback. 183
Article 2. PBAF/cBAF reorganization on H3.3 chromatin regulates BMAL1 activity in the absence of circadian negative feedback. 183

Acknowledgements

The past four years linked to this thesis work have been extremely intense and challenging. I was entirely living for my research project, putting anything else aside. There were many moments when I felt like there are more lows than ups in science and research in general. Despite all the challenges, and not only the technical ones, that I encountered in the laboratory, I never thought of giving up. I truly believe that if one puts all their efforts and good intensions into achieving something, one will be successful in his/her accomplishments. I also truly believe that everything becomes possible if one has deep motivation and is surrounded by people allowing him/her to progress and move forward. I am very grateful for people and mentors that I met on my scientific journey, especially for those that helped me and allowed me to evolve. Many people played a significant role and I would like to deeply acknowledge them.

First, I would like to thank my supervisor, Dr. Kiran Padmanabhan, for his belief in me, his strong support in conducting my thesis research project and for all the challenges and precious life lessons. By giving me the space to learn, explore and discover, he allowed me to grow not only scientifically, but also personally- for which I am very grateful.

I would like to thank all the team members. My special thanks go to Damien Sery for his critical help with circadian tissue collections and mentoring for mice handling. I would also like to thank especially Dr. Aurélie Peticca for all the bioinformatic analysis related to the ChIP-sequencing present in this thesis, which allowed us to get new insights into my work.

I would like to thank as well our collaborators Prof. Yutaka Suzuki and Dr. Masahide Seki, as well as Kazumi Abe and Shota Takashima from the Department of Computational Biology and Medical Sciences of the University of Tokyo for their help with sequencing. In addition, I would like to acknowledge Dr. Adeline Page and Dr. Frédéric Delolme from PSF facility for their help with mass spectrometry experiments and Nadine Aguilera for animal husbandry at PBES facility, SFR Biosciences (UMS3444/CNRS, US8/Inserm, ENS de Lyon, UCBL). I would also like to thank Benjamin Gillet, Sandrine Hughes and Yves Dusabyinema at the sequencing platform at IGFL for their advice, as well as Jean-Louis Thoumas and the PEHR mouse facility.

Additionally, I would like to thank my thesis tracking committee members, Dr. Benjamin Loppin and Dr. Jean-Christophe Andrau for their guidance.

My immense gratitude goes to the organizations supporting my PhD thesis research. I am very grateful for the 3-year PhD fellowship from the doctoral school ED 340 BMIC, ENS de Lyon and for the 4th year PhD fellowship from the “Fondation ARC pour la recherche sur le cancer”.

Their trust in me and financial support allowed me to fully conduct and achieve my thesis project and gave me the opportunity to make my initial steps into the academic scientific career.

I would also like to thank and express my gratitude towards all the jury members, Prof. Dr. Urs Albrecht, Dr. Armelle Corpet, Dr. Matthieu Gérard, Dr. Aline Probst and Prof. Marie Sémon for taking their time in evaluating my work. For those that I had a chance to meet personally before my PhD defense, as well for their advice for the next steps in my scientific career.

Special thanks go to the reviewers of my thesis, Dr. Armelle Corpet, MCU and Prof. Dr. Urs Albrecht for their time, reviews and beyond. I would particularly like to thank Armelle for encouraging young women and making them realize that they have their legit place in science. I would also like to thank Urs for his valuable advice that he gave me during our discussion at EBRS Chronobiology School in Munich, where we first met several years ago, on learning how to recognize the right opportunity for me, among all the others, in order to become successful.

On a personal note, I would like to thank my very first internship tutor Dr. Pascal Maurice, whom I had a chance to meet very early on during my Bachelor's degree studies. His kindness and professionalism allowed me to truly immerse myself in research, making me feel in the laboratory at a place where I belong. His approach to any scientific question and challenge with enthusiasm truly inspired me and became the approach I carry within me ever since.

I also thank Prof. Arnaud Haudrechy for his everlasting support and advice throughout my studies, as well as for making me believe more in myself.

I would as well like to thank Dr. Julie Carnesecchi for our discussions, her support and encouragements during my PhD thesis.

Last, but not least, I would like to thank my whole family and friends for their unconditional love and support. Especially, I thank my parents, Nina and Matej, for allowing me to explore the world and for giving me the space to find my passion for science, when they let me to leave home so young in order to pursue my dreams. I also thank my sister Paulínka for her presence in my life and her support throughout all the challenging times. I would like to thank as well my 'French family', especially Marie-Christine and Serge that I am very lucky to have in my life and very grateful for all their help and support when I initially came to France and throughout all the time of my studies and stay in France. Special thanks go as well to all my friends, Zuzka, Léa, Khushi, Pavel, Yevhenii, Amélie, Tamara, Marianne, Nat, Céline, Alenka and Dušan for all their careful listening, advice, help and their true support and friendship. Without your support, I would not be at a place where I am today. Thank you!

Abstract

In mammals, robust circadian clocks coordinate gene-expression programs in a tissue-specific manner. Rhythmic binding of the core-clock transcription factors (TF) BMAL1-CLOCK on chromatin results in a 'day to night' dynamics in chromatin states and in turn, ~10-15% of transcriptome in every tissue is cycling. In order to allow BMAL1-CLOCK rhythmic binding at 'specific time and place' on the genome, chromatin has to be accessible and such dynamic changes in chromatin states epigenetically encoded. Therefore, how chromatin architecture gets reorganized upon BMAL1-CLOCK binding, remains an active field of research.

Over the past decades, it has been shown that circadian clock machinery is tightly linked with dynamics in chromatin landscapes. Deposition of epigenetic marks, such as acetylation or methylation of histone proteins, nucleosome remodeling and circadian gene expression are closely coordinated. Core-clock factors are directly involved in the recruitment of chromatin-modifying enzymes and deposition of epigenetic signatures, including histone variants, such as H2A variant, H2A.Z. Dynamic incorporation and/or eviction of H2A.Z within nucleosomes near transcription start sites (TSS) is highly concomitant with incorporation of the H3 histone variant, H3.3. In dividing cells, it has been shown that H3.3/H2A.Z histone variants are incorporated within the same nucleosomes at promoters and TSS, generating extremely labile, easily removable dual-variant nucleosomes. Nevertheless, while H2A.Z role in 24hr rhythms and chromatin dynamics is well established across species, the role of H3.3 in clock function remains unknown.

Therefore, we aimed to study the link between the histone variant H3.3 and the molecular machinery of mammalian circadian clocks. In other words, how could H3.3 nucleosomes shape the chromatin architecture to contribute to 24hr transcriptional dynamics in close connection with circadian core-clock regulators in murine tissues, such as liver. Purification of specific H3.3 liver protein complexes over circadian time allowed us to identify dynamic assembly of PBAF/cBAF chromatin remodelers with the core-clock TF BMAL1 on H3.3 variant chromatin. We found that H3.3 deposition is cycling over time, and PBAF/cBAF-BMAL1 assemble on dynamic H3.3 nucleosomes marked with specific epigenetic marks such as H3K115ac and H3K122ac, resulting in their fragility. Furthermore, circadian clock disruption (*Per* knock-out mouse models) results in a higher loading of H3.3 on chromatin and maintenance of fragile H3.3 'day-time-like' epigenetic landscapes. Moreover, near-total depletion of ARID2 and BRG1 shared ATPase subunits respectively lead to disassembly of PBAF and reorganization of cBAF chromatin remodelers, followed by a 'switch' to cBAF/BRM complexes. In addition, the absence of circadian feedback results in increased BMAL1 binding on chromatin due to the higher accessibility of BMAL1-CLOCK binding sites. All of these events

highlight a permanently active ‘day-time like’ chromatin state upon circadian disruption, implicating H3.3.

Last, but not least, circadian disruption is implicated in several disorders such as metabolic syndrome and sleep loss, neurodegenerative diseases and cancer,- all of which have a strong epigenetic component, including mutations in H3.3 and chromatin remodelers. Better understanding of the physiological link between chromatin dynamics and circadian transcription would allow better understanding of disease development and its progression, as well as an aid in the development of novel therapeutic approaches.

Key words: circadian clocks, chromatin dynamics, fragile nucleosomes, histone variants, H3.3, PBAF/cBAF chromatin remodelers, circadian clock disruption, *Per1*$^{-/-}$, *Per2*$^{-/-}$ knockout

Résumé

Chez les mammifères, les oscillations circadiennes robustes coordonnent des programmes d'expression de gènes de manière tissu-spécifique. La liaison rythmique des facteurs de transcription de l'horloge circadienne BMAL1-CLOCK à la chromatine entraîne une dynamique journalière dans les états chromatiniens. En conséquence, ~10-15% du transcriptome de chaque tissu cycle. Afin de permettre la liaison rythmique de BMAL1-CLOCK à un temps et un endroit spécifique du génome, la chromatine doit être accessible et ces changements dynamiques d'états chromatiniens encodés épigénétiquement. Par conséquent, la manière dont l'architecture chromatinienne est réorganisée lors de la liaison de BMAL1-CLOCK reste un domaine de recherche active.

Au cours des dernières décennies, il a été montré que la machinerie de l'horloge circadienne est liée avec la dynamique au sein des paysages chromatiniens. Le dépôt de marques épigénétiques, comme acétylation ou méthylation des histones, le remodelage de nucléosomes et l'expression circadienne des gènes sont étroitement coordonnés. Les facteurs de l'horloge sont directement impliqués dans le recrutement des enzymes modificatrices de la chromatine, ainsi que la déposition des signatures épigénétiques- notamment des variants d'histones, comme le variant de l'histone H2A, le H2A.Z. L'incorporation et/ou éviction dynamique de H2A.Z au sein des nucléosomes près de sites de début de transcription (TSS) est concomitante avec l'incorporation de variant de H3, le H3.3. Il a été montré que dans les cellules au cours de division, les variants H3.3/H2A.Z sont incorporés au sein des mêmes nucléosomes au niveaux des promoteurs et des TSS, générant des nucléosomes double-variants qui sont très instables et mobiles. Néanmoins, tandis que le rôle de H2A.Z dans les rythmes circadiens et la dynamique de la chromatine est bien établi à travers les espèces, le rôle de H3.3 dans la fonction de l'horloge circadienne reste inconnu.

Ainsi, on a eu pour but d'étudier le lien entre le variant d'histone H3.3 et la machinerie moléculaire de l'horloge circadienne chez les mammifères. Autrement dit, comment les nucléosomes contenant H3.3 pourraient moduler l'architecture de la chromatine et contribuer à la dynamique transcriptionnelle au cours de 24h, en lien étroit avec les régulateurs clefs de l'horloge dans les tissus murins, comme le foie. La purification des complexes protéiques spécifiques de H3.3 dans le foie au cours de 24h nous a permis d'identifier que les remodeleurs chromatiniens PBAF/cBAF s'assemblent dynamiquement avec le facteur de transcription BMAL1 sur la chromatine marquée par H3.3. Par ailleurs, on a montré que l'incorporation de H3.3 au sein de la chromatine est rythmique au cours du temps et que PBAF/cBAF-BMAL1 s'assemble dynamiquement avec des nucléosomes H3.3 décorés par des marques épigénétiques comme H3K115ac et H3K122ac, rendant ces nucléosomes instables et mobiles (fragiles). De plus, la perturbation de l'horloge circadienne (modèle de

souris *Per* knock-out) conduit à une augmentation de H3.3 sur la chromatine, ainsi qu'à un maintien des paysages épigénétiques marqués par des nucléosomes H3.3 fragiles. La perte presque totale de ARID2 et de la sous unité ATPasique BRG1, mène respectivement au désassemblage de PBAF, ainsi qu'à une réorganisation des remodeleurs cBAF/BRG1, suivie par la favorisation des complexes cBAF/BRM. De plus, l'absence de feedback circadien résulte en une augmentation de fixation de BMAL1 sur la chromatine, due à l'augmentation de l'accessibilité des sites de liaison de BMAL1-CLOCK. Tous ces événements mènent à un état chromatinien actif en permanence lors de la perturbation circadienne, impliquant le variant H3.3.

Enfin, les dérèglements de l'horloge circadienne sont impliqués dans plusieurs maladies comme le syndrome métabolique, perturbations de sommeil, maladies neurodégénératives et les cancers- toutes ces maladies ont une forte composante épigénétique, dont les mutations au sein de H3.3 et les remodeleurs chromatiniens. Meilleure compréhension du lien physiologique entre la dynamique de la chromatine et la transcription circadienne permettrait de mieux comprendre la mise en place et la progression de ces maladies, ainsi que d'apporter une aide pour le développement des approches thérapeutiques nouvelles.

Mots clés : horloge circadienne, dynamique de la chromatine, nucléosomes fragiles, variants d'histones, H3.3, remodeleurs chromatiniens PBAF/cBAF, perturbation des rythmes circadiens, *Per1*$^{-/-}$, *Per2*$^{-/-}$ knockout

List of figures

Figure 1. Circadian regulation of key hepatic metabolic processes 25
Figure 2. The core-clock regulatory feedback loops (simplified model) 26
Figure 3. Chromatin organization 30
Figure 4. Three-dimensional chromatin organization within the nucleus 31
Figure 5. Landscape of histone post-translational modifications 32
Figure 6. ATP-dependent remodeling mechanism of SWI/SNF complexes 34
Figure 7. Multistep assembly process of BAF and PBAF complexes. 35
Figure 8. Overview of canonical and variant histone deposition 38
Figure 9. Alterations in histone variants and their consequences: example of H3 and H2A variants 39
Figure 10. Main structural differences between the histone variant H3.3 and canonical histones H3.1/2. 45
Figure 11. Proposed model of the H3.3/H2A.Z dual-variant nucleosome involvement in transcriptional regulation 47
Figure 12. Native purification of H3.3A liver protein complexes 72
Figure 13. Day-time specific H3.3A complexes contain BMAL1-CLOCK 73
Figure 14. Rhythmic assembly of H3.3-PBAF-BMAL1 complexes 75
Figure 15. Circadian dynamics of H3.3A nucleosomes 77
Figure 16. H3.3A enrichment on wild-type vs. PerKO chromatin 78
Figure 17. H3.3A occupancy at rhythmic transcripts in wild-type vs. PerKO livers 79
Figure 18. H3.3A occupancy at CTCF sites in wild-type vs. PerKO livers 80
Figure 19. Disassembly of H3.3-PBAF-BMAL1 complexes in PerKO livers 82
Figure 20. Remodeler switch from PBAF-cBAF/BRG1 to cBAF/BRM in the absence of PER 84
Figure 21. Day-time specific fragile H3.3A nucleosomes mark clock-disrupted chromatin 86
Figure 22. Expression levels of H3.3A and its specific chaperones 86
Figure 23. cBAF/BRM-BMAL1 complexes assemble with H3K115ac-marked fragile nucleosomes in PerKO 88
Figure 24. Circadian clock disruption leads to enhanced BMAL1 binding on chromatin 89
Figure 25. Increased presence and turnover of BMAL1 on chromatin in PerKO 90
Figure 26. Impact of H3.3 on circadian clock function 91
Figure 27. Reanalysis of published datasets for PBAF and BAF specific components siRNA screens 92
Figure 28. Proposed model illustrating changes in BMAL1 targeting on H3.3 variant chromatin in wildtype animals and in the absence of circadian negative feedback 95

Figure S1. Timeline of major early discoveries in the field of mammalian circadian research 118
Figure S2. Detailed model of the mammalian core-clock mechanism 119
Figure S3. Differential enrichment of PBAF/cBAF components in H3.3A complexes in wild-type vs. PerKO livers 120

List of tables

Table 1. Mammalian SWI/SNF complexes: shared and specific subunits of PBAF and cBAF 35
Table 2. List of core canonical histones with their corresponding variants in mammals.....36
Table 3. List of reagents, chemicals and products with their corresponding references 50
Table 4. Buffer composition for DNA extraction from ear punches 53
Table 5. PCR mix for 20 reactions and PCR program.....53
Table 6. Buffer composition for nuclei isolation from liver tissues.....55
Table 7. Buffer composition for native purification of interacting protein complexes 57
Table 8. 5X SDS-blue loading dye 61
Table 9. Antibodies 62
Table 10. ChIP elution buffer 64
Table 11. Buffer composition for cross-linked ChIP 67
Table 12. Master mix for one RT-qPCR reaction.....67
Table 13. RT-qPCR program 68
Table S1. Mass spectrometry analysis of detected peptides of PBAF/cBAF components in H3.3A complexes in wild-type vs. PerKO livers.....121
Table S2. ChIP Tapestation profiles and fragment length.....125
Table S3. Primer sequences.....129

List of abbreviations

+/-	heterozygous
ARC	Association pour la Recherche sur le Cancer
ARID1A	AT-rich interactive domain-containing protein 1A
ARID1B	AT-rich interactive domain-containing protein 1B
ARID2	AT-rich interactive domain-containing protein 2
ARNTL	Aryl Hydrocarbon receptor nuclear translocator-like protein 1
ASF-1	Anti-silencing function 1
ATP	Adenosine triphosphate
ATRX	Alpha-thalassemia/mental retardation syndrome X-linked protein
BAH	Bromo-adjacent homology
BD	Bromodomain
bHLH	Basic helix-loop-helix
BMAL1	Basic helix-loop-helix ARNT-like protein 1
BMIC	Biologie Moléculaire Intégrative et Cellulaire
BRD7	Bromodomain-Containing Protein 7
BRD9	Bromodomain-Containing Protein 9
BRG1	Brahma-related gene 1
BRM	Brahma
BSA	Bovine Serum Albumin
CABIN1	Calcineurin-binding protein 1
$CaCl_2$	Calcium chloride
CAF-1	Chromatin assembly factor 1
cBAF	Canonical BRG1/Brahma Associated Factor
CBP	CREB-binding protein
CCG	Clock-controlled genes
CDK	Cyclin-dependent kinase
cDNA	Complementary Deoxyribonucleic acid
CHD	Chromodomain Helicase DNA-Binding
ChIP	Chromatin Immunoprecipitation
CK	Casein Kinase
CLOCK	Circadian Locomotor Output Cycles Kaput
CO_2	Carbon dioxide
CRY	Cryptochrome
CT	Circadian Time
CTCF	CCCTC binding factor
dATP	Deoxyadenosine triphosphate
DAXX	Death-associated protein 6
Dbp	D Site-Binding Protein
dCTP	Deoxycytidine triphosphate
DDR	DNA damage response
dGTP	Deoxyguanosine triphosphate
DKO	Double Knock-out
DMEM	Dulbecco's Modified Eagle Medium
DMSO	Dimethyl Sulfoxide
DNA	Deoxyribonucleic acid
DNTP	Deoxynucleotide triphosphate
DPF1/2/3	Double PHD Fingers 1/2/3
dsDNA	Double stranded Deoxyribonucleic acid
DSPD	Delayed sleep phase disorder
DTT	Dithiothreitol
dTTP	Deoxythymidine Triphosphate
ECL	Electrochemiluminescence
EDTA	Ethylenediaminetetraacetic acid
EGTA	Ethylene glycol-bis (β-aminoethyl ether)-N,N,N′,N′-tetraacetic acid
ENCODE	Encyclopedia of DNA elements
ENS	Ecole Normale Supérieure
EtOH	Ethanol

FACT	Facilitates chromatin transcription
FASPS	Familial advanced sleep phase syndrome
f/f	Flox/Flox
FBS	Fetal Bovine Serum
FH	FLAG-FLAG-HA
GEO	Gene Expression Omnibus
H_2O	Water
H3f3a	H3 Histone Family Member 3A
H3f3b	H3 Histone Family Member 3B
HA	Human influenza hemagglutinin
HAT	Histone Acetyl Transferase
HCC	Hepatho Cellular Carcinoma
HCl	Hydrochloric acid
HDAC	Histone Deacetylase
HDM	Histone Demethylase
HIRA	Histone Cell Cycle Regulation Defective Homolog A
HMG	High Mobility Group
HMT	Histone Methyl Transferase
HP1α	Heterochromatin protein 1 alpha
INO80	Inositol requiring mutant 80
IgG	Immunoglobulin G
IP	Immunoprecipitation
ISWI	Imitation SWItch
JARID	Jumonji, AT-Rich Interaction Domain
JMJD	Jumonji Domain containing
KCl	Potassium chloride
KO	Knock-out
KOH	Potassium hydroxide
LAD	Lamina-associated domain
LC-MS/MS	Liquid Chromatography coupled with Tandem Mass Spectrometry
mAb	Monoclonal Antibody
MEF	Mouse Embryonic Fibroblasts
mESc	Mouse embryonic stem cells
MG132	Carbobenzoxy- l -leucyl- l -leucyl- l-leucinal peptide
$MgCl_2$	Magnesium chloride
MLL	Mixed Lineage Leukemia
MNase	Micrococcal nuclease
MOPS	3- (N-morpholino)propanesulfonic acid
MYST	Moz, Ybf2/Sas3, Sas2, Tip60
mRNA	Messenger Ribonucleic acid
mSWI/SNF	Mammalian SWItch/Sucrose non-fermentable
NaCl	Sodium chloride
NAD	Nicotinamide adenine dinucleotide
$NaHCO_3$	Sodium Bicarbonate
NAMPT	Nicotinamide phosphoribosyl-transferase
NaOH	Sodium Hydroxide
NAP-1	Nucleosome assembly protein 1
ncBAF	Non-canonical BRG1/Brahma Associated Factor
Nfil3	Nuclear factor, interleukin-3 regulated
NLB	Nuclear Lysis Buffer
NP-40	Nonidet P-40
NPAS2	Neuronal PAS domain protein 2
Nr1d1	Nuclear receptor subfamily 1 group D member 1
Nr1d2	Nuclear receptor subfamily 1 group D member 2
NuRD	Nucleosome Remodeling Deacetylase
pAb	Polyclonal Antibody
PAR-bZip	Proline and acidic amino acid-rich - basic leucine zipper
PAS	PER-ARNT-SIM
PBAF	Polybromo-associated BRG1/Brahma Associated Factor
PBRM1	Polybromo-1

PBS	Phosphate-buffered saline
PCR	Polymerase Chain Reaction
PE	Paired-End
PER	Period
Ph:Ch:I	Phenol:Chloroform:Isoamyl
PHF10	PHD Finger Protein 10
Pol II	RNA Polymerase II
PRC	Polycomb Repressive Complex
pRGC	Photosensitive retinal ganglion cells
PTMs	Post-Translational Modifications
REST	RE1-Silencing Transcription factor
RH	Relative Humidity
RNA	Ribonucleic acid
ROR	RAR-related orphan receptors
ROS	Reactive Oxygen Species
Rps9	Ribosomal Protein S9
RSC	Remodeling the Structure of Chromatin
RT-qPCR	Real-Time- quantitative Polymerase Chain Reaction
SAHF	Senescence-associated heterochromatin foci
SCN	Suprachiasmatic Nucleus
SDS	Sodium Dodecyl Sulfate
SDS-PAGE	Sodium Dodecyl Sulfate-Polyacrylamide Gel Electrophoresis
SEM	Standard Error of the Mean
Seq	Sequencing
SETD	SET Domain-Containing
SIN3A	SIN3 Transcription Regulator Family Member A
SINEs	Short Interspersed Nuclear Elements
siRNA	Small interfering ribonucleic acid
SIRT	Sirtuin
SMARC	SWI/SNF-related matrix-associated actin-dependent regulator of chromatin
SRC	Steroid receptor co-activator -1
SS18/L1	Synovial Sarcoma Translocated To X Chromosome Protein
SUV39H1/2	Suppressor of variegation 3-9 homolog 1/2
SWI/SNF	SWItch/Sucrose Non-Fermentable
SWR	SWI2/SNF2-Related Chromatin Remodeling Complex
TAD	Topologically-associated domain
TAE	Tris-base, acetic acid and EDTA
Taq	Thermus aquaticus
TE	Transposable Element
TF	Transcription factor
TIM	Timeless
TKO	Triple Knock-out
TSS	Transcriptional Start Sites
TTFL	Transcriptional-Translational Feedback Loop
UBN1/2	Ubinuclein 1/2
UCSC	University of California Santa Cruz
UTR	Untranslated region
WT	Wild-type

Introduction

1. Circadian rhythms: from molecular mechanisms to physiology

1.1 Circadian clocks: an important feature for organismal fitness and homeostasis

Almost every living organism on Earth, from cyanobacteria to mammals, have evolved biological oscillators, among which circadian clocks (*circa diem,* about a day) drive approximately 24h rhythms in gene expression, physiology and behavior. Such robust autonomous oscillations allow organisms to adapt and to anticipate daily changes in their environment [1, 2]. Anticipation of external environmental cues (*Zeitgebers*, 'time-giver'), such as alternations in light-dark cycles, feeding time, as well as variations in temperature, by circadian oscillators is critical for internal organismal homeostasis [1, 2].

1.1.1 Discovery of circadian rhythms: from plants to mammals

The very first scientific observation of rhythmic behavior was made by the French astronomer Jean Jacques d'Ortous de Mairan in 1729, while studying the leaf movement of a mimosa plant, *Mimosa pudica* [3]. While mimicking physiological conditions (12h light:12h dark), he observed that the Mimosa leaves unfold during the day and fold during the night. Such movement was systematically repeated over time, along with day/night alternation. Interestingly, while placing the Mimosa plant in a light-tight dark room (constant darkness), he observed that the leaves continued to rhythmically unfold during the 'day-time' and fold during the 'night', even in the absence of light. In his publication *Observation botanique- Histoire de l'Académie Royale des Sciences* [4], de Mairan describes for the first time that an external cue such as light, is not necessary for the oscillations in Mimosa leaf movement,- highlighting that rhythmic behavior persists in the absence of external environmental cues and such oscillations are therefore very likely to be endogenous [3, 4]. In addition, de Mairan hypothesized that temperature cycles might influence the plant ability to sense time, contributing to their rhythmic behavior. In 1832, a Swiss botanist Augustin Pyramus de Candolle noted that Mimosa leaves unfold earlier each day and measured a period slightly shorter than 24h. Rhythmic leaf folding displayed a period of 22.5h, providing therefore evidence that such rhythms are internal [5].

Following these observations, it took nearly 200 years to finally acknowledge that circadian rhythms in behavior, such as photoperiodism in plants, are indeed regulated by endogenous clock which responds and can be synchronized to external stimuli. It was Erwin Bünning, a German biologist, that in the 1930s conducted the studies on bean plant leaf movement and noted that placing the bean plant under constant light conditions results in a free-running rhythmic leaf movement that has a period slightly longer than 24h (24.4h) [3]. It took no longer to characterize the first genes involved in organismal behavior [6, 7]. In the 1960s,

while performing mutagenesis screens to study genes involved in pupal eclosion and locomotor activity rhythms of the fruit fly *Drosophila melanogaster*, Ronald J. Konopka and Seymour Benzer identified three single-gene mutants mapped on the same locus on the X chromosome [6]. These mutants displayed important alterations in eclosion and locomotor activity rhythms, such as shortening or lengthening of the 24h period, resulting respectively in rhythms of approximately 19h or 28h, as well as mutants displaying arrhythmicity in described phenomena. They named this gene *Period*,- however at that time, the scientific community remained restrictive to the possibility that a single gene could control complex organismal behavior [6, 7].

Nevertheless, their discoveries led to a new era of investigating the molecular mechanisms behind circadian rhythms [3, 8]. During the 1980s, three scientists- Jeffrey C. Hall, Michael Rosbash and Michael W. Young, along with their colleagues, independently cloned and identified *Period* (*Per*) as the first clock gene in *Drosophila* [9, 10]. Their further studies provided important insights into molecular mechanisms of circadian clocks. They found that in Drosophila heads, *Per* mRNA levels display free-running circadian rhythms peaking in the early night, followed by oscillations and a peak of the PER protein levels 4-6h later [11, 12]. Moreover, a nonsense mutation in *Per* gene abolished oscillations in its mRNA levels and affected behavioral rhythms of the flies, which was rescued by *Per* gene transfer of the wild-type fly [13]. Furthermore, they characterized PER as a nuclear protein that rhythmically shuttles between the cytoplasm and the nucleus [14]. In addition, overexpression of the PER protein inhibited oscillations in *Per* mRNA levels, leading therefore to establishment of a regulatory model, where PER protein directly modulates its own gene expression [11, 12]. Identification of the second clock gene 10 years later, *Timeless* (*Tim*), revealed a close connection with PER regulatory mechanism [15, 16]. Indeed, TIM was shown as essential for PER nuclear entry, oscillations in PER levels, and establishment of pupal eclosion and locomotor activity rhythms [17, 18, 19]. A model of transcriptional-translational feedback loop (TTFL) to establish 24h oscillations in gene expression, protein levels and behavior was proposed. In parallel, a positive limb of the feedback loop was characterized thanks to the discovery of the mammalian mouse *Clock* gene by Joseph Takahashi and colleagues [20, 21, 22], followed by identification of its partner BMAL1 [23] - both being essential for circadian behavior. BMAL1-CLOCK were further identified as positive drivers of transcriptional oscillations, and their orthologs CYCLE [24] and CLOCK [25], as positive transcription factors of *Per* and *Tim* in *Drosophila*. All of these initial findings led progressively to the identification of the whole regulatory molecular network of circadian clock in *Drosophila* and mammals (Figure S1), and in parallel as well in other organisms. Established core-clock TTFL mechanism was further challenged by the discovery of the auxiliary post-transcriptional and post-translational regulators of the main core-clock

factors, such as *Doubletime* gene in *Drosophila*, encoding for the casein kinase CK1 and its orthologs in mammals, being involved in the stability of the PERIOD protein [26, 27, 28]. These 'auxiliary' regulators are involved in the maintenance of the 24h period in transcriptional-translational processes, which would usually last from several minutes to maximum few hours in eukaryotic cells [29].

In 2017, the Nobel Prize in Physiology or Medicine was jointly awarded to Jeffrey C. Hall, Michael Rosbash and Michael W. Young *for their discoveries of molecular mechanisms controlling the circadian rhythm* [30]. Nevertheless, the main question in the field, *i.e.* understanding how the molecular core-clock machinery generates and sustain the delay of 24h in 'fast' biochemical processes such as transcription and translation, still remains an active field of research.

1.1.2 Universal properties of circadian oscillators

Properties of circadian oscillators were first fully described in 1960 by Colin Stephenson Pittendrigh, based mainly on initial discoveries including observations in *Drosophila* behavioral rhythms [31]. Circadian clocks are characterized as endogenous, self-sustaining and cell-autonomous pacemakers (see Box 1 for the definitions and terminology). They are free-running and extremely robust oscillators with a physiological timing error of only few minutes every 24h. In addition, they are inherent and ubiquitous (*i.e.* present in every cell). Despite their endogenous, self-sustaining properties, circadian clocks are responding to external environmental cues to synchronize organisms with their environment [31, 32]. Therefore, these oscillators are entrainable by the external environmental cues, called *Zeitgebers*. However, these daily biological rhythms remain temperature-compensated (Box 1) [2, 31, 33].

Box 1. Definitions of main, key properties of circadian rhythms and terminology.

- Circadian rhythms. *Circa diem* (about a day) rhythms are biological rhythms whose free-running period (τ_{FR}) reflects the approximation of the period of the Earth's rotation.
- Period. Refers to the time biological oscillator takes to complete one cycle. For circadian oscillations, the period is approximately 24h.
- Free-running period (τ_{FR}). The length of time that an organismal endogenous rhythm takes to repeat, in the absence of environmental timing cues. τ_{FR} can be measured in constant experimental conditions (*e.g.* constant darkness). It is not a fixed, but rather flexible feature of a given organism, adjustable to spontaneous and induced shifts (*e.g.* travelling across different time zones), within a certain range of values.

The free-running property of circadian rhythms goes along with their characteristics of being endogenous and self-sustaining.

- Endogenous, self-sustaining. Circadian oscillators are intrinsic ('work from within') to an organism. They are able to 'self-generate' rhythmic and repetitive variations in physiological phenomena in the absence of external cues.
- Cell-autonomous. Circadian rhythms occur autonomously at both, cellular and tissue levels, meaning they are able to occur independently of surrounding cells or tissues (outside of an organism). Recordings of individual cell and even tissue rhythms have been made in culture systems *in vitro**.
- Robust. Robustness of circadian clocks refers to their remarkable precision. As it has been previously described in CS Pittendrigh's properties of circadian rhythms, observed physiological timing error of circadian period might be less than 2min in one cycle of 24h.
- Inherent. Circadian rhythms are innate to an organism.
- Ubiquitous. This property not only refers to the fact that almost all living organisms on Earth evolved circadian oscillators, but also to their levels of organization (*i.e.* present in every tissue and virtually in every single cell) and as well their roles in various biological processes- from rhythms in DNA synthesis to complex organismal behavior.
- Entrainable. Circadian clocks sense and are sensitive to various external environmental cues such as light/dark cycles, temperature variations and fasting/feeding cycles. These cues were named as *Zeitgebers* ('time-givers' or synchronizers) by the German biologist Jürgen Aschoff**. Entrainable property of circadian oscillators refers to the coupling of an observable rhythm in an organism to a given *Zeitgeber*. In other words, endogenous clock that responds to the sensed environmental cue (stimulus), adjusts the internal rhythm of an organism to its environment, resulting in a shared, synchronized period.
- Temperature-compensated. Reflects the ability of circadian clocks to maintain a relatively constant free-running period, which is not affected upon variations in external environmental temperature.

* 34, 35, 36, 37; ** 32

Nevertheless, these key properties remain characteristic of circadian oscillators in any given species.

Given that circadian clocks are simultaneously endogenous and entrainable, two different concepts of time-perception and definition related to the experimental conditions have been established in the field (Box 2).

Box 2. Concepts of time related to the experimental conditions.

- Zeitgeber time (ZT). Is defined as a time, referring to the external environmental cues, such as alternation of light/dark cycles. Therefore, studies of circadian entrainment are performed under experimental conditions mimicking the environment of an organism. *E.g*. 12h light: 12h dark conditions, where the first time point ZT0 corresponds to the beginning of the light exposure (day-time) and 12h later, ZT12 time point, to the beginning of the darkness (night-time).
- Circadian time (CT). In contrary, circadian time is defined by endogenous circadian clocks of an organism placed under constant conditions (*e.g*. constant darkness), without any reference to external environmental cues. Therefore, in order to conduct a circadian experiment and study the intrinsic roles of organismal clocks in biological processes, animals are usually entrained for two weeks upon 12h light:12h dark cycles, following which they are placed under constant darkness prior experiment. Thus, CT0 refers to the first time point in constant darkness- beginning of the subjective day-time, and 12h later, CT12 time point to the beginning of the subjective night-time.

1.2 Organization levels of circadian clocks in mammals

In mammals, circadian clocks are present within the whole organism: in every tissue and virtually in every single cell. They are hierarchically organized into two groups, which consist of the main, central pacemaker called the master clock located in the brain, and the peripheral oscillators found in all remaining tissues of the body [1, 8].

1.2.1 Suprachiasmatic nuclei: the master clock

Composed of ~20,000 neurons, the Suprachiasmatic nuclei (SCN) reside within a tiny region of the brain, the hypothalamus, located just above the optic chiasma [1, 8]. The importance of the SCN in circadian rhythms was discovered while investigating various brain structures for their potential role as a pacemaker for the whole organism, by performing brain lesion experiments in rats [38, 39]. SCN lesions resulted in loss of behavioral rhythms, such as locomotor activity [39]. Interestingly, upon intact SCN transplantation to SCN-lesioned animals, behavioral rhythms were restored with a period length characteristic of the donor [40, 41]. Moreover, in genetically-modified arrhythmic mice, transplantation of the SCN from wild-type littermates resulted in a

full restoration of circadian rhythms at behavioral level [42], indicating the primary role of the SCN as a main brain oscillator. In addition, in dispersed cultures, individual SCN neurons are able to generate circadian oscillations in clock gene expression and neuronal firing,- independently, in a cell-autonomous manner [43, 44]. However, for the proper SCN function as the main brain circadian pacemaker, intact neuronal network within the SCN is needed [45, 46, 47].

In order to synchronize peripheral oscillators in remaining organs, including the secondary brain oscillators, the SCN integrates information received from the light input, initially perceived by the photosensitive retinal ganglion cells (pRGC) [48]. The photic cues are then transmitted from the retina directly to the SCN [49], which in turn convert the received information into a multitude of neuronal and hormonal cues that synchronize the clocks in peripheral tissues [1, 8, 50]. Moreover, the master clock integrates signals from the periphery and such interplay between circadian clocks at various levels across organism results in establishment of overall synchrony between organismal external and internal environments (homeostasis) [1, 8].

1.2.2 Peripheral oscillators

Peripheral oscillators are found in every organ, as well as in every single cell. Being synchronized by the central SCN pacemaker, tissue clocks drive ~24h rhythms in local gene expression programs [50, 51, 52]. Although organ-specific genes involved in regulation of key metabolic processes of a given tissue oscillate at their own pace, the core-clock genes remain in synchrony across multiple tissues [53]. As an output, such coordination results in rhythmicity of approximately 10-15% of the expressed genome, cycling in a tissue-specific manner [51, 52, 53]. In addition, as for the SCN, peripheral tissue oscillators continue to sustain circadian rhythms independently of external and internal synchronizing cues, when cultured *in vitro* [34, 35, 36, 37, 50].

1.2.3 Example of a mammalian peripheral clock: liver at the center of the interplay between circadian timing system and metabolism

Liver is one of the most well studied and characterized peripheral oscillators, very likely due to its central role in metabolism and the close connection between circadian clocks and metabolic pathways [54].

In mammals, liver consists of four main lobes, hundreds of thousands hepatic lobules and is highly vascularized [55]. Hepatic vein network consists mainly of portal and central veins. Such vein network generates gradients in oxygen and nutrient concentrations, signaling pathways, as well as gradients in gene expression programs along the portal-central axis [55]. The polarization of hepatic lobules leads to liver zonation, resulting in a spatial compartmentalization of key metabolic pathways [56]. In addition, liver harbors various cell types.

While the liver post-mitotic quiescent cells, hepatocytes, represent approximately 80-90% of the tissue, liver contains as well non-parenchymal cells, Kupffer (hepatic macrophage-like) cells, liver sinusoidal endothelial cells, Ito (hepatic stellate) cells, intrahepatic cholangiocytes and epithelial biliary tree cells, which results in important cell-type heterogeneity [57].

Liver, the central metabolic crossroad of the organism, is involved in regulation of several metabolic processes such as carbohydrate and lipid metabolism, synthesis of bile acid and hormones, transport of nutrients, processing of amino acids and detoxification. All of these are highly rhythmic processes, tightly linked to circadian clock regulation [54, 58, 59]. Liver is synchronized by several systemic cues, such as feeding/ fasting cycles, oscillations in body temperature, oxygen levels, hormones and metabolites, and in turn, liver rhythmicity can be as well driven by the liver clock itself (Figure 1) [58, 60, 61, 62]. As an output, approximately 15-20% of the hepatic transcriptome is cycling, followed by oscillations in hepatic proteome, including post-translational modifications such as phosphorylation and acetylation, and metabolome [63, 64, 65]. For instance, the enzymatic activity of the histone deacetylase SIRT1 (Sirtuin 1) is dependent on nicotinamide adenine dinucleotide (NAD^+) metabolite, which acts as a cofactor. NAD^+ levels oscillate, as well as the levels of its regulatory enzyme NAMPT (Nicotinamide phosphoribosyl-transferase). In turn, SIRT1-mediated deacetylation responds to rhythmically changing NAD^+/NADH ratio [66]. Indeed, SIRT1 activity was shown concomitant with acetylation status of the core-clock transcription factor BMAL1 and histone H3 at circadian promoters in murine livers [67]. In addition, SIRT1-mediated deacetylation of PER2 was shown important for its degradation/stability, playing important role in circadian molecular mechanism [68]. Moreover, liver-specific *Sirt1* knock-out resulted in impairment of circadian rhythms *in vivo* [67]. In addition, it has been shown that mutations in the core clock genes such as *Bmal1*, result in alterations of key metabolic functions, such as impairment of glucose homeostasis, highlighting the key role of the core-clock molecular machinery in liver physiology and homeostasis [69].

The importance of the food-intake timing (food availability along with feeding time) as the main *Zeitgeber* to keep the liver clock in sync has been demonstrated in early 2000 [70, 71]. In these studies, where rats and mice were exposed to a time-restricted feeding (*e.g.* access to food only during the day-time) under light/dark and constant darkness conditions, the imposed restricted food availability resulted in a phase-shift of ~10-12 hours in circadian gene expression within peripheral oscillators (mainly observed in the liver). In contrary, the phase of cyclic gene expression within the SCN master clock remained unaffected [70, 71]. Furthermore, liver rhythms were shifted very rapidly, within 2 days. While the phase-resetting occurred faster in the liver than in other peripheral tissues, such as kidney, pancreas or heart, the phases of circadian gene expression were found to be similar in all these tissues after one week of restricted feeding [70, 71]. Thus, these studies provided important cues in understanding of the

relationship between the central pacemaker and the peripheral tissues. In summary, the coupling between the SCN master clock and peripheral oscillators is primarily dependent on the timing and food availability [72]. Metabolic changes due to the time-restricted feeding result in uncoupling of the peripheral oscillators from the SCN. Such phase-shift in circadian gene expression occurs progressively and gradually in peripheral oscillators, affecting primarily the liver [70, 71]. This indicates that peripheral oscillators are able to function independently of the central pacemaker, which was further confirmed by additional studies in which lesions in SCN did not abolish circadian rhythms in peripheral tissues, but led rather to desynchrony among different organs [73]. Despite important uncoupling among oscillators during the first initial days after the phase-shift (can be experienced as a jet lag), peripheral oscillators are able to adjust within following days to the imposed *Zeitgeber* and function again in synchrony. Such adjustments highlight remarkable plasticity and adaptability of the circadian timing system.

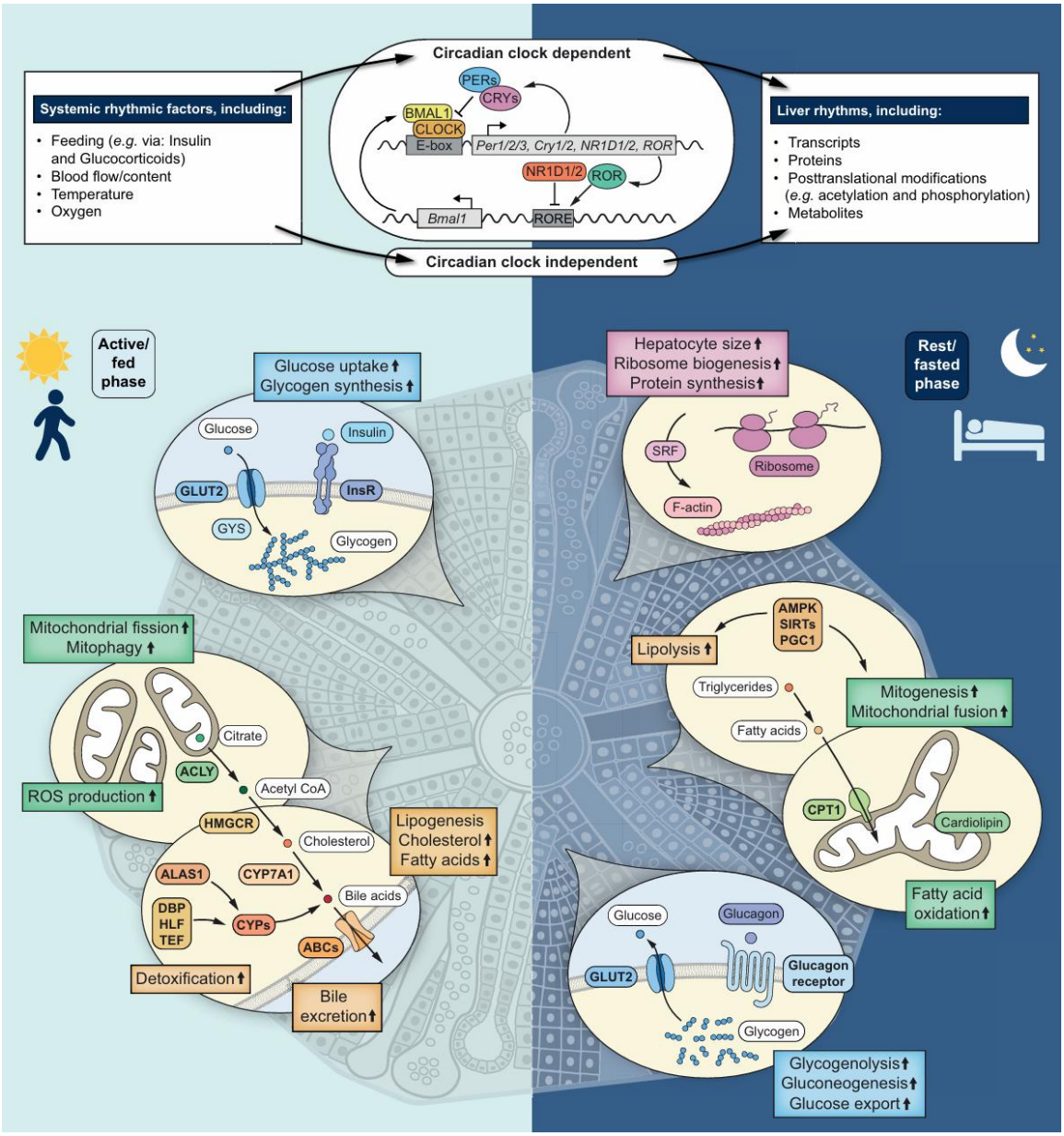


Figure 1. Circadian regulation of key hepatic metabolic processes. Regulation of liver-specific metabolic processes are tightly linked with circadian rhythms. The active phase (day-time for humans and night-time for mice), is accompanied by lipid synthesis and storage, glycogen synthesis, detoxification, as well as mitochondrial fission associated with production of reactive oxygen species (ROS). In contrary, the rest phase (night-time for humans and day-time for mice) is linked with lipolysis, gluconeogenesis, protein synthesis, oxidation of fatty acids and mitochondrial fusion. In addition, hepatocyte size also oscillates over 24h, depending on the diet and feeding schedule [74]. *Figure from Aviram R, Manella G, Asher G. J Hepatol. 2021* [58].

1.3 Molecular mechanisms of mammalian circadian clocks

Circadian rhythms are built on approximately 24h transcriptional-translational feedback loops (TTFL), subdivided into the core-clock and auxiliary TTFL (Figure 2), which are highly conserved across species [8, 75, 76].

In mammals, the core molecular clock comprises primarily four key actors. Two transcriptional activators: the basic helix-loop-helix (bHLH) - PER-ARNT-SIM (PAS) transcription factors (TFs) BMAL1 (Brain and Muscle ARNT-Like 1) and CLOCK (Circadian Locomotor Output Cycles Kaput), along with its paralog NPAS2 (Neuronal PAS domain protein 2), and two transcriptional repressor protein families: PERIOD (PER, encoded by *Per1, Per2* and *Per3*) and CRYPTOCHROME (CRY, encoded by *Cry1* and *Cry2*) [75].

At the beginning of the day, upon initiation of the active clock phase, TF heterodimer BMAL1-CLOCK binds to their specific circadian E-box sequences (CACGTG) on DNA, which leads to chromatin opening and transcriptional activation of thousands of clock-controlled genes (CCGs). Among these genes are found as well their own repressors, *Per* and *Cry*. Therefore, in the early night, upon sufficient accumulation of PER and CRY proteins in the cytoplasm, PER-CRY form heterodimeric complexes which translocate to the nucleus to repress BMAL1-CLOCK activity and block their own synthesis. Following circadian cycle starts the next day, upon phosphorylation and proteasomal degradation of PER-CRY repressive complexes, where BMAL1-CLOCK become active again, establishing thus ~24h TTFL [75, 76, 77].

In parallel, a secondary ‘auxiliary’ feedback loop is generated by the nuclear receptors REV-ERBα and REV-ERBβ (encoded respectively by *Nr1d1* and *Nr1d2* genes) and ROR (RAR-related orphan receptors) α, β and γ, whose transcriptional activation is controlled by BMAL1-CLOCK. In return, REV-ERBs and RORs regulate BMAL1-CLOCK activity by respectively acting as repressors and activators of *Arntl* (*Bmal1*) gene expression [75, 78]. Additional level of regulation of the primary core-clock feedback loop is mediated by casein kinases such as CK1δ (Casein Kinase 1 delta) and CK1ε (Casein Kinase 1 epsilon), which are implicated in PER phosphorylation and thus its stability, being involved in the E3 ubiquitin ligase pathways of proteasomal degradation [77]. In addition, another auxiliary loop contributes

to the rhythmic regulations of transcriptional-translational processes within the cell (Figure S2). Expression of *Nfil3* (Nuclear factor, interleukin-3 regulated) is as well negatively regulated by REV-ERBs and in contrary, positively regulated by RORs. In turn, NFIL3 represses the PAR-bZip factor DBP (D-box binding protein) which mediates rhythms in RORs nuclear receptors [75].

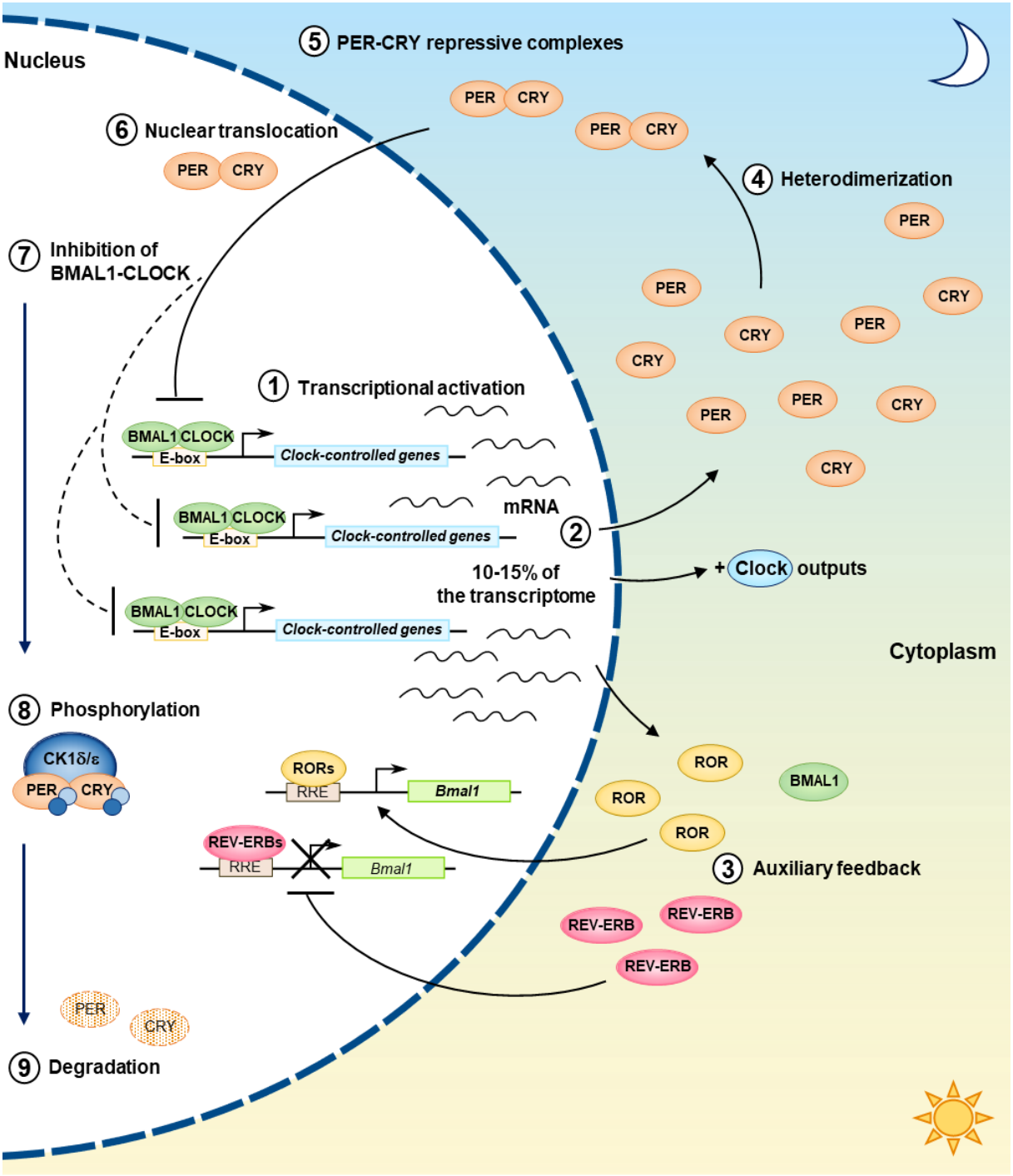


Figure 2. The core-clock regulatory feedback loops (simplified model). At the beginning of the day, BMAL1-CLOCK bind to their specific E-boxes to turn on transcription of thousands of genes (1). Approximately 10-15% of the expressed genome is cycling (2). The main core-clock loop sustains

auxiliary feedback loops, which in turn positively (RORs) or negatively (REV-ERBs) regulate *Bmal1* expression (3). Among BMAL1-CLOCK target genes are *Per* and *Cry*, their own repressors. Therefore, upon sufficient accumulation of PER and CRY proteins in the cytoplasm, they heterodimerize (4) to form PER-CRY repressive complexes (5). PER-CRY translocate to the nucleus (6) to repress BMAL1-CLOCK activity and establish facultative heterochromatin during the night (7). Towards the beginning of the next day, PER-CRY get phosphorylated by CK1δ/ε (8). These phosphorylations are followed by their targeting to proteasome, and therefore their degradation (9). BMAL1-CLOCK become active again and a new circadian clock cycle starts at the beginning of the next day. Rhythmic binding of BMAL1-CLOCK and PER-CRY on chromatin along with auxiliary regulatory mechanisms, generate ~24h transcriptional-translational dynamics. *Figure inspired by the figure 2 in Takahashi JS. Nat Rev Genet. 2017* [75], *see Figure S2. Created with Inkscape*.

Together, the core-clock and auxiliary circadian feedback loops establish ~24h dynamic changes in chromatin architecture and therefore in chromatin states - generating transcriptionally active regions of the genome (euchromatin) during the day-time, followed by silencing of gene expression and establishment of facultative heterochromatin during the night.

1.4 Circadian clock disruption in diseases

Circadian rhythms are involved in regulation of various (if not all), biological and physiological processes, such as sleep-wake cycles, hormone secretion, redox state, xenobiotic metabolism, as well as immune and inflammatory processes, being therefore critical for organismal homeostasis [62, 79]. In addition, circadian clocks are also involved in regulation of cell proliferation and DNA damage repair. The molecular core-clock machinery gates the cells through division by rhythmically regulating the core cell cycle factors involved in mitotic checkpoints, both at transcriptional and post-translational levels [80]. In parallel, DNA damage response (DDR) pathways, such as DNA damage and repair, apoptosis and transcriptional reprogramming, are also gated by circadian clocks. Rhythmic assembly of DNA repair machinery with the core-clock complexes, as well as rhythmic expression of key DDR regulators, result in coordination of circadian oscillators with DNA damage checkpoints, playing a key role in cell survival [81, 82, 83].

Given their crucial role in organismal fitness and physiology, disruption of circadian rhythms by either genetic (*e.g.* mutations in core-clock genes) and epigenetic alterations in its key regulators, or even by environmental stress (*e.g*. night-shift work resulting in chronic jet lag, unhealthy modern lifestyle) leads to development and progression of multiple disorders and diseases. For instance, mutations in human Per2 gene have been described as perturbators of the free-running period, resulting in circadian sleep disorders in humans. More precisely, PER2 is implicated in Familial advanced sleep phase syndrome (FASPS), where the S662G mutation located within the CK1ε binding-domain, results in hypo phosphorylation of

PER2 [84, 85]. As a consequence, PER2 hypo phosphorylation would accelerate its autorepression, by decreasing the time of PER2 nuclear retention. These would result in phase-advanced molecular rhythms, shortening therefore the period of the clock cycle and the resting phase [86, 87]. In contrary, genetic variations in Cry1 are involved in the Delayed sleep phase disorder (DSPD). The gain-of-function CRY1 variant displays enhanced affinity for BMAL1 and CLOCK, which leads to downregulation of key clock target genes, lengthening therefore the period of circadian rhythm, characterized by a persistent delay of sleep onset [88].

In addition, alterations in core-clock genes, resulting from mutations or upregulation, are implicated in onset and progressive development of tumors in various cancers. For instance, PER2 is also known to function as a tumor suppressor [89, 90], implicated in regulation of cell cycle-related genes (*e.g*. *c-Myc*, *p53*, *p21*, *wee1*), cyclin-dependent kinases (CDK), CDK inhibitory checkpoints and epithelial-mesenchymal transition [91, 92, 93].

Moreover, disruption of coordination among oscillators within organism occurs due to the loss of synchrony between internal circadian clocks and external environmental timing cues. Such phenomenon is called circadian misalignment and is often characteristic for the night-shift workers [94]. It has been shown that while exposed to controlled circadian misalignment conditions mimicking the night-shift work (*e.g*. long-lasting light exposure during the night time), subjects experienced imbalances in glucose homeostasis, appetite control and energy expenditure [95, 96]. In addition, studies of circadian misalignment induced by high-fat diet time-restricted feeding regimes in mice, led to a significant increase in weight of animals fed during the day, when compared to those fed during their physiological timining at night, promoting diet-induced obesity [97, 98]. Overall, circadian misalignment is associated with defects in glucose tolerance and insulin resistance, increasing the risk of obesity and diabetes [69, 97, 98, 99]. Additionally, due to light exposure and feeding at the ‘wrong time of the day’, night-shift workers are as well more prone to tumor development [100, 101].

Overall, circadian rhythm disruption is directly involved in sleep disorders, metabolic syndrome, obesity, diabetes, cardiovascular diseases, neurodegenerative diseases and multiple cancers, as well as pathological aging [102, 103, 104, 105, 106, 107]. All of these highlight opportunities in development of novel therapeutic approaches, such as the concept of chronotherapy. Chronotherapy consists in optimizing treatment success by delivering the ‘right drug at the right time’ of the day to the patients, based on their internal rhythms. Optimal administration timing of any therapeutic or medical treatment (*e.g*. drug, radiation, surgery) promotes reduction of side effects and therefore improves patient prognosis [62, 108, 109].

2. Chromatin dynamics and epigenetic signatures

2.1 Chromatin organization: general overview

In eukaryotic cells, the fundamental structural and functional unit of chromatin is the nucleosome, which consists of ~ 147 base pairs of DNA wrapped around an octamer of histone proteins, among which two copies of each of H2A, H2B, H3 and H4 canonical histones constitute its core [110, 111, 112].

Nucleosome assembly is a highly dynamic process which begins with an incorporation of H3-H4 tetramer on chromatin, followed by a subsequent deposition of two H2A-H2B heterodimers and DNA wrapping around the newly formed histone core. *De novo* nucleosome assembly and incorporation on chromatin occurs during the replication S phase of the cell cycle [112]. This process is mediated by the specific chaperone proteins: CAF-1 (Chromatin assembly factor 1) [113, 114] and ASF-1 (Anti-silencing function 1) [115, 116] involved in deposition of the H3-H4 tetramer and the FACT (Facilitates chromatin transcription) [117, 118] and NAP1 (Nucleosome assembly protein 1) [119] H2A-H2B specific chaperones. Nucleosomes, along with the linker H1 histone, are involved in DNA packaging and multiple layers of chromatin compaction mediated by the histone proteins result in its organization of a higher-ordered structure (Figure 3) [120].

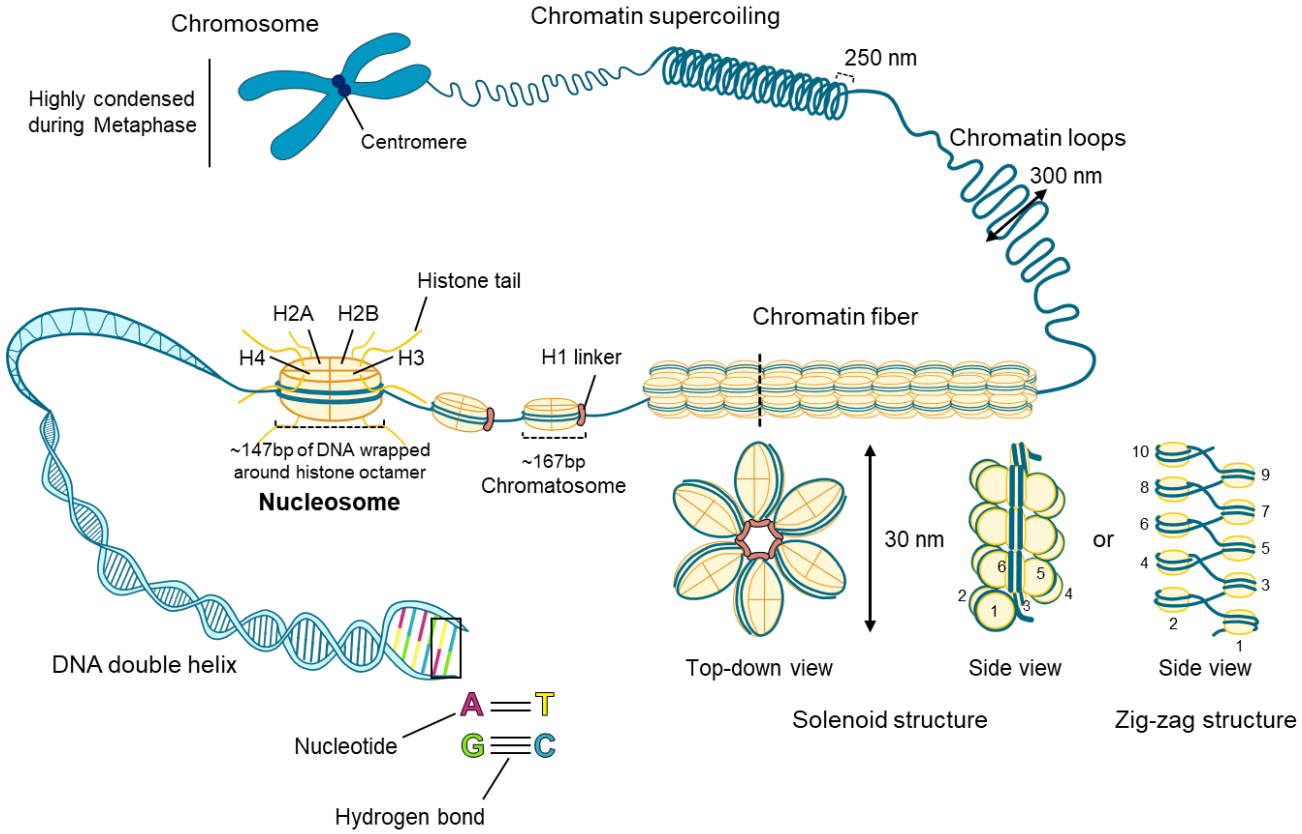


Figure 3. Chromatin organization *in vitro*. In eukaryotic nuclei, chromatin is organized into a higher-ordered structure due to the several layers of its compaction. Negatively charged sugar-phosphate backbone allows DNA to wrap around positively charged histone proteins, which constitute the core of the nucleosome [110, 111]. Nucleosomes, along with the H1 linker histone are further involved in DNA compaction, resulting in formation of a 30nm chromatin fiber [121]. Two main models have been proposed so far for the 30nm fiber formation- a solenoid secondary structure, or a zig-zag nucleosomal stretches [121, 122]. Chromatin fiber then further folds into chromatin loops, averaging ~300nm in length, which further coil into a 250nm wide fibers. Chromatin supercoiling results in a highly condensed chromatin, which compacts into chromosomes during the cell division in Metaphase [120]. *Created with Inkscape.*

Additional levels of chromatin organization exist within the nucleus (Figure 4) [123, 124]. In eukaryotic cells, nucleus is further organized into distinct chromosomal territories, which are subdivided into A (active) and B (inactive) compartments harboring respectively actively transcribed and silenced genes [125, 126]. The interchromatin compartment represents a 'chromatin-free space' separating the different chromosomal territories [124]. Within these territories, other regulatory domains can be found, such as nuclear bodies- distinct local environments with their specific functions (*e.g.* transcription factory, stress-response) [127, 128], lamina-associated domains (LADs)- zones in which chromatin contacts the nuclear lamina, harboring mainly silent genes, and topologically-associated domains (TADs) which are involved in mediating interactions between the gene-distal cis-regulatory sequences (enhancers) and their target genes [124, 129]. Such three-dimensional nuclear-chromatin organization plays a key role in gene regulation [123, 124, 129].

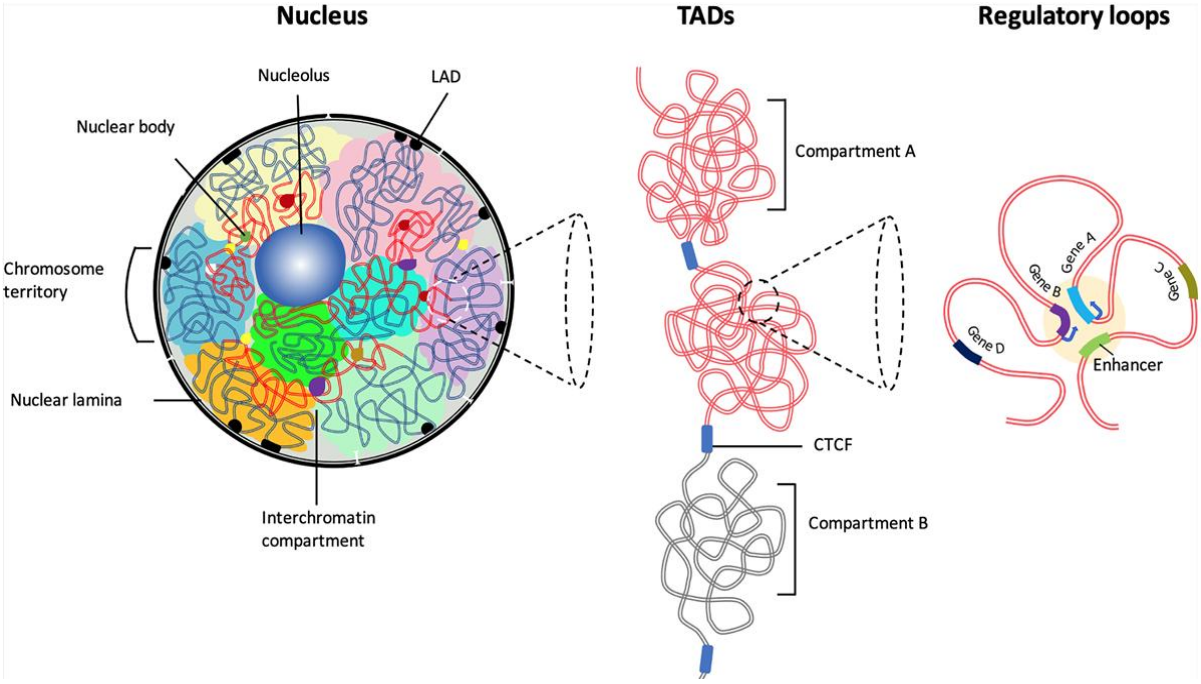


Figure 4. Three-dimensional chromatin organization within the nucleus. Chromatin organization into distinct chromosomal territories and regulatory domains results in highly regulated gene expression in space and time. *Figure from Pongubala JMR, Murre C. Front Immunol. 2021* [124].

2.2 Epigenetic mechanisms establishing dynamic chromatin changes

Dynamic transitions in chromatin states and its architecture are modulated by several key epigenetic players: chromatin modifying enzymes, known as '*writers, readers, erasers*', epigenetic signatures such as DNA methylation and histone post-translational modifications (PTMs) (*e.g.* acetylation, methylation, phosphorylation, ubiquitination, sumoylation, *etc.*), chromatin remodelers, and as well by incorporation of histone variants on chromatin. All of which play an important role in transcriptional regulation, both as activators and repressors in a context-dependent manner [130, 131, 132].

2.2.1 Example of epigenetic signatures: post-translational modifications of histones

Histones are marked by a multitude of PTMs, whose combination would serve as an *epigenetic code*. They play a role in key biological processes, such as transcriptional regulation, DNA replication and repair, cell cycle and differentiation, as well in zygotic genome activation and development [133, 134, 135]. Such PTMs are present on histone tails (*e.g.* H3K4me3, H3K27ac), as well as on histone globular core domains located within the nucleosome dyad, also known as lateral surface PTMs (*e.g.* H3K115ac, H3K122ac). Being involved in modulation of chromatin architecture, they can act either directly by affecting nucleosome-nucleosome interactions, inducing local chromatin alterations to drive transcriptional activation or repression, as well as indirectly, requiring recruitment of their '*readers*' and/or '*erasers*' to have an effect at a larger genomic scale [133]. Conceptually, acetylation of histones is linked with transcriptional activity, whereas histone methylation with genome silencing. Nevertheless, it is known that methylation marks can be as well involved in transcriptional regulation as activators in a context-dependent manner. As an example, tri-methylation of lysine 4 of histone 3 (H3K4me3) bookmarks the genome prior transcriptional activation [136, 137], whereas di-methylation of lysine 9 of histone 3 (H3K9me2), genomic regions prior silencing [133, 134].

Among canonical histones, the histone H3 is one of the most marked. Multiple combinations in histone PTMs (Figure 5) result from highly regulated spatio-temporal recruitment of chromatin modifiers involved in their deposition or removal, such as histone acetyl transferases (HATs) (*e.g.* p300 and CBP from the EP300 family; Tip60 from the MYST family) and histone methyl transferases (HMTs) (*e.g.* SUV39H1/2 and SETD2 enzymes, MLL and PRC families) [134]- the *writers*. And among *erasers*, histone deacetylases (HDACs) (*e.g.* HDAC1-11, SIRT1-7) and histone demethylases (HDMs) (*e.g.* JARID and JMJD families) [138].

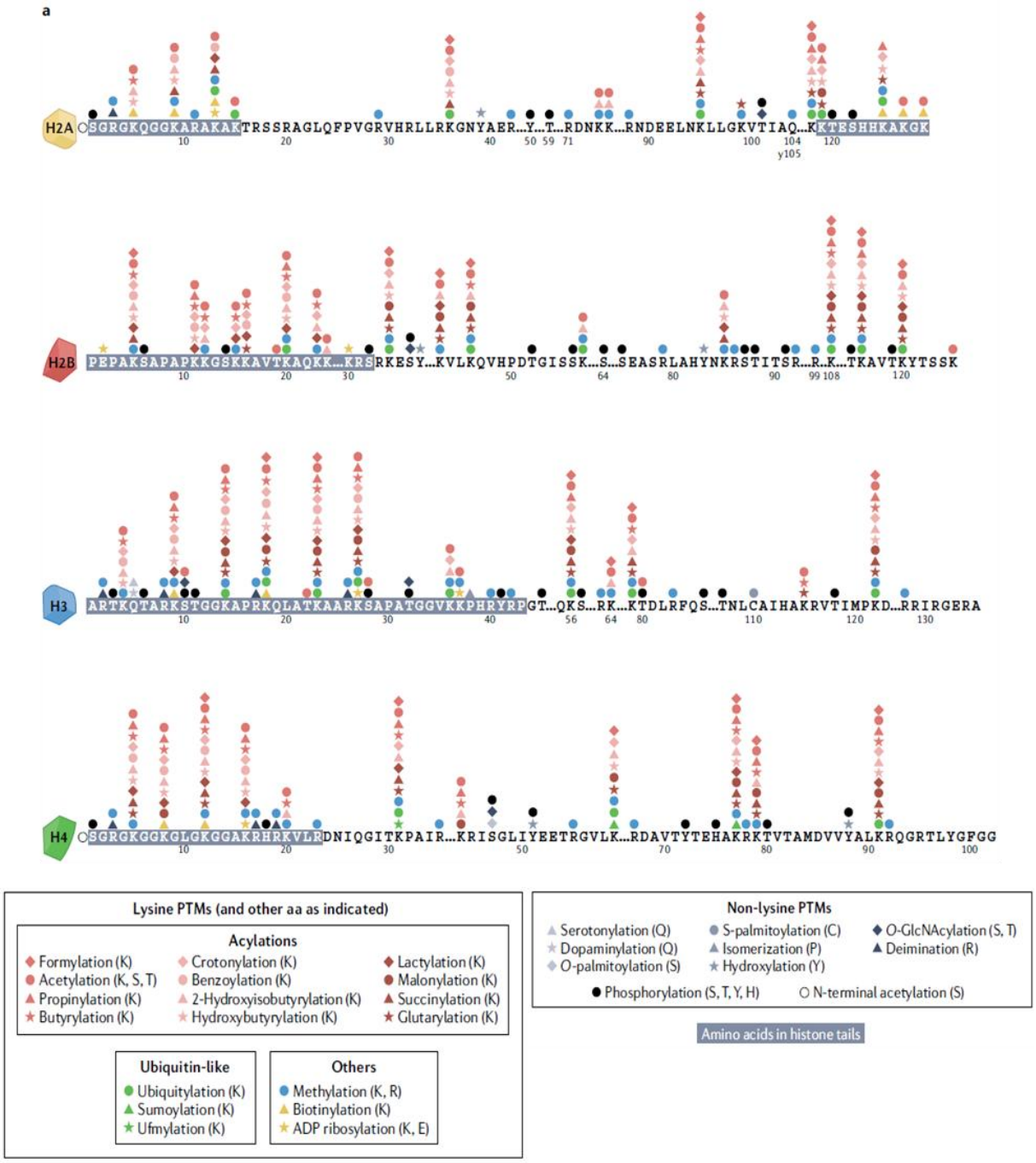


Figure 5. Landscape of histone post-translational modifications. Among canonical histones, the histone H3 is the most marked, highlighting its versatile roles in key biological processes. Histone post-translational modifications occur mainly on lysines (K) in N-terminal histone tails (*e.g.* lysine 4 of the histone H3). Several modifications might occur as well at their lateral surface located near the nucleosome dyad, modulating thus nucleosomal stability (*e.g.* lysine 115 of the histone H3). *Figure adapted from Millán-Zambrano G, Burton A et al. Nat Rev Genet. 2022* [133].

2.2.2 Chromatin remodelers of the SWI/SNF family

Chromatin remodeling complexes play a critical role in shaping the chromatin architecture, regulating DNA accessibility and thus, gene expression programs. In mammals, four different

families of ATP-dependent chromatin remodelers have been characterized: the mammalian SWI/SNF (mSWI/SNF) family, the INO80/SWR family (including INO80, p400/TIP60 and SRCAP complexes), the ISWI family, and the CHD/NuRD complex family [139].

Remodelers from the SWI/SNF (SWItch/Sucrose non-fermentable) family were first identified in two independent screens in yeast *Saccharomyces cerevisiae*, in which mutations resulted both in alterations in yeast mating type switch and their inability to ferment sucrose [140, 141]. These ~1-2 megadalton multiprotein complexes are highly conserved from yeast to mammals [142, 143]. Very early on, initial purifications of mammalian SWI/SNF complexes have revealed biochemical heterogeneity in their composition and identified key roles of the different subunits in targeting these complexes to DNA, being involved in transcriptional regulation [144, 145, 146, 147]. Overall, remodeling activity of SWI/SNF complexes is involved in multiple key biological processes, such as gene expression, cell growth and mitotic progression, development and neurogenesis, DNA damage response and repair. Processes, in which they can act as both activators and repressors, in a context dependent manner [142, 148, 149, 150, 151, 152].

ATP-dependent SWI/SNF complexes are involved in physical remodeling of chromatin architecture by three different modes: repositioning of nucleosomes, nucleosome ejection and eviction of histone dimers from chromatin [139]. By using energy from ATP hydrolysis, they slide the DNA around nucleosomes and the remodeling occurs in four to five key steps (Figure 6) [153, 154]. The translocase domain of the remodeler (consisting of the torsion and tracking subdomains) binds to the nucleosomal DNA, located approximately two turns from the dyad of the nucleosome. Upon remodeler binding followed by ATP hydrolysis, the torsion subdomain performs a directional DNA translocation, disengaging contacts between histones and DNA. This action results in creation of a transient intranucleosomal DNA loop that propagates around the nucleosome (Figure 6A) [154]. The loop resolution occurs when unwrapped DNA reaches the exit site, resulting in nucleosome repositioning or ejection, following which the remodeler resets to its original position to ensure a new remodeling cycle. In addition, during translocation phase, reverse translocation or DNA sliding might occur, being followed by immediate nucleosome repositioning without formation of intranucleosomal DNA loops (Figure 6B) [153].

The mSWI/SNF complexes include the PBAF (Polybromo-associated BAF), the cBAF (canonical BRG1/BRM associated factor) and the ncBAF (non-canonical BRG1/BRM associated factor) chromatin remodelers [155, 156]. These complexes display a large core of shared subunits, including the mutually exclusive catalytic ATPase subunits BRG1 (Brahma-related gene 1) and BRM (Brahma). The complex identity is shaped by their specific subunits (Table 1). PBAF complexes are characterized by PBRM1 (Polybromo-1), ARID2 (AT-rich interactive domain-containing protein 2), BRD7 (Bromodomain-Containing Protein 7) and PHF10 (PHD Finger Protein 10) subunits. cBAF complexes are characterized by ARID1A/B

(AT-rich interactive domain-containing protein 1A/ 1B), DPF1/2/3 (Double PHD Fingers 1/2/3) and SS18/L1 (Synovial Sarcoma Translocated To X Chromosome Protein).

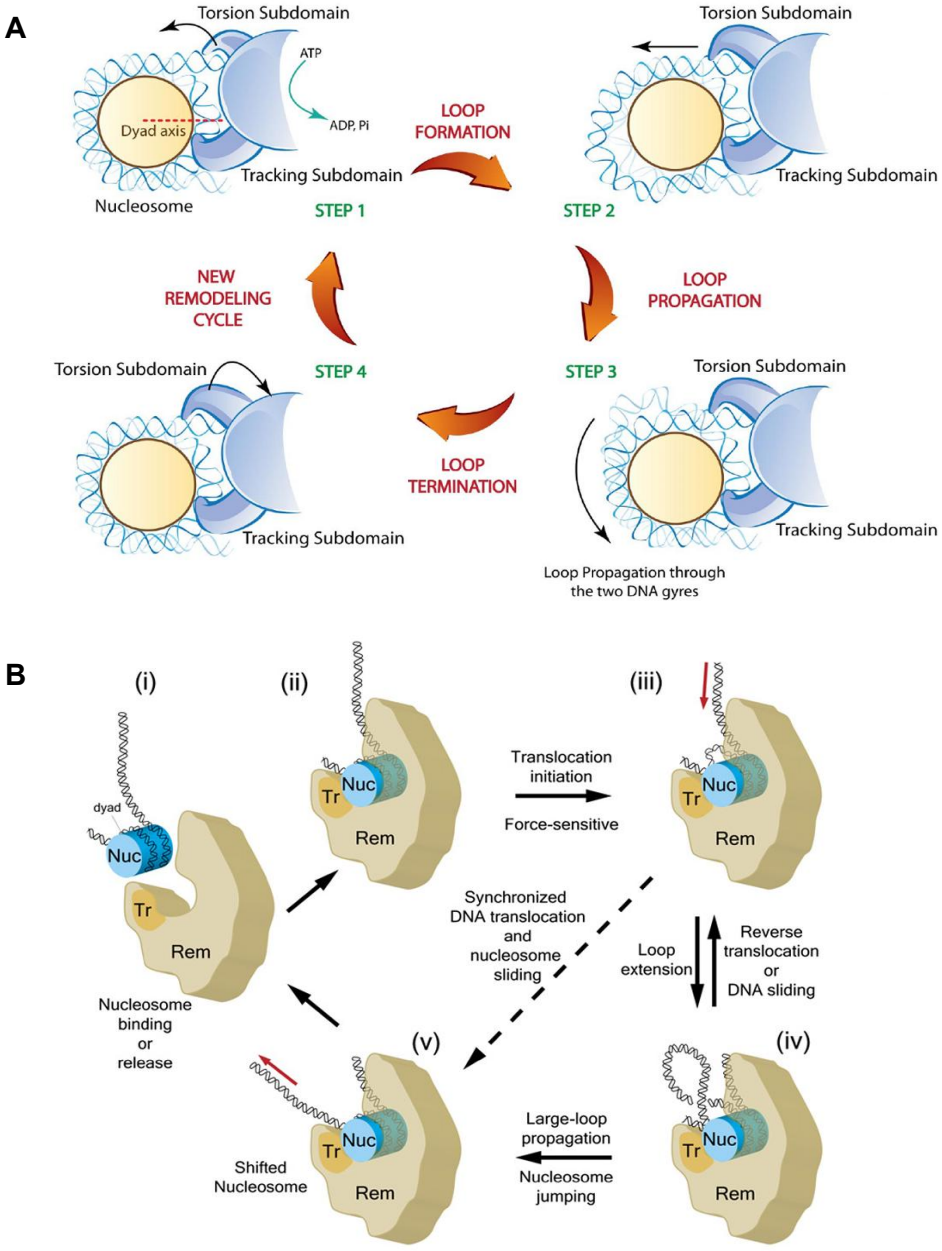


Figure 6. ATP-dependent remodeling mechanism of SWI/SNF complexes. Figure 6A summarizes the four key steps in nucleosomal remodeling: binding of the remodeler to the nucleosome and activation of the remodeling cycle upon ATP hydrolysis (step 1), disengagement of histone-DNA contacts and DNA loop formation (step 2), propagation of the loop (step 3) followed by its resolution and resetting of the remodeler position (step 4). Figure 6B highlights alternative way of nucleosome repositioning by reverse translocation or direct DNA sliding without loop formation. *Figures 6A and 6B respectively from Tang L, Nogales E, Ciferri C. Prog Biophys Mol Biol. 2010* [154] *and Zhang Y et al. Mol Cell. 2006* [153].

Both PBAF and cBAF complexes assemble in a multistep process, wherein ARIDs play an essential role in determining their identity (Figure 7) [155]. Once the core common subunits

are assembled, integration of one of the ARID subunits becomes critical, giving rise to PBAF (integration of ARID2) or cBAF (integration of ARID1A or ARID1B) complexes, followed by assembly of their remaining specific subunits. Integration of two copies of PBRM1 terminates the assembly of the PBAF complex [155].

Table 1. Mammalian SWI/SNF complexes: shared and specific subunits of PBAF and cBAF.

Shared	PBAF-specific	cBAF-specific
SMARCA2 (BRM) SMARCA4 (BRG1) SMARCB1 (BAF47) SMARCC1/2 (BAF155/170) SMARCD1/2/3 (BAF60A/B/C) SMARCE1 (BAF57) ACTL6A/B (BAF53A/B); β-Actin BCL7A/B/C; BCL11 A/B	PBRM1 (BAF180) ARID2 (BAF200) BRD7 PHF10 (BAF45A)	- ARID1A/B (BAF250A/B) - DPF1/2/3 (BAF45B/D/C) SS18/SS18L1

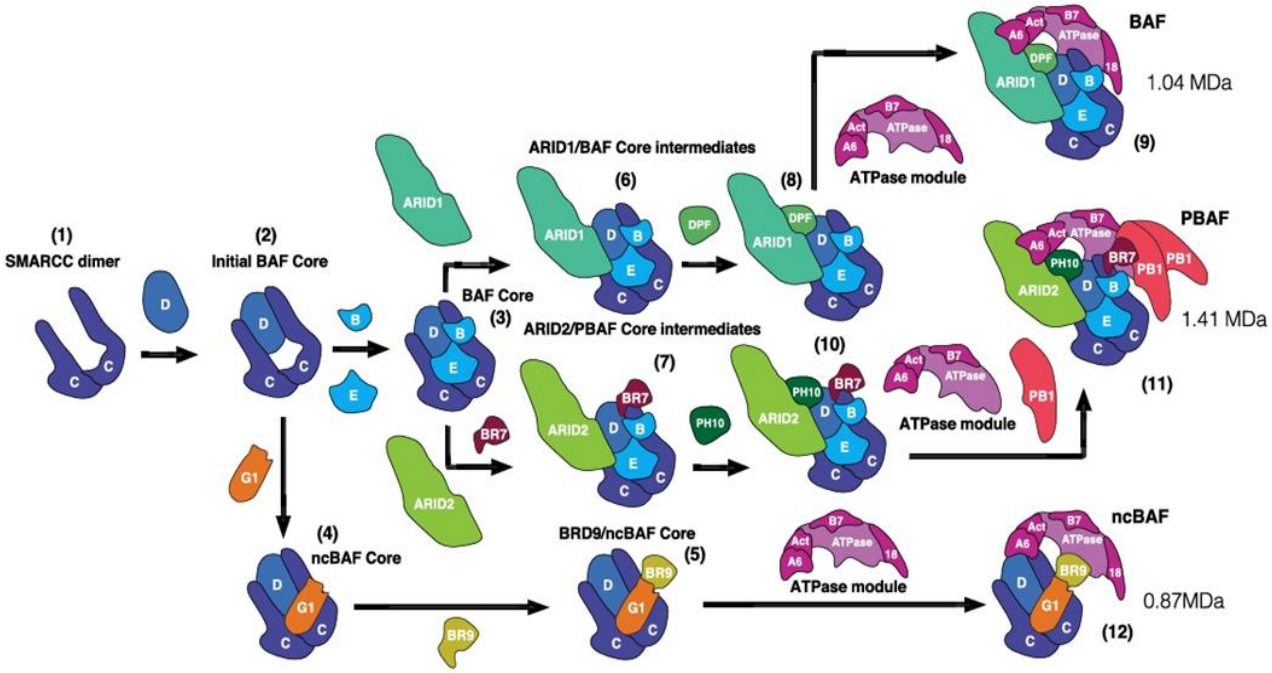


Figure 7. Multistep assembly process of cBAF and PBAF complexes. Upon assembly of the core module (highlighted in blue), integration of the specific ARID subunit (highlighted in green) mediates the fate decision of assembling either cBAF (ARID1A/B) or PBAF (ARID2) complexes. ARID-mediated branching is then followed by assembly of the ATPase module (highlighted in purple), including mutually exclusive BRG1 and BRM catalytic subunits. The assembly follows along with the integration of remaining specific subunits of both complexes- the PBAF complex formation terminates with integration of two copies of the PBRM1 subunit (highlighted in red). The ncBAF complex assembly is mediated *via* GLTSCR1/1L and BRD9 integration. Abbreviations: core module (blue) B- SMARCB1, C- SMARCC1/2, D- SMARCD1/2/3, E- SMARCE1; shared ATPase module (purple) A6- ACTL6A, Act- β-Actin, ATPase-

SMARCA2 (BRM) or SMARCA4 (BRG1), B7- BCL7A/B/C; remaining specific subunits: BR7- BRD7, BR9- BRD9, DPF- DPF1/2/3, G1- GLTSCR1/1L, PH10- PHF10, 18- SS18/L1. *Figure adapted from Mashtalir N et al. Cell. 2018* [155].

While ARIDs, BRDs, PHF10/DPFs subunits are homologous between these complexes, PBRM1 stands for a unique feature of the PBAF complex [142, 155]. PBRM1 is a lysine-acetyl and methyl *reader* that targets the PBAF complex to chromatin, directly engaging with nucleosomes *via* its multiple bromodomains [157, 158]. Bromodomains BD2 and BD4 are essential, since they are directly involved in nucleosome remodeling, recognizing acetyl histone marks. Bromodomains BD1 and BD5 enhance respectively BD2 and BD4 activity. In contrary, BD3 attenuates PBRM1 activity [157]. The role of BD6 remains unknown. In addition, PBRM1 contains two BAH (Bromo-adjacent homology) domains that are directly involved in recognition of methyl histone marks [159, 160]. Direct contact of PBRM1 with DNA is mediated by its HMG (High mobility group) domain [157]. Along with PBRM1, other specific subunits are as well involved in complex targeting to DNA, however their precise roles during the process of chromatin remodeling remain still unclear. Moreover, SWI/SNF subunits are as well characterized as key tumor-suppressors and their alterations are present in more than 20% of various cancers [161].

2.2.3 Histone variants: general overview

Additional layer of epigenetic regulation in chromatin dynamic changes is mediated by incorporation of the histone variants into nucleosomes [132]. In mammals, every canonical histone displays a variant counterpart (Table 2) that modulates nucleosomal stability and therefore chromatin properties and architecture [132, 162]. For example, a single copy of H2A.Z within nucleosome generates extremely stable nucleosomes involved in chromatin compaction. In contrary, incorporation of the histone variant H3.3 creates more unstable nucleosomes [132, 163]. In addition, variant-containing nucleosomes can be either heterotypic, in which both canonical histone and its variant counterpart are present, or homotypic, in which a specific histone variant replaces both copies of its canonical counterparts [164, 165, 166].

Table 2. List of core canonical histones with their corresponding variants in mammals.

H2A	H2B	H3	H4
H2A.X	H2BK1	H3.3A	H4.G (H4.7)
H2A.Z.1	H2B.N	H3.3B	
H2A.Z.2.1, H2A.Z.2.2	H2BFWT	H3.T (H3.4)	
macroH2A.1.1, macroH2A.1.2	H2BFM	H3.5	
macroH2A.2	TSH2B	H3.X	
H2A.B1	H2B1B/D/H/J/K/L/M/N/O	H3.Y	
H2A.B2/3	H2B2F/E	CenH3/CENP-A	
H2A.P	H2B3B		
H2A.J			
TH2A			

Histone variants are highly conserved across species and differ from their canonical counterparts mainly within their histone fold domain- either to a larger extent (*e.g.* H2A.Z shares 60% of homology with canonical H2A), or only by few amino acids (*e.g.* H3.3 differs by 4 to 5 amino acids from canonical H3.2 and H3.1 respectively) [167, 168]. Genes encoding for histone variants differ in several key aspects from the genes encoding for their canonical counterparts. In terms of genomic organization, canonical histone genes are organized in clusters, they are intronless and lack polyA tails. In contrast, histone variant genes are single copy genes located within distinct genomic locations, they contain exons and introns and their mRNAs are polyadenylated [169]. Moreover, main difference resides in their deposition pathways, including their specific chaperones (Figure 8) [132]. While canonical histones are deposited on chromatin in a replication-dependent (DNA synthesis-coupled) manner, the histone variants are mainly incorporated within nucleosomes in a replication-independent manner, throughout the cell cycle [132, 168].

Given that the same histone variant can be incorporated by different chaperone complexes into distinct genomic locations, histone variants can act as both, positive and negative regulators of specific gene expression programs [132, 162, 168]. Moreover, they act often in combination with histone PTMs and/or other histone variants [162]. Histone variants play essential roles in transcriptional activation, due to their location at enhancers, promoters and transcriptional start sites (TSS), as well as in gene silencing and heterochromatin formation, while being located near centromeric and telomeric regions [132, 162]. They are as well involved during the cell cycle progression, DNA replication, chromosome segregation and chromosome integrity. They also play a role in DNA damage response and repair, during embryonic development, cell differentiation and aging [162, 170]. Due to their versatile roles in multiple biological processes, alterations in their structure, expression and/or deposition pathways lead to development and progression of many diseases, including cancers [162]. Specific examples of alterations in H2A and H3 histone variants linked to their respective diseases are illustrated in Figure 9 [162].

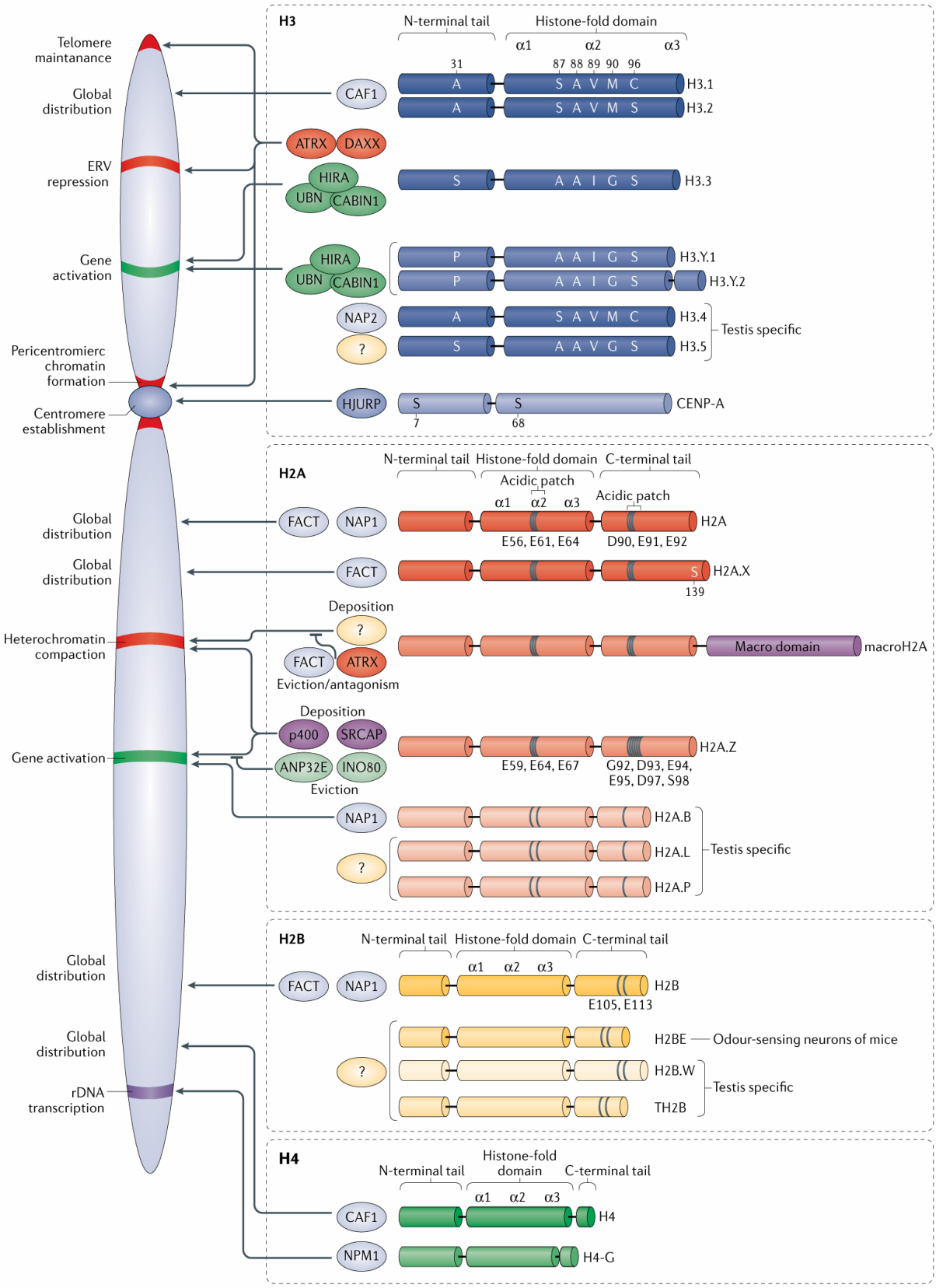


Figure 8. Overview of canonical and variant histone deposition. Schematic overview of main differences, specific chaperone complexes, distinct genomic locations and key implications in transcriptional regulation of canonical histones and histone variants in mice. *Figure from Martire S, Banaszynski LA. Rev Mol Cell Biol. 2020* [132].

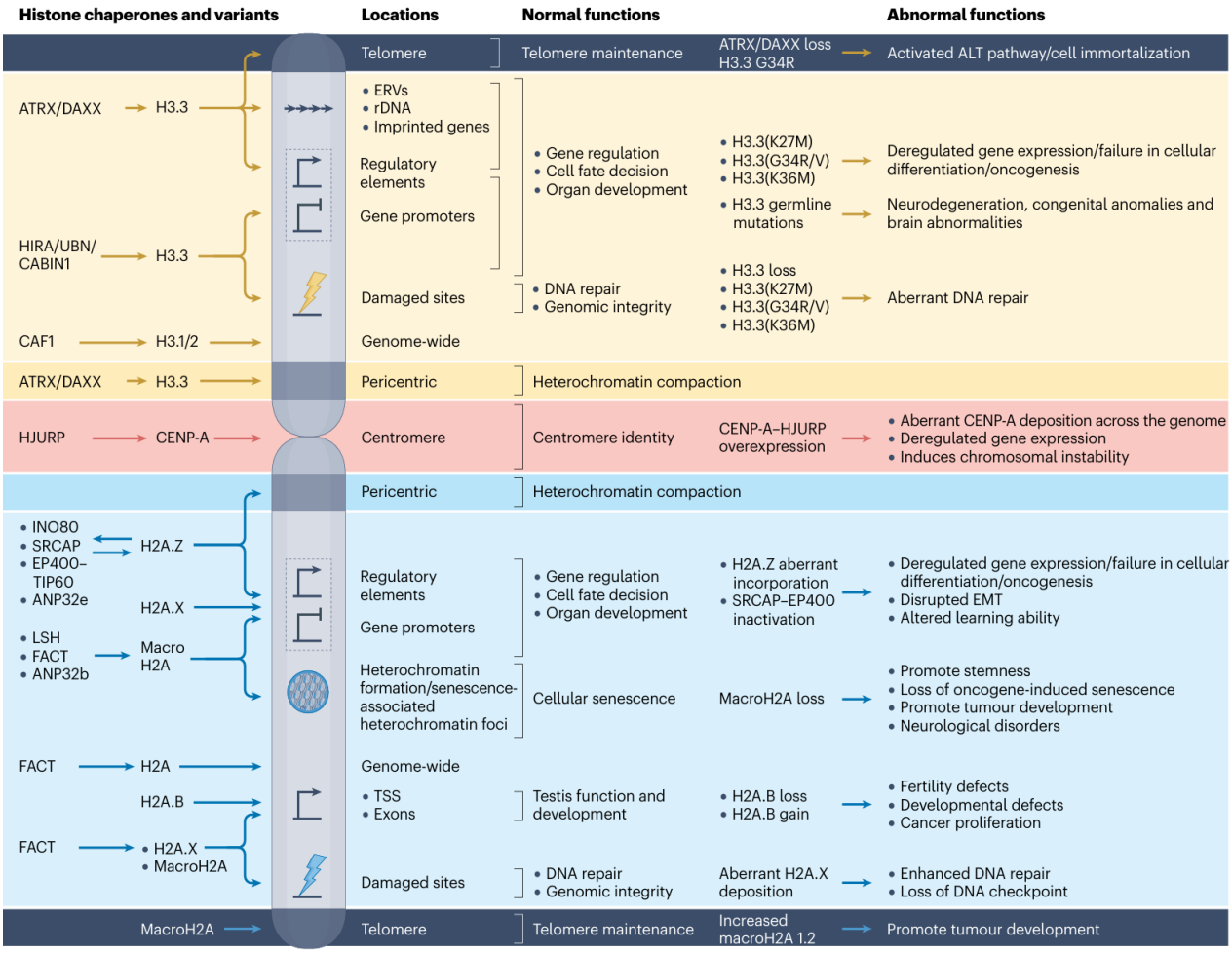


Figure 9. Alterations in histone variants and their consequences: example of H3 and H2A variants. Histone variants are involved in many essential regulatory mechanisms maintaining organismal homeostasis. Their mutations and/or alterations in their deposition pathways lead to abnormal cellular functions, resulting in development and progression of multiple diseases. *Figure from Wong LH, Tremethick DJ. Nat Rev Genet. 2025* [162].

3. Interplay between chromatin dynamics and circadian clocks

3.1 Crosstalk between circadian clocks and epigenome

How is chromatin architecture being reorganized in order to allow, and upon, BMAL1-CLOCK rhythmic binding at 'specific time and place' on the genome? Changes in chromatin architecture mediated by the epigenetic signatures and nucleosome remodeling modulate accessibility of regulatory factors binding to DNA [171, 172]. In turn, binding of the core-clock machinery sets a 24h dynamics in chromatin organization. Therefore, such rhythmic regulation of chromatin states results in a close coordination between establishment of the specific epigenetic landscapes and circadian gene expression programs [51, 75, 76, 173].

3.1.1 Dynamics in histone marks and chromatin accessibility

At clock genes and CCGs, histone tail PTMs undergo rhythmic oscillations and in turn, dynamic PTMs generate day vs. night rhythmicity in chromatin landscapes [51, 75, 76, 174, 175]. Rhythmic deposition of histone acetyl marks near clock-gene promoters and enhancers (*e.g.* H3K27ac, H3K9ac) results from the recruitment of HATs by the core-clock machinery. Moreover, it has been shown that rhythms in histone H3 acetylation levels at clock *loci* and RNA Polymerase II (Pol II) recruitment are co-occurrent with their steady-state mRNA dynamics in murine livers [176]. BMAL1-CLOCK heterodimer rhythmically interacts with p300 and CBP (CREB binding protein) HATs. While p300 HAT was found within CLOCK-specific complexes [176], it has been proposed that CBP is directly recruited by BMAL1 to mediate transactivation of BMAL1-CLOCK specific targets [177]. In addition, the core CLOCK TF displays intrinsic HAT activity. CLOCK shares sequence similarity, along with enzymatic specificity for H3-H4 histones with the nuclear receptor co-activator ACTR/SRC-1 (Steroid receptor co-activator- 1) HAT [178]. Finally, ACTR/SRC-1 is also known to interact and form a multimeric complex with p300 and CBP HATs [179, 180]. It has been proposed that CLOCK, p300 and CBP HATs may as well display redundant activities, since they share the same histone targets (*e.g.* H3K9, H3K14). However, it is also speculated that CLOCK, p300 and CPB work in tandem at different phases of the circadian transcriptional activation, and therefore, their function might be cooperative in a time-dependent manner [75, 76]. For instance, BMAL1-CLOCK are known to function as pioneer TFs, thus the intrinsic HAT activity of CLOCK TF could play an important role in histone acetylation and nucleosome eviction in the early activation phase of circadian cycle [178, 181]. On the other hand, directly engaging with BMAL1-CLOCK heterodimer, p300 and CBP HATs would acetylate flanking nucleosomes of BMAL1-CLOCK target sites to further loosen chromatin and allow transcriptional activation in the later activation phase of circadian cycle [176, 177].

In turn, histone deacetylation is as well rhythmically regulated by HDACs (*e.g.* SIRT1, HDAC3). For instance, in murine livers, while SIRT1-mediated deacetylation rhythmically

occurs at core-clock genes and their targets [67], HDAC3 interaction with REV-ERBα and their recruitment at regulatory sites of genes involved in lipid metabolism is required for hepatic lipid homeostasis [182]. Another example involves PER-CRY-mediated repression of the core-clock targets. PER-CRY dynamically interact with the SIN3A (SIN3 Transcription Regulator Family Member A) co-repressor, which acts as a scaffold of repressive complexes and in parallel, with the NuRD (Nucleosome Remodeling Deacetylase) repressive complex, both containing HDAC1 and HDAC2 deacetylases [183, 184].

Moreover, rhythmic recruitment of HMTs results in dynamic changes in histone methylation levels over 24h. Deposition of the H3K4me3 mark is dynamically regulated at TSS and enhancers of clock and CCGs during the active phase of circadian cycle. Rhythmicity in H3K4me3 is mediated by the MLL (Mixed Lineage Leukemia) family of HMTs, MLL1 and MLL3, which are dynamically recruited by the core-clock machinery and have been shown to promote robust transcriptional oscillations of the core-clock gene promoters, such as *Bmal1*, *Per2*, *Cry1* and *Rev-erbα*, in murine livers [185, 186]. In contrary, deposition of the H3K9me2 mark near circadian E-boxes results in gene silencing [187]. Mediated by the SUV39H (Suppressor of variegation 3-9 homolog) methyltransferase, di-methylation of H3K9 at circadian E-boxes leads to recruitment of HP1α (Heterochromatin protein 1 alpha), resulting in repression of core-clock genes and their targets. In addition, it has been hypothesized that SUV39H/HP1α-mediated epigenetic silencing of clock targets might be maintained until BMAL1-CLOCK initiate new circadian cycle, contributing therefore to circadian facultative heterochromatin formation during the repressive clock phase [187].

3.1.2 H2A.Z histone variant chromatin state dynamics at clock *loci*

In *Neurospora crassa*, rhythmic recruitment of the FACT chaperone at the *frq* promoter (*Frequency*, equivalent of mammalian *Period*) generates 24h occupancy dynamics in H2A.Z-contaning nucleosomes [188]. H2A.Z levels impact the binding of the White Collar Complex (WCC, equivalent to mammalian BMAL1-CLOCK), correlating with transcriptional regulation of the *frq* gene and such mechanism is highly conserved across species, including *Arabidopsis thaliana* and *Drosophila* clock neurons [188, 189, 190].

In mammals, replication-independent H2A.Z deposition is mediated by p400-Tip60 and SRCAP (SWI2-SNF2-related CBP activator protein) remodeling complexes which are distinct from the FACT chaperone. Transcriptionally poised and/or active TSS are enriched in H2A.Z-containing nucleosomes, displaying rapid turnover [191]. Indeed, displacement of the acetylated +1 H2A.Z nucleosome by RNA Polymerase II complex committed to elongation coincides with active gene transcription. Nucleosomes enriched in H2A.Z are also found at insulators, flanking CTCF (CCCTC-binding factor) binding sites that mediate long-range chromosomal interactions

by facilitating contacts between distal promoter-enhancer regions [192]. Moreover, in murine livers, genome-wide Chromatin-immunoprecipitation followed by sequencing (ChIP-seq) experiments revealed that rhythmic changes in H2A.Z nucleosome occupancy occur at clock and CCGs, upon BMAL1-CLOCK binding on DNA, suggesting that BMAL1-CLOCK dynamically regulates DNA accessibility to adjacent TF through remodeling of H2A.Z-containing nucleosomes and act therefore as pioneer TFs [181].

We recently showed (see Article 1) that H2A.Z deposition near clock TSS and enhancers occurs during the repressive phase of circadian cycle, being mediated by PER-YL1 complexes. Moreover, in this study, I have contributed to further uncover the link between CTCF and molecular core-clock machinery (see Figure 6h of Article 1). Purification of endogenous PER2 complexes from soluble liver chromatin revealed a time-dependent interaction with CTCF, during the later stage of the repressive clock phase, suggesting that PER2-mediated deposition of H2A.Z might occur at insulator regions in order to establish rhythmic facultative heterochromatin [193].

In addition, H2A.Z double knockout (*H2afz*$^{-/-}$, *H2afv*$^{-/-}$) results in complete loss of circadian cellular rhythms, indicating that epigenetic components, such as H2A.Z histone variant, play a critical role in establishment of the 24h TTFL [193]. However, whether other histone variants play a role in circadian chromatin dynamics along with the link with BMAL1-CLOCK binding remains to be explored.

3.1.3 Circadian chromatin remodeling

In *Neurospora crassa*, dynamic remodeling of nucleosomes occurs upon WCC binding at C-box sequences (equivalent to E-boxes in mammals) near *frq* promoter. It has been shown that WC-1, which forms the WCC along with WC-2 (equivalent to the BMAL1-CLOCK heterodimer in mammals), recruits SWI/SNF remodelers at *frq* regulatory sites. Such recruitment results in remodeling of nucleosomes and chromatin looping to promote enhancer-promoter interactions, which leads to transcriptional activation of *frq* gene. The authors propose a model in which WC-1 -SWI/SNF complexes activate *frq* expression, initiating thereby activation of the circadian cycle [194].

As mentioned before, it is known that H2A.Z deposition/eviction is rhythmically regulated near TSS of *frq* in *Neurospora crassa* [188] and in yeast, it has been shown that H2A.Z nucleosomes at TSS are remodeled by the PBAF-like RSC (Remodeling the Structure of Chromatin) remodeling complex of the SWI/SNF family [195]. In addition, in yeast, BAF-mediated nucleosome remodeling acts in synergy with Pol II to make chromatin accessible for adjacent TFs [196]. However, whether the observed 24h dynamics of H2A.Z containing nucleosomes in *Neurospora crassa* might be linked to circadian remodeling, and whether remodeling of H2A.Z nucleosomes by the RSC complex in yeast occurs in a circadian manner, remains unknown.

In mammals, it has been proposed that RORα and BMAL1 activity promotes hepatic chromatin decompaction to facilitate REV-ERBα binding on chromatin later on, during the repressive phase of circadian cycle. Indeed, REV-ERBα loading on chromatin was shown to be facilitated by the rhythmic recruitment of the SRC-2/PBAF SWI/SNF remodeler complexes during the active clock phase and loss of SRC-2 or PBAF resulted in impairment of REV-ERBα loading and low-amplitude rhythms [197].

Nevertheless, very little is known about the mechanism through which SWI/SNF chromatin remodelers cooperate with the core-clock machinery to establish 24h chromatin dynamics.

4. H3.3 histone variant

4.1 The H3 histone family: key modulators of chromatin states

In mammals, the H3 histone family comprises the two canonical H3.1/H3.2 histones and six H3 variants (Table 2), *e.g.* H3.3 (H3.3A and H3.3B), CenH3/CENP-A and testis-specific H3T. The H3 variants are involved in nucleosome stability and maintenance of genome integrity, playing roles in multiple biological processes (Figure 9) ranging from transcriptional regulation to cell division, zygotic genome activation and embryonic development [132, 162].

4.2 The H3.3 histone variant

Evolutionary speaking, the canonical H3 variant H3.3 is one of the most conserved proteins in all eukaryotes. In mammals, H3.3 is mainly encoded by *H3f3a* and *H3f3b* genes, giving rise to H3.3A and H3.3B proteins respectively [169]. In mice, *H3f3a* and *H3f3b* genes are located within distinct places of the genome, respectively on chromosomes 1 and 11. While they differ in their nucleotide sequences and their mRNAs in 5' and 3' UTRs, they code for identical proteins in terms of their amino acid sequence and structure [169]. Additionally, thirteen other genes similar to H3.3 have been identified in mice, remaining exclusive to the mouse genome since no orthologs have been found in rat species and humans [198].

The H3.3 variants differ only by 4 to 5 amino acids from their canonical counterparts H3.2 and H3.1 respectively. The key differences reside within their fold domain on residues 87, 89 and 90 (Figure 10), playing an important role in H3.3 recognition by its specific chaperones. In addition, H3.3 differs in residue 31, where the alanine from the canonical H3.1/2 histones is replaced by serine, whose phosphorylation is playing important roles in mitotic progression and cell cycle regulation [169, 199].

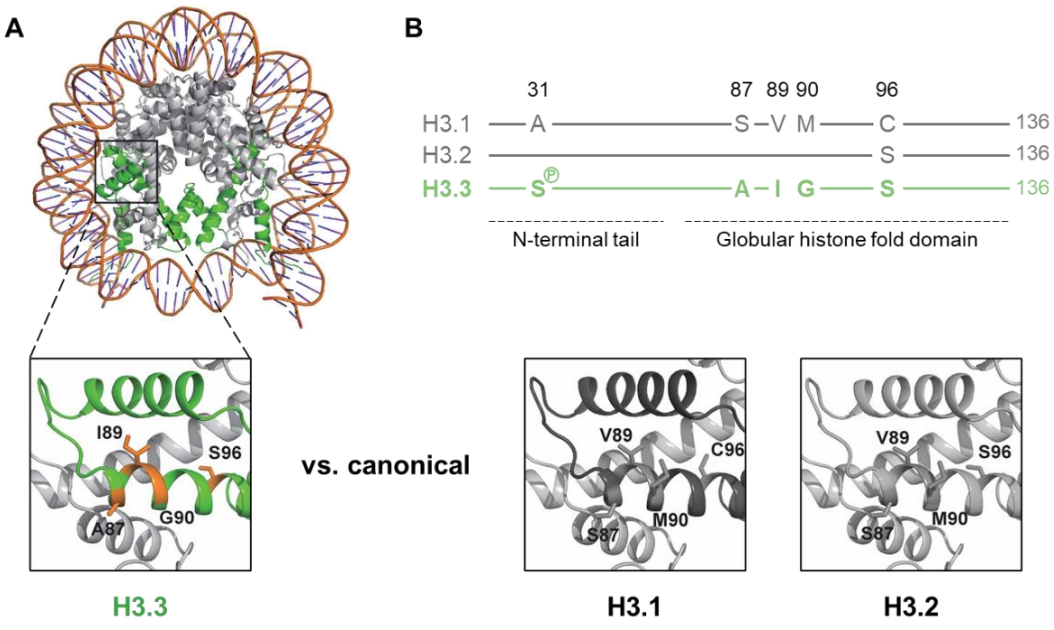


Figure 10. Main structural differences between the histone variant H3.3 and canonical histones H3.1/2. Figure 10A shows the crystal structure of an H3.3 containing nucleosome with a zoom on the histone fold domain, highlighting the differences between the H3.3 variant and H3.1/2 histones. Figure 10B summarizes the overall key differences between the three H3 variant proteins. *Figure 10A adapted from Tachiwana H et al. Acta Crystallogr D Biol Crystallogr. 2011* [200].

4.2.1 Specific deposition pathways of H3.3 variant

H3.3 variant deposition is mediated by two specific chaperone complexes, HIRA (Histone cell cycle Regulation defective homolog A) and DAXX (Death domain-associated protein), which incorporates H3.3 into distinct genomic regions (Figure 8) [201, 202, 203].

HIRA chaperone complex assembles with UBN1/2 (Ubinuclein 1/2) subunits involved in direct recognition, binding of the H3.3 variant and its deposition on chromatin and with CABIN1 (Calcineurin-binding protein 1) subunit which is involved in the stability of the chaperone complex [201, 204, 205]. The HIRA-mediated deposition results in enrichment of H3.3 nucleosomes near promoters and enhancers of transcriptionally active, as well inactive genes, establishing the poised chromatin state prior transcriptional activation [169, 201, 202]. In dividing cells, HIRA chaperone complex is implicated in regulation of RNA Pol II presence at TSS and regulatory elements, playing crucial role in gene expression and has been linked as well to temporary H3.3 deposition at centromeres prior CENP-A loading, where H3.3 acts as a placeholder for the centromeric variant in late Metaphase/ early G1 phase of the cell cycle [206, 207]. In addition, HIRA-mediated H3.3 deposition has been shown critical for early embryonic development and cell pluripotency. Moreover, HIRA has been shown implicated in formation of senescence-associated heterochromatin foci (SAHF) formation, further supporting the role of H3.3 variant in age-related processes [207, 208, 209].

The second specific H3.3 chaperone DAXX is associated in complex with ATRX (alpha-thalassemia/mental retardation syndrome X-linked protein) subunit, a member of ATP-dependent chromatin remodelers. DAXX-mediated H3.3 incorporation occurs at telomeric regions and pericentric heterochromatin (Figure 8) [169, 201, 210]. Although within this complex, the chaperone activity is exclusively related to DAXX, its cooperation with ATRX has been shown critical for accumulation of the H3.3 at telomeric regions [169]. Additionally, as for HIRA, DAXX is essential during mouse development, since its loss causes massive apoptosis, leading to embryonic lethality in mice [210, 211].

4.2.2 H3.3 as a key transcriptional regulator and beyond

Being involved in modulation of chromatin states, H3.3 plays important roles in regulation of gene expression [202, 207]. Positioned at enhancers and promoters of actively transcribed genes, labeled H3.3 nucleosomes by active PTMs (*e.g.* H3K4me3) prime transcriptional activation, and display rapid replication-independent turnover. In addition, this replication-independent

turnover of H3.3 nucleosomes at enhancers of active genes has been shown to correlate with Pol II dynamics [212, 213]. In contrary, while being labeled by repressive PTMs (*e.g.* H3K9me3), H3.3 nucleosomes are found at transcriptionally inactive regions of the genome, displaying a slow turnover [213].

Along its regulatory roles in gene expression, both H3.3A and H3.3B variants are as well involved in regulation and maintenance of genome integrity during mammalian development [214, 215]. In mice, complete loss of H3.3 variant leads to mitotic defects and developmental retardation resulting in early embryonic lethality and in cells, H3.3 depletion results in cell death indicating essential role of the H3.3 variant in cell survival [215]. Moreover, H3.3-mediated regulation of lifespan and its age-linked accumulation in post-mitotic cells indicates that H3.3 incorporation and turnover would as well play an important regulatory role in shaping chromatin landscapes during physiological aging [208, 207].

4.2.3 Fragile H3.3/H2A.Z dual-variant nucleosomes

Deposition of H3.3 variant on chromatin modulates nucleosome stability and combination of H3.3/H2A.Z histone variants within the same nucleosome results in formation of highly mobile, unstable, dual-variant fragile nucleosomes [163, 191, 212].

In vitro, H3.3/H2A.Z dual-variant nucleosomes are highly sensitive to salt concentrations and therefore, they are as well very likely to be less stable than replication-coupled nucleosomes containing canonical histones *in vivo* [212]. In addition, positioned H2A.Z nucleosomes at promoters of inactive genes are removed from chromatin upon transcriptional activation and their depletion has been shown concomitant with H3.3 deposition at these sites [212, 216]. The knockdown of H3.3 results in inhibition of Tip60 and SRCAP recruitment to promoter regions of retinoic acid-inducible genes, indicating that H3.3 is involved in the recruitment of H2A.Z specific chaperones at these sites [212].

The dual-variant nucleosomes would prevent the deposition of stable canonical nucleosomes around those regulatory sites to facilitate DNA accessibility to Pol II transcriptional machinery, adjacent TFs and other regulatory complexes (Figure 11) [212]. Recently, HIRA chaperone complex has been shown to mediate the co-deposition of H3.3 and H2A.Z variants into nucleosomes at promoters and TSS of poised genes prior transcriptional activation in mouse embryonic stem cells (mESc), by co-regulating SRCAP recruitment at these sites [217]. However, whether the establishment of H3.3 and H3.3/H2A.Z dual-variant chromatin could occur at promoters and TSS of clock and CCGs to generate 24h dynamics in chromatin landscapes remains unknown.

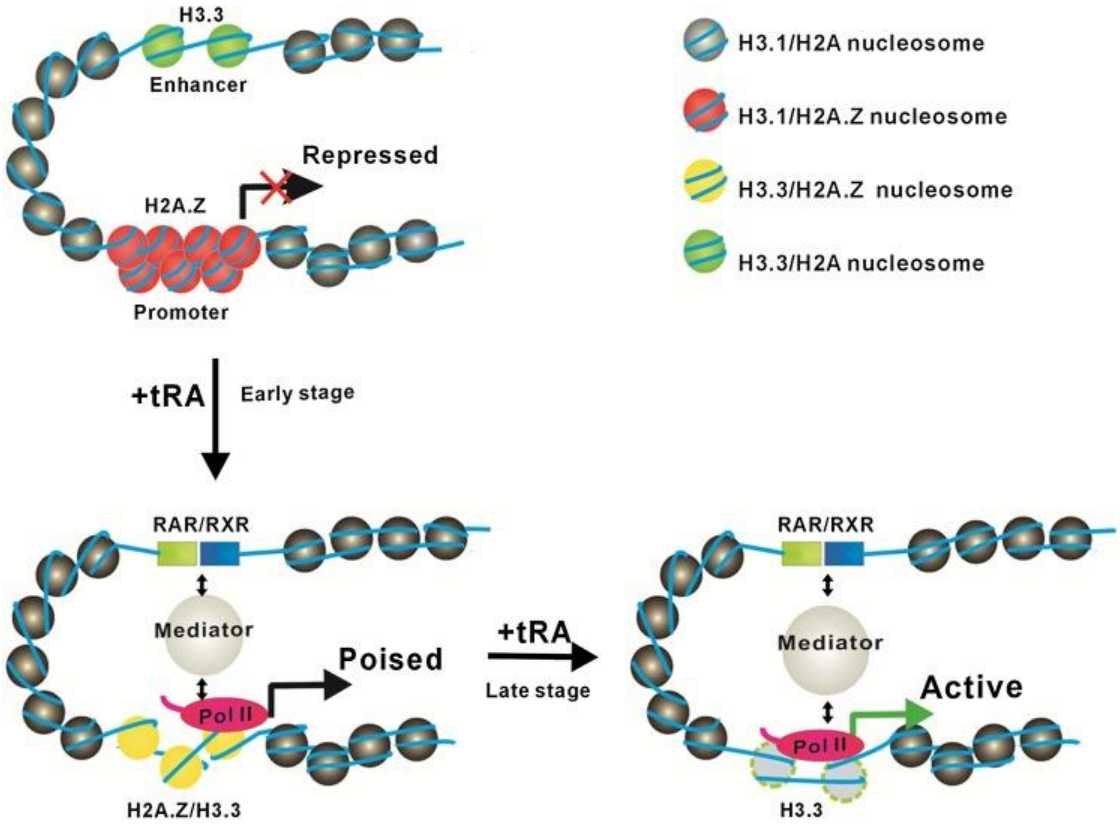


Figure 11. Proposed model of the H3.3/H2A.Z dual-variant nucleosome involvement in transcriptional regulation. Example of retinoic acid-inducible gene expression. H2A.Z nucleosomes are present at promoters of transcriptionally silenced genes. Upon induction, co-deposition of H3.3 variant into H2A.Z-containing nucleosomes results in formation of extremely labile dual-variant nucleosomes prior transcriptional activation, during the poised state. Recruitment of Pol II, associated regulatory complexes and chromatin remodelers leads to nucleosome remodeling and eviction of dual-variant nucleosomes, followed by transcriptional activation. *Figure from Chen P et al. Genes Dev. 2013* [212].

5. Research hypotheses and aims

5.1 Scientific context and hypotheses

Given the implication of H2A.Z histone variant in circadian clock function in many species [181, 188, 193], we wondered whether other histone variants such as H3.3, could play a role in chromatin state dynamics at clock *loci*. Therefore, we aimed to study the link between the histone variant H3.3 and the molecular machinery of mammalian circadian clocks. In other words, how could H3.3 nucleosomes shape the chromatin architecture to contribute to 24hr transcriptional dynamics in close connection with circadian core-clock regulators in murine tissues, such as liver.

H3f3a and *H3f3b* gene expression is cycling over time in multiple murine tissues, such as liver, kidney and heart (data can be found on CircaDB, circadian gene expression profile database). However, whether H3.3 variants play a role in establishment of 24h chromatin rhythms in mammals remains unknown. We therefore hypothesized that H3.3 could contribute to circadian clock function, generating 24h chromatin dynamics. To do so, i) H3.3 nucleosomes would be enriched at clock *loci* and their deposition and/or removal would follow 24h dynamics, and ii) H3.3 would assemble with the main core-clock factors in dynamic complexes over time.

Since H3.3 variant family comprises two main variants, H3.3A and H3.3B, whose expression is differentially cycling in murine livers, we initially aimed to uncover potential differences in their implication in establishment of mammalian circadian rhythms, by studying their roles independently. However, while studying the role of both H3.3 variants in parallel, we encountered some unexpected technical issues and therefore, we further focused on the histone variant H3.3A.

5.2 Mouse models and aims of the project

To study the role of H3.3A in circadian rhythms, and since H3.3A differs from its canonical H3 counterparts only by 4-5 amino acids, we used a conditional knock-in mouse model, in which a FLAG-FLAG-HA-tag (FH) sequence was inserted in frame with the N-terminus of a single H3.3A allele, as described in [218]. Such heterozygous FH-H3.3A$^{+/-}$ mouse model allows to conduct specific biochemical studies, targeting exclusively H3.3A and associated protein complexes. This mouse model was kindly provided to us from Dr. Stefan Dimitrov. In addition, Dr. Padmanabhan lab has generated a FH-H3.3A$^{+/-}$ *Per1*$^{-/-}$, *Per2*$^{-/-}$ knockout mouse line in order to assess potential changes in H3.3A chromatin landscape upon circadian clock disruption. The *Per1*$^{-/-}$, *Per2* $^{Brdm-/-}$ mice were kindly provided to us by Prof. Marie-Paule Felder Schmittbuhl and Prof. Urs Albrecht.

Having these mouse models in hand, we aimed to 1) characterize specific H3.3A protein complexes over time, while seeking for interactions with the core-clock and epigenetic factors involved in chromatin dynamics - by performing H3.3A complex purification followed by mass spectrometry analysis and immunoprecipitation experiments; 2) assess H3.3A nucleosome occupancy over time genome-wide and with a particular focus on BMAL1-CLOCK binding sites, TSS of BMAL1-CLOCK target genes and CTCF sites - by performing ChIP-seq experiments and 3) study the impact of circadian clock disruption on H3.3A chromatin landscapes and its interacting complexes in FH-H3.3A$^{+/-}$ *Per1*$^{-/-}$, *Per2*$^{-/-}$ murine livers.

Materials and methods

Materials

1. Reagents, chemicals and products used in this work

All the reagents, chemicals and products that have been used are listed below in their respective categories in alphabetical order (Table 3). Antibodies and equipment are listed in their respective sections in Methods.

Table 3. List of reagents, chemicals and products with their corresponding references.

Product name	Supplier	Reference
Chemicals and reagents		
2-Mercaptoethanol	Sigma-Aldrich	M3148
2-Propanol	Supelco	1096341000
Acetic acid	Sigma-Aldrich	33209-2.5L-M
Agarose standard	Euromedex	LE-8200-B
Biophenol/Chloroform/Isoamyl alcohol	Biosolve	169723
BSA	Sigma-Aldrich	A2153
Bromophenol blue	Sigma-Aldrich	B8026
$CaCl_2$	Euromedex	T885
Chloroform	VWR Chemicals	22711.290
DC protein assay reagents	Bio-Rad	5000116
DTT	Sigma-Aldrich	D9779
EDTA	Euromedex	EU0007-C
EGTA	Sigma-Aldrich	E4378
Ethidium bromide solution	Honeywell-Fluka	46057
EtOH	ThermoFisher Scientific	10375842
Formaldehyde solution	Sigma-Aldrich	F8775
Glycerol	Euromedex	EU3550
Glycine	Euromedex	26-128-6405
HCl	Sigma-Aldrich	258148
HEPES	Euromedex	10-110-A
KCl	Honeywell-Fluka	60129
KOH	Honeywell-Fluka	2214732
$MgCl_2$ hexahydrate	Sigma-Aldrich	M2670
NaCl	Euromedex	1112-A
$NaHCO_3$	Sigma-Aldrich	S6014-500G
NaOH	Honeywell-Fluka	71690

Non-fat dried milk	Local supermarket	-
NP-40 (IGEPAL® CA-630)	Sigma-Aldrich	I8896
PBS 1X without magnesium, calcium	Dominique-Dutscher	L0615-500
PBS 10X without magnesium, calcium	Dominique-Dutscher	X0515-500
RIPA lysis buffer	Invitrogen, ThermoFisher	89901
SDS	Sigma-Aldrich	L3771
Spermine	Sigma-Aldrich	85590
Spermidine	Sigma-Aldrich	S0266
Sucrose	Euromedex	200-301-B
TAE 50X	Euromedex	EU0201
Tris-base	Euromedex	200923-A
Triton X-100	Eurobio Scientific	GAUTTR00-01
TRIzol LS Reagent	Invitrogen, ThermoFisher	10296010
Tween 20	Sigma-Aldrich	P9416
Universal SYBR Green Supermix	Bio-Rad	1725121
Enzymes, peptides and inhibitors		
Enzymes		
Nuclease S7 (batch number 53964400)	Roche, Merck	10107921001
Proteinase K	NEB Molecular Biology Grade	P8107S
Peptides		
3xFLAG peptide	Sigma-Aldrich	F4799
Inhibitors		
Aprotinin	Sigma-Aldrich	A4529
Chymostatin	Sigma-Aldrich	C7268
cOmplete, EDTA-free Protease Inhibitor Cocktail	Roche, Merck	5056489001
Leupeptin	Sigma-Aldrich	L8511
MG132 proteasome inhibitor	Sigma-Aldrich	M7449
Resins and beads		
Anti-FLAG M2 Affinity Gel	Sigma-Aldrich	A2220
Dynabeads A	Invitrogen, ThermoFisher	10002D
Dynabeads G	Invitrogen, ThermoFisher	10004D
Kits		
DNA-related		
IScript cDNA Synthesis kit	Bio-Rad	1708891
NEBNext UltraII DNA Library Prep Kit for Illumina sequencing	NEB Molecular Biology Grade	E7645S/L, E7103S/L
QIAquick PCR Purification Kit	QIAGEN	28104
Qubit dsDNA HS Assay Kit	Invitrogen, ThermoFisher	Q32854
Protein-related		
SilverQuest Silver Staining kit	Invitrogen, ThermoFisher	LC6070

Subcellular Protein Fractionation Kit for Cultured Cells	ThermoFisher Scientific	PI78840
Subcellular Protein Fractionation Kit for Tissues	ThermoFisher Scientific	PI87790
Ladders		
100bp Opti-DNA Marker	abm	G016
1kb Opti-DNA Marker	abm	G106
Prestained Protein Ladder Plus	Euromedex	06P-0211
Western-blotting		
0.2µm nitrocellulose membranes	(Amersham) Sigma-Aldrich	GE10600004
ECL Prime western blotting reagent	CYTIVA	RPN2232
Mini-Cell XCell SureLock system for precast gels with accessories	Invitrogen, ThermoFisher	EI0001
Mini-PROTEAN® Tetra Cell, 2-Gel system for vertical electrophoresis and western-blotting with accessories	Bio-Rad	1658005
Novex NuPAGE 4-12% Bis-Tris gradient precast gels 10W 1.0mm	Invitrogen, ThermoFisher	NP0321BOX
Novex NuPAGE 4-12% Bis-Tris gradient precast gels 10W 1.5mm	Invitrogen, ThermoFisher	NP0335BOX
Novex NuPAGE 4-12% Bis-Tris gradient precast gels 15W 1.5mm	Invitrogen, ThermoFisher	NP0336BOX
Novex NuPAGE SDS MOPS Running buffer (20X)	Invitrogen, ThermoFisher	NP000102
Cell culture		
4-OHT, cis/trans-4-hydroxytamoxifen	Sigma-Aldrich	H6278
Dexamethasone	Sigma-Aldrich	D4902
D-Luciferin Sodium Salt	PJK GmbH	102131
DMEM-high glucose medium	Sigma-Aldrich	D5796
DMSO	Sigma-Aldrich	D2650
Fetal Bovine Serum	(Gibco), ThermoFisher	A5256701
HEPES Buffer solution (1M)	(Gibco), ThermoFisher	15630056
Penicillin-Streptomycin (10 000 U/ml)	(Gibco), ThermoFisher	15140122
Sodium Bicarbonate 7.5% solution	(Gibco), ThermoFisher	25080094
Trypsin-EDTA (1X) 0.05%, phenol red	(Gibco), ThermoFisher	25300054
Genotyping		
5X Green GoTaq Reaction Buffer	Promega	M7911
Set of dATP, dCTP, dGTP, dTTP	Promega	U1330
Taq DNA Polymerase	ThermoFisher Scientific	18038026
Others		
38.5ml Ultra-clear polypropylene tubes	Beckman Coulter	326823
Black 24 well plate with flat and clear bottom for high-throughput microscopy	Ibidi	82426 (ibiTreat)
CryoPure tubes, 2ml	Sarstedt	72.380

Cryogenic Vials, 2ml	(Corning), ThermoFisher	431386
Freezing container Mr. Frosty	ThermoFisher Scientific	5100-0001
Hard-Shell PCR 96-well thin wall plates	Bio-Rad	HSP9655
High Sensitivity D5000 ScreenTape with associated reagents	Agilent	5067-5592, 5067-5593

Methods

1. Mouse models, genotyping and tissue collections

Genetically modified heterozygous FLAG-FLAG-HA-tag (FH) - H3.3A$^{+/-}$, FH-H3.3A$^{+/-}$ *Per1*$^{-/-}$, *Per2*$^{-/-}$ knock-out (KO) mouse lines and wild-type (WT) C57Bl/6 male mice were used in this thesis work. The FH-H3.3A$^{+/-}$ heterozygous mouse line has been generated as described previously [218]. FH-H3.3A$^{+/-}$ littermates were obtained by crossing FH-H3.3A$^{+/-}$ with WT mice. Male FH-H3.3A$^{+/-}$ heterozygous mice were kept for the study. The FH-H3.3A$^{+/-}$ *Per1*$^{-/-}$, *Per2*$^{-/-}$ KO mouse line was generated by crossing FH-H3.3A$^{+/-}$ with *Per1*$^{-/-}$, *Per2*$^{-/-}$ KO mice.

Mouse genotypes were identified using genomic DNA from ear punches as follows. Ear punches were incubated in 40µl of solution A for 20min at 95°C, followed by neutralization, tissue dissociation and homogenization of extracts with 40µl of solution B. Buffer composition is described in Table 4. PCR reactions were performed with 3.5µl of total extract and 17.5µl of PCR mix with T100 Thermal Cycler (Bio-Rad), as described in Table 5. Primers used for genotyping are described in Table 16. Primer sequences. DNA fragments were separated on 2% agarose gel, using TAE 1X buffer, at 135V for 25min. DNA was visualized with ultra-violet light and Bio-print Mega-Capt software.

Table 4. Buffer composition for DNA extraction from ear punches.

Buffer	Components (stock)	Final concentration
Solution A	0.5M EDTA-NaOH pH 8.0	0.2mM
	10M NaOH	25mM
Solution B	1M Tris-HCl pH 5	40mM

Table 5. PCR mix for 20 reactions and PCR program.

Components (stock)	Volume for 20 reactions
Millipore H_2O	216µl
5X Green GoTaq Buffer	80µl
Forward primer at 5µM	20µl
Reverse primer at 5µM	20µl

DNTP mix at 10mM	8µl
Taq DNA Polymerase at 5U/µl	6µl
PCR program	
Step	**Temperature, time**
1. Polymerase activation	94°C, 5min
2. Denaturation	94°C, 45sec
3. Annealing	54°C, 45sec
4. Extension	72°C, 1min
5. Go to step 2., 34 more times	
6.	72°C, 10min
7.	12°C, infinite hold

Animals were housed under a temperature-controlled, 12h:12h light-dark cycles, and were fed *ad libitum*. All mice used in this study were from 10- to 17-weeks old male littermates. Aged-matched littermates were randomly assigned to experimental groups. Prior tissue collection, mice were entrained to a 12h:12h light-dark cycle in temperature and humidity-controlled ventilated cabinets (~22 °C, 30% RH) for 2 weeks and then kept in constant darkness. Mice were euthanized at CT0, 4, 8, 12, 16 and 20 under the red light, and tissues dissected under the room light. Animal procedures were carried out according to the French guidelines for care and use of experimental animals and approved by the ethical committee of the ENS Lyon and the French ministry of science under APAFIS no. 5212-2016032914413553.

Liver tissues from FH-H3.3A$^{+/-}$ and WT animals were collected at 1 day in constant darkness and from FH-H3.3A$^{+/-}$ *Per1*$^{-/-}$, *Per2*$^{-/-}$ KO animals at 1 or 4 days in constant darkness. Livers were mainly processed fresh, followed by nuclei purification immediately after tissue isolation, or fresh-frozen and stored at -80°C until use.

2. Nuclei isolation from murine livers

Nuclei were purified as described previously in [219]. Briefly, isolated livers were cut into small pieces using sterile blades. Tissue pieces were transferred to a dounce homogenizer on ice and grinded in 3ml of PBS 1X containing protease inhibitors for 15-20 times with a loose pestle A. Tissue homogenate was filtered through gauze, volume completed to 5ml with PBS 1X containing protease inhibitors, transferred back to the dounce homogenizer and covered with a part of 2.2M homogenizing sucrose solution (25ml total per sample) containing protease inhibitors, spermine, spermidine and DTT. The tissue homogenate was next dounced in sucrose solution for 15-20 times with pestle A, followed by a tighter pestle B for 3-5 times. The homogenate was then transferred to Falcons containing remaining homogenizing sucrose

solution and mixed well by inversion. Entire homogenate (approximately 30ml total) was then layered on a 2.05M cushion sucrose solution (9ml) containing protease inhibitors, spermine, spermidine and DTT in 38.5ml Ultra-clear polypropylene tubes (Beckman Coulter). Nuclei were separated by ultracentrifugation using the SW32 Ti Swinging-Bucket Rotor for 45min at 25,000g, 4°C with OPTIMA XPN 80 ultracentrifuge (Beckman Coulter).

Post-separation, cytoplasmic upper part was removed and pelleted nuclei resuspended in 2ml of 1X Nuclear Lysis Buffer (NLB) containing protease inhibitors, spermine and spermidine. Nuclei were transferred into 2ml Eppendorf tubes and centrifuged at 4500rpm (1902g) for 5min. Supernatant was removed, nuclei again resuspended in 1ml of 1X NLB containing protease inhibitors, spermine and spermidine, aliquoted and pelleted at 4500rpm for 4min30. They were stored in 1X NLB containing protease inhibitors, spermine and spermidine at -80°C until further use. Buffer composition is described in Table 6.

Table 6. Buffer composition for nuclei isolation from liver tissues.

Buffer	Components (stock)	Final concentration
2.2M Sucrose Homogenizing solution stock	Sucrose	2.2M
	1M HEPES-KOH pH 7.6	10mM
	2M KCl	15mM
	0.5M EDTA-NaOH pH 8.0	2mM
	Protease inhibitors at 10mg/ml*: Leupeptin, Aprotinin, Chymostatin (dissolved in Millipore H_2O)	0.5mM
	0.1M Spermine* (dissolved in Millipore H_2O)	0.15mM
	1M Spermidine* (dissolved in Millipore H_2O)	0.5mM
	1M DTT* (dissolved in Millipore H_2O)	0.5mM
2.05M Sucrose Cushion solution stock	Sucrose	2.05M
	1M HEPES-KOH pH 7.6	10mM
	2M KCl	15mM
	0.5M EDTA-NaOH pH 8.0	2mM
	Protease inhibitors at 10mg/ml*: Leupeptin, Aprotinin, Chymostatin	0.5mM
	0.1M Spermine*	0.15mM
	1M Spermidine*	0.5mM
	1M DTT*	0.5mM
Nuclear Lysis Buffer 10X stock	1M HEPES-KOH pH 7.6	10mM
	2M KCl	100mM
	0.5M EDTA-NaOH pH 8.0	0.1mM

Nuclear Lysis Buffer 1X	10 times diluted NLB 10X stock with Millipore H_2O	1X
	50% glycerol*	10%
	50X protease inhibitor cocktail*	1X
	0.1M Spermine*	0.15mM
	1M Spermidine*	0.5mM
	1M DTT*	0.5mM

*****_Added freshly, prior nuclei isolation._

3. Native purification of H3.3A protein complexes for mass spectrometry analysis

Nuclei were initially isolated from FH-H3.3A$^{+/-}$ livers collected at CT4,8 and CT16, 20 (pooled time-points) for preliminary analysis of native H3.3A complexes. Based on the preliminary analysis and after the purification conditions were established, nuclei isolated from FH-H3.3A$^{+/-}$ livers collected at CT8 and CT20 and FH-H3.3A$^{+/-}$ *Per1*$^{-/-}$, *Per2*$^{-/-}$ KO livers collected at CT20 were used for the native purification of H3.3A protein complexes. In parallel, nuclei from WT livers collected at random time points were used as a negative control for the purification experiments.

Total nuclear protein quantity was estimated by lysing 10µl of purified nuclei with 60ul of RIPA lysis buffer for 20min on ice and sonicated for 6 cycles on Diagenode bioruptor (30s on/ 30s off) at 4°C, followed by centrifugation at 14,000rpm (18,407g) for 10min. Released proteins in the supernatant were quantified using DC protein assay (Bio-Rad).

MNase-digested nuclear extracts were prepared from one full liver (~1.4mg of total protein) for each condition according to Khan *et al*. 2020 [220] with modifications, as follows. Nuclei were washed twice in 500µl of Buffer A containing protease inhibitors and centrifuged at 4500rpm (1902g) for 4min30. Nuclear pellets were resuspended in 300µl of Cutting Buffer and 100µl of freshly diluted MNase (Nuclease S7, Roche 10107921001, batch number 53964400) in Cutting buffer was added at 10U final per sample. To digest chromatin to mononucleosomes, samples were vortexed at low speed and incubated in water-bath at 37°C for 7min, vortexed every 1min30. After digestion, samples were kept on ice and MNase activity was stopped by adding 16µl of EGTA-NaOH pH 8.0 at 20mM final. Samples were vortexed and centrifuged at 1300g for 5min. The totality of the supernatant was kept in separate tubes on ice as S1 MNase-digested fraction. Remaining pellets were resuspended in 400µl of TE buffer containing protease inhibitors and incubated on end-to-end rotator for 30min at 4°C. After incubation, samples were centrifuged at 13,000g for 5min and the totality of the supernatant was kept in separate tubes on ice as S2 TE-soluble fraction. Salt concentration was adjusted for the totality of both, S1 and S2 fractions as follows. With equal sample volume

of 2XE buffer for the S1 fraction, and with half of the sample volume of 3XD buffer for the S2 fraction, added dropwise on vortex. Samples were centrifuged at 13,000g for 5min and supernatants from both fractions were pooled together respectively for each condition in separate tubes, kept on ice as nuclear extracts. All centrifugation steps were performed at 4°C and all vortex steps at the lowest speed.

Prior purification, 5% of each nuclear extract was saved as input for further analysis. Nuclear extracts were incubated with 300µl of 50% slurry prewashed Anti-FLAG M2 Affinity Gel agarose beads (Sigma-Aldrich), over-night (18h) on an end-to-end rotator at 4°C. After incubation, samples were centrifuged at 1500rpm (211g), 2min and the unbound fraction was isolated. Sequential washing steps were applied to remove non-specific binding, as follows. Beads were washed 4 times with 1ml of 1XD buffer made from 3XD, followed by 4 washes with 1ml of 1XD buffer made from 3XD + 0.5% Triton X-100, followed by 2 washes with 1ml of 1XD buffer without Triton X-100. Each washing step was done on rotation for 5min, followed by centrifugation at 1500rpm, 2min. After the final wash, beads were dried and specifically-bound proteins eluted by a tandem elution with the 3xFLAG peptide (Sigma-Aldrich). Both elution steps were performed with 100µl of the 3xFLAG peptide at 500µg/ml final concentration, resuspended and diluted in TEGN buffer, for 3h at room temperature with tilting mode. Both eluates were pooled respectively for each condition and 40% of eluates kept to further assess the specificity of the pull-down by silver staining and western-blotting. Remaining eluates were submitted for Mass Spectrometry analysis. Buffer composition is described in Table 7.

Table 7. Buffer composition for native purification of interacting protein complexes.

Buffer	**Components (stock)**	**Final concentration**
Buffer A	1M HEPES-KOH pH 8	10mM
	1M KCl	10mM
	1M $MgCl_2$	1.5mM
	1M Sucrose	340 mM
	50% Glycerol	10%
	50X protease inhibitor cocktail*	1X
	1M DTT*	1mM
Cutting buffer	1M NaCl	15mM
	1M KCl	60mM
	1M Tris-HCl pH 7.5	10mM
	1M $CaCl_2$	2mM
MNase stock at 50U/µl	1M Tris-HCl pH 7.5	10mM
	5M NaCl	50mM

was resuspended and stored in 'MNase storage buffer'	0.5M EDTA-NaOH pH 8.0	1mM
	100% glycerol	50%
TE buffer	1M Tris-HCl pH 8.0	10mM
	0.5M EDTA-NaOH pH 8.0	1mM
	50X protease inhibitor cocktail*	1X
2XE buffer	1M HEPES-KOH pH 7.5	30mM
	4M NaCl	225mM
	1M $MgCl_2$	3mM
	10% Triton X-100	0.4%
	50% glycerol	20%
3XD buffer	1M HEPES-KOH pH 7.5	60mM
	4M NaCl	450mM
	1M $MgCl_2$	4.5mM
	0.5M EGTA-NaOH pH 8.0	0.6mM
	10% Triton X-100	0.6%
	50% glycerol	30%
1XD buffer from 3XD	3 times diluted 3XD buffer	1X
1XD buffer from 3XD + 0.5% Triton X-100	3 times diluted 3XD buffer	1X
	10% Triton X-100	0.5%
1XD buffer without Triton X-100	1M HEPES-KOH pH 7.5	20mM
	4M NaCl	150mM
	1M $MgCl_2$	1.5mM
	0.5M EGTA-NaOH pH 8.0	0.2mM
	50% glycerol	10%
TEGN buffer	1M Tris-HCl pH 7.65	20mM
	0.5M EDTA-NaOH pH 8.0	0.1mM
	50% glycerol	10%
	5M NaCl	150mM
	10% NP-40	0.01%

*****_Added freshly, prior purification; Millipore H_2O was added in all buffers to complete till the final volume._

Enrichment for mononucleosomes was verified on the unbound fractions. 200µl of each unbound fraction was mixed with 200µl of Phenol:Chloroform:Isoamyl (Ph:Ch:I) alcohol 25:24:1 and centrifuged at 14,000rpm for 5min, 4°C. Transparent aqueous phase was transferred into new Eppendorf tubes and equal volume of Ph:Ch:I alcohol was added. Samples were vortexed at high speed and centrifuged at 14,000rpm for 5min, 4°C. Transparent aqueous phase was transferred into new Eppendorf tubes. To precipitate the DNA, 3M sodium acetate pH 5.2 at 15% final and 100% EtOH at 2.5X final concentration were

added to the samples. DNA precipitation was performed at -20°C over-night. Following precipitation, samples were centrifuged at 14,000rpm for 10min, 4°C. Supernatant was removed and precipitated DNA pellets washed in 500µl of 75% EtOH. Samples were centrifuged at 14,000rpm for 5min, pellets air-dried for 15min and finally resuspended in 30µl of TE buffer. DNA quantity was measured on Nanodrop 2000c spectrophotometer (ThermoFisher Scientific). 0.5µg of DNA was mixed with 6X DNA loading dye at 1X final concentration and loaded on 1.2% agarose gel. Separation of DNA fragments was performed with TAE 1X buffer, at 135V for 25min. DNA digestion profile was visualized with ultra-violet light and Bio-print Mega-Capt software.

4. LC-MS/MS analysis

Label-free quantitative Mass Spectrometry analysis was performed at Protein Sciences Facility - SFR BioSciences (UAR3444/US8) in Lyon, using Q Exactive HF (Thermo Scientific) Mass Spectrometer coupled with nanoUHPLC U3000 (Thermo Scientific). Briefly, samples were reduced and alkylated with tris-(2-carboxyethyl) phosphine/ iodoacetamide (TCEP/IAA) and fixed on SP3 beads prior digestion. Beads were washed with 80% ethanol and protein digested in ammonium bicarbonate (100mM), using Lys-C/Trypsin protease (enzyme/protein ratio: 1/100) for 18 h at 37°C. Supernatants with peptides were recovered after centrifugation at 20,000g for 1min and peptide concentration was determined for each sample by quantitative fluorometric peptide assay (Thermo Scientific) to inject 400 ng of peptides in the nanoLC-MS/MS system.

The two biological replicates for each condition were injected in triplicates and loaded on a C18 Acclaim PepMap100 trap-column 300 µm ID x 5 mm, 5 µm, 100Å, (Thermo Scientific) for 3.0 minutes at 20 µL/min with 2% ACN, 0.05% TFA in H2O and then separated on a C18 Acclaim Pepmap100 nano-column, 50 cm x 75 µm i.d, 2 µm, 100 Å (Thermo Scientific) with a 60 minutes linear gradient from 3.2% to 40% buffer B (A: 0.1% FA in H2O, B: 0.1% FA in ACN), from 40% to 90% of B in 2 min, hold for 10 min and returned to the initial conditions in 1 min for 14 min. The total duration was set to 90 minutes with a flow rate of 300 nL/min and the oven temperature was kept constant at 40°C.

Samples were analyzed with a TOP20 DDA HCD method: MS data were acquired in a data dependent strategy selecting the fragmentation events based on the 20 most abundant precursor ions in the survey scan (350-1600 Th). The resolution of the MS scan was 60,000 at m/z 200 Th and for MS/MS scan the resolution was set to 15,000 at m/z 200 Th. Parameters for acquiring HCD MS/MS spectra were as follows: normalized collision energy = 27 and an isolation window width of 2 m/z. The precursors with unknown charge state, charge state of 1

and 8 or greater than 8 were excluded. Peptides selected for MS/MS acquisition were then placed on an exclusion list for 20 s using the dynamic exclusion mode to limit duplicate spectra.

Sample file was treated with Proteome Discoverer 2.5 software (Thermo Scientific), using SEQUEST HT research engine and Swiss-Prot Mus musculus database (august 2021 release, 17500 entries), supplemented with protein contaminant database. Precursor mass tolerance was set at 10 ppm and fragment mass tolerance was set at 0.02 Da, and up to 2 missed cleavages were allowed. Oxidation (M), phosphorylation (S, T, Y), acetylation (Protein N-terminus) were set as variable modifications and carbamidomethylation (C) as fixed modification. False discovery rate (FDR) of peptide identifications was calculated by the Percolator algorithm method, and a cut-off FDR value of 1 % was used. Protein quantification was done by Label Free Quantification (LFQ) approach, and LFQ abundance values were obtained and normalized to the total peptide amount. Protein quantitation was performed with precursor ions quantifier node in Proteome Discoverer 2.5 software with protein quantitation based on pairwise ratios and hypothesis t-test. Proteins were considered as differentially expressed between the two conditions when FC > 2 and p-value < 0.05. Adjusted p-values were obtained by applying the Benjamini-Hochberg procedure. Generated data files were further analyzed taking into account following parameters in order to determine specific candidates of FH-H3.3A pull-down: 'not found in WT', number of peptides, number of unique peptides, Score Sequest HT: Sequest HT, abundance ratio and adjusted p-value abundance ratio for each peptide of given protein.

Data availability: All Mass Spectrometry proteomics datasets are available *via* ProteomeXchange at https://www.ebi.ac.uk/pride/archive/projects/PXD061974, with identifier PXD061974.

5. Native immunoprecipitation and western-blotting

Native immunoprecipitation (IP) experiments were mainly performed on MNase-digested nuclear extracts from wild-type, FH-H3.3A$^{+/-}$ and FH-H3.3A$^{+/-}$ *Per1*$^{-/-}$, *Per2*$^{-/-}$ KO nuclei purified from livers collected either every 4h over 24h, or at CT8 and CT20. Nuclei from WT livers collected at random timepoints, or isotype matched Anti-Mouse IgG antibody (Jackson Immuno Research) were used as negative controls for the IP experiments.

Nuclear extracts were prepared as described above for H3.3A complex purification, according to Khan *et al*. 2020 [220] with few following modifications. ~530µg of total protein were used for the IP, with all buffer volumes reduced by half and diluted MNase was used at 5U per sample. Prior IP, 5% of each nuclear extract was saved as input, mixed with 1.5X SDS-blue loading dye containing DTT (Table 8), denatured at 80°C for 7min and stored at -20°C for

further analysis. Nuclear extracts were incubated overnight (18h) on an end-to-end rotator at 4°C with 2 - 4.5µg of following antibodies: anti-HA-Tag, anti-PBRM1/BAF180, anti-BMAL1, anti-BRG1/SMARCA4, anti-SMARCA2 and anti-Acetyl-Histone H3 (Table 9). Following overnight incubation with antibodies, equal volume of Protein A and Protein G Dynabeads (Invitrogen) mix (12.5-30µl total) was added per sample and nuclear extracts were incubated on an end-to-end rotator for 3-4h at 4°C. Unbound fraction was isolated and beads were washed 2-3 times with 500µl of 1XD buffer made from 3XD, on rotation at 4°C for 5min. After final wash, beads were resuspended in 35µl of 2.5X SDS-blue loading dye containing DTT and proteins eluted for 10min at room temperature, with shaking mode. Protein eluates were transferred to separate tubes, denatured at 80°C for 7min and stored at -20°C.

Table 8. 5X SDS-blue loading dye.

Components (stock)	Final concentration
SDS powder	340mM
50% glycerol	25%
1M Tris-HCl pH 6.8	310mM
β-Mercaptoethanol	3.58M
Pinch of Bromophenol blue	-
1M DTT*	100mM

*****_Added freshly, prior use._

SDS-PAGE electrophoresis was performed using precast Novex NuPAGE 4-12% Bis-Tris gradient gels and NuPAGE SDS MOPS Running buffer (20X) (Invitrogen) at 1X final. Prestained Protein Ladder Plus (Euromedex) was used as a reference marker for protein size. For each IP experiment, 0.6-1% of input and one-third of IP eluates were loaded per lane. Transfer was performed on 0.2µm nitrocellulose membranes (Amersham) at constant current (0.4A) for 2-3h at 4°C, using NuPAGE SDS MOPS Running buffer at 1X with 5% ethanol. After transfer, membranes were rinsed with Millipore water and incubated in 5% non-fat dry milk-PBS 1X blocking solution for 30min at room temperature. After blocking, membranes were first rinsed with Millipore water, then with PBS 1X- 0.1% Tween 20 wash buffer prior overnight incubation at 4°C with respective primary antibodies. After incubation with primary antibodies, membranes were washed 2-3 times with PBS 1X- 0.1% Tween 20 wash buffer for 5-10min and incubated with respective anti-rabbit or anti-mouse secondary antibodies (Table 9) for 1h - 1h30 at room temperature. Membranes were washed 2-3 times with PBS 1X- 0.1% Tween 20 wash buffer for 5-10min, and incubated with ECL Prime western blotting reagent (CYTIVA) prior developing. Image acquisitions were performed using ChemiDoc Imaging system (Bio-Rad) and ImageLab software (version 6.0.1).

Following antibodies were used for IP experiments and western-blotting.

Table 9. Antibodies.

Reference	Dilutions for western-blotting	
Primary antibodies		
HA-Tag (C29F4) Rabbit mAb* (Cell Signaling, #3724)	1:1000	3% BSA - PBS 1X
PBRM1/BAF180 (E9X2Z) Rabbit mAb* (Cell Signaling, #89123)	1:1000	3% BSA - PBS 1X
ARID2 (GT7311) Mouse mAb (Sigma-Aldrich, SAB2702340)	1:500	3% BSA - PBS 1X
ARID2 (GT7311) Mouse mAb (GENETEX, GTX632011)	1:500	3% BSA - PBS 1X
BRG1/SMARCA4 Rabbit pAb* (Bethyl Laboratories, A300-813A)	1:500	3% BSA - PBS 1X
BRD7 Rabbit pAb (Proteintech, 51009-2-AP)	1:500	3% BSA - PBS 1X
PHF10 Mouse mAb (Proteintech, 66341-1-Ig)	1:500	3% BSA - PBS 1X
PHF10 Rabbit pAb (GENETEX, GTX116314)	1:500	3% BSA - PBS 1X
BMAL1 Rabbit pAb* (Bethyl Laboratories, A302-616A)	1:1000	3% BSA - PBS 1X
CLOCK Mouse mAb (MBL, D334-3)	1:500	3% BSA - PBS 1X
Histone H3.1/3.2 (1D4F2) Mouse mAb* (Active Motif, 61629)	1:500	3% BSA - PBS 1X
Tri-Methyl-Histone H3 (Lys4) Rabbit pAb (Cell Signaling, #9727)	1:500	3% BSA - PBS 1X
Acetyl-Histone H3 (Lys115) Rabbit pAb* (PTM Bio, PTM-170)	1:1000	3% BSA - PBS 1X
Histone H3 (acetyl K122) Rabbit pAb (Abcam, ab33309)	1:500	3% BSA - PBS 1X
Histone H2A.Z Rabbit pAb (Active Motif, 39113)	1:1000	3% BSA - PBS 1X
Homemade H2A.Z Rabbit pAb (kind gift from Stefan Dimitrov)	1:500	3% BSA - PBS 1X
ARID1B Rabbit pAb (GENETEX, GTX130708)	1:500	3% BSA - PBS 1X
SMARCA2 (HL1115) Rabbit mAb* (GENETEX, GTX636330)	1:500	3% BSA - PBS 1X

Histone H3 Rabbit pAb (Proteintech, 17168-1-AP)	1:2000	1% milk- PBS 1X
Histone H4 Rabbit pAb (Proteintech, 16047-1-AP)	1:2000	1% milk- PBS 1X
U2AF65 Rabbit mAb (Abcam, ab197031)	1:500	3% BSA - PBS 1X
HIRA (clone WC119) Mouse mAb (Sigma-Aldrich, 04-1488)	1:500	3% BSA - PBS 1X
DAXX anti-Mouse (Precision antibody)	1:500	3% BSA - PBS 1X
IgG negative control antibody used for the immunoprecipitation		
IgG antibody (Jackson ImmunoResearch, 315-005-003)*		
Secondary antibodies		
Peroxidase Goat Anti-Rabbit IgG (H+L) (Jackson ImmunoResearch, 111-035-144)	1:10,000	5% milk- PBS 1X
Goat Anti-Mouse IgG (H+L)- HRP Conjugate (Bio-Rad, #1706516)	1:5000 - 1:10,000	

***Antibody used as well for the IP and ChIP experiments.*

If the proteins of interest were migrating at the same size, mainly different gels and membranes were used. In some cases, primary anti-ARID2 mouse antibody was used first and after extensive stringent washing for few hours, membranes were probed in primary anti-BRG1 rabbit antibody. Before probing in primary rabbit antibody, extensively washed membranes were incubated with the anti-mouse secondary antibody and developed to verify the removal of the signal. Membranes were probed in the following order: PBRM1 and CLOCK (migrating at different sizes, both probed on the same membranes); ARID2 and BRG1 (migrating at similar sizes, probed mainly on different membranes); BMAL1 and BRD7 (migrating at similar sizes, probed on different membranes); PHF10 (probed on different membranes); ARID1B and BRM/SMARCA2 (migrating at similar sizes, probed on different membranes). The histones, histone variants and histone marks were probed mainly on different membranes, except HA-tag (H3.3A) and H2A.Z, migrating at different sizes.

6. Native chromatin immunoprecipitation-sequencing

Native chromatin-immunoprecipitation experiments were performed on MNase-digested nuclear extracts from FH-H3.3A$^{+/-}$ and FH-H3.3A$^{+/-}$ *Per1*$^{-/-}$, *Per2*$^{-/-}$ KO nuclei purified from livers collected either every 4h over 24h, or at CT8 and CT20. Nuclear extracts were prepared with ~350 - 530µg of total protein, according to Khan *et al*. 2020 [220] and as described above for the IP experiments. DNA quantity in nuclear extracts was measured on Nanodrop 2000c

spectrophotometer. ~15-30µg of chromatin was used per sample for ChIP experiments and 1% of each nuclear extract was saved as input. Inputs from CT0 - CT20 circadian nuclear extracts (related to FH-H3.3A ChIP) and inputs from CT8 and CT20 (related to H3.1/3.2 and BMAL1 ChIP) nuclear extracts were pooled together and stored at -80°C for further analysis. Nuclear extracts were incubated overnight (18h) on an end-to-end rotator at 4°C with 2 - 4µg of following antibodies: anti-HA-Tag, anti-Histone H3.1/3.2 and anti-BMAL1 (Table 9). Following overnight incubation with antibodies, equal volume of Protein A and Protein G Dynabeads mix (25µl total) was added per sample and nuclear extracts were incubated on an end-to-end rotator for 3-4h at 4°C. Unbound fraction was isolated and beads were washed 3 times with 250µl of 1XD buffer made from 3XD, on rotation at 4°C for 5min. After final wash, beads were resuspended in 100µl of ChIP Elution buffer (Table 10) and co-immunoprecipitated DNA eluted at 65°C, with shaking mode at 600rpm for 15min. Recovered eluates and inputs were treated with Proteinase K (NEB Molecular Biology Grade) at 10mg/ml final concentration, at 37°C for 2h30, followed by DNA purification using QIAquick PCR Purification Kit (QIAGEN). Purified ChIP DNA was stored at -80°C until further analysis. Concentration of purified DNA samples was assessed on Qubit 4 Fluorometer (Invitrogen) using Qubit dsDNA HS Assay Kit (Invitrogen). Quality of purified DNA samples was assessed on Agilent 4150 TapeStation System using High Sensitivity D5000 ScreenTape assay (Agilent) and analyzed with Agilent TapeStation Software 5.1 prior sequencing.

Table 10. ChIP elution buffer.

Components (stock)	Final concentration
10% SDS	1%
1M $NaHCO_3$	100mM

7. Data filtering, ChIP-Seq analysis and graphical representation

Sequencing was performed at the sequencing platform at the Department of Computational Biology and Medical Sciences of the University of Tokyo in collaboration with Pr. Yutaka Suzuki and Dr. Masahide Seki. All bioinformatic analysis was done by Dr. Aurélie Peticca from Padmanabhan laboratory, as follows.

Sequencing libraries were prepared with NEBNext UltraII DNA Library Prep Kit for Illumina sequencing, enriching for fragments from 100-150bp with the 0.9X beads. 150b paired-end (PE) sequencing was performed on Illumina NovaSeq6000 system using NovaSeqS4 flow cell. Approximately 30,000,000+ PE reads were obtained for each replicate. These were filtered to remove poor quality reads (Q<20), short reads (<75b) and Illumina adapters using cutadapt

4.5, the results were visualized using FastQC 0.12.1. The trimmed reads from each replicate were then mapped separately on the mouse genome GRCm39 with Bowtie2 2.5.4 [221] using --very-sensitive --no-mixed --no-discordant and --dovetail options. Samtools 1.18 [222], command view -F 1804 -q 20 -f 2, was used to remove poor quality mappings (<20), unmapped reads and their mate, non-primary alignments and reads not correctly matched. The resulting alignment was then filtered to remove duplicates and blacklisted regions, following ENCODE recommendations [223], using Picard MarkDuplicates 3.1.1 (Broad Institute 2019) and Bedtools intersect 2.30.0 [224] respectively. The alignment of each replicate was then down-sampled to ensure that the same number of sequences were present for each replicate of the same ChIP Seq sample, and thus avoid over-representation of any one of them. This sub-sampling was carried out using samtools view, and the alignments were sorted using samtools sort. The input samples (ChIP seq control samples) were processed in the same way as the others samples.

In order to compare the alignments obtained for each sample and represent them, deepTools 3.5.5 [225] was selected to create a matrix of intensity scores (computeMatrix --beforeRegionStartLength 1000 --afterRegionStartLength 1000, combined with plotProfile) from the normalized alignments (bamcoverage --normalizeUsing RPGC --Mnase --maxFragmentLength 200 --minFragmentLength 80). These were then plotted either as a heatmap (plotHeatmap) or as an average profile plot (plotProfile). The regions of interest studied in these graphs were the regions of interest were the CLOCK-BMAL1 binding sites recovered from the work of Trott and Menet (2018) [226], the CTCF binding sites from ENCODE project and the SINEs class annotation from UCSC Genome Browser (https://genome-euro.ucsc.edu/). If the sites were not annotated for the mm39 mouse genome, then the coordinates were converted using UCSC genome (https://genome.ucsc.edu/cgi-bin/hgLiftOver).

Data availability: All ChIP-seq datasets are available at https://www.ncbi.nlm.nih.gov/geo/query/acc.cgi?acc=GSE284165, with accession number GSE284165. All scripts are available at https://github.com/Thrylia/ChIP_HA-Complexe.

8. Cross-linked ChIP-qPCR

Cross-linked material was directly prepared during the nuclei purification from isolated livers as following. Tissues were grinded in PBS 1X without protease inhibitors. Filtered tissue homogenates were then cross-linked with Formaldehyde solution (Sigma) at 1% final on rotation for 5min at room temperature, followed by quenching with Glycine at 150mM final on rotation for 3min at room temperature. Subsequent nuclei purification steps remained unchanged and done as described above and in [219], except that Glycine at 150mM final was

added to the 2.2M and 2.05M sucrose solutions prior ultracentrifugation step. Purified nuclei were stored in NLB 1X containing protease inhibitors, spermine, spermidine and DTT, at -80°C until further use.

To proceed for chromatin preparation, cross-linked nuclei were washed once with 200µl of 1X Ripperger buffer, pelleted at 4000rpm (1503g) for 2min and resuspended again in 100µl of 1X Ripperger buffer. 110µl of 1X Ripperger buffer containing 2% SDS was added to the samples and after immediate homogenization, samples were incubated on ice for 30min, vortexed at low speed every 10min during the incubation time. Samples were then sonicated 4 times for 3 cycles on Diagenode bioruptor (30s on/ 30s off; total 12 cycles) to obtain a smear between 100 - 300bp with enrichment for mononucleosomes at 150bp. In between each 4 cycles, samples were quickly warmed up at 37°C to dissolve precipitated SDS. Following sonication, samples were centrifuged at 10,000rpm (9391g) for 10min and supernatants kept as cross-linked chromatin for the ChIP experiments, stored at -80°C until further use. All centrifugation steps were done at 4°C.

In order to determine DNA concentration prior ChIP experiments, 5% of cross-linked chromatin were decrosslinked in ChIP Elution buffer for 2h at 65°C, treated with Proteinase K at 10mg/ml final concentration for 1h30 at 37°C and DNA purified using QIAquick PCR Purification Kit. DNA quantity was measured on Nanodrop 2000c spectrophotometer and sonication efficiency visualized on 1.2% agarose gel with ultra-violet light and Bio-print Mega-Capt software. For each ChIP, 30µg of cross-linked chromatin were mixed with 1X Ripperger buffer containing 1% Triton X-100 to get the final concentration of SDS at 0.1% within samples to avoid its precipitation at 4°C. 10% of each sample were kept as input. ChIP was performed respectively with 2.5µg and 4µg of anti-BRG1/SMARCA4 and anti-SMARCA2 antibody (Table 9), overnight (18h) on an end-to-end rotator at 4°C. Following overnight incubation with antibodies, equal volume of Protein A and Protein G Dynabeads mix (30µl total) was added per sample and chromatin was incubated on an end-to-end rotator for 3-4h at 4°C. Unbound fraction was isolated and beads were first washed 2 times with 500µl of Wash buffer 1 for 5min, followed by one wash with 500µl of Wash buffer 2 for 5min. All washes were done on rotation at 4°C. After final wash, beads were resuspended in 100µl of ChIP Elution buffer and co-immunoprecipitated DNA eluted at 65°C, with shaking mode at 600rpm for 20min. Recovered eluates and inputs were decross-linked at 65°C for 2h and treated with Proteinase K at 10mg/ml for 1h30 at 37°C, followed by DNA purification using QIAquick PCR Purification Kit. Purified ChIP DNA was stored at -80°C until further analysis. Buffer composition is described in Table 11.

Table 11. Buffer composition for cross-linked ChIP.

Buffer	Components (stock)	Final concentration
Ripperger buffer 10X stock	1M Tris-HCl pH 7.5	200mM
	5M NaCl	1.5M
	0.5M EDTA-NaOH pH 8.0	20mM
1X Ripperger buffer	10 times diluted Ripperger buffer 10X stock with Millipore H_2O	1X
1X Ripperger buffer + 2% SDS	10 times diluted Ripperger buffer 10X stock with Millipore H_2O	1X
	10% SDS	2%
1X Ripperger buffer + 1% Triton X-100	10 times diluted Ripperger buffer 10X stock with Millipore H_2O	1X
	10% Triton X-100	1%
Wash buffer 1	10% SDS	0.1%
	10% Triton X-100	1%
	0.5M EDTA-NaOH pH 8.0	2mM
	1M Tris-HCl pH 8.1	20mM
	5M NaCl	150mM
Wash buffer 2	10% SDS	0.1%
	10% Triton X-100	1%
	0.5M EDTA-NaOH pH 8.0	2mM
	1M Tris-HCl pH 8.1	20mM
	5M NaCl	500mM

Real-time qPCR reactions were performed as follows. Each sample was deposited in three wells as technical replicates on Hard-Shell PCR 96-well thin wall plates (Bio-Rad). Reaction master mixes (Table 12) were prepared using ITaq Universal SYBR Green Supermix (Bio-Rad) and specific forward/ reverse primer sets. RT-qPCR were performed with CFX96 Real-Time PCR Detection System (Bio-Rad), using the program described in Table 13, and analyzed by CFX Maestro Software (version 2.3). Enrichment at clock-gene E-boxes (*Per1, Dbp, Per2, Reverbα, Cry2, Rorc*) was assessed, calculated as percentage of the immunoprecipitated input. All the results are represented as the average ± SEM of three independent biological replicates. Primers for these regions [227] were synthesized by Eurogentec; primer sequences are available in the Table 16. Primer sequences.

Table 12. Master mix for one RT-qPCR reaction.

Components (stock)	Volume for one reaction
Primer mix (5µM of each, forward/ reverse primers)	2µl

Millipore H_2O	2µl
ITaq Universal SYBR Green Supermix	5µl

Table 13. RT-qPCR program.

Step	Temperature, time
1. Polymerase activation	95°C, 3min
2. Denaturation	95°C, 10sec
3. Annealing	60°C, 20sec
+ Plate Read	
4. Go to step 2., 39 more times	
5. Melt Curve 60°C to 95°C, increment 0.5°C for 5sec	
+ Plate Read	

9. mRNA expression levels and RT-qPCR

Whole liver extracts from FH-H3.3A$^{+/-}$ and FH-H3.3A$^{+/-}$ *Per1*$^{-/-}$, *Per2*$^{-/-}$ KO livers collected at CT8 and CT20 were obtained during the nuclei purification as follows. Tissues were grinded in PBS 1X containing protease inhibitors and aliquots of tissue homogenates were stored at -80°C until further use. Total RNA was extracted from whole liver extracts with TRIzol LS Reagent (Invitrogen) according to manufacturer's instructions and quantified on Nanodrop 2000c spectrophotometer. cDNA was prepared from 2µg of purified RNA using IScript cDNA Synthesis kit (Bio-Rad) according to manufacturer's instructions and diluted 5 times prior further application.

Real-time qPCR reactions were performed as described above, with following modifications. Each sample was deposited in two to three wells as technical replicates on Hard-Shell PCR 96-well thin wall plates. All the results are represented as the average ± SEM of three independent biological replicates of relative expression calculated with the $2^{-\Delta\Delta Ct}$ method and normalized to *Rps9* cDNA levels. Primer sequences were mainly obtained from the Harvard PrimerBank database and synthesized by Eurogentec; they are available in the Table 16. Primer sequences.

10. Real-time bioluminescence monitoring assay of circadian oscillations in cultured cells

FLAG-HA-H3.3B f/f animals were crossed to H3.3A f/f strain [228] and embryos were sacrificed at E14 to generate mouse embryonic fibroblasts. Cell lines were cultured at 37°C with a 5%

CO_2 atmosphere in DMEM-high glucose medium (Sigma-Aldrich) supplemented with 10% FBS (Gibco) and 1% penicillin-streptomycin at 25 units/ml (ThermoFisher).

Circadian bioluminescence rhythms were monitored on confluent wild-type and tamoxifen-treated double-floxed FH-H3.3A$^{-/-}$, FH-H3.3B$^{-/-}$ ERT2-Cre Bmal1: luciferase reporter mouse embryonic fibroblasts. To obtain H3.3A, H3.3B double knock-out (H3.3 DKO), cells were treated with 4-OHT, cis/trans-4-hydroxytamoxifen (Sigma-Aldrich) at 5µM for 3.5 - 4 days and knock-out efficiency was verified by western-blotting. Both WT and H3.3 DKO cells were seeded at high confluency in a black 24 well plate with flat and clear bottom for high-throughput microscopy (Ibidi) and cells were synchronized with Dexamethasone (Sigma-Aldrich) at 100nM for 1h30. After synchronization, cell culture medium was replaced, supplemented with HEPES (Gibco) at 10mM, sodium bicarbonate solution (Gibco) at 1% and 200µM of D-Luciferin Sodium Salt (PJK GmbH) and bioluminescence was monitored in both, WT and H3.3 DKO cells at 4th day post-tamoxifen treatment with LumiCycle 96 luminometer for circadian biology (ACTIMETRICS). LumiCycle Data Analysis software (ACTIMETRICS, version 3.100) was used to visualize the data, to perform detrending analysis and calculation of oscillation period and amplitude.

For cryopreservation of the cell lines, cells were trypsinized, transferred into Falcons and pelleted at 120g for 5min. Medium supernatant was nearly totally removed, cell pellet resuspended in the remaining medium with gentle shaking of the Falcon. DMEM-high glucose medium supplemented with DMSO (1:10 dilution; Sigma-Aldrich) was added slowly on the resuspended cell pellet dropwise, while shaking the Falcon and cell suspension was transferred into cryogenic vials. Vials were first stored at -80°C in a freezing container (Nalgene) for one week, then transferred and stored in liquid nitrogen.

11. Subcellular protein tissue fractionation

Nucleoplasm and chromatin fractions were extracted from FH-H3.3A$^{+/-}$ and FH-H3.3A$^{+/-}$ *Per1*$^{-/-}$, *Per2*$^{-/-}$ KO liver pieces collected at CT8 and CT20, using Subcellular Protein Fractionation Kit for Tissues (Thermo Scientific) according to the manufacturer's instructions. Whole liver lysates were obtained by incubating small liver pieces from the same tissues as for the fractionation in 70µl of RIPA lysis buffer for 30min on ice, then sonicated for 6 cycles on Diagenode bioruptor (30s on/ 30s off) at 4°C, followed by centrifugation at 14,000rpm for 10min. Proteins from all fractions were quantified using DC protein assay.

12. MG132 treatment and subcellular protein fractionation

Unsynchronized confluent murine wild-type and *Per1*$^{-/-}$,*Per2*$^{-/-}$,*Per3*$^{-/-}$ triple-knockout (PerTKO) lung fibroblasts were treated with MG132 proteasome inhibitor (Sigma-Aldrich) for 4h prior chromatin extraction. Subcellular protein fractionation was performed using Subcellular Protein Fractionation Kit for Cultured Cells (Thermo Scientific) according to the manufacturer's instructions. Whole cell lysates were obtained by incubating a part of the same cell pellets that were used for the fractionation in 60µl of RIPA lysis buffer for 20min on ice, then sonicated for 6 cycles on Diagenode bioruptor (30s on/ 30s off) at 4°C, followed by centrifugation at 14,000rpm for 10min. Proteins from all fractions were quantified using DC protein assay.

13. Reanalysis of published siRNA screens

To verify whether specific PBAF and BAF complex components have an impact on circadian clock regulation, we searched and reanalyzed data from the previously published genome-wide siRNA screen for modifiers of the circadian clock [229]. Data from all available replicates for the siRNAs of target genes, *Cry2* positive and negative controls were taken into account from all plates. Technical duplicates for given control siRNAs were averaged to obtain a single value and thus in total four traces for each siRNA, corresponding to two averaged duplicates from each plate. For the siRNAs of target genes, since one technical duplicate was available on each plate, obtained values were kept without calculating the average and the four traces correspond to individual technical replicates. Statistical analysis for period length was performed with available data from the published study (see NIHMS144235-supplement-01 file [229] for period distribution for negative and positive control siRNA, respectively 25.20 h ± 0.55 for and 29.43 h ± 0.65; BioGPS centralized gene-annotation portal [230] with Circadian Layout plugin -- Circadian Genomics Screen Database - BioGPS - your Gene Portal System for respective target siRNA made available by the authors of the genome wide RNAi screen [229]). For Phf10 screen, data from only one replicate were available in the database.

Results

1. Characterization of liver-specific H3.3A protein complexes over time

1.1 Establishment of the purification method and encountered challenges

To characterize specific H3.3A protein complexes over time in murine livers, we needed to establish a suitable purification method. Very few publications provide detailed methods on purification of histone variant complexes. Moreover, such methods are essentially described for cell culture models, in which the given histone variant is often being overexpressed- in contrary to our FH-H3.3A$^{+/-}$ and FH-H3.3A$^{+/-}$ *Per1*$^{-/-}$, *Per2*$^{-/-}$ mouse models, where H3.3 is expressed at endogenous levels [218]. In addition, the complexity of mouse liver tissues resides in important cell-type heterogeneity with a majority of non-dividing cells in quiescent state, and the limited amount of material that can be used to conduct experiments.

Several challenges were encountered in order to adapt already existing protocols described for cell culture models [220] to purify H3.3A complexes from murine livers. First step required efficient isolation of the liver nuclei from a crude tissue homogenate enriched in fat, mitochondria and proteases [219]. Next, in order to purify protein complexes that assemble on mononucleosomes harboring histone variants and underlying DNA, chromatin has to be digested with MNase (Micrococcal nuclease)- a nuclease that cuts DNA preferentially on its naked sites to release nucleosomes from chromatin [231]. Since MNase activity can vary from batch to batch, establishment of the correct conditions to digest and enrich chromatin for mononucleosomes, while avoiding over digestion and DNA degradation, was not straightforward.

Therefore, to establish conditions under which we could efficiently purify native H3.3A complexes from murine livers, we made several adjustments in the purification process over time to the original protocol from Khan *et al*. 2020 [220] (described in Methods section). These adjustments were related to the initial protein concentration, MNase (concentration and digestion time), immunoprecipitation and increased stringency during the washing steps post-immunoprecipitation in order to massively reduce non-specific background (Figure 12). The wild-type non-tagged animals were used as negative controls for the H3.3A protein complex purification.

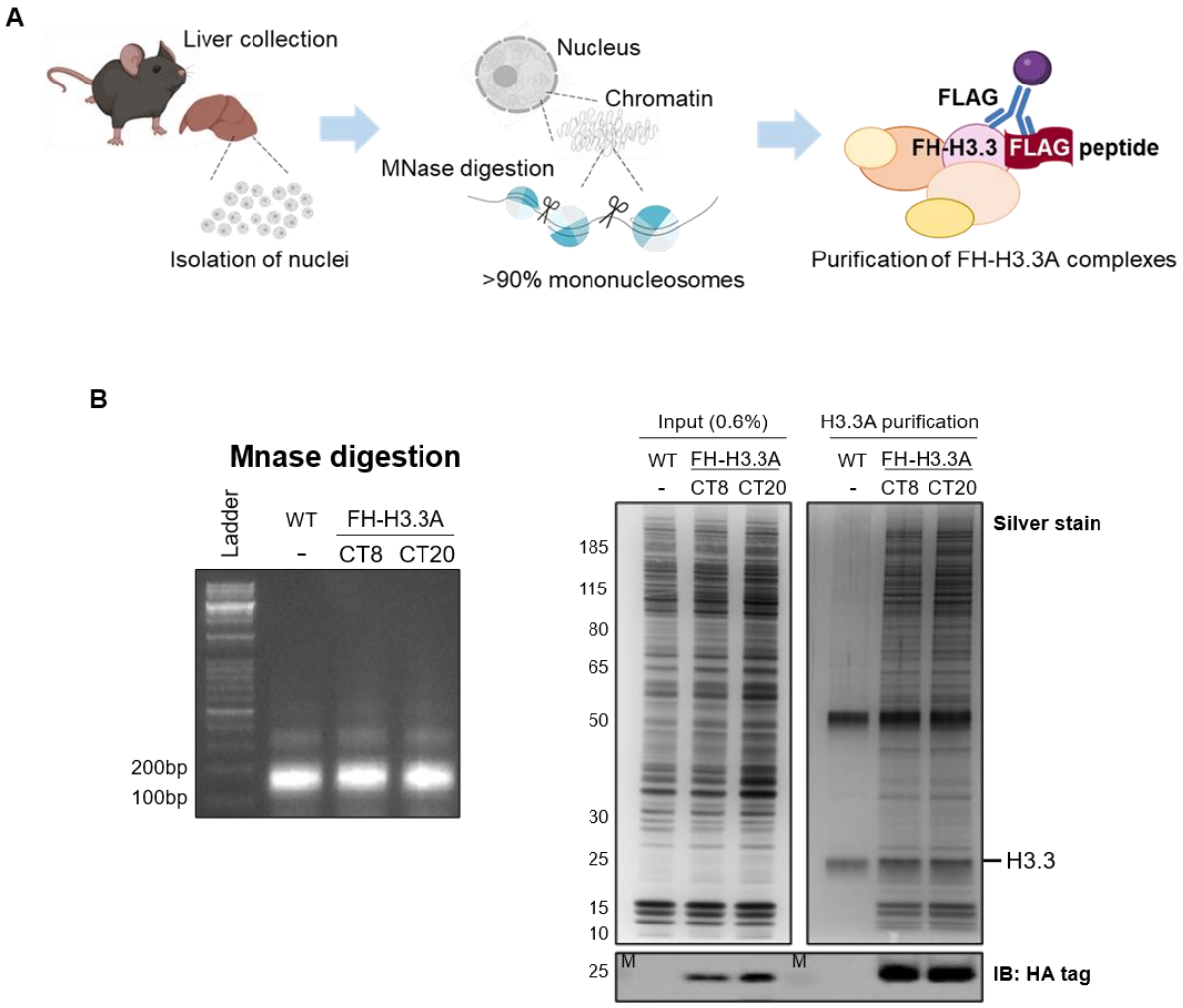


Figure 12. Native purification of H3.3A liver protein complexes. (A) Workflow of native H3.3A purification method from mononucleosome (~150bp) -enriched soluble FH-H3.3A wild-type and PerKO liver chromatin, followed by mass spectrometry. (B) Verification of soluble chromatin fraction enrichment in mononucleosomes on 1.2% agarose gel (left panel), and of the purification method specificity by silver staining, comparing wild-type negative control (only IgG light and heavy chains are visible, migrating respectively ~28 and 55kDa) with FH-H3.3A purifications (right panel). Results are representative of *n* > 3 independent biological replicates. M corresponds to the protein ladder; sizes are indicated in kDa.

1.2 H3.3A day-time dependent assembly with BMAL1-CLOCK transcription factors

To uncover H3.3A chromatin states over time, we first purified H3.3A nucleosome complexes from FH-H3.3A$^{+/-}$ liver chromatin at two opposite circadian times (CT) with a 12h resolution, corresponding to the peak (subjective day-time) and trough (subjective night-time) of BMAL1-CLOCK activity. In parallel, we as well analyzed H3.3A complexes in FH-H3.3A$^{+/-}$ *Per1*$^{-/-}$, *Per2*$^{-/-}$ (PerKO) livers to gain insights into variant chromatin landscapes upon circadian clock disruption.

To characterize H3.3A nucleosome complexes at day vs. night time points, the FH-H3.3A$^{+/-}$ (wild-type) and FH-H3.3A$^{+/-}$ PerKO animals were raised under controlled conditions and sacrificed in constant darkness during the subjective day at CT8 and night at CT20 for the wild-type, and at CT20 for the PerKO mice. Liver tissue collection was then subsequently followed by isolation of liver nuclei and preparation of soluble chromatin fractions enriched in mononucleosomes. We then performed a native HA-tag immunoprecipitation (IP) experiments and analyzed the purified complexes for the presence of the core-clock transcription factors BMAL1-CLOCK (Figure 13).

H3.3A complexes assembled with both BMAL1 and CLOCK during the active clock phase at CT8. These complexes were absent during the repressive phase of the circadian cycle at CT20, and interestingly, BMAL1-CLOCK were no longer present in H3.3A complexes in the PerKO livers. In addition, we noted that H3.3A nucleosome complexes retained H2A.Z at both time points in wild-type, as well as in PerKO liver chromatin. However, they did not include canonical H3.1/2 histones at any of these time points, suggesting that FH-H3.3A variant forms mainly homotypic nucleosomes, harboring one copy of the tagged and remaining untagged H3.3 histone variants.

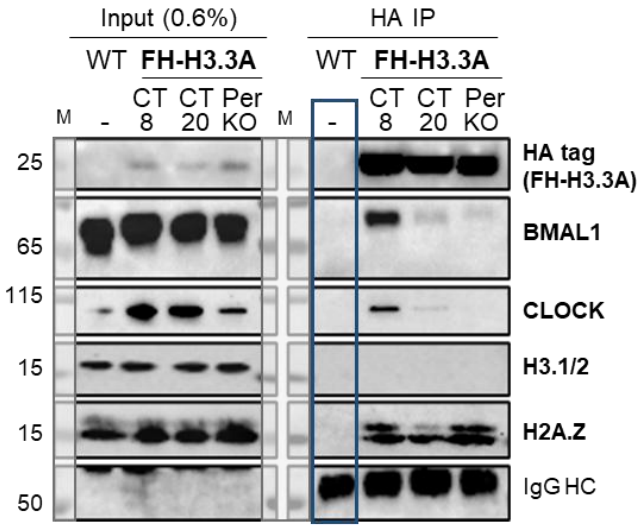


Figure 13. Day-time specific H3.3A complexes contain BMAL1-CLOCK. Native HA-tag IP on soluble chromatin at circadian times CT8 and CT20 from FH-H3.3A wild-type and FH-H3.3A PerKO mouse livers. Chromatin from non-tagged wild-type livers was used as a negative control (indicated in blue box). 0.6% of the nuclear extracts were loaded as Input. Immunoblotting was performed for HA epitope to identify FH-H3.3A, BMAL1, CLOCK, H3.1/2 and H2A.Z. Results are representative of *n* = 3 independent biological replicates. M corresponds the protein ladder; sizes are indicated in kDa.

1.3 Identification of SWI/SNF PBAF chromatin remodelers as main H3.3A interactors

We next scaled up the H3.3A complex purification from liver nuclei to identify H3.3A interactors by mass spectrometry analysis. Soluble chromatin enriched for mononucleosomes from day- and night- time points and the PerKO was generated as before, followed by native anti-FLAG IP and gradually increasing stringent washing conditions. H3.3A complexes were then eluted with the FLAG peptide. Chromatin from non-tagged wild-type animals served as negative control and purified fractions were verified by silver staining prior to mass spectrometry (MS) analysis (Figure 12B, right panel).

While MS analysis did not reveal any significant differences in known H3.3 specific chaperones (data not shown), we identified a significant reduction in specific components of the PBAF complex and the shared ATPase subunit BRG1 in the H3.3A interactome generated from PerKO livers (Table 14, Figure S3), suggesting that the absence of circadian negative feedback due to the loss of PER could compromise establishment of H3.3-PBAF complexes.

1.4 Circadian PBAF-BMAL1 complex assembles on dynamic H3.3 variant chromatin

Would PBAF complex assemble on H3.3A chromatin along with BMAL1 over time? To address whether the assembly of PBAF-BMAL1 is dynamic on H3.3A variant nucleosomes, we first performed native HA-tag IP on soluble chromatin from FH-H3.3A$^{+/-}$ livers collected at circadian times CT0-CT20, with a 4h resolution (*i.e.* livers collected every 4h over 24h). Wild-type non-tagged liver chromatin collected at random time points was used as a negative control.

Since the FH-H3.3A animals used in this study are heterozygous, H3.3 nucleosomes could, in principle, harbor either a canonical H3 histone or the untagged native H3.3 copy, as indicated before (Figure 13). The absence of canonical histones H3.1/2 in the H3.3A complex across all circadian times indicated that the IP enriches for homotypic H3.3 nucleosomes (Figure 14A). Moreover, we found that PBAF remodeling complexes (PBRM1, ARID2 and the shared BRG1 subunit) assemble on H3.3 nucleosomes independently of circadian time, whereas BMAL1 was enriched on H3.3 chromatin during the subjective daytime, peaking at CT8 (Figure 14A).

To address whether endogenous PBAF complexes associate with BMAL1, we performed native PBRM1 IP from soluble chromatin from non-tagged wild-type livers, collected at circadian times CT0-CT20. An isotype-matched IgG antibody was used as a negative control. PBRM1 co-immunoprecipitated with other specific PBAF complex components, including ARID2, BRD7, PHF10, as well as the shared ATPase subunit BRG1 across all time points, with only subtle differences between CTs. The most notable differences were observed for PBRM1-BRG1 interaction, including all BRG1 isoforms, peaking at CT8 and then again later on at CT16 and CT20 (Figure 14B). Such differences would potentially reflect the activity

of the remodeling complex, given that the presence of the catalytic ATPase subunit is needed for nucleosome remodeling and/or the time-dependent availability of the BRG1 subunit which is shared between the PBAF and BAF complexes.

However, while PBAF complexes assembled at all time points, PBAF-BMAL1 complexes were specifically enriched during the active clock phase at CT4 and CT8 (Figure 14B), consistent with previous observations on H3.3A complexes (Figure 14A).

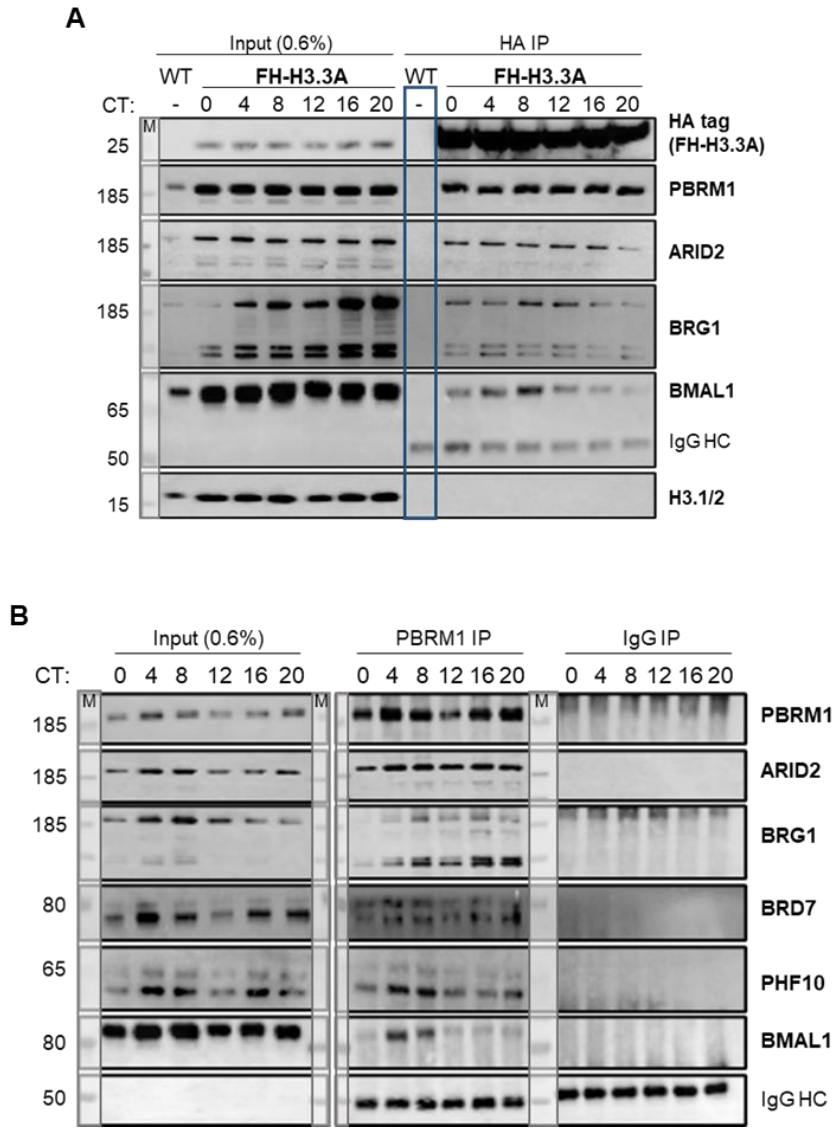


Figure 14. Rhythmic assembly of H3.3-PBAF-BMAL1 complexes. (A) Native HA-tag IP on soluble FH-H3.3A chromatin over circadian times. Wild-type chromatin used as a negative control (indicated in blue box). Pooled nuclei from three different animals per time point were used for the immunoprecipitation experiment. (B) Native PBRM1 IP on soluble wild-type liver chromatin over circadian times. IgG antibody was used as a negative control. 0.6% of the nuclear extracts were loaded as Input. Immunoblotting was performed for HA epitope to identify FH-H3.3A (A), specific PBAF complex components, BRG1 and BMAL1 (A and B). M corresponds to the protein ladder; sizes are indicated in kDa. Results are representative of *n* = 3 independent biological replicates.

2. Rhythmicity in H3.3A nucleosome occupancy

2.1 H3.3A variant generates 24h chromatin dynamics at clock *loci*

Would the presence of H3.3A nucleosomes on liver chromatin follow a 24h dynamics? To address this question, we performed native HA-tag ChIP-seq experiments on soluble chromatin enriched for mononucleosomes from FH-H3.3A$^{+/-}$ livers collected over circadian time (Table 15).

We found that H3.3A nucleosomes are rhythmically enriched at TSS of BMAL1-CLOCK target genes, as well as binding sites, peaking during the subjective day-time at CT4 (Figure 15A, B). In addition, well-positioned H3.3A nucleosomes were found downstream of the TSS of BMAL1-CLOCK target genes, extending up to nearly 1kb at all time points, whereas those positioned upstream of the TSS were mainly detected during the active clock phase (Figure 15A). Moreover, circadian E-box sequences were flanked by H3.3A nucleosomes (Figure 15B). Such observed dynamics at clock-target genes and circadian E-boxes remained specific to these sites, since no rhythms were detected in H3.3A nucleosome occupancy at other regions of the genome, such as short interspersed nuclear element (SINE) repeats (Figure 15C) and intergenic regions (Figure 15D). Furthermore, the time of enrichment of H3.3A nucleosomes at clock-target genes preceded the peak of recruitment of BMAL1-CLOCK and coincided with recruitment of active Pol II [51, 181, 232].

In parallel, as a control, we also performed H3.1/2 ChIP-seq at CT8 and CT20 to assess potential differences in enrichment between H3.3 variant and H3 canonical nucleosomes. We found that variant H3.3A nucleosomes are overall specifically enriched at TSS, including BMAL1-CLOCK target genes, when compared to the canonical H3.1/2 (Figure 15E).

2.2 Impact of circadian clock disruption on H3.3A chromatin landscapes

We therefore wondered what is happening to H3.3A nucleosomal landscapes in PerKO livers. To address this, we performed native HA-tag ChIP-seq, along with the control ChIP-seq for canonical H3.1/2 histones in FH-H3.3A$^{+/-}$ PerKO livers, as described previously. We found that H3.3A nucleosomes were overall specifically enriched in PerKO liver chromatin, when compared to H3.1/2 nucleosomes (Figure 16A). Remarkably, H3.3A enrichment in PerKO livers was higher than in wild-type livers at both CT8 and CT20 (Figure 16A) and no such important enrichment was detected at SINE repeats or intergenic regions (Figure 16B, C).

We further noticed higher enrichment of H3.3A nucleosomes at BMAL1-CLOCK target genes and binding sites in PerKO chromatin when compared to the wild-type livers across all circadian times, as well as input samples (Figure 16D, Figure 24B).

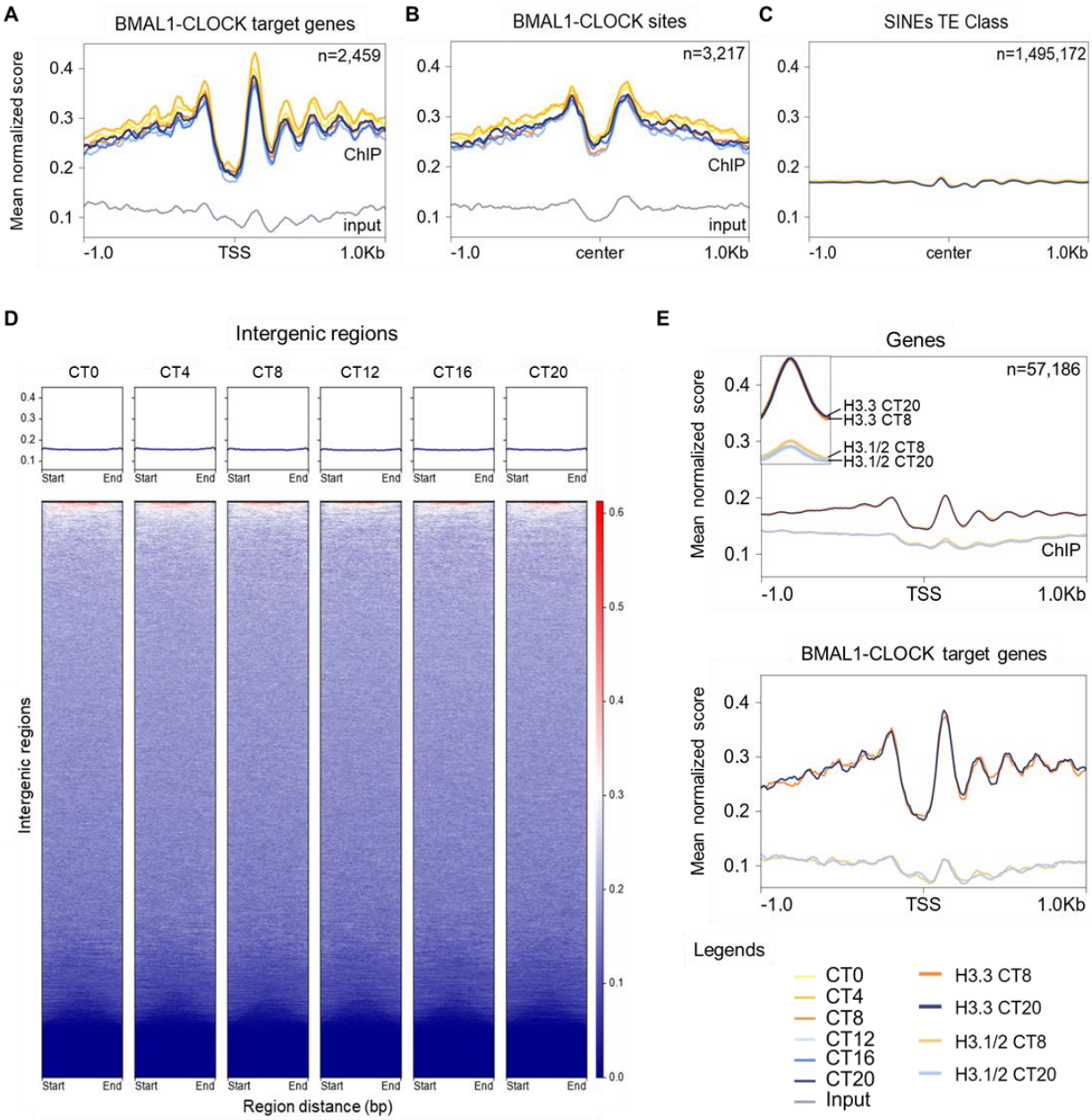


Figure 15. Circadian dynamics of H3.3A nucleosomes. (A-C) Native FH-H3.3A circadian ChIP-seq at BMAL1-CLOCK target genes (A), BMAL1-CLOCK binding sites (B) and SINE repeats (C). Input signal was plotted along with the normalized ChIP signal on the same graph. Y-axis corresponds to the mean of normalized scores per genomic region. X-axis represents the distance from the TSS or the center of the given site/region (± 1kb). Each color represents a given CT, with yellow/orange for the day- and blue colors for the night-time points, as indicated in legends. (D) H3.3A occupancy at intergenic regions. Y-axis corresponds to the mean of normalized scores per genomic regions. X-axis represents the region distance in bp. Heat-map represents an alternative visualization of H3.3A enrichment at intergenic regions. (E) Native FH-H3.3A and H3.1/2 ChIP-seq. H3.3A enrichment compared to canonical H3.1/2 at TSS of all genes and at TSS of BMAL1-CLOCK target genes. ChIP-seq graph axes were represented as indicated previously in (A-C). All results were obtained from *n* = 3 independent biological replicates.

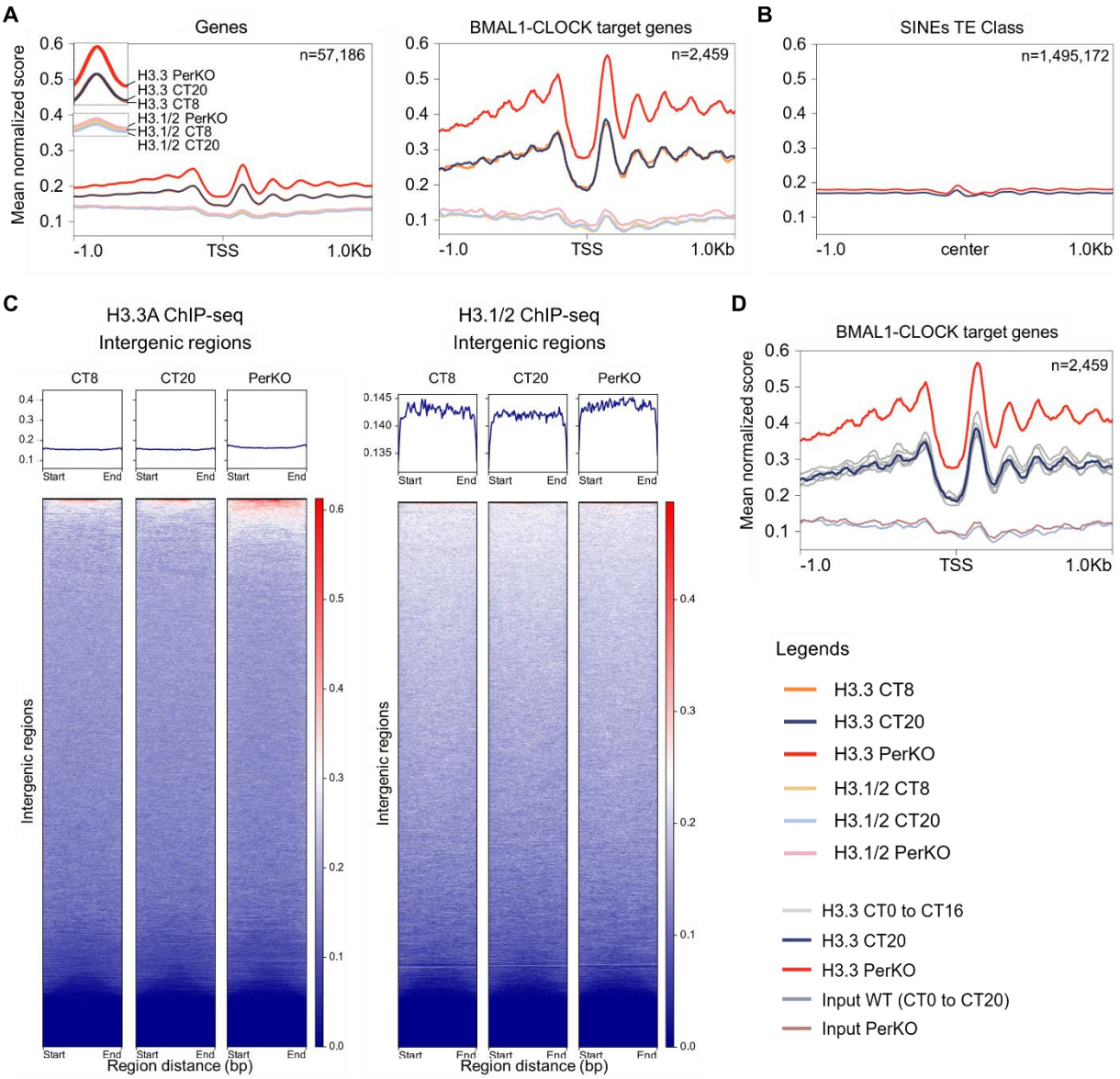


Figure 16. H3.3A enrichment on wild-type vs. PerKO chromatin. (A) Native FH-H3.3A and H3.1/2 ChIP-seq in FH-H3.3A wild-type and PerKO livers at TSS of all genes and BMAL1-CLOCK target genes, plotted on the same graph. (B) H3.3A nucleosome occupancy at SINE repeats in wild-type and PerKO livers. Highlighted is H3.3A enrichment at CT20 in blue and in PerKO in red. Y-axis corresponds to the mean of normalized scores per genomic region. X-axis represents the distance from the TSS (A) or the center of the SINE region (B) (± 1kb). (C) H3.3A and H3.1/2 enrichment at intergenic regions. Y-axis corresponds to the mean of normalized scores per genomic regions. X-axis represents the region distance in bp. Heat-map represents an alternative visualization of H3.3A and H3.1/2 enrichment at intergenic regions. (D) Enrichment of H3.3A nucleosomes in wild-type and PerKO livers compared to the respective inputs. Highlighted is H3.3A enrichment at CT20 in blue compared to the enrichment in PerKO in red and respective inputs; CT0-CT16 are represented in light grey, as indicated in the legend. ChIP-seq graph axes were represented as indicated previously in (A). All results were obtained from *n* = 3 independent biological replicates.

Since not all BMAL1-CLOCK target genes are expressed in the same phase, we analyzed H3.3A occupancy at TSS generating rhythmic transcripts that are either in-phase or out-of-phase with BMAL1 binding, as well as arrhythmic transcripts as defined in [226]. While overall enrichment of H3.3A nucleosomes was noted in all three transcript subclasses in PerKO chromatin, differences in nucleosome positioning were observable. Well-positioned H3.3A nucleosomes were enriched downstream of the TSS that generate transcripts in-phase with BMAL1 binding, whereas the two other subclasses displayed TSS-flanking nucleosomes (Figure 17).

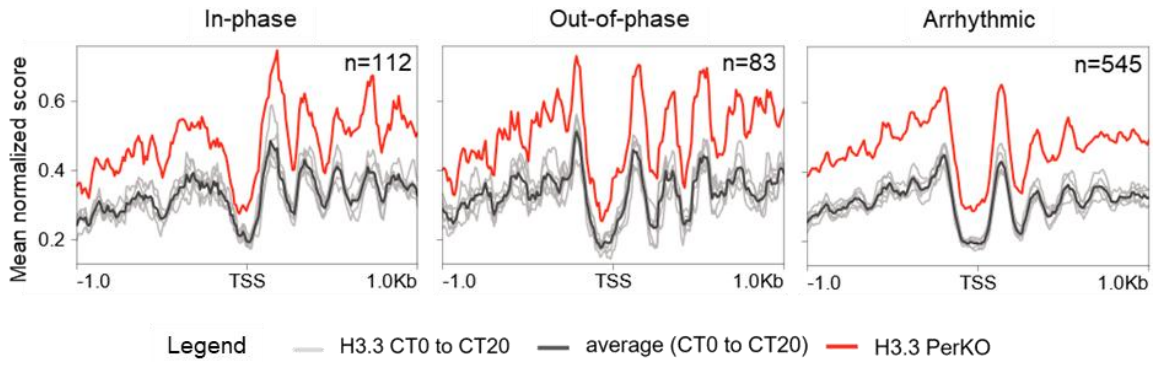


Figure 17. H3.3A occupancy at rhythmic transcripts in wild-type vs. PerKO livers. Mean H3.3A occupancy at TSS of BMAL1-CLOCK targeted rhythmic transcripts in-phase, out-of-phase and arrhythmic transcripts in wild-type and PerKO. Y-axis corresponds to the mean of normalized scores per genomic region. X-axis represents the distance from the TSS (± 1kb). Results were obtained from *n* = 3 independent biological replicates.

Moreover, H3.3 is also known to mark MNase sensitive CTCF sites, particularly in the context of H3.3/H2A.Z dual-variant nucleosomes [233, 234, 235]. We therefore assessed H3.3A occupancy at CTCF sites and found that H3.3A nucleosomes were highly enriched at CTCF sites associated with target genes that contained either BMAL1-CLOCK binding sites or were co-enriched for PER2 and BMAL1 relative to the genome-wide background (all CTCF sites) in wild-type, and even more enriched in PerKO liver chromatin (Figure 18).

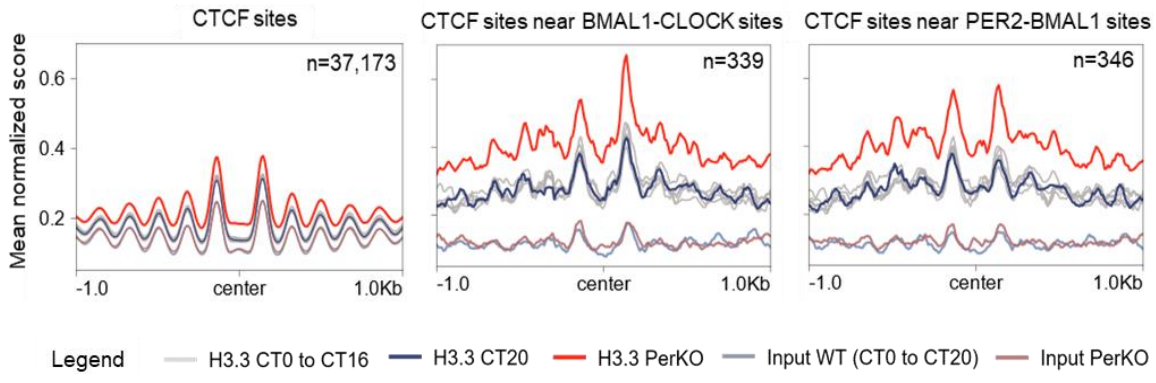


Figure 18. H3.3A occupancy at CTCF sites in wild-type vs. PerKO livers. Mean H3.3A occupancy at CTCF sites alone or CTCF sites overlapping with BMAL1-CLOCK and PER2-BMAL1 binding sites. Y-axis corresponds to the mean of normalized scores per genomic region. X-axis represents the distance from the center of the site (± 1kb). Results were obtained from *n* = 3 independent biological replicates.

3. Reorganization of chromatin remodelers upon circadian disruption

3.1 Loss of ARID2 leads to PBAF complex disassembly in the absence of PER

Given the previously observed rearrangements of H3.3A chromatin architecture and a significant decrease in key PBAF components in FH-H3.3A complexes in PerKO livers (Table 14, Figure S3), we hypothesized that PBAF complex assembly on H3.3 chromatin might be altered in the absence of circadian negative feedback.

To investigate this, we performed native HA-tag IP experiments on soluble chromatin from FH-H3.3A$^{+/-}$ wild-type and H3.3A$^{+/-}$ PerKO livers, using non-tagged wild-type liver chromatin as negative controls, as described previously. Consistent with our previous findings (Figure 14A), H3.3A interaction with specific PBAF components and BRG1 ATPase was slightly higher during the subjective day at CT8, when compared to CT20, along with BMAL1 present within H3.3A complexes specifically during the daytime (see Quantification of immunoprecipitation experiments in the Supplementary Materials section). These interactions were considerably reduced in PerKO livers, and a near-total depletion of ARID2, along with the reduction in BRG1 subunit in PerKO nuclear extracts indicated disruption of PBAF complex assembly (Figure 19A). Despite the reduction in ARID2 and BRG1, total PBRM1 protein levels were unaffected in PerKO liver tissues (input fractions).

Therefore, to confirm depletion of PBAF complexes in PerKO livers, we immunoprecipitated endogenous PBRM1 complexes from FH-H3.3A$^{+/-}$ wild-type and H3.3A$^{+/-}$ PerKO livers collected both at CT8 and CT20, using an isotype-matched IgG antibody as a negative control. We found that upon circadian clock disruption, PBRM1 failed to interact with ARID2, BRD7, PHF10 and its interaction with BRG1 was as well highly reduced, resulting in PBAF complex disassembly. BMAL1 was found enriched within the daytime PBAF complexes and was no longer detectable in PBRM1 complexes in the absence of PBAF, in PerKO livers (Figure 19B). In addition, PBRM1-associated PBAF complexes were enriched for H3.3A at CT8, while H2A.Z was detected at both CT8 and CT20 time points. In contrary, PBRM1 no longer interacted with H3.3A or H2A.Z in PerKO livers (Figure 19B).

These findings suggest that PBAF and BMAL1 complexes associate mainly with daytime chromatin marked by H3.3 nucleosomes. Thus, the decrease of ARID2 and BRG1 in PerKO livers disrupts the PBAF and very likely cBAF/BRG1 complexes on chromatin.

Moreover, observed reduction in specific PBAF and BRG1 subunits in PerKO livers appears to be independent of transcriptional regulation, since no significant differences were observed between wild-type and PerKO livers for the key components *Pbrm1*, *Arid2*, *Brd7*, *Phf10*, and the *Brg1* ATPase subunit at mRNA levels (Figure 19C). As a control, *Per1* mRNA levels were depleted as expected, consistent with the disruption of circadian feedback in PerKO tissues. Thus, these findings suggest that the loss of PBAF and BRG1 subunits in PerKO livers would very likely arise from post-translational mechanisms, being consistent with previous studies implicating similar pathways in chromatin remodeler subunit dynamics [142, 155].

3.2 Remodeler 'switch' to cBAF/BRM complexes marks the clock-disrupted state in PerKO livers

Could a remodeler switch to canonical BAF complexes replace the PBAF loss of function in PerKO livers? In melanoma cell lines, ARID2 depletion leads to PBAF complex disassembly and redistribution of remaining subunits, followed by a remodeler switch from PBAF to cBAF complexes. This switch is associated with increased chromatin accessibility, as well with enhanced binding of adjacent transcription factors [236]. Given the reduction of ARID2 in PerKO soluble chromatin, we hypothesized that a similar switch to cBAF remodeler complexes might occur to regulate BMAL1 function in the absence of PER.

To address this, we performed native BRG1 and BRM IP experiments on soluble chromatin from FH-H3.3A$^{+/-}$ wild-type and H3.3A$^{+/-}$ PerKO livers as before and analyzed the purified cBAF complexes for the presence of BMAL1 and ARID1B subunit (Figure 20). BMAL1 co-immunoprecipitated with BRG1-associated complexes during the active clock phase at CT8. In contrary, BMAL1-BRG1 interaction was reduced at CT20 and lost in PerKO livers (Figure 20A). ARID1B co-immunoprecipitated with BRG1 at both, CT8 and CT20 time points. In PerKO livers, we observed a decrease in BRG1 and ARID1B protein levels in nuclear extracts (input fractions), resulting in disrupted assembly of cBAF/BRG1 complexes (Figure 20A). Interestingly, despite the notable reduction of ARID1B subunit in total protein levels in PerKO input fraction, cBAF/BRM complex assembly remained unaffected in the absence of PER (Figure 20B). Moreover, BMAL1 co-immunoprecipitated with BRM at CT8 and CT20, and surprisingly BRM-BMAL1 interaction remained unaffected in PerKO livers (Figure 20B). Consistent with these findings, ChIP-qPCR experiments revealed that BRG1 ChIP levels were significantly reduced in PerKO livers, while no significant differences were observed for BRM ChIP levels at E-boxes of clock genes (*Per1*, *Per2*, *Cry2*), as well as clock-target genes (*Dbp, Rev-erbα* and *Rorc*) (Figure 20C, D). All of these suggest that ARID2 and BRG1 depletion in PerKO livers leads to PBAF and cBAF/BRG1 complex disassembly, followed by a remodeler 'switch' to cBAF/BRM complexes. In addition, maintenance of cBAF/BRM-BMAL1 complexes could very likely target BMAL1 at E-boxes in the absence of circadian negative feedback.

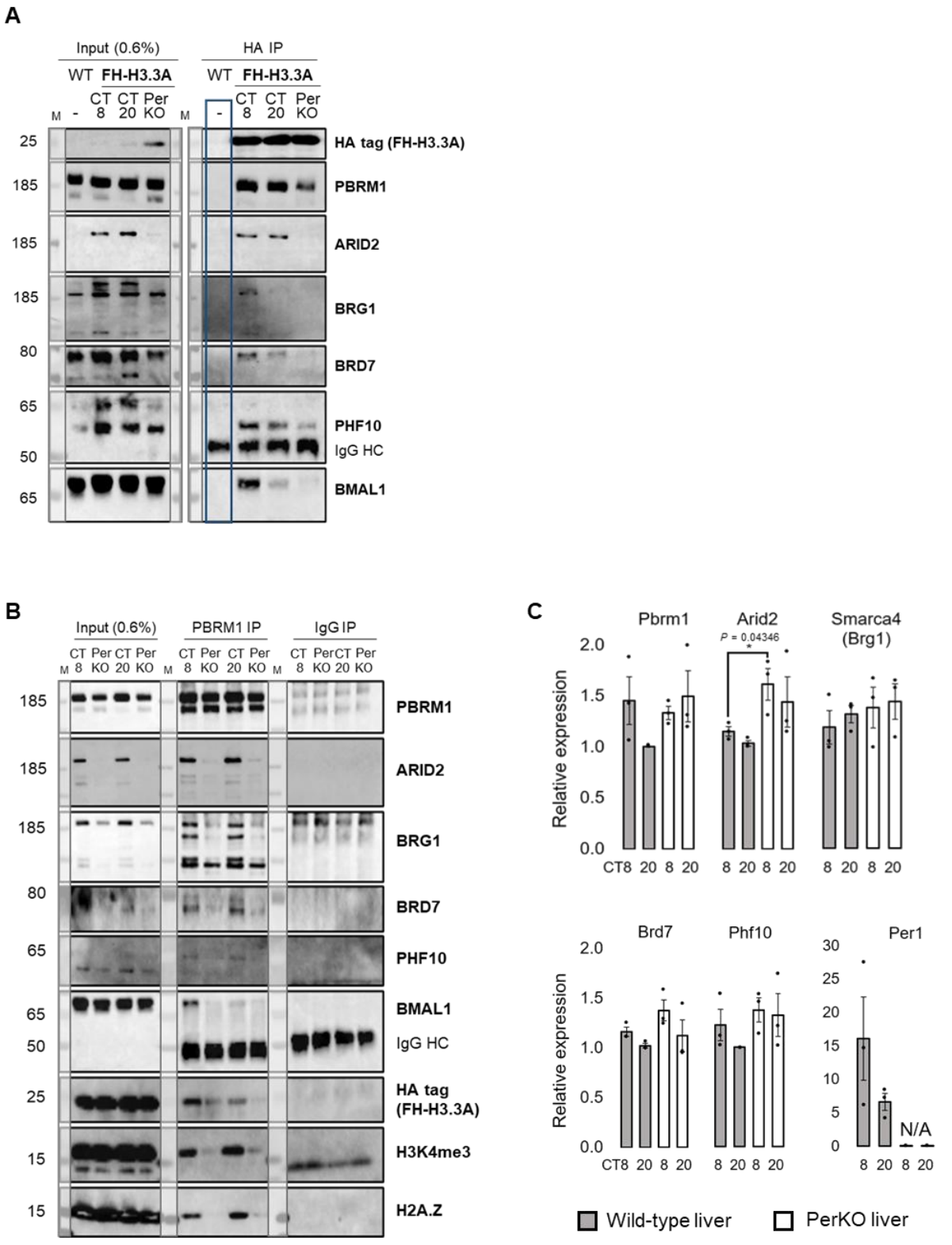


Figure 19. Disassembly of H3.3-PBAF-BMAL1 complexes in PerKO livers. (A) Native HA-tag IP on soluble FH-H3.3A wild-type and PerKO chromatin. Non-tagged wild-type chromatin was used as a negative control (indicated in blue box). (B) Native PBRM1 IP on soluble FH-H3.3A wild-type and PerKO chromatin. IgG antibody was used as a negative control. Immunoblotting was performed for HA epitope (FH-H3.3A), specific PBAF complex components, BRG1 and BMAL1 (A,B). M corresponds to the protein

ladder; sizes are indicated in kDa. Results are representative of *n* = 3 to 4 independent biological replicates. (C) mRNA relative expression levels of specific PBAF components and shared ATPase subunit *Brg1* normalized to *Rps9*; *Per1* was used as control. Results are represented as mean ± SEM with individual points indicated for each replicate. P-values were calculated for all PBAF components between wild-type CT8 and PerKO CT8, and between wild-type CT20 and PerKO CT20 with paired, one-tailed Welch's (unequal variance) t-test; P-values were not significant, except for *Arid2* CT8 time point; **P* = 0.04346. Results are representative of *n* = 3 independent biological replicates.

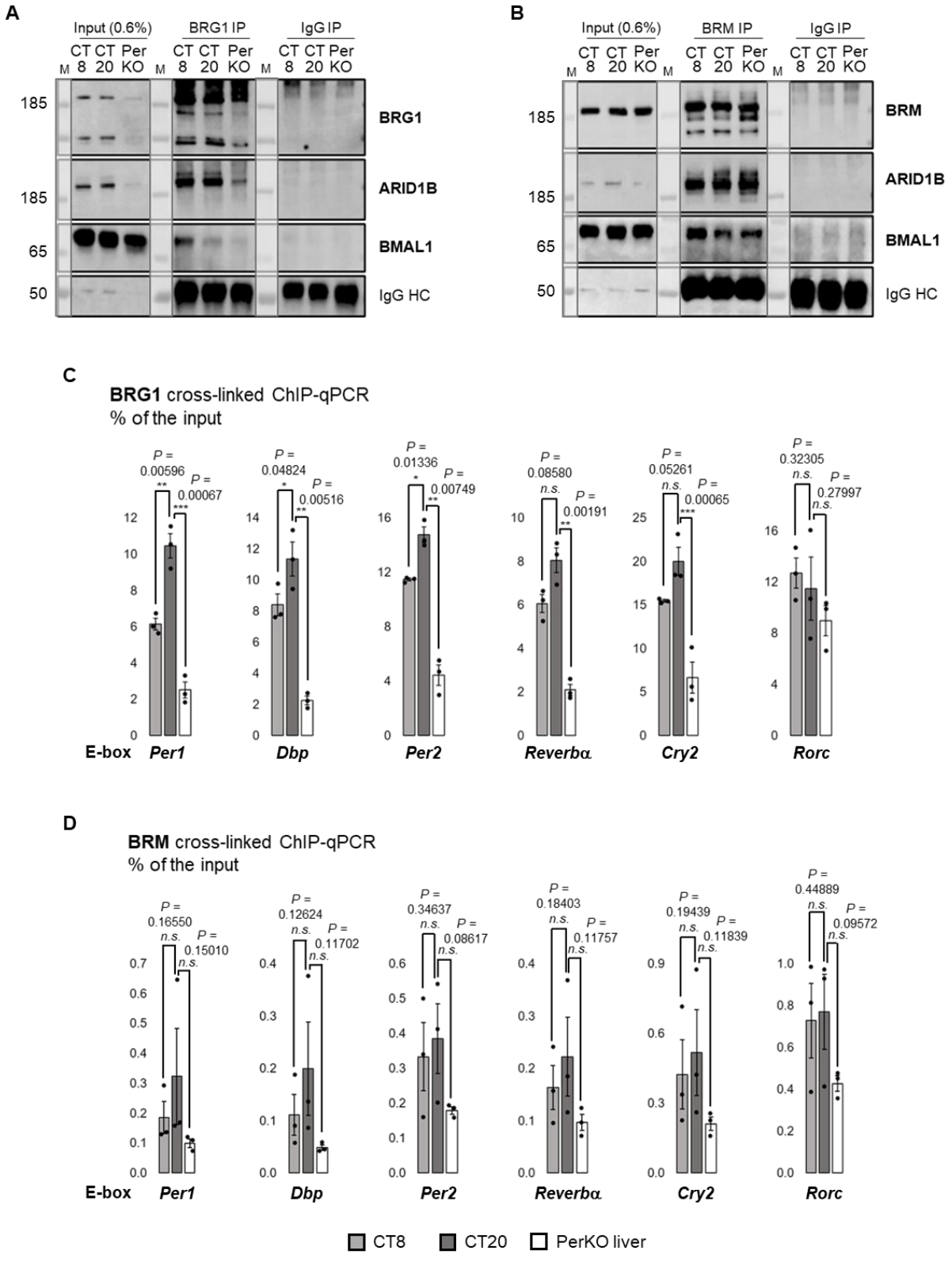


Figure 20. Remodeler switch from PBAF-cBAF/BRG1 to cBAF/BRM in the absence of PER. (A) Native BRG1 IP and (B) native BRM IP on soluble FH-H3.3A wild-type and PerKO chromatin. IgG antibody was used as a negative control. 0.6% of the nuclear extracts were loaded as Input. Immunoblotting was performed for BRG1 (A), BRM (B), ARID1B (specific BAF complex component) and BMAL1 (A,B). M corresponds to the protein ladder; sizes are indicated in kDa. Results are representative

of *n* = 3 independent biological replicates. (C,D) BRG1 and BRM cross-linked ChIP-qPCR. Enrichment at *Per1*, *Dbp*, *Per2*, *Rev-erbα*, *Cry2* and *Rorc* E-boxes was assessed, calculated as percentage of the input. Results are represented as the average ± SEM of *n* = 3 independent biological replicates. P-values were calculated either with paired, one-tailed t-test or paired Welch's (unequal variance) t-test.

4. Alterations in fragile H3.3A chromatin states and BMAL1 binding

Complexes from the mSWI/SNF family display different preferences for histone PTMs and histone variants. Thus, the composition of a given nucleosome dictates preferential binding of either PBAF or cBAF complexes to chromatin. Active PBAF complexes have a strong preference for histone H3 PTMs (*e.g.* H3K115ac, H3K122ac) and dual-variant H3.3/H2A.Z nucleosomes [156]. Moreover, it has been shown that H3K115ac and H3K122ac lateral surface PTMs, mark fragile H3.3 nucleosomes and are linked to active chromatin states [237, 238]. We therefore wondered how fragile H3.3A nucleosomes shape 24h chromatin landscapes and how these could be altered in the absence of negative feedback.

4.1 BMAL1-CLOCK is recruited to fragile H3.3 nucleosomes during the active phase

BMAL1-CLOCK is known to function as a pioneer transcription factor, binding directly to nucleosomes, interacting with the acidic patch, to remodel chromatin [181, 239]. We hypothesized that BMAL1-CLOCK recognizes fragile H3.3 nucleosomes marked by H3K115ac and H3K122ac and aimed to determine whether this interaction is altered in PerKO livers.

To address this, we used the HA-tag IP from Figure 13 and analyzed the purified complexes for these specific acetyl marks, as well as H3K4me3 associated with active promoters (Figure 21). We found that homotypic H3.3 nucleosomes were marked with H3K4me3, H3K115ac/H3K122ac marks during the active clock phase at CT8. We observed near complete loss of these marks 12h later, at CT20 during the repressive clock phase. Surprisingly, chromatin from PerKO livers was enriched for fragile H3K115ac/H3K122ac nucleosome marks, including the active H3K4me3 mark, reflecting a persistent daytime-like 'active' chromatin state (Figure 21). However, BMAL1-CLOCK co-immunoprecipitated with fragile H3K115ac/H3K122ac-marked homotypic H3.3 nucleosomes only during the active clock phase in wild-type, and failed to bind fragile H3.3 nucleosomes in PerKO livers, despite the persistent 'daytime-like' dual-variant chromatin state (Figure 21).

Observation that FH-H3.3A nucleosomes did not co-immunoprecipitated canonical H3.1/2 histones suggested that BMAL1-CLOCK binding favors the H3.3 variant and remodeling by PBAF/cBAF complexes in wild-type livers. Interestingly, the noted increase in H3.3 deposition in PerKO chromatin (Figure 16A, B, D) was not reflected in higher levels of H3.3A mRNA expression (Figure 22A), neither in H3.3A total protein levels, which remained unchanged across most replicates (N > 6, Figure 22A). We therefore wondered if changes in

H3.3-specific chaperones could explain the higher loading of H3.3 in PerKO chromatin. However, the nuclear protein levels of the primary H3.3 chaperones, HIRA and DAXX, were not consistently altered across multiple samples (*n* = 4, Figure 22B).

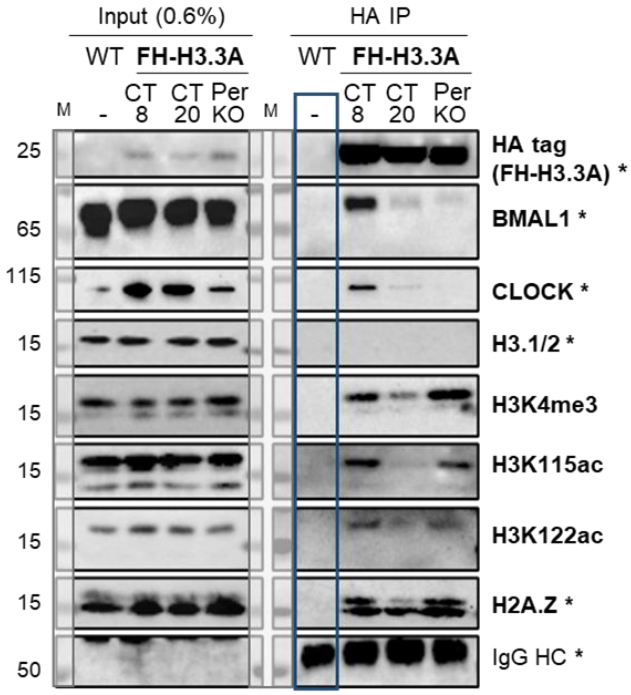


Figure 21. Day-time specific fragile H3.3A nucleosomes mark clock-disrupted chromatin. Native HA-tag IP on soluble FH-H3.3A wild-type and PerKO chromatin. Non-tagged wild-type chromatin was used as a negative control (indicated in blue box). 0.6% of the nuclear extracts were loaded as Input. Immunoblotting was performed for HA epitope (FH-H3.3A), BMAL1, CLOCK, H3.1/2, H2A.Z (as shown in Figure 13, marked with *) and for H3K4me3, H3K115ac, and H3K122ac. M corresponds to the protein ladder; sizes are indicated in kDa. Results are representative of *n* = 3 independent biological replicates.

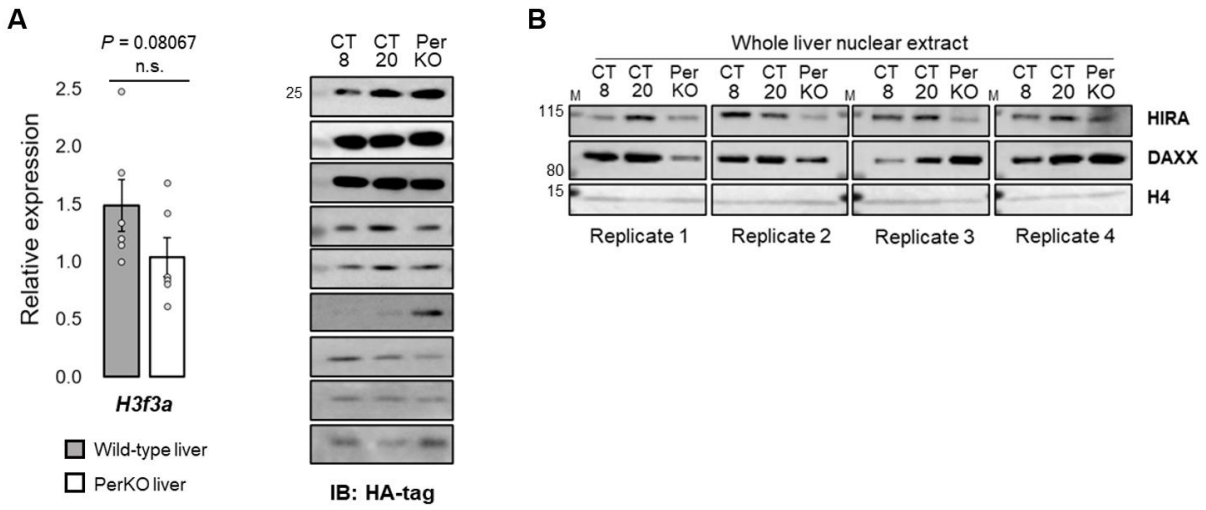


Figure 22. Expression levels of H3.3A and its specific chaperones. (A) mRNA relative expression levels of *H3f3a* normalized to *Rps9*. Shown is the average of *H3f3a* relative expression at CT8 and CT20

in wild-type and PerKO livers. Results are representative of *n* = 3 independent biological replicates and represented as mean ± SEM, with individual points indicated for each replicate. P-value between wild-type and PerKO was calculated with paired, one-tailed t-test; *P-value = 0.08067*, non-significant. In addition, shown are protein levels of H3.3A in input fractions across multiple experiments. (B) HIRA and DAXX nuclear protein levels at day- vs. night-time points in wild-type and PerKO livers. 5ug of total nuclear proteins were loaded; H4 was used as loading control. M corresponds to the protein ladder; sizes are indicated in kDa. Shown are results from *n* = 4 independent biological replicates.

4.2 Identification of two different subsets of H3K115ac-marked fragile nucleosomes

We next wondered if overall H3K115ac-marked nucleosomes retained BMAL1-CLOCK in PerKO chromatin. To address this, we purified endogenous H3K115ac nucleosome complexes from FH-H3.3A$^{+/-}$ wild-type and H3.3A$^{+/-}$ PerKO livers as described before, using an antibody that is not able to distinguish between canonical H3.1/2 and the H3.3 variant. Native H3K115ac pull-down revealed two different subsets of fragile nucleosomes that harbor either the H3.3 and/or H3.1/2 canonical histones (Figure 23). Moreover, we found that BMAL1 and CLOCK proteins consistently associate with H3K115ac-marked fragile nucleosomes at subjective day and night-time in the wild-type, as well in PerKO chromatin. In addition, H3K115ac co-immunoprecipitated with H3.3A, H2A.Z, and H3K122ac marks in all conditions. These findings indicate that circadian TF complexes interact with canonical and variant H3 nucleosomes that are indeed fragile.

We as well analyzed the H3K115ac complexes for components of the SWI/SNF remodeler subunits and found, that fragile H3K115ac nucleosomes retained PBAF (PBRM1, ARID2) and shared BRG1/BRM ATPase subunits at both CT8 and CT20 (Figure 23). However, consistent with the overall reduction of ARID2 and BRG1 protein levels in PerKO livers observed earlier, assembly of the PBAF and cBAF/BRG1 complexes was disrupted on H3K115ac nucleosomes in the absence of PER. Remarkably, cBAF/BRM complex assembly on H3K115ac nucleosomes remained unaffected in PerKO chromatin, suggesting a preferential interaction of BRM remodelers with fragile canonical or variant H3 nucleosomes independently of circadian feedback (Figure 23).

4.3 Fragile H3.3 chromatin in PerKO livers enhances BMAL1 E-box accessibility

We therefore wondered whether increased loading of fragile H3.3 nucleosomes in PerKO chromatin, as well as the maintenance of cBAF/BRM-BMAL1 remodeling complexes would impact BMAL1 binding in the absence of PER. To address this, we performed native BMAL1 ChIP-seq on soluble mononucleosome-enriched chromatin from FH-H3.3A$^{+/-}$ wild-type and H3.3A$^{+/-}$ PerKO livers collected at CT8 and CT20 (Figure 24). Unlike for crosslinked BMAL1 ChIP-seq [51], we observed only a weak enrichment of BMAL1 on chromatin. Nevertheless, BMAL1 was enriched at H3.3 nucleosome positions that flank BMAL1-CLOCK sites, with a

greater signal at CT8 centered on the binding site as well as on the flanking nucleosomes (Figure 24A). Strikingly, PerKO chromatin revealed significantly enhanced BMAL1 enrichment centered at BMAL1-CLOCK sites (Figure 24B).

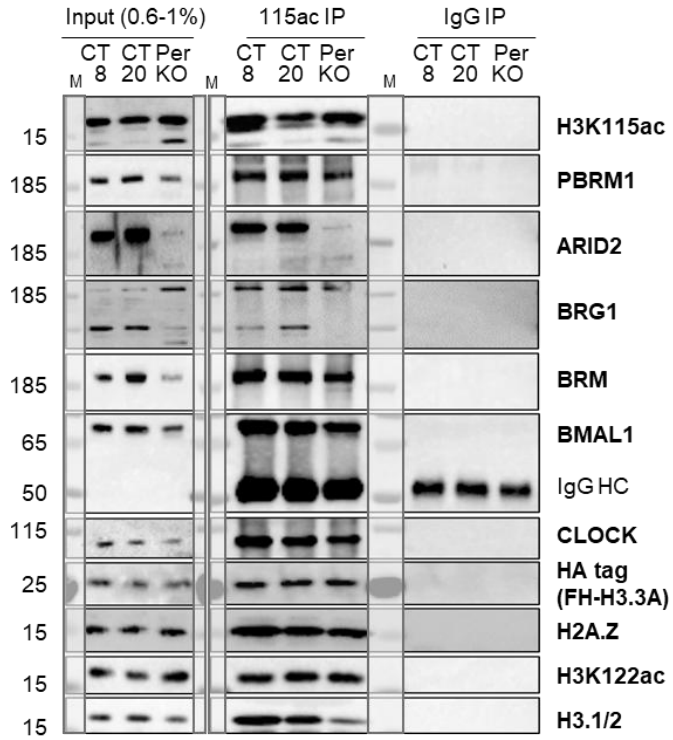


Figure 23. cBAF/BRM-BMAL1 complexes assemble with H3K115ac-marked fragile nucleosomes in PerKO. Native H3K115ac IP on soluble FH-H3.3A wild-type and PerKO chromatin. IgG antibody was used as a negative control. 0.6-1% of the nuclear extracts were loaded as Input. Immunoblotting was performed for H3K115ac, PBAF/cBAF components, BMAL1, CLOCK, HA epitope (FH-H3.3A), H2A.Z, H3K122ac and H3.1/2. M corresponds to the protein ladder; sizes are indicated in kDa. Results are representative of *n* = 3 independent biological replicates.

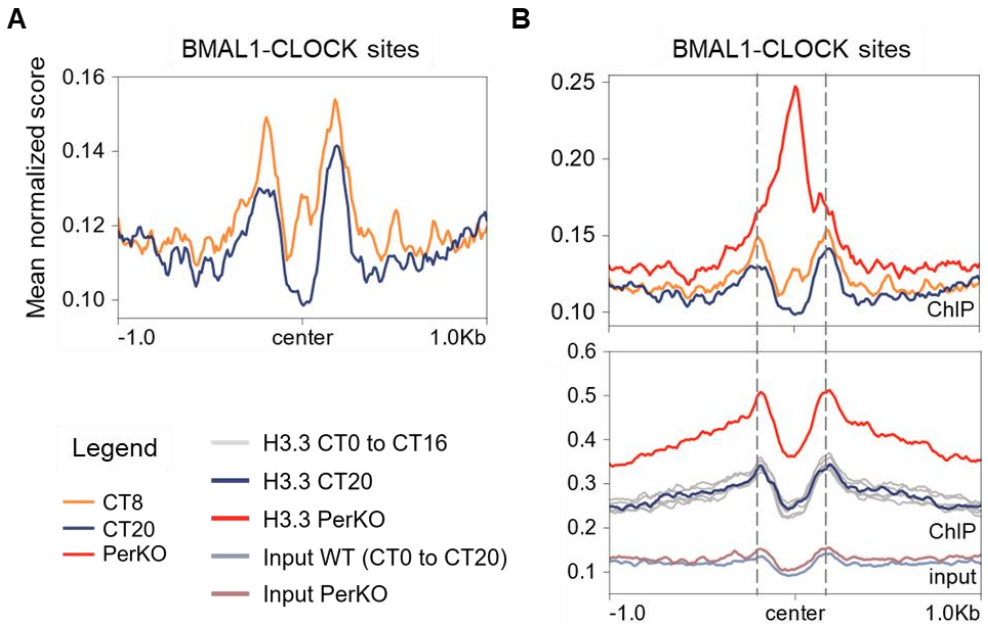


Figure 24. Circadian clock disruption leads to enhanced BMAL1 binding on chromatin. Mean BMAL1 (A, B- upper panel) and H3.3A (B- lower panel) occupancy at circadian E-boxes at CT8 and CT20 on FH-H3.3A wild-type and PerKO chromatin. Y-axis corresponds to the mean of normalized scores per genomic regions. X-axis represents the distance from the center of BMAL1-CLOCK binding site (± 1kb). Each color represents a given CT, with orange for the day-, blue for the night-time points, and red for the PerKO, as indicated in the legend. Results were obtained from *n* = 3 independent biological replicates.

These findings suggest that the fragile H3.3 chromatin landscape and altered remodeling dynamics in PerKO livers render BMAL1-CLOCK binding sites more accessible. The reduced association of BMAL1 with H3.3 complexes in PerKO chromatin (Figure 13) could potentially be explained by BMAL1 targeting to E-boxes located within linker DNA regions, by the presence of differentially modified subtype of H3.3 nucleosomes, and/or an increased BMAL1 turnover at these sites.

4.4 BMAL1 turnover in the absence of circadian feedback

It is known that BMAL1 activity is high in the absence of circadian negative feedback [240, 241]. We therefore wondered whether the increase in BMAL1 binding on PerKO chromatin could be linked with an increase in its turnover.

We first aimed to determine endogenous BMAL1 protein levels on PerKO liver chromatin. While BMAL1 protein levels peaked at CT8 in the wild-type animals as expected, we observed an appreciable enrichment of BMAL1 on PerKO chromatin when compared to CT20 in the wild-type (Figure 25A). Next, to address whether BMAL1 turnover on chromatin is higher in the absence of PER, we treated wild-type and *Per1*$^{-/-}$, *Per2*$^{-/-}$, *Per3*$^{-/-}$ triple knockout (PerTKO) fibroblasts with proteasome inhibitor MG132. Since BMAL1 stability and turnover

are regulated by the ubiquitin-proteasome pathway [242], we hypothesized that upon proteasome inhibition, we might stabilize and capture more BMAL1 on chromatin (Figure 25B). While overall BMAL1 protein levels were reduced in PerTKO cells, BMAL1 chromatin levels were slightly increased following MG132 treatment.

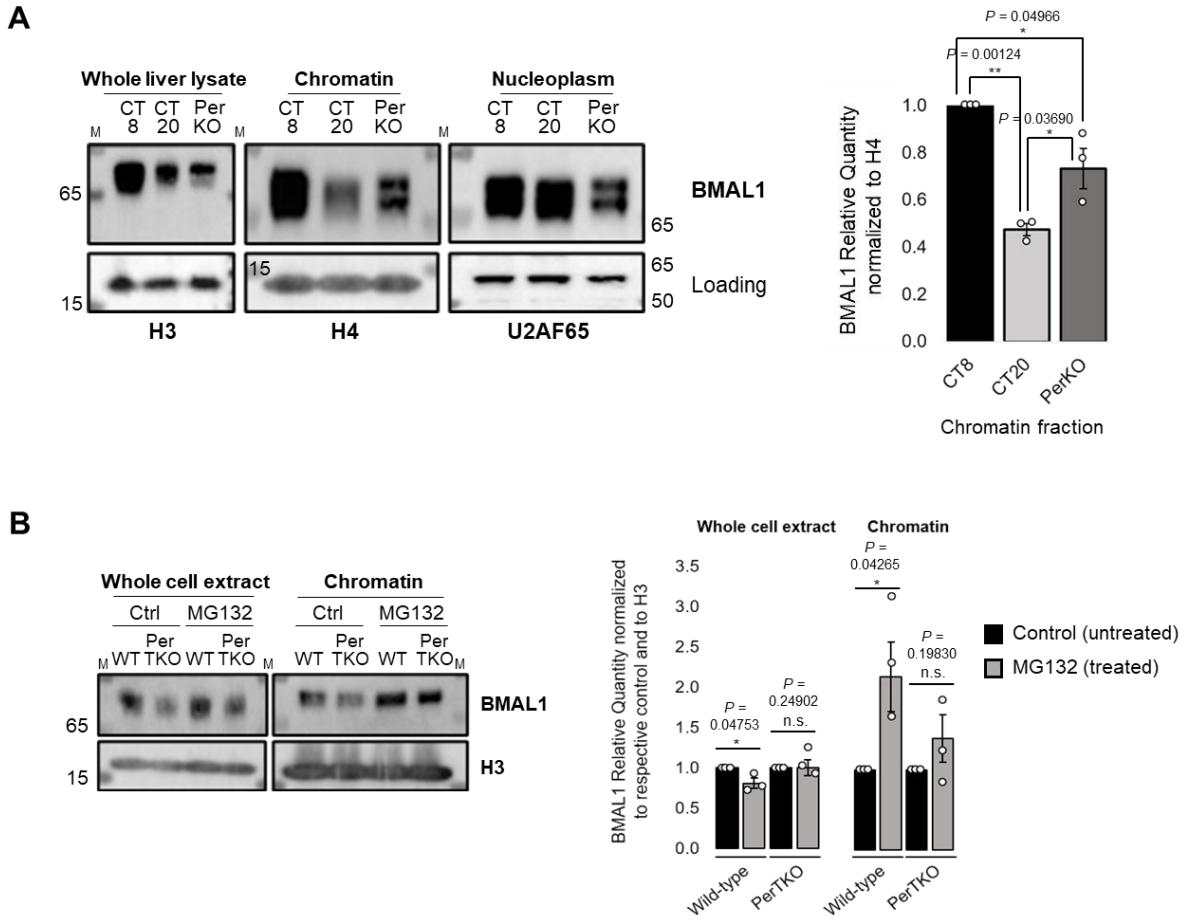


Figure 25. Presence and turnover of BMAL1 on chromatin in PerKO. (A) BMAL1 protein levels in whole liver lysate, chromatin and nucleoplasm fractions. 15ug of protein were loaded; H3, H4 and U2AF65 were used as loading controls. Bar graph shows the mean ± SEM of BMAL1 relative quantity on chromatin normalized to H4 (and setting CT8 as reference at 1), with individual points of normalized ratios indicated for each replicate. (B) BMAL1 protein levels in wild-type or PerTKO lung fibroblasts. 3ug of protein were loaded for the whole cell extract and 10ug for chromatin; H3 was used as loading control. BMAL1 levels are shown in untreated (Ctrl) or treaded (MG132) cells with proteasome inhibitor MG132 at 10uM 4h prior extraction. Bar graph shows the mean ± SEM of BMAL1 relative quantity on chromatin normalized to H3, and to the control samples respective to each condition, with individual points indicated for each replicate. P-values were calculated with paired, one-tailed t-test (A) or with paired, one-tailed Welch's (unequal variance) t-test (B). Results are representative of *n* = 3 independent biological replicates. M corresponds to the protein ladder; sizes are indicated in kDa.

5. Impact on circadian clock function

5.1 Role of H3.3 in circadian clock function

Finally, we aimed to understand whether H3.3 plays a role in circadian clock function. As both *H3f3a* and *H3f3b* encode identical H3.3 proteins, we generated H3.3A and H3.3B knockout mouse embryonic fibroblasts (MEFs) by crossing homozygous floxed strains.

To determine if H3.3 is important for clock function, the double-floxed MEFs were stably transduced with a Bmal1:Luciferase reporter and a Tamoxifen-inducible Cre recombinase. Tamoxifen treatment resulted in a significant reduction of H3.3 protein levels within 4 days (Figure 26). Following the 4th day of tamoxifen treatment, we recorded bioluminescence from the confluent fibroblast cultures for 7 consecutive days. We observed that H3.3 depletion caused a significant shortening of the circadian period by nearly 2 hours when compared to the H3.3 wild-type (floxed) controls (Figure 26), indicating a critical role for the H3.3 variant in maintaining core oscillator function.

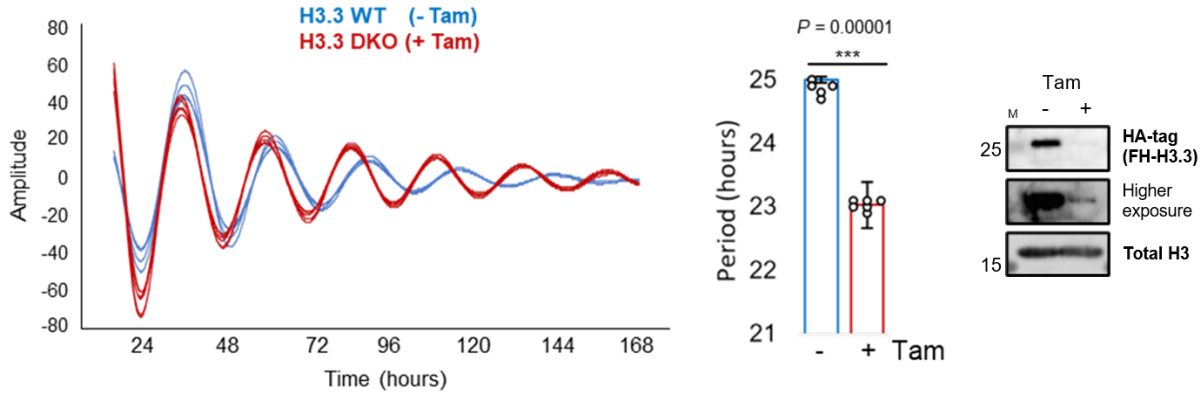


Figure 26. Impact of H3.3 on circadian clock function. Real-time bioluminescence recordings of synchronized wild-type f/f (in blue) and H3.3 double knock-out (in red) mouse embryonic fibroblasts expressing Bmal1:Luciferase reporter. Detrended analysis over 7d of measurements is shown. Results are representative of *n* = 5 (wild-type) and *n* = 6 (knock-out) replicates; the bar graph shows the calculated period length represented as mean ± SEM with individual points indicated for each replicate. P-value between wild-type and H3.3DKO was calculated with paired, one-tailed t-test; ****P* = 1.12542E-05. Knock-out efficiency was confirmed by western-blotting. M, protein ladder; sizes are indicated in kDa

5.2 Impact of specific PBAF/cBAF components on circadian rhythms

Given the observed reorganization of H3.3 chromatin landscapes and remodeling complexes in PerKO, we wondered whether loss of PBAF/cBAF specific and shared ATPase subunits could result in alterations of circadian rhythms. To address this, we analyzed previously published datasets for circadian clock modifiers [229]. Overall, loss of SWI/SNF subunits had limited effects on circadian clock function (Figure 27).

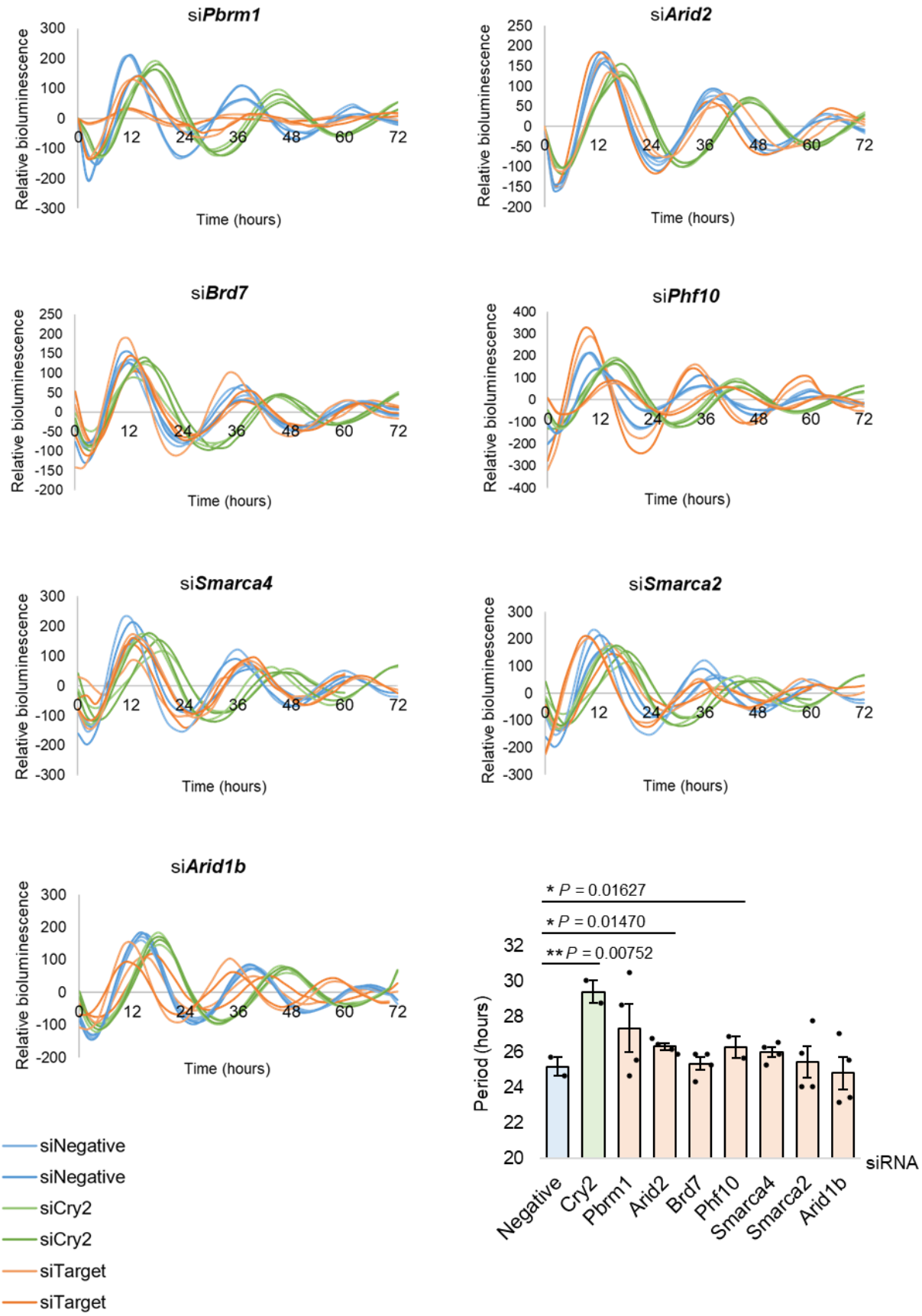


Figure 27. Reanalysis of published datasets for PBAF and BAF specific components siRNA screens. Real-time bioluminescence recordings of Bmal1: Luciferase rhythms is U2OS cell line post-

knock-down of specific PBAF and BAF components, reanalyzed from published datasets of genome-wide siRNA screens [229]. Shown are negative control siRNA (blue), *Cry2* siRNA (green) and specific PBAF or BAF components as target siRNA (orange). Y-axis represents relative bioluminescence and X-axis the time of recordings in hours. Every available replicate for a given siRNA on corresponding plate was taken into account for the analysis. Statistical analysis for period length was performed with available data from the published study [229]. Results are represented as mean ± s.e.m. with individual points indicated for all available replicates. P-values were calculated with paired, one-tailed t-test, comparing the negative siRNA to target siRNA values. Significant P-values are directly marked on the graph: positive control *Cry2*, ***P* = 0.00752; *Arid2*, **P* = 0.01470; *Phf10*, **P* = 0.01627. Remaining P-values were not significant: *Pbrm1*, *P* = 0.10539; *Brd7*, *P* = 0.41778; *Smarca 4*, *P* = 0.06671; *Smarca2*, *P* = 0.38670; *Arid1b*, *P* = 0.37158.

Discussion

Proposed model, open questions and perspectives

Taken all together, we describe and propose a model, in which dynamic fragile H3.3 nucleosomes establish time-specific chromatin landscapes promoting assembly of BMAL1-CLOCK and PBAF-cBAF/BRG1 remodeling complexes (Figure 28A). We find that H3.3 deposition/eviction is dynamic over time, peaking during the active phase of circadian cycle, between CT0 and CT8. The day-time H3.3 nucleosomes are enriched in lateral surface histone marks, such as H3K115ac and H3K122ac, rendering them highly mobile and unstable (fragile) [237, 238]. We also found that such nucleosomes are marked by the active H3K4me3 mark during the subjective day-time at CT8. Observed rhythmicity in H3.3 deposition and related PTMs is concomitant with the active transcription phase in murine livers [51]. Fragile H3.3 nucleosomes assist BMAL1-CLOCK binding and therefore contribute to circadian transcriptional activation. In addition, PBAF complexes assemble rhythmically along with BMAL1 transcription factor on H3.3 variant chromatin during the active clock phase at CT4 and CT8 (Figure 14). Observed subsequent decrease in H3.3 nucleosomes at clock *loci* at CT12 (Figure 15A, B) suggests active remodeling of these nucleosomes by the PBAF complex. Additional SWI/SNF cBAF remodeling complexes dynamically assemble with BMAL1. While BMAL1 association with the cBAF/BRG1 remodeler remains specific to the subjective day-time phase, peaking on chromatin at CT8, the assembly of cBAF/BRM-BMAL1 complexes happens during both, the subjective day- and night-time phases.

Circadian clock disruption results in overall increase of H3.3 loading on chromatin in PerKO livers, including clock *loci*. These nucleosomes maintain their fragility, establishing ‘day-time like’ chromatin landscapes. Despite the ‘day-time like’ chromatin states favored in PerKO livers, we found that circadian clock disruption is accompanied by structural reorganization of remodeling complexes (Figure 28B). In the absence of PER, we observe a nearly-total depletion of ARID2 and BRG1 shared ATPase subunits within the nucleus, resulting in disassembly of PBAF complexes. While no changes occur at mRNA levels for PBAF specific complex components upon PER removal, observed near-total loss of ARID2 at protein levels indicates that the inability to assemble PBAF complexes in the absence of negative feedback results very likely from post-translational modifications of ARID2 protein and/or alterations of its stability.

Could the loss of function of the PBAF complex be compensated by the remaining SWI/SNF BAF remodelers? Observed reduction of the shared ATPase BRG1 and cBAF-specific ARID1B subunits leads to disruption of the cBAF/BRG1 remodeling complexes along

with their interaction with BMAL1. Surprisingly, the assembly of the cBAF/BRM remodelers, as well as their association with BMAL1 remains unaffected in the absence of PER, suggesting that maintenance of cBAF/BRM remodelers favors BMAL1 ON/OFF chromatin states upon circadian clock disruption. In addition, we found that the absence of circadian negative feedback leads to increased BMAL1 binding on chromatin due to the increased accessibility of BMAL1-CLOCK binding sites, very likely rendered accessible by higher loading of fragile H3.3 nucleosomes. Moreover, the absence itself of the repressive phase mediated by PER results in higher BMAL1 activity as shown in previous studies [240, 241].

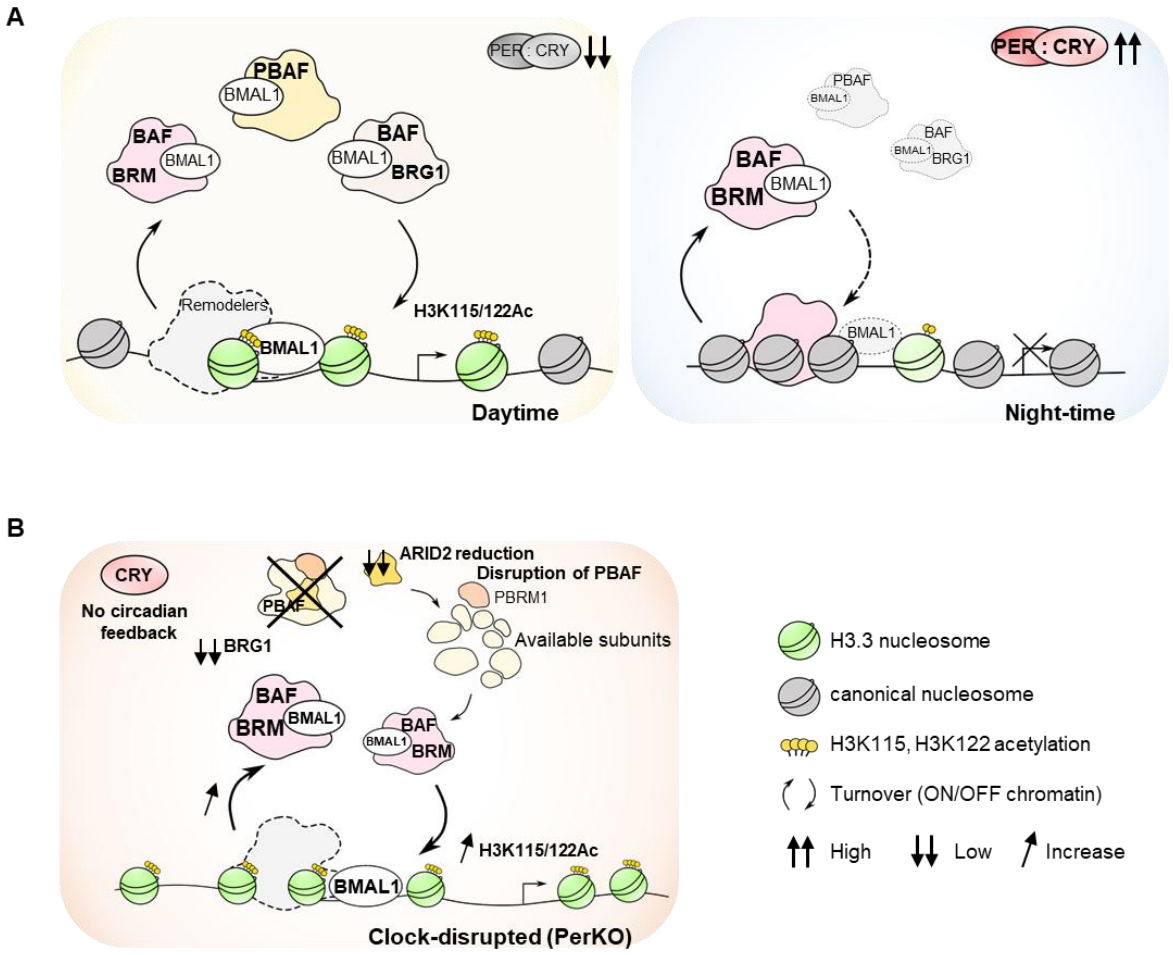


Figure 28. Proposed model illustrating changes in BMAL1 targeting on H3.3 variant chromatin in wildtype animals and in the absence of circadian negative feedback. (A) Under physiological conditions, fragile H3.3 nucleosomes are enriched at TSS and BMAL1- CLOCK binding sites during the active clock phase. These nucleosomes serve as regulatory hubs for assembly of BMAL1-SWI/SNF chromatin remodeling complexes (PBAF, cBAF/BRG1 and cBAF/BRM). In addition, BMAL1-cBAF/BRM complexes persist during the repressive clock phase. (B) Circadian clock disruption is characterized by enrichment of fragile H3.3 nucleosomes, along with the loss of PBAF and cBAF/BRG1 complexes. Such changes lead to more open, 'day-time like' chromatin states, increased BMAL1 binding and reorganization of SWI/SNF remodeling complexes. BMAL1-cBAF/BRM complexes remain unaffected

and target BMAL1 activity at its genomic binding sites, very likely rendered more accessible by higher loading of fragile H3.3 nucleosomes on chromatin.

All of these events characterize establishment of transcriptionally active, 'day-time like' chromatin states upon circadian clock disruption, implicating H3.3 variant and the cross-talk between the core-clock transcription factor BMAL1 and SWI/SNF chromatin remodelers. In addition, these rearrangements are reflective of the effect of loss of PER and thus, the absence of circadian negative feedback in general. Nevertheless, several outstanding questions remain regarding the role of H3.3 and chromatin remodelers in clock function.

In *Neurospora crassa*, dynamic assembly of the WCC with SWI/SNF BAF-like complexes at *frq* regulatory sites (C-boxes) is followed by rhythmic chromatin remodeling and activation of the *frq* gene expression [194]. Furthermore, authors show that such remodeling is accompanied by the loss of H3 containing nucleosomes within few hours at these regulatory sites [194]. These findings could suggest following outcomes: i) either the SWI/SNF complex rhythmically evicts H3 nucleosomes at C-boxes, generating straightforwardly nucleosome-depleted regions (NDR) during the initiation phase of transcription, or ii) very likely, evicted H3 containing nucleosomes could be replaced by the fragile nucleosomes marked with H3.3 (eviction of the H3-H4 dimer or tetramer, being subsequently replaced by H3.3-H4) to render chromatin more accessible during the initial stage of the clock active phase. In that case, the H3.3 histone variant would serve as a 'bookmark' for recruitment of SWI/SNF remodelers.

At the beginning of our investigation, we were wondering whether similar mechanism to WCC-mediated recruitment of SWI/SNF remodelers described in *Neurospora* could occur in murine livers, involving H3.3. By studying the link between PBAF/cBAF remodelers and H3.3A, along with the core-clock complexes, we discovered a mechanism underlying circadian transcriptional regulation by BMAL1-CLOCK.

In our study, we found that unlike H3 canonical nucleosomes, H3.3A containing nucleosomes are dynamically enriched at clock regulatory sites over 24h. Additionally, the overall increase of H3.3A nucleosomes at TSS of genes observed at CT8 and CT20 when compared to the canonical H3.1/2 histones in wild-type animals (Figure 15E) is very likely reflecting findings from previous studies, where authors showed that in healthy ('cancer-free') hepatocytes, the overall proportion of H3.3 variant is higher than the proportion of H3.1/2 [208]. Therefore, the observed dynamics of BMAL1-CLOCK day-time specific recruitment to H3.3A nucleosomes is most likely mediated by H3.3-specific H3K115 and H3K122 acetylation, since our purification of FH-H3.3A protein complexes revealed formation of homotypic H3.3 nucleosomes within these complexes (Figure 14A and Figure 21). To address and confirm if marked fragile H3.3A nucleosomes occupy the TSS of clock target genes, performing the ChIP-reChIP experiment, using anti-HA-tag antibody (for the initial ChIP), subsequently

followed by the use of anti-H3K115ac antibody (for the reChIP), would be highly informative. Moreover, to better understand the dynamics of homotypic H3.3 vs. heterotypic H3.3-H3.1/2 nucleosomes, instead of bioinformatically mapping the overlapping regions on the genome between FH-H3.3A and H3.1/2 ChIP-seq experiments that we performed independently, the variant-canonical H3 ChIP-reChIP could as well bring more accurate answers. Initially, I tried to uncover the dynamics of heterotypic H3.3A-H3.1/2 nucleosomes by performing sequential IP experiments and assessed the outcome by western-blotting. While FH-H3.3A IP followed by H3.1/2 IP systematically failed to detect canonical H3.1/2 histones in H3.3A complexes, the very preliminary reverse experiments starting with H3.1/2 IP followed by FH-H3.3A IP indicated a presence of modified FH-H3.3A band migrating at a different, lower size than the main form, which migrates ~28kDa on the polyacrylamide gels. While we do not have any clues about this modified FH-H3.3A form, these preliminary data suggested existence of a subset of modified H3.3A-H3.1/2 heterotypic nucleosomes forming constantly at all time-points (data not shown). These preliminary findings further supported our model, in which we propose that the day-time specific dynamic recruitment of BMAL1-CLOCK to H3.3A nucleosomes is mediated by day-time H3.3-specific H3K115 and H3K122 acetylation marks.

Furthermore, findings on H2A.Z circadian dynamics at clock *loci* and CTCF sites established in many species [188, 189, 190], as well as dynamic remodeling of H2A.Z containing nucleosomes by the RSC PBAF-like remodeler in yeast [195], lead to following open questions in respect with our study on fragile H3.3 nucleosome dynamics at these regulatory sites. Would fragile H3.3/H2A.Z dual-variant nucleosomes serve as epigenomic 'bookmarks' at clock *loci* for the core-clock machinery, following 24h dynamics in their formation and/or eviction? For instance, night-time PER-mediated deposition of H2A.Z variant establishing facultative heterochromatin during the repressive clock phase at clock *loci* [193] could be eventually followed by the co-regulated deposition of H3.3 at these sites during the active clock phase to initiate transcription as observed in mESc at enhancers and promoters of genes [217], resulting in formation of fragile dual-variant nucleosomes. Additionally, H3.3/H2A.Z nucleosomes could be rhythmically remodeled by the SWI/SNF complexes at these sites. Regular ChIP-seq experiments for specific components of PBAF/cBAF remodelers would allow to identify genomic regions at which dynamic remodeling of H3.3 and potentially of H3.3/H2A.Z dual-variant nucleosomes might occur. While native ChIP-seq experiments for PBAF specific complex components that we performed failed to specifically enrich these components on chromatin (data not shown), the cross-linked ChIP-seq experiments that could not have been performed due to the limited number of samples and lack of time, might bring the answers- at this stage, at least, for the remodeling of specific regions marked by the H3.3A variant by evaluating the overlap between respective immunoprecipitated regions genome-wide.

Moreover, the presence of H3.3A nucleosomes detected at CTCF sites, as described previously for H2A.Z [192, 233] suggests potential co-deposition of these two variants prior transcriptional activation. From the circadian perspective, time-dependent interaction of PER2 with CTCF during the repressive clock phase suggests that PER2-mediated deposition of H2A.Z variant is occurring at insulators during the night-time in order to establish facultative heterochromatin [193]. Therefore, the observed dynamic enrichment of H3.3A variant at CTCF sites in our study highly suggests co-deposition of this variant to H2A.Z containing nucleosomes, resulting very likely in opening of CTCF-mediated chromatin boundaries set by incorporation of H2A.Z during the previous night. If true, fragile H3.3/H2A.Z nucleosomes would dynamically form over 24h at these sites, prior transcriptional activation during the active clock phase.

Although all of these events could very likely occur, lack of experimental data keeps currently these suggestions at a hypothetical level. The H3.3 ChIP- H2A.Z reChIP experiments could bring potential answers to these questions. Overall, such type of experiments remains however extremely challenging and difficult to perform. Mainly due to the lack of information in current published protocols on how the reChIP experiments were performed and achieved- *e.g*. missing information on chromatin quantity used at both steps, as well as insufficient description of subsequent elution/immunoprecipitation methods, and lack of information on optimal buffer composition for each step [243, 244, 245]. In addition, a great initial amount of chromatin would be needed, since the fraction of H3.3/H2A.Z dual-variant nucleosomes might very likely be minor, if formation of such nucleosomes would occur only at specific gene regulatory sites for instance, rather than at the genome-wide level.

Nevertheless, towards the end of my PhD thesis, I tried to establish a method, which would allow to specifically reChIP associated H2A.Z variants to H3.3 containing nucleosomes, without any non-specific background. Despite the first very promising preliminary results, showing mononucleosomal DNA enrichment post-reChIP, as well as specific co-immunoprecipitation of H2A.Z with H3.3 at both ChIP-reChIP steps assessed by western-blotting, the following two trials were not successful. The promising initial results were not reproducible and important variations were observed in the two following trials- where either only a background levels of mononucleosomal DNA were detected post-reChIP in one trial, or serious concerns about the non-specificity of H2A.Z enrichment were raised due to the sticking background and its enrichment in the negative control in another trial. Unfortunately, due to the lack of time, I was not able to try to further improve this method, and therefore all the questions and hypotheses discussed above remain open.

Upon circadian clock disruption, we observed important changes in H3.3 chromatin architecture. Increased deposition of fragile H3.3A nucleosomes on chromatin in the absence

of PER, suggests that either activity along with the turnover, and/or the protein levels of H3.3-specific chaperones might as well be higher. However, inconsistent changes observed in protein levels of know H3.3 chaperones HIRA and DAXX in PerKO livers (Figure 22B), indicated that potential other liver-specific chaperones of H3.3 variant might be involved.

Degradation of the totality of DNA followed by the purification of liver-specific complexes that assemble with H3.3A independently of chromatin and mass spectrometry analysis, highlighted the presence of other known histone chaperones (data not shown) that might be worth further exploration in order to assess whether their protein levels might increase and whether they could play a role in higher loading of H3.3 on liver chromatin in the absence of negative feedback. Moreover, observed increase of fragile H3.3A nucleosomes at BMAL1-CLOCK binding sites in PerKO liver chromatin, results in more accessible binding sites within the linker DNA, accompanied with increase of BMAL1 activity. All of these events indicate that chromatin is trapped in transcriptionally active, 'day-time like' state in PerKO mice lacking functional circadian oscillators. Furthermore, overall observed increase in H3.3 incorporation in PerKO liver chromatin suggests accelerated rate of hepatic aging, since important H3.3 accumulation has been observed with age in several murine tissues [208].

In addition, structural reorganization of chromatin remodelers due to the loss of ARID2 and reduction in BRG1 and ARID1B protein levels might as well explain and result in observed changes in H3.3 chromatin architecture in PerKO livers. It has been recently shown that the loss of cBAF-specific ARID1A subunit leads to misexpression of sex-linked genes, which is accompanied by changes in H3.3 occupancy and distribution [246]. Authors noted that ARID1A KO leads to an increase and a shift of H3.3 accumulation from intergenic to promoter-proximal regions of the genome on X and Y chromosomes, resulting therefore in enrichment of H3.3 variant at TSS of sex-linked genes and concomitantly, in its depletion at intergenic regions [246].

It has been proposed that dynamic regulation of gene expression programs by circadian core-clock machinery and chromatin remodelers is tightly linked [76]. Indeed, circadian clock drives rhythmic gene expression and promotes time-specific recruitment of chromatin remodelers. Along with their recruitment, rhythmic activation of chromatin remodelers by the core-clock machinery might as well occur. In turn, remodeling complexes would regulate accessibility of the core-clock transcription factors to DNA [76]. Nevertheless, how circadian clocks and chromatin remodelers cooperate to establish 24h dynamics in chromatin states is still not fully understood. Our study brings more insights into these regulatory mechanisms and how remodelers work in hand with BMAL1-CLOCK TF and fragile H3.3 nucleosomes in order to establish dynamic chromatin landscapes. Additionally, we also uncovered how these mechanisms are altered upon circadian clock disruption, which is accompanied by structural reorganization of chromatin remodelers towards the cBAF-BRM remodeler due to disruption

of PBAF/cBAF-BRG1 complexes. Therefore, it is very likely that disassembly of the PBAF complexes in PerKO disrupts previously described auxiliary feedback mediated by SRC-2 - PBAF - REV-ERBα [197], resulting very likely in alterations in hepatic metabolism and physiology. However, reanalysis of published datasets [229] (Figure 27) showed that loss of individual SWI/SNF subunits has only limited effects on circadian clock function in cell culture systems. This suggests that very likely, loss of one of the complex components does not have an immediate effect on transcription of clock genes due to their functional redundancy. This could be further confirmed by performing specific knock-downs of individual complex components, followed by RT-qPCR analysis of mRNA expression levels of several core-clock genes in depleted cells. Alternatively, more visible effects might be noted upon combinatory attenuation of several PBAF/cBAF subunits in parallel in cell culture models, however potentially affecting cell viability.

In a recent study done in *Drosophila*, it has been shown that despite the constitutive BRM protein expression, binding of BRM remodeler to clock *loci* occurs in a circadian manner, peaking during the repressive phase [247]. This study further supports previous findings in *Drosophila* about the repressive role of BRM remodeler in circadian gene expression, where its catalytic activity has been shown to increase nucleosome density at clock *loci* to restrain transcription during the later stages of the active clock phase. On the other hand, BRM non-catalytic activity limits core-clock TF binding to the target clock gene promoters during the repressive phase [248]. These findings suggest that the observed interaction between cBAF/BRM remodeler and BMAL1 at both CT8 and CT20 in our model, could reflect distinct BMAL1-BRM complexes. The catalytically active BRM-BMAL1 complex during the active clock phase at CT8,- limiting transcriptional activity of clock targets, and catalytically inactive BRM-BMAL1 complex during the repressive clock phase at CT20,- promoting BMAL1 off-chromatin state.

Furthermore, it is important to note that observed structural reorganization of chromatin remodelers resulting in a ‘switch’ from PBAF/cBAF-BRG1 to cBAF-BRM complexes in PerKO livers reflects more likely a maintenance of cBAF-BRM complexes upon circadian clock disruption rather than the ‘switch’. Indeed, the absence of PER favors maintenance of BRM-associated remodeling complexes as main SWI/SNF remodelers, which could in turn modulate BMAL1 activity in response to its enhanced binding on chromatin in clock-disrupted livers, in respect to what has been proposed for the dual role of the catalytic and non-catalytic function of BRM complexes at clock genes in *Drosophila* [248].

While we do not have detailed mechanistic insights into what exactly triggers this remodeler ‘switch’, we found that loss of PER is sufficient to promote PBAF complex disassembly due to the loss of ARID2, as well as cBAF-BRG1 complex disruption due to the reduction of BRG1, along with the subsequent repurposing of available remodeler subunits.

Similar phenomena have been observed in ARID2-deficient melanoma cancer cell lines, where loss of ARID2 results in disassembly of PBAF complexes, followed by repurposing of the remaining subunits and a preferential shift towards cBAF chromatin remodelers [236]. In addition, a recent study in these ARID2-deficient melanoma cancer cell lines showed that disruption of the PBAF complex leads to upregulation of neuronal genes by altering ability of the REST (RE1 silencing transcription factor) TF to inactivate its targets [249]. Would the loss of ARID2 in these melanoma patient-derived cell lines lead to alterations in period of circadian rhythms, and/or would these cell lines naturally lack functional clocks? Could disruption of the PBAF complexes lead to similar changes in H3.3 chromatin architecture in these ARID2-deficient cell lines, as well as upregulation of BMAL1 targets as observed in PerKO livers? While answers to these questions remain unknown for now, all of these findings strongly indicate the link between circadian clock disruption and epigenetic alterations linked to cancer. Moreover, subunits of SWI/SNF remodeling complexes are mutated in more than 20% of various cancers, mainly with alterations occurring in PBRM1, ARID2 and BRG1 subunits [142, 161]. In addition, driver mutations in H3.3 variants (*e.g.* H3.3G34R/V) have been shown implicated in several cancers, such as pediatric glioblastomas [250] and alterations in H3.3 chromatin landscapes are involved in development of hepatocellular carcinoma (HCC) [251]. Taken all together, observed rearrangements in H3.3 chromatin architecture, along with structural reorganization of chromatin remodelers upon circadian clock disruption in our study highlight chromatin states characteristic of epigenetic alterations implicated in cancer onset and progression.

Finally, multiple studies on H3.3 role in transcriptional regulation and H3.3-specific interactors have been conducted in dividing cells in culture, such as MEFs or HeLa cells, where H3.3 was stably expressed as a fusion protein with C-terminal 2X FLAG-2X HA epitope tag [210, 252, 253]. In our study, we aimed to establish conditions under which we could purify native H3.3 complexes from circadian mouse liver tissues to further study implication of the H3.3 histone variants in establishment of 24h dynamic chromatin states at clock *loci*. Unlike in the previous studies in cell culture systems, we used mouse models expressing N-terminal FLAG-FLAG-HA -tagged H3.3A variant at endogenous levels [218]. Here we showed for the first time that H3.3A deposition is dynamic in murine tissues, such as liver, and how H3.3A is involved in establishment of 24h dynamics in chromatin landscapes, along with BMAL1 TF and SWI/SNF chromatin remodelers. Additionally, it would be worth to further address the impact of H3.3 deletion on expression levels of core-clock genes, as well as specific PBAF/cBAF complex components. Nevertheless, generating reliable knock-out of main H3.3A and H3.3B variants in mouse models, along with all thirteen other genes similar to H3.3 identified in mice [198], as well as knock-out of their specific chaperones, remains rather challenging task,- yet could be

highly informative to gain further insights into H3.3 role in circadian clock function and rearrangements of chromatin landscapes in the absence of H3.3.

References

1. Dibner, C., Schibler, U. & Albrecht, U. The Mammalian Circadian Timing System: Organization and Coordination of Central and Peripheral Clocks. *Annu. Rev. Physiol.* **72**, 517–549 (2010).

2. Merrow, M., Spoelstra, K. & Roenneberg, T. The circadian cycle: daily rhythms from behaviour to genes. *EMBO Rep* **6**, 930–935 (2005).

3. Huang, R.-C. The discoveries of molecular mechanisms for the circadian rhythm: The 2017 Nobel Prize in Physiology or Medicine. *Biomedical Journal* **41**, 5–8 (2018).

4. Bibnum. Observation botanique (Jean-Jacques de Mairan, 1729). (2013) doi:10.58079/LZXV.

5. Emery, P., Klarsfeld, A., Stanewsky, R. & Shafer, O. T. Sensitive Timing: A Reappraisal of Chronobiology's Foundational Texts. *J Biol Rhythms* **38**, 245–258 (2023).

6. Konopka, R. J. & Benzer, S. Clock Mutants of *Drosophila melanogaster*. *Proc. Natl. Acad. Sci. U.S.A.* **68**, 2112–2116 (1971).

7. Takahashi, J. S. The 50th anniversary of the Konopka and Benzer 1971 paper in PNAS: "Clock Mutants of *Drosophila melanogaster* ". *Proc. Natl. Acad. Sci. U.S.A.* **118**, e2110171118 (2021).

8. Patke, A., Young, M. W. & Axelrod, S. Molecular mechanisms and physiological importance of circadian rhythms. *Nat Rev Mol Cell Biol* **21**, 67–84 (2020).

9. Reddy, P. *et al.* Molecular analysis of the period locus in Drosophila melanogaster and identification of a transcript involved in biological rhythms. *Cell* **38**, 701–710 (1984).

10. Rosbash, M. A 50-Year Personal Journey: Location, Gene Expression, and Circadian Rhythms. *Cold Spring Harb Perspect Biol* **9**, a032516 (2017).

11. Hardin, P. E., Hall, J. C. & Rosbash, M. Feedback of the Drosophila period gene product on circadian cycling of its messenger RNA levels. *Nature* **343**, 536–540 (1990).

12. Zeng, H., Hardin, P. E. & Rosbash, M. Constitutive overexpression of the Drosophila period protein inhibits period mRNA cycling. *The EMBO Journal* **13**, 3590–3598 (1994).

13. Bargiello, T. A., Jackson, F. R. & Young, M. W. Restoration of circadian behavioural rhythms by gene transfer in Drosophila. *Nature* **312**, 752–754 (1984).

14. Liu, X. *et al.* The period gene encodes a predominantly nuclear protein in adult Drosophila. *J. Neurosci.* **12**, 2735–2744 (1992).

15. Sehgal, A., Price, J. L., Man, B. & Young, M. W. Loss of Circadian Behavioral Rhythms and *per* RNA Oscillations in the *Drosophila* Mutant *timeless*. *Science* **263**, 1603–1606 (1994).

16. Price, J. L., Dembinska, M. E., Young, M. W. & Rosbash, M. Suppression of PERIOD protein abundance and circadian cycling by the Drosophila clock mutation timeless. *The EMBO Journal* **14**, 4044–4049 (1995).

17. Saez, L. & Young, M. W. Regulation of Nuclear Entry of the Drosophila Clock Proteins Period and Timeless. *Neuron* **17**, 911–920 (1996).

18. Gekakis, N. *et al.* Isolation of *timeless* by PER Protein Interaction: Defective Interaction Between *timeless* Protein and Long-Period Mutant PER^{L}. *Science* **270**, 811–815 (1995).

19. Suri, V. TIMELESS-dependent positive and negative autoregulation in the Drosophila circadian clock. *The EMBO Journal* **18**, 675–686 (1999).

20. Vitaterna, M. H. *et al.* Mutagenesis and Mapping of a Mouse Gene, *Clock* , Essential for Circadian Behavior. *Science* **264**, 719–725 (1994).

21. King, D. P. *et al.* Positional Cloning of the Mouse Circadian Gene. *Cell* **89**, 641–653 (1997).

22. Antoch, M. P. *et al.* Functional Identification of the Mouse Circadian Clock Gene by Transgenic BAC Rescue. *Cell* **89**, 655–667 (1997).

23. Gekakis, N. *et al.* Role of the CLOCK Protein in the Mammalian Circadian Mechanism. *Science* **280**, 1564–1569 (1998).

24. Rutila, J. E. *et al.* CYCLE Is a Second bHLH-PAS Clock Protein Essential for Circadian Rhythmicity and Transcription of Drosophila period and timeless. *Cell* **93**, 805–814 (1998).

25. Allada, R., White, N. E., So, W. V., Hall, J. C. & Rosbash, M. A Mutant Drosophila Homolog of Mammalian Clock Disrupts Circadian Rhythms and Transcription of period and timeless. *Cell* **93**, 791–804 (1998).

26. Kloss, B. *et al.* The Drosophila Clock Gene double-time Encodes a Protein Closely Related to Human Casein Kinase Iε. *Cell* **94**, 97–107 (1998).

27. Price, J. L. *et al.* double-time Is a Novel Drosophila Clock Gene that Regulates PERIOD Protein Accumulation. *Cell* **94**, 83–95 (1998).

28. Lowrey, P. L. *et al.* Positional Syntenic Cloning and Functional Characterization of the Mammalian Circadian Mutation *tau*. *Science* **288**, 483–491 (2000).

29. Lenstra, T. L., Rodriguez, J., Chen, H. & Larson, D. R. Transcription Dynamics in Living Cells. *Annu Rev Biophys* **45**, 25–47 (2016).

30. Callaway, E. & Ledford, H. Medicine Nobel awarded for work on circadian clocks. *Nature* **550**, 18–18 (2017).

31. Pittendrigh, C. S. Circadian Rhythms and the Circadian Organization of Living Systems. *Cold Spring Harbor Symposia on Quantitative Biology* **25**, 159–184 (1960).

32. Aschoff, J. Circadian Rhythms in Man: A self-sustained oscillator with an inherent frequency underlies human 24-hour periodicity. *Science* **148**, 1427–1432 (1965).

33. Period (Tau, τ) of Circadian Rhythm. in *Encyclopedia of Neuroscience* (eds. Binder, M. D., Hirokawa, N. & Windhorst, U.) 3117–3117 (Springer Berlin Heidelberg, Berlin, Heidelberg, 2009). doi:10.1007/978-3-540-29678-2_4479.

34. Balsalobre, A., Damiola, F. & Schibler, U. A Serum Shock Induces Circadian Gene Expression in Mammalian Tissue Culture Cells. *Cell* **93**, 929–937 (1998).

35. Herzog, E. D., Geusz, M. E., Khalsa, S. B. S., Straume, M. & Block, G. D. Circadian rhythms in mouse suprachiasmatic nucleus explants on multimicroelectrode plates. *Brain Research* **757**, 285–290 (1997).

36. Welsh, D. K., Yoo, S.-H., Liu, A. C., Takahashi, J. S. & Kay, S. A. Bioluminescence Imaging of Individual Fibroblasts Reveals Persistent, Independently Phased Circadian Rhythms of Clock Gene Expression. *Current Biology* **14**, 2289–2295 (2004).

37. Liu, A. C. *et al.* Intercellular Coupling Confers Robustness against Mutations in the SCN Circadian Clock Network. *Cell* **129**, 605–616 (2007).

38. Moore, R. Y. & Eichler, V. B. Loss of a circadian adrenal corticosterone rhythm following suprachiasmatic lesions in the rat. *Brain Research* **42**, 201–206 (1972).

39. Stephan, F. K. & Zucker, I. Circadian Rhythms in Drinking Behavior and Locomotor Activity of Rats Are Eliminated by Hypothalamic Lesions. *Proc. Natl. Acad. Sci. U.S.A.* **69**, 1583–1586 (1972).

40. Lehman, M. *et al.* Circadian rhythmicity restored by neural transplant. Immunocytochemical characterization of the graft and its integration with the host brain. *J. Neurosci.* **7**, 1626–1638 (1987).

41. Ralph, M. R., Foster, R. G., Davis, F. C. & Menaker, M. Transplanted Suprachiasmatic Nucleus Determines Circadian Period. *Science* **247**, 975–978 (1990).

42. Sujino, M. *et al.* Suprachiasmatic Nucleus Grafts Restore Circadian Behavioral Rhythms of Genetically Arrhythmic Mice. *Current Biology* **13**, 664–668 (2003).

43. Green, D. J. & Gillette, R. Circadian rhythm of firing rate recorded from single cells in the rat suprachiasmatic brain slice. *Brain Research* **245**, 198–200 (1982).

44. Welsh, D. K., Logothetis, D. E., Meister, M. & Reppert, S. M. Individual neurons dissociated from rat suprachiasmatic nucleus express independently phased circadian firing rhythms. *Neuron* **14**, 697–706 (1995).

45. Welsh, D. K., Takahashi, J. S. & Kay, S. A. Suprachiasmatic Nucleus: Cell Autonomy and Network Properties. *Annu. Rev. Physiol.* **72**, 551–577 (2010).

46. Yamaguchi, S. *et al.* Synchronization of Cellular Clocks in the Suprachiasmatic Nucleus. *Science* **302**, 1408–1412 (2003).

47. Shan, Y. *et al.* Dual-Color Single-Cell Imaging of the Suprachiasmatic Nucleus Reveals a Circadian Role in Network Synchrony. *Neuron* **108**, 164-179.e7 (2020).

48. Berson, D. M., Dunn, F. A. & Takao, M. Phototransduction by Retinal Ganglion Cells That Set the Circadian Clock. *Science* **295**, 1070–1073 (2002).

49. Moore, R. Y. & Lenn, N. J. A retinohypothalamic projection in the rat. *J of Comparative Neurology* **146**, 1–14 (1972).

50. Yamazaki, S. *et al.* Resetting Central and Peripheral Circadian Oscillators in Transgenic Rats. *Science* **288**, 682–685 (2000).

51. Koike, N. *et al.* Transcriptional Architecture and Chromatin Landscape of the Core Circadian Clock in Mammals. *Science* **338**, 349–354 (2012).

52. Storch, K.-F. *et al.* Extensive and divergent circadian gene expression in liver and heart. *Nature* **417**, 78–83 (2002).

53. Mavroudis, P. D., DuBois, D. C., Almon, R. R. & Jusko, W. J. Daily variation of gene expression in diverse rat tissues. *PLoS ONE* **13**, e0197258 (2018).

54. Asher, G. & Sassone-Corsi, P. Time for Food: The Intimate Interplay between Nutrition, Metabolism, and the Circadian Clock. *Cell* **161**, 84–92 (2015).

55. Droin, C. *et al.* Space-time logic of liver gene expression at sub-lobular scale. *Nat Metab* **3**, 43–58 (2021).

56. Manco, R. & Itzkovitz, S. Liver zonation. *Journal of Hepatology* **74**, 466–468 (2021).

57. Azimifar, S. B., Nagaraj, N., Cox, J. & Mann, M. Cell-Type-Resolved Quantitative Proteomics of Murine Liver. *Cell Metabolism* **20**, 1076–1087 (2014).

58. Aviram, R., Manella, G. & Asher, G. The liver by day and by night. *Journal of Hepatology* **74**, 1240–1242 (2021).

59. Panda, S. Circadian physiology of metabolism. *Science* **354**, 1008–1015 (2016).

60. Schmutz, I., Albrecht, U. & Ripperger, J. A. The role of clock genes and rhythmicity in the liver. *Molecular and Cellular Endocrinology* **349**, 38–44 (2012).

61. Huang, R. *et al.* Multi-omics profiling reveals rhythmic liver function shaped by meal timing. *Nat Commun* **14**, 6086 (2023).

62. Sulli, G., Manoogian, E. N. C., Taub, P. R. & Panda, S. Training the Circadian Clock, Clocking the Drugs, and Drugging the Clock to Prevent, Manage, and Treat Chronic Diseases. *Trends in Pharmacological Sciences* **39**, 812–827 (2018).

63. Wang, Y. *et al.* A proteomics landscape of circadian clock in mouse liver. *Nat Commun* **9**, 1553 (2018).

64. Robles, M. S., Humphrey, S. J. & Mann, M. Phosphorylation Is a Central Mechanism for Circadian Control of Metabolism and Physiology. *Cell Metabolism* **25**, 118–127 (2017).

65. Ferrell, J. M. & Chiang, J. Y. L. Circadian rhythms in liver metabolism and disease. *Acta Pharmaceutica Sinica B* **5**, 113–122 (2015).

66. Nakahata, Y., Sahar, S., Astarita, G., Kaluzova, M. & Sassone-Corsi, P. Circadian Control of the NAD^+ Salvage Pathway by CLOCK-SIRT1. *Science* **324**, 654–657 (2009).

67. Nakahata, Y. *et al.* The NAD+-Dependent Deacetylase SIRT1 Modulates CLOCK-Mediated Chromatin Remodeling and Circadian Control. *Cell* **134**, 329–340 (2008).

68. Asher, G. *et al.* SIRT1 Regulates Circadian Clock Gene Expression through PER2 Deacetylation. *Cell* **134**, 317–328 (2008).

69. Lamia, K. A., Storch, K.-F. & Weitz, C. J. Physiological significance of a peripheral tissue circadian clock. *Proc. Natl. Acad. Sci. U.S.A.* **105**, 15172–15177 (2008).

70. Damiola, F. *et al.* Restricted feeding uncouples circadian oscillators in peripheral tissues from the central pacemaker in the suprachiasmatic nucleus. *Genes Dev.* **14**, 2950–2961 (2000).

71. Stokkan, K.-A., Yamazaki, S., Tei, H., Sakaki, Y. & Menaker, M. Entrainment of the Circadian Clock in the Liver by Feeding. *Science* **291**, 490–493 (2001).

72. Mendoza, J. Circadian Clocks: Setting Time By Food. *J Neuroendocrinology* **19**, 127–137 (2007).

73. Yoo, S.-H. *et al.* PERIOD2::LUCIFERASE real-time reporting of circadian dynamics reveals persistent circadian oscillations in mouse peripheral tissues. *Proc. Natl. Acad. Sci. U.S.A.* **101**, 5339–5346 (2004).

74. Sinturel, F. *et al.* Diurnal Oscillations in Liver Mass and Cell Size Accompany Ribosome Assembly Cycles. *Cell* **169**, 651-663.e14 (2017).

75. Takahashi, J. S. Transcriptional architecture of the mammalian circadian clock. *Nat Rev Genet* **18**, 164–179 (2017).

76. Papazyan, R., Zhang, Y. & Lazar, M. A. Genetic and epigenomic mechanisms of mammalian circadian transcription. *Nat Struct Mol Biol* **23**, 1045–1052 (2016).

77. Etchegaray, J.-P. *et al.* Casein Kinase 1 Delta Regulates the Pace of the Mammalian Circadian Clock. *Molecular and Cellular Biology* **29**, 3853–3866 (2009).

78. Guillaumond, F., Dardente, H., Giguère, V. & Cermakian, N. Differential Control of Bmal1 Circadian Transcription by REV-ERB and ROR Nuclear Receptors. *J Biol Rhythms* **20**, 391–403 (2005).

79. Fagiani, F. *et al.* Molecular regulations of circadian rhythm and implications for physiology and diseases. *Sig Transduct Target Ther* **7**, 41 (2022).

80. Feillet, C., Van Der Horst, G. T. J., Levi, F., Rand, D. A. & Delaunay, F. Coupling between the Circadian Clock and Cell Cycle Oscillators: Implication for Healthy Cells and Malignant Growth. *Front. Neurol.* **6**, (2015).

81. Kondratov, R. V. & Antoch, M. P. Circadian proteins in the regulation of cell cycle and genotoxic stress responses. *Trends in Cell Biology* **17**, 311–317 (2007).

82. Gery, S. *et al.* The Circadian Gene Per1 Plays an Important Role in Cell Growth and DNA Damage Control in Human Cancer Cells. *Molecular Cell* **22**, 375–382 (2006).

83. Yang, Y. *et al.* Checkpoint kinases regulate the circadian clock after DNA damage by influencing chromatin dynamics. *Nucleic Acids Research* **53**, gkaf162 (2025).

84. Vanselow, K. *et al.* Differential effects of PER2 phosphorylation: molecular basis for the human familial advanced sleep phase syndrome (FASPS). *Genes Dev* **20**, 2660–2672 (2006).

85. Mignot, E. & Takahashi, J. S. A Circadian Sleep Disorder Reveals a Complex Clock. *Cell* **128**, 22–23 (2007).

86. Toh, K. L. *et al.* An h *Per2* Phosphorylation Site Mutation in Familial Advanced Sleep Phase Syndrome. *Science* **291**, 1040–1043 (2001).

87. Pavithra, S. *et al.* PER2 gene and its association with sleep-related disorders: A review. *Physiology & Behavior* **273**, 114411 (2024).

88. Patke, A. *et al.* Mutation of the Human Circadian Clock Gene CRY1 in Familial Delayed Sleep Phase Disorder. *Cell* **169**, 203-215.e13 (2017).

89. Fu, L., Pelicano, H., Liu, J., Huang, P. & Lee, C. C. The Circadian Gene Period2 Plays an Important Role in Tumor Suppression and DNA Damage Response In Vivo. *Cell* **111**, 41–50 (2002).

90. Su, X. *et al.* The circadian clock gene PER2 plays an important role in tumor suppression through regulating tumor-associated genes in human oral squamous cell carcinoma. *Oncology Reports* **38**, 472–480 (2017).

91. Xiong, H. *et al.* Loss of the clock gene PER2 is associated with cancer development and altered expression of important tumor-related genes in oral cancer. *Int J Oncol* (2017) doi:10.3892/ijo.2017.4180.

92. Hwang-Verslues, W. W. *et al.* Loss of corepressor PER2 under hypoxia up-regulates OCT1-mediated EMT gene expression and enhances tumor malignancy. *Proc. Natl. Acad. Sci. U.S.A.* **110**, 12331–12336 (2013).

93. Wang, Z., Li, L. & Wang, Y. Effects of Per2 overexpression on growth inhibition and metastasis, and on MTA1, nm23-H1 and the autophagy-associated PI3K/PKB signaling pathway in nude mice xenograft models of ovarian cancer. *Mol Med Rep* **13**, 4561–4568 (2016).

94. Koronowski, K. B. & Sassone-Corsi, P. Communicating clocks shape circadian homeostasis. *Science* **371**, eabd0951 (2021).

95. Buxton, O. M. *et al.* Adverse Metabolic Consequences in Humans of Prolonged Sleep Restriction Combined with Circadian Disruption. *Sci. Transl. Med.* **4**, (2012).

96. McHill, A. W. *et al.* Impact of circadian misalignment on energy metabolism during simulated nightshift work. *Proc. Natl. Acad. Sci. U.S.A.* **111**, 17302–17307 (2014).

97. Arble, D. M., Bass, J., Laposky, A. D., Vitaterna, M. H. & Turek, F. W. Circadian Timing of Food Intake Contributes to Weight Gain. *Obesity* **17**, 2100–2102 (2009).

98. Kohsaka, A. *et al.* High-Fat Diet Disrupts Behavioral and Molecular Circadian Rhythms in Mice. *Cell Metabolism* **6**, 414–421 (2007).

99. Stenvers, D. J., Scheer, F. A. J. L., Schrauwen, P., La Fleur, S. E. & Kalsbeek, A. Circadian clocks and insulin resistance. *Nat Rev Endocrinol* **15**, 75–89 (2019).

100. Masri, S., Kinouchi, K. & Sassone-Corsi, P. Circadian clocks, epigenetics, and cancer. *Current Opinion in Oncology* **27**, 50–56 (2015).

101. Lingas, E. C. A Narrative Review of the Carcinogenic Effect of Night Shift and the Potential Protective Role of Melatonin. *Cureus* **15**, e43326 (2023).

102. Xie, Y. *et al.* New Insights Into the Circadian Rhythm and Its Related Diseases. *Front. Physiol.* **10**, 682 (2019).

103. Lin, Y. *et al.* The role of circadian clock in regulating cell functions: implications for diseases. *MedComm* **5**, e504 (2024).

104. Masri, S. & Sassone-Corsi, P. The emerging link between cancer, metabolism, and circadian rhythms. *Nat Med* **24**, 1795–1803 (2018).

105. Elvira, A.-L. The Circadian Timing System: A Recent Addition in the Physiological Mechanisms Underlying Pathological and Aging Processes. *aging dis* (2014) doi:10.14336/ad.2014.0500406.

106. Manoogian, E. N. C. & Panda, S. Circadian rhythms, time-restricted feeding, and healthy aging. *Ageing Research Reviews* **39**, 59–67 (2017).

107. Rijo-Ferreira, F. & Takahashi, J. S. Genomics of circadian rhythms in health and disease. *Genome Med* **11**, 82 (2019).

108. Mormont, M. & Levi, F. Cancer chronotherapy: Principles, applications, and perspectives. *Cancer* **97**, 155–169 (2003).

109. Adam, D. Core Concept: Emerging science of chronotherapy offers big opportunities to optimize drug delivery. *Proc Natl Acad Sci U S A* **116**, 21957–21959 (2019).

110. Luger, K., Mäder, A. W., Richmond, R. K., Sargent, D. F. & Richmond, T. J. Crystal structure of the nucleosome core particle at 2.8 Å resolution. *Nature* **389**, 251–260 (1997).

111. Luger, K. & Richmond, T. J. DNA binding within the nucleosome core. *Current Opinion in Structural Biology* **8**, 33–40 (1998).

112. Mello, J. A. & Almouzni, G. The ins and outs of nucleosome assembly. *Current Opinion in Genetics & Development* **11**, 136–141 (2001).

113. Verreault, A., Kaufman, P. D., Kobayashi, R. & Stillman, B. Nucleosome Assembly by a Complex of CAF-1 and Acetylated Histones H3/H4. *Cell* **87**, 95–104 (1996).

114. Smith, S. & Stillman, B. Purification and characterization of CAF-I, a human cell factor required for chromatin assembly during DNA replication in vitro. *Cell* **58**, 15–25 (1989).

115. Agez, M. *et al.* Structure of the Histone Chaperone Asf1 Bound to the Histone H3 C-Terminal Helix and Functional Insights. *Structure* **15**, 191–199 (2007).

116. English, C. M., Adkins, M. W., Carson, J. J., Churchill, M. E. A. & Tyler, J. K. Structural Basis for the Histone Chaperone Activity of Asf1. *Cell* **127**, 495–508 (2006).

117. Belotserkovskaya, R. *et al.* FACT Facilitates Transcription-Dependent Nucleosome Alteration. *Science* **301**, 1090–1093 (2003).

118. Hondele, M. *et al.* Structural basis of histone H2A–H2B recognition by the essential chaperone FACT. *Nature* **499**, 111–114 (2013).

119. D'Arcy, S. *et al.* Chaperone Nap1 Shields Histone Surfaces Used in a Nucleosome and Can Put H2A-H2B in an Unconventional Tetrameric Form. *Molecular Cell* **51**, 662–677 (2013).

120. Li, G. & Reinberg, D. Chromatin higher-order structures and gene regulation. *Current Opinion in Genetics & Development* **21**, 175–186 (2011).

121. Tremethick, D. J. Higher-Order Structures of Chromatin: The Elusive 30 nm Fiber. *Cell* **128**, 651–654 (2007).

122. Krietenstein, N. & Rando, O. J. Mesoscale organization of the chromatin fiber. *Current Opinion in Genetics & Development* **61**, 32–36 (2020).

123. Cremer, T. & Cremer, C. Chromosome territories, nuclear architecture and gene regulation in mammalian cells. *Nat Rev Genet* **2**, 292–301 (2001).

124. Pongubala, J. M. R. & Murre, C. Spatial Organization of Chromatin: Transcriptional Control of Adaptive Immune Cell Development. *Front. Immunol.* **12**, 633825 (2021).

125. Harris, H. L. *et al.* Chromatin alternates between A and B compartments at kilobase scale for subgenic organization. *Nat Commun* **14**, 3303 (2023).

126. Oji, A., Choubani, L., Miura, H. & Hiratani, I. Structure and dynamics of nuclear A/B compartments and subcompartments. *Current Opinion in Cell Biology* **90**, 102406 (2024).

127. Shan, L., Li, P., Yu, H. & Chen, L.-L. Emerging roles of nuclear bodies in genome spatial organization. *Trends in Cell Biology* **34**, 595–605 (2024).

128. Morimoto, M. & Boerkoel, C. The Role of Nuclear Bodies in Gene Expression and Disease. *Biology* **2**, 976–1033 (2013).

129. McArthur, E. & Capra, J. A. Topologically associating domain boundaries that are stable across diverse cell types are evolutionarily constrained and enriched for heritability. *The American Journal of Human Genetics* **108**, 269–283 (2021).

130. Biswas, S. & Rao, C. M. Epigenetic tools (The Writers, The Readers and The Erasers) and their implications in cancer therapy. *European Journal of Pharmacology* **837**, 8–24 (2018).

131. Becker, P. B. & Workman, J. L. Nucleosome Remodeling and Epigenetics. *Cold Spring Harbor Perspectives in Biology* **5**, a017905–a017905 (2013).

132. Martire, S. & Banaszynski, L. A. The roles of histone variants in fine-tuning chromatin organization and function. *Nat Rev Mol Cell Biol* **21**, 522–541 (2020).

133. Millán-Zambrano, G., Burton, A., Bannister, A. J. & Schneider, R. Histone post-translational modifications — cause and consequence of genome function. *Nat Rev Genet* **23**, 563–580 (2022).

134. Liu, R. *et al.* Post-translational modifications of histones: Mechanisms, biological functions, and therapeutic targets. *MedComm* **4**, e292 (2023).

135. Sotomayor-Lugo, F. *et al.* The Dynamics of Histone Modifications during Mammalian Zygotic Genome Activation. *IJMS* **25**, 1459 (2024).

136. Wang, H. & Helin, K. Roles of H3K4 methylation in biology and disease. *Trends in Cell Biology* **35**, 115–128 (2025).

137. Wang, H. *et al.* H3K4me3 regulates RNA polymerase II promoter-proximal pause-release. *Nature* **615**, 339–348 (2023).

138. Kooistra, S. M. & Helin, K. Molecular mechanisms and potential functions of histone demethylases. *Nat Rev Mol Cell Biol* **13**, 297–311 (2012).

139. Sokpor, G., Castro-Hernandez, R., Rosenbusch, J., Staiger, J. F. & Tuoc, T. ATP-Dependent Chromatin Remodeling During Cortical Neurogenesis. *Front. Neurosci.* **12**, 226 (2018).

140. Stern, M., Jensen, R. & Herskowitz, I. Five SWI genes are required for expression of the HO gene in yeast. *Journal of Molecular Biology* **178**, 853–868 (1984).

141. Neigeborn, L. & Carlson, M. GENES AFFECTING THE REGULATION OF *SUC2* GENE EXPRESSION BY GLUCOSE REPRESSION IN *SACCHAROMYCES CEREVISIAE*. *Genetics* **108**, 845–858 (1984).

142. Hodges, C., Kirkland, J. G. & Crabtree, G. R. The Many Roles of BAF (mSWI/SNF) and PBAF Complexes in Cancer. *Cold Spring Harb Perspect Med* **6**, a026930 (2016).

143. Singh, A., Modak, S. B., Chaturvedi, M. M. & Purohit, J. S. SWI/SNF Chromatin Remodelers: Structural, Functional and Mechanistic Implications. *Cell Biochem Biophys* **81**, 167–187 (2023).

144. Wang, W. *et al.* Purification and biochemical heterogeneity of the mammalian SWI-SNF complex. *EMBO J* **15**, 5370–5382 (1996).

145. Wang, W. *et al.* Diversity and specialization of mammalian SWI/SNF complexes. *Genes Dev.* **10**, 2117–2130 (1996).

146. Wang, W. *et al.* Architectural DNA binding by a high-mobility-group/kinesin-like subunit in mammalian SWI/SNF-related complexes. *Proc. Natl. Acad. Sci. U.S.A.* **95**, 492–498 (1998).

147. Biggar, S. R. Continuous and widespread roles for the Swi-Snf complex in transcription. *The EMBO Journal* **18**, 2254–2264 (1999).

148. Khavari, P. A., Peterson, C. L., Tamkun, J. W., Mendel, D. B. & Crabtree, G. R. BRG1 contains a conserved domain of the SWI2/SNF2 family necessary for normal mitotic growth and transcription. *Nature* **366**, 170–174 (1993).

149. Zhu, Z. *et al.* Mitotic bookmarking by SWI/SNF subunits. *Nature* **618**, 180–187 (2023).

150. Chmykhalo, V. K. *et al.* SWI/SNF Complex Connects Signaling and Epigenetic State in Cells of Nervous System. *Mol Neurobiol* **62**, 1536–1557 (2025).

151. Abu Sailik, F., Emerald, B. S. & Ansari, S. A. Opening and changing: mammalian SWI/SNF complexes in organ development and carcinogenesis. *Open Biol.* **14**, 240039 (2024).

152. Gong, F., Chiu, L.-Y. & Miller, K. M. Acetylation Reader Proteins: Linking Acetylation Signaling to Genome Maintenance and Cancer. *PLoS Genet* **12**, e1006272 (2016).

153. Zhang, Y. *et al.* DNA Translocation and Loop Formation Mechanism of Chromatin Remodeling by SWI/SNF and RSC. *Molecular Cell* **24**, 559–568 (2006).

154. Tang, L., Nogales, E. & Ciferri, C. Structure and function of SWI/SNF chromatin remodeling complexes and mechanistic implications for transcription. *Progress in Biophysics and Molecular Biology* **102**, 122–128 (2010).

155. Mashtalir, N. *et al.* Modular Organization and Assembly of SWI/SNF Family Chromatin Remodeling Complexes. *Cell* **175**, 1272-1288.e20 (2018).

156. Mashtalir, N. *et al.* Chromatin landscape signals differentially dictate the activities of mSWI/SNF family complexes. *Science* **373**, 306–315 (2021).

157. Slaughter, M. J. *et al.* PBRM1 bromodomains variably influence nucleosome interactions and cellular function. *Journal of Biological Chemistry* **293**, 13592–13603 (2018).

158. Cai, W. *et al.* PBRM1 acts as a p53 lysine-acetylation reader to suppress renal tumor growth. *Nat Commun* **10**, 5800 (2019).

159. Petell, C. J. *et al.* The bromo-adjacent homology domains of PBRM1 associate with histone tails and contribute to PBAF-mediated gene regulation. *Journal of Biological Chemistry* **299**, 104996 (2023).

160. Karki, M. *et al.* A cytoskeletal function for PBRM1 reading methylated microtubules. *Sci. Adv.* **7**, eabf2866 (2021).

161. Malone, H. A. & Roberts, C. W. M. Chromatin remodellers as therapeutic targets. *Nat Rev Drug Discov* **23**, 661–681 (2024).

162. Wong, L. H. & Tremethick, D. J. Multifunctional histone variants in genome function. *Nat Rev Genet* **26**, 82–104 (2025).

163. Jin, C. & Felsenfeld, G. Nucleosome stability mediated by histone variants H3.3 and H2A.Z. *Genes Dev.* **21**, 1519–1529 (2007).

164. Colino-Sanguino, Y., Clark, S. J. & Valdes-Mora, F. The H2A.Z-nucleosome code in mammals: emerging functions. *Trends in Genetics* **38**, 516 (2022).

165. Horikoshi, N., Arimura, Y., Taguchi, H. & Kurumizaka, H. Crystal structures of heterotypic nucleosomes containing histones H2A.Z and H2A. *Open Biol.* **6**, 160127 (2016).

166. Arimura, Y. *et al.* Crystal structure and stable property of the cancer-associated heterotypic nucleosome containing CENP-A and H3.3. *Sci Rep* **4**, 7115 (2014).

167. Talbert, P. B. & Henikoff, S. Histone variants at a glance. *Journal of Cell Science* **134**, jcs244749 (2021).

168. Hegazy, Y. A. *et al.* Histone variants: The bricks that fit differently. *Journal of Biological Chemistry* **301**, 108048 (2025).

169. Szenker, E., Ray-Gallet, D. & Almouzni, G. The double face of the histone variant H3.3. *Cell Res* **21**, 421–434 (2011).

170. Yi, S.-J. & Kim, K. New Insights into the Role of Histone Changes in Aging. *IJMS* **21**, 8241 (2020).

171. Quina, A. S., Buschbeck, M. & Di Croce, L. Chromatin structure and epigenetics. *Biochemical Pharmacology* **72**, 1563–1569 (2006).

172. Bowman, G. D. & Poirier, M. G. Post-Translational Modifications of Histones That Influence Nucleosome Dynamics. *Chem. Rev.* **115**, 2274–2295 (2015).

173. Vollmers, C. *et al.* Circadian Oscillations of Protein-Coding and Regulatory RNAs in a Highly Dynamic Mammalian Liver Epigenome. *Cell Metabolism* **16**, 833–845 (2012).

174. Ripperger, J. A. & Schibler, U. Rhythmic CLOCK-BMAL1 binding to multiple E-box motifs drives circadian Dbp transcription and chromatin transitions. *Nat Genet* **38**, 369–374 (2006).

175. Lowrey, P. L. & Takahashi, J. S. Genetics of Circadian Rhythms in Mammalian Model Organisms. in *Advances in Genetics* vol. 74 175–230 (Elsevier, 2011).

176. Etchegaray, J.-P., Lee, C., Wade, P. A. & Reppert, S. M. Rhythmic histone acetylation underlies transcription in the mammalian circadian clock. *Nature* **421**, 177–182 (2003).

177. Lee, Y. *et al.* Coactivation of the CLOCK–BMAL1 complex by CBP mediates resetting of the circadian clock. *Journal of Cell Science* **123**, 3547–3557 (2010).

178. Doi, M., Hirayama, J. & Sassone-Corsi, P. Circadian Regulator CLOCK Is a Histone Acetyltransferase. *Cell* **125**, 497–508 (2006).

179. Spencer, T. E. *et al.* Steroid receptor coactivator-1 is a histone acetyltransferase. *Nature* **389**, 194–198 (1997).

180. Chen, H. *et al.* Nuclear Receptor Coactivator ACTR Is a Novel Histone Acetyltransferase and Forms a Multimeric Activation Complex with P/CAF and CBP/p300. *Cell* **90**, 569–580 (1997).

181. Menet, J. S., Pescatore, S. & Rosbash, M. CLOCK:BMAL1 is a pioneer-like transcription factor. *Genes Dev.* **28**, 8–13 (2014).

182. Feng, D. *et al.* A Circadian Rhythm Orchestrated by Histone Deacetylase 3 Controls Hepatic Lipid Metabolism. *Science* **331**, 1315–1319 (2011).

183. Duong, H. A., Robles, M. S., Knutti, D. & Weitz, C. J. A Molecular Mechanism for Circadian Clock Negative Feedback. *Science* **332**, 1436–1439 (2011).

184. Kim, J. Y., Kwak, P. B. & Weitz, C. J. Specificity in Circadian Clock Feedback from Targeted Reconstitution of the NuRD Corepressor. *Molecular Cell* **56**, 738–748 (2014).

185. Katada, S. & Sassone-Corsi, P. The histone methyltransferase MLL1 permits the oscillation of circadian gene expression. *Nat Struct Mol Biol* **17**, 1414–1421 (2010).

186. Valekunja, U. K. *et al.* Histone methyltransferase MLL3 contributes to genome-scale circadian transcription. *Proc. Natl. Acad. Sci. U.S.A.* **110**, 1554–1559 (2013).

187. Duong, H. A. & Weitz, C. J. Temporal orchestration of repressive chromatin modifiers by circadian clock Period complexes. *Nat Struct Mol Biol* **21**, 126–132 (2014).

188. Liu, X. *et al.* DNA Replication Is Required for Circadian Clock Function by Regulating Rhythmic Nucleosome Composition. *Molecular Cell* **67**, 203-213.e4 (2017).

189. Tong, M. *et al.* The Evening Complex Establishes Repressive Chromatin Domains Via H2A.Z Deposition. *Plant Physiol.* **182**, 612–625 (2020).

190. Liu, Z. *et al.* Splice variants of DOMINO control Drosophila circadian behavior and pacemaker neuron maintenance. *PLoS Genet* **15**, e1008474 (2019).

191. Thakar, A. *et al.* H2A.Z and H3.3 Histone Variants Affect Nucleosome Structure: Biochemical and Biophysical Studies. *Biochemistry* **48**, 10852–10857 (2009).

192. Fu, Y., Sinha, M., Peterson, C. L. & Weng, Z. The Insulator Binding Protein CTCF Positions 20 Nucleosomes around Its Binding Sites across the Human Genome. *PLoS Genet* **4**, e1000138 (2008).

193. Tartour, K. *et al.* Mammalian PERIOD2 regulates H2A.Z incorporation in chromatin to orchestrate circadian negative feedback. *Nat Struct Mol Biol* **29**, 549–562 (2022).

194. Wang, B., Kettenbach, A. N., Gerber, S. A., Loros, J. J. & Dunlap, J. C. Neurospora WC-1 Recruits SWI/SNF to Remodel frequency and Initiate a Circadian Cycle. *PLoS Genet* **10**, e1004599 (2014).

195. Brahma, S. & Henikoff, S. RSC-Associated Subnucleosomes Define MNase-Sensitive Promoters in Yeast. *Molecular Cell* **73**, 238-249.e3 (2019).

196. Brahma, S. & Henikoff, S. The BAF chromatin remodeler synergizes with RNA polymerase II and transcription factors to evict nucleosomes. *Nat Genet* **56**, 100–111 (2024).

197. Zhu, B. *et al.* Coactivator-Dependent Oscillation of Chromatin Accessibility Dictates Circadian Gene Amplitude via REV-ERB Loading. *Molecular Cell* **60**, 769–783 (2015).

198. Maehara, K. *et al.* Tissue-specific expression of histone H3 variants diversified after species separation. *Epigenetics & Chromatin* **8**, 35 (2015).

199. Hake, S. B. *et al.* Serine 31 phosphorylation of histone variant H3.3 is specific to regions bordering centromeres in metaphase chromosomes. *Proc. Natl. Acad. Sci. U.S.A.* **102**, 6344–6349 (2005).

200. Tachiwana, H. *et al.* Structures of human nucleosomes containing major histone H3 variants. *Acta Crystallogr D Biol Crystallogr* **67**, 578–583 (2011).

201. Ray-Gallet, D. & Almouzni, G. The Histone H3 Family and Its Deposition Pathways. in *Histone Mutations and Cancer* (eds. Fang, D. & Han, J.) vol. 1283 17–42 (Springer Singapore, Singapore, 2021).

202. Shi, L., Wen, H. & Shi, X. The Histone Variant H3.3 in Transcriptional Regulation and Human Disease. *Journal of Molecular Biology* **429**, 1934–1945 (2017).

203. Goldberg, A. D. *et al.* Distinct Factors Control Histone Variant H3.3 Localization at Specific Genomic Regions. *Cell* **140**, 678–691 (2010).

204. Xiong, C. *et al.* UBN1/2 of HIRA complex is responsible for recognition and deposition of H3.3 at cis-regulatory elements of genes in mouse ES cells. *BMC Biol* **16**, 110 (2018).

205. Choi, J., Kim, T. & Cho, E.-J. HIRA vs. DAXX: the two axes shaping the histone H3.3 landscape. *Exp Mol Med* **56**, 251–263 (2024).

206. Delaney, K., Weiss, N. & Almouzni, G. The cell-cycle choreography of H3 variants shapes the genome. *Molecular Cell* **83**, 3773–3786 (2023).

207. Bano, D., Piazzesi, A., Salomoni, P. & Nicotera, P. The histone variant H3.3 claims its place in the crowded scene of epigenetics. *Aging* **9**, 602–614 (2017).

208. Tvardovskiy, A., Schwämmle, V., Kempf, S. J., Rogowska-Wrzesinska, A. & Jensen, O. N. Accumulation of histone variant H3.3 with age is associated with profound changes in the histone methylation landscape. *Nucleic Acids Research* **45**, 9272–9289 (2017).

209. Piazzesi, A. *et al.* Replication-Independent Histone Variant H3.3 Controls Animal Lifespan through the Regulation of Pro-longevity Transcriptional Programs. *Cell Reports* **17**, 987–996 (2016).

210. Drané, P., Ouararhni, K., Depaux, A., Shuaib, M. & Hamiche, A. The death-associated protein DAXX is a novel histone chaperone involved in the replication-independent deposition of H3.3. *Genes Dev.* **24**, 1253–1265 (2010).

211. Sun, C. *et al.* The histone chaperone function of Daxx is dispensable for embryonic development. *Cell Death Dis* **14**, 565 (2023).

212. Chen, P. *et al.* H3.3 actively marks enhancers and primes gene transcription via opening higher-ordered chromatin. *Genes Dev.* **27**, 2109–2124 (2013).

213. Kraushaar, D. C. *et al.* Genome-wide incorporation dynamics reveal distinct categories of turnover for the histone variant H3.3. *Genome Biol* **14**, R121 (2013).

214. Tang, M. C. W. *et al.* Contribution of the Two Genes Encoding Histone Variant H3.3 to Viability and Fertility in Mice. *PLoS Genet* **11**, e1004964 (2015).

215. Jang, C.-W., Shibata, Y., Starmer, J., Yee, D. & Magnuson, T. Histone H3.3 maintains genome integrity during mammalian development. *Genes Dev.* **29**, 1377–1392 (2015).

216. Jin, C. *et al.* H3.3/H2A.Z double variant–containing nucleosomes mark 'nucleosome-free regions' of active promoters and other regulatory regions. *Nat Genet* **41**, 941–945 (2009).

217. Yang, Y. *et al.* HIRA complex presets transcriptional potential through coordinating depositions of the histone variants H3.3 and H2A.Z on the poised genes in mESCs. *Nucleic Acids Research* **50**, 191–206 (2022).

218. Fontaine, E. *et al.* Dual role of histone variant H3.3B in spermatogenesis: positive regulation of piRNA transcription and implication in X-chromosome inactivation. *Nucleic Acids Research* **50**, 7350–7366 (2022).

219. Lichtsteiner, S., Wuarin, J. & Schibler, U. The interplay of DNA-binding proteins on the promoter of the mouse albumin gene. *Cell* **51**, 963–973 (1987).

220. Khan, K. A., Ng, M. K. & Cheung, P. The Use of Mononucleosome Immunoprecipitation for Analysis of Combinatorial Histone Post-translational Modifications and Purification of Nucleosome-Interacting Proteins. *Front Cell Dev Biol* **8**, 331 (2020).

221. Langmead, B. & Salzberg, S. L. Fast gapped-read alignment with Bowtie 2. *Nat Methods* **9**, 357–359 (2012).

222. Danecek, P. *et al.* Twelve years of SAMtools and BCFtools. *GigaScience* **10**, giab008 (2021).

223. Amemiya, H. M., Kundaje, A. & Boyle, A. P. The ENCODE Blacklist: Identification of Problematic Regions of the Genome. *Sci Rep* **9**, 9354 (2019).

224. Quinlan, A. R. & Hall, I. M. BEDTools: a flexible suite of utilities for comparing genomic features. *Bioinformatics* **26**, 841–842 (2010).

225. Ramírez, F. *et al.* deepTools2: a next generation web server for deep-sequencing data analysis. *Nucleic Acids Res* **44**, W160–W165 (2016).

226. Trott, A. J. & Menet, J. S. Regulation of circadian clock transcriptional output by CLOCK:BMAL1. *PLoS Genet* **14**, e1007156 (2018).

227. Lande-Diner, L., Stewart-Ornstein, J., Weitz, C. J. & Lahav, G. Single-cell analysis of circadian dynamics in tissue explants. *MBoC* **26**, 3940–3945 (2015).

228. Tang, M. C. W., Jacobs, S. A., Wong, L. H. & Mann, J. R. Conditional allelic replacement applied to genes encoding the histone variant H3.3 in the mouse. *Genesis* **51**, 142–146 (2013).

229. Zhang, E. E. *et al.* A Genome-wide RNAi Screen for Modifiers of the Circadian Clock in Human Cells. *Cell* **139**, 199–210 (2009).

230. Wu, C., Jin, X., Tsueng, G., Afrasiabi, C. & Su, A. I. BioGPS: building your own mash-up of gene annotations and expression profiles. *Nucleic Acids Res* **44**, D313–D316 (2016).

231. Chereji, R. V., Bryson, T. D. & Henikoff, S. Quantitative MNase-seq accurately maps nucleosome occupancy levels. *Genome Biol* **20**, 198 (2019).

232. Le Martelot, G. *et al.* Genome-Wide RNA Polymerase II Profiles and RNA Accumulation Reveal Kinetics of Transcription and Associated Epigenetic Changes During Diurnal Cycles. *PLoS Biol* **10**, e1001442 (2012).

233. Wen, Z., Zhang, L., Ruan, H. & Li, G. Histone variant H2A.Z regulates nucleosome unwrapping and CTCF binding in mouse ES cells. *Nucleic Acids Research* **48**, 5939–5952 (2020).

234. Millau, J.-F. & Gaudreau, L. CTCF, cohesin, and histone variants: connecting the genome. *Biochem. Cell Biol.* **89**, 505–513 (2011).

235. Weth, O. *et al.* CTCF induces histone variant incorporation, erases the H3K27me3 histone mark and opens chromatin. *Nucleic Acids Research* **42**, 11941–11951 (2014).

236. Carcamo, S. *et al.* Altered BAF occupancy and transcription factor dynamics in PBAF-deficient melanoma. *Cell Reports* **39**, 110637 (2022).

237. Tropberger, P. *et al.* Regulation of Transcription through Acetylation of H3K122 on the Lateral Surface of the Histone Octamer. *Cell* **152**, 859–872 (2013).

238. Sengupta, D., Friman, E. T., Illingworth, R. S., Bickmore, W. A. & Kumar, Y. Acetylation of H3K115 at the nucleosome dyad is associated with fragile nucleosomes at active regulatory sites. Preprint at https://doi.org/10.1101/2023.11.10.566531 (2023).

239. Michael, A. K. *et al.* Cooperation between bHLH transcription factors and histones for DNA access. *Nature* **619**, 385–393 (2023).

240. Preitner, N. *et al.* The Orphan Nuclear Receptor REV-ERBα Controls Circadian Transcription within the Positive Limb of the Mammalian Circadian Oscillator. *Cell* **110**, 251–260 (2002).

241. Chikhaoui, L. *et al.* Circadian PERIOD proteins sculpt the mammalian alternative splicing landscape. Preprint at https://doi.org/10.1101/2024.12.23.630108 (2024).

242. Kwon, I. *et al.* BMAL1 Shuttling Controls Transactivation and Degradation of the CLOCK/BMAL1 Heterodimer. *Molecular and Cellular Biology* **26**, 7318–7330 (2006).

243. Nekrasov, M., Soboleva, T. A., Jack, C. & Tremethick, D. J. Histone variant selectivity at the transcription start site: H2A.Z or H2A.Lap1. *Nucleus* **4**, 431–437 (2013).

244. Nekrasov, M. *et al.* Histone H2A.Z inheritance during the cell cycle and its impact on promoter organization and dynamics. *Nat Struct Mol Biol* **19**, 1076–1083 (2012).

245. Soutoglou, E. & Talianidis, I. Coordination of PIC Assembly and Chromatin Remodeling During Differentiation-Induced Gene Activation. *Science* **295**, 1901–1904 (2002).

246. Menon, D. U., Chakraborty, P., Murcia, N. & Magnuson, T. ARID1A governs the silencing of sex-linked transcription during male meiosis in the mouse. *eLife* **12**, RP88024 (2024).

247. Tabuloc, C. A. *et al.* CLOCK and TIMELESS regulate rhythmic occupancy of the BRAHMA chromatin-remodeling protein at clock gene promoters. *PLoS Genet* **19**, e1010649 (2023).

248. Kwok, R. S., Li, Y. H., Lei, A. J., Edery, I. & Chiu, J. C. The Catalytic and Non-catalytic Functions of the Brahma Chromatin-Remodeling Protein Collaborate to Fine-Tune Circadian Transcription in Drosophila. *PLoS Genet* **11**, e1005307 (2015).

249. Grossi, E. *et al.* The SWI/SNF PBAF complex facilitates REST occupancy at repressive chromatin. *Molecular Cell* S109727652500303X (2025) doi:10.1016/j.molcel.2025.03.026.

250. Schwartzentruber, J. *et al.* Driver mutations in histone H3.3 and chromatin remodelling genes in paediatric glioblastoma. *Nature* **482**, 226–231 (2012).

251. Reddy, D., Bhattacharya, S., Shah, S., Rashid, M. & Gupta, S. DNA methylation mediated downregulation of histone H3 variant H3.3 affects cell proliferation contributing to the development of HCC. *Biochimica et Biophysica Acta (BBA) - Molecular Basis of Disease* **1868**, 166284 (2022).

252. Tagami, H., Ray-Gallet, D., Almouzni, G. & Nakatani, Y. Histone H3.1 and H3.3 Complexes Mediate Nucleosome Assembly Pathways Dependent or Independent of DNA Synthesis. *Cell* **116**, 51–61 (2004).

253. Nakatani, Y. & Ogryzko, V. Immunoaffinity Purification of Mammalian Protein Complexes. in *Methods in Enzymology* vol. 370 430–444 (Elsevier, 2003).

Supplementary materials

List of supplementary materials

Supplementary Figure 1

Figure S1. Timeline of major early discoveries in the field of mammalian circadian research.

Supplementary Figure 2

Figure S2. Detailed model of the mammalian core-clock mechanism.

Supplementary Figure 3

Figure S3. Differential enrichment of PBAF/cBAF components in H3.3A complexes in wild-type vs. PerKO livers.

Supplementary Table 1

Table S1. Mass spectrometry analysis of detected peptides of PBAF/cBAF components in H3.3A complexes in wild-type vs. PerKO livers (Table 14).

Supplementary Table 2

Table S2. ChIP fragment length and Tapestation profiles (Table 15).

Supplementary Table 3

Table S3. Primer sequences (Table 16).

Quantification of immunoprecipitation experiments

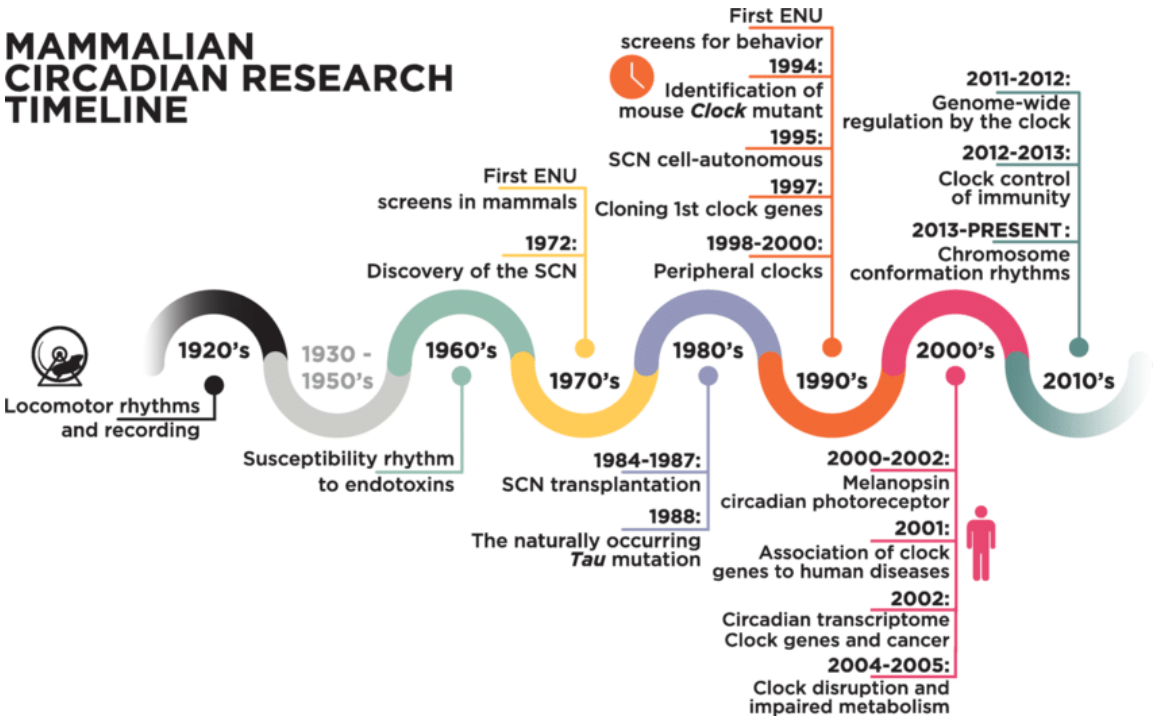


Figure S1. Timeline of major early discoveries in the field of mammalian circadian research. Overview of major findings in establishment of molecular clock mechanisms and their role in physiology. Since 2010s, one of the major axes in the field focuses on rhythms in chromatin dynamics and how they in turn influence rhythms in physiology. *Figure from Rijo-Ferreira F, Takahashi JS. Genome Med. 2019* [107].

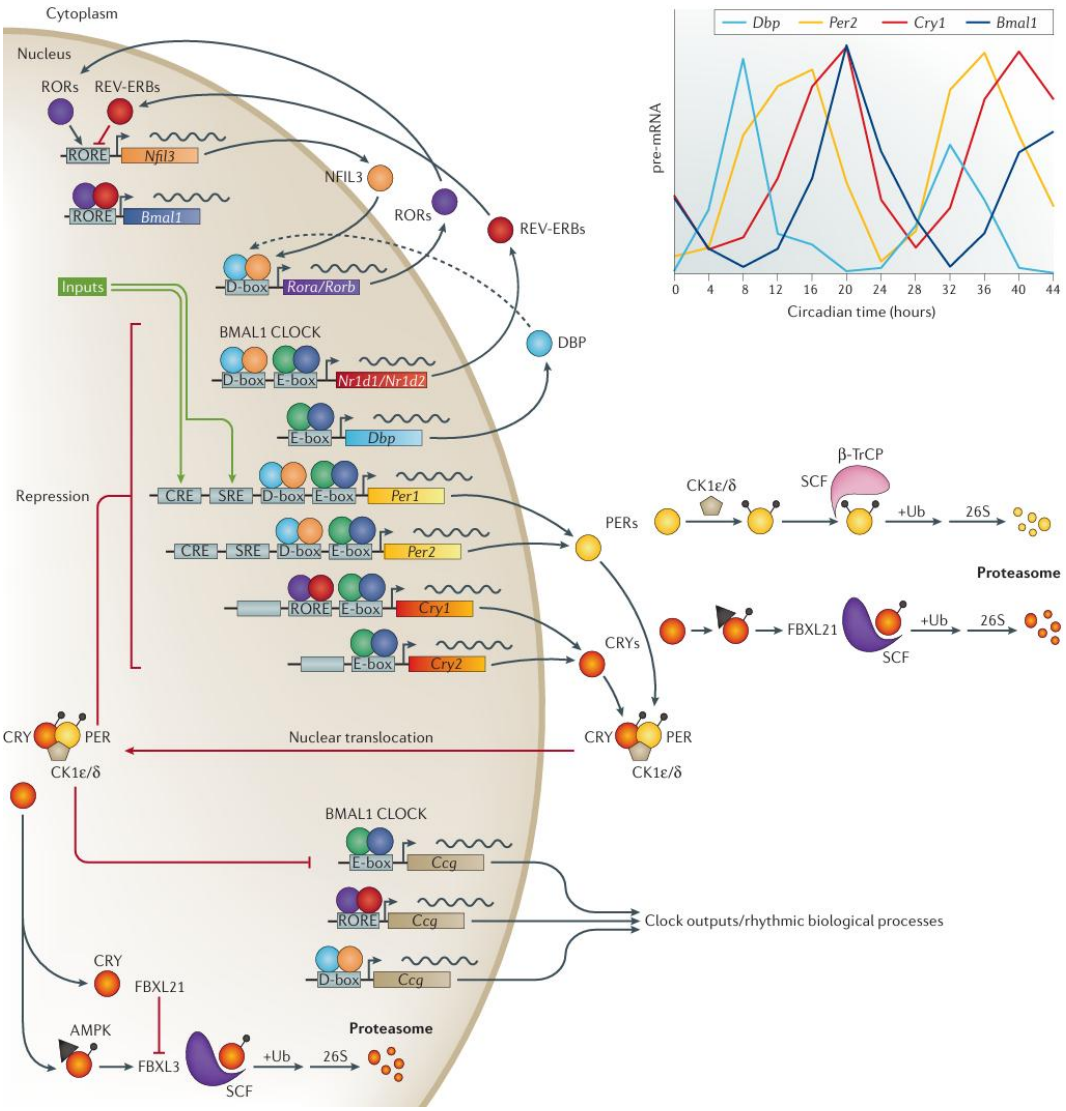


Figure S2. Detailed model of the mammalian core-clock mechanism. The core-clock regulatory network in mammals comprises bHLH-PAS transcription factors BMAL1 and CLOCK, which activate Per1, Per2, Cry1, Cry2 genes. Their protein products in turn interact with BMAL1-CLOCK and repress their own synthesis. In parallel, stability of PER and CRY proteins is regulated by the E3 ubiquitin ligase pathways. In addition, BMAL1-CLOCK rhythmically regulate expression of Nr1d1 and Nr1d2 genes, respectively encoding for the nuclear receptors REV-ERBα and REV-ERBβ. In turn, REV-ERBs negatively regulate expression of Arntl1 (Bmal1) and Nfil3 (encoding for the nuclear factor, interleukin-3 regulated). Bmal1 and Nfil3 expression is positively regulated by the retinoic acid-related orphan receptor α and β (RORα/β; respectively encoded by Rora and Rorb). In addition, NFIL3 represses the PAR-bZip factor DBP (D-box binding protein) which mediates rhythms in RORs nuclear receptors. These are the main TTFLs involved in transcriptional regulations of the majority of cycling genes. As an output, differential rhythms in transcription are being established, highlighted by the different RNA profiles on the right upper panel (given is the example of the mouse liver). Furthermore, additional regulations of ~24h transcriptional rhythms are mediated by the CCGs (the rhythmic output genes), and casein kinases 1 (CK1), involved in stability of PER proteins. Remaining abbreviations on the figure: AMPK, 5´ AMP-activated protein kinase; CRE, cAMP response element; FBX, F-box protein; SCF, SKP1-cullin-F-box protein; SRE, serum response element; Ub, ubiquitin. *Legend is adapted from the original description. Figure from Takahashi JS. Nat Rev Genet. 2017* [75].

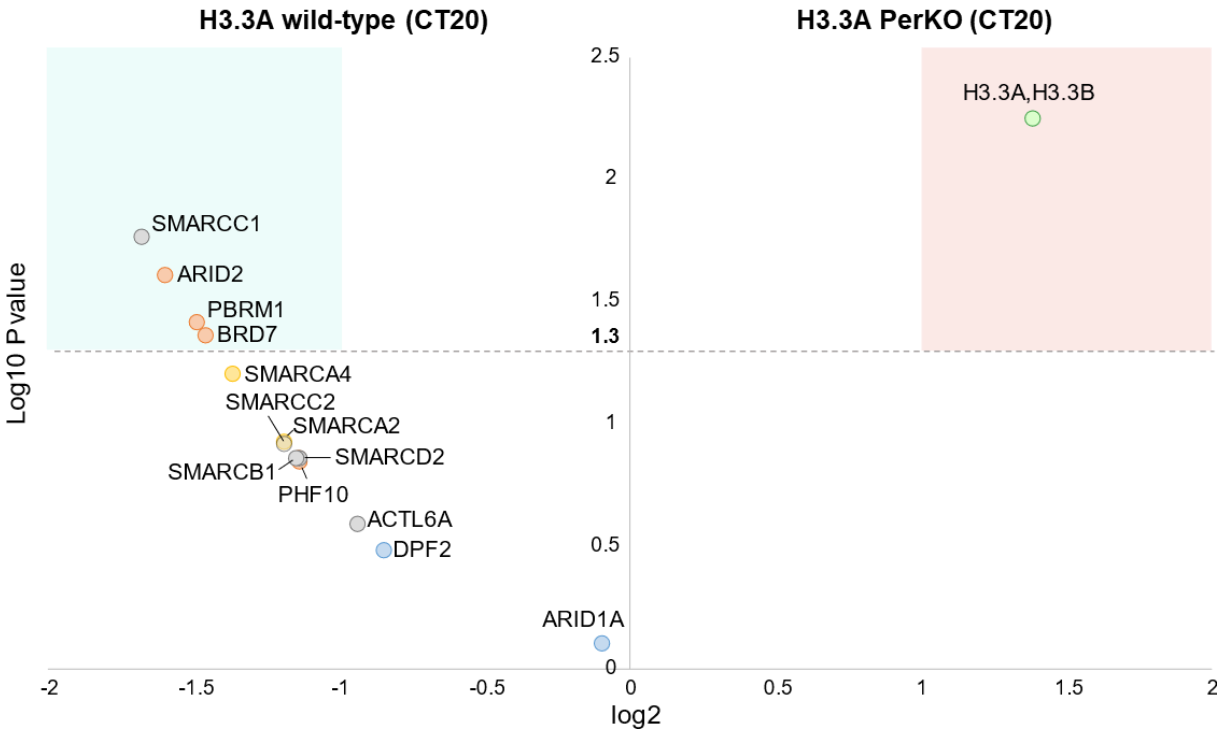


Figure S3. Differential enrichment of PBAF/cBAF components in H3.3A complexes in wild-type vs. PerKO livers. Volcano plot visualization of differential enrichment of specific PBAF (orange), specific cBAF (blue), shared ATPase subunits (yellow) and common core PBAF/cBAF components (grey) in wild-type vs. PerKO H3.3A complexes at CT20. Shown is also enrichment of H3.3 (green). Significant enrichment is highlighted in blue box for wild-type and in red box for PerKO. Shown are results from one biological replicate, based on the preliminary initial mass spectrometry analysis.

Table 14. Mass spectrometry analysis of detected peptides of PBAF/cBAF components in H3.3A complexes in wild-type vs. PerKO livers.

Biological replicate 1: highlighted in green are peptides that are significantly missing in H3.3A interactome in PerKO livers vs. in red are peptides that are significantly enriched.

Protein name	Detected peptides (sequence)	Abundance ratio: (H3.3A PerKO Night) / (H3.3A Night)	Abundance Ratio Adj. P-Value: (H3.3A PerKO Night) / (H3.3A Night)	Master Protein Accessions
PBRM1	AQHPDYSFGELSR	0.189	0.66023233	Q8BSQ9
Accession number	ATSPSSSVSGDFDDGHHSVPTPGPSR	0.01	2.85769E-17	Q8BSQ9
Q8BSQ9	ATSPSSSVSGDFDDGHHSVPTPGPSR	0.01	2.85769E-17	Q8BSQ9
	DGAAYFYGPIFIHPEETEHEPTK	0.094	0.191451535	Q8BSQ9
	DIDLLAK	0.076	0.157622571	Q8BSQ9
	ELARRDDIEDGDSMISSATSDTGSAK	0.01	2.85769E-17	Q8BSQ9
	ELGPLPDDDDMASPK	0.168	0.577378403	Q8BSQ9
	ELGPLPDDDDMASPK	0.158	0.292245966	Q8BSQ9
	EPSPLLEK	0.146	0.52713715	Q8BSQ9
	GAHTTMADALWR	0.677	0.826095857	Q8BSQ9
	HYNEEGSQVYNDAHILEK	0.102	0.377711861	Q8BSQ9
	KAEIEHHEMTK	0.01	2.85769E-17	Q8BSQ9
	KIQLLEAK	0.01	2.85769E-17	Q8BSQ9
	IIEHNIRNDK	0.087	0.061731772	Q8BSQ9
	LLHSEAYLK	0.157	0.558368272	Q8BSQ9
	IILEPMDLK	0.111	0.289115649	Q8BSQ9
	LISELFQK	0.01	2.85769E-17	Q8BSQ9
	LPSHWLK	0.093	0.215184288	Q8BSQ9
	LSAIFLR	0.01	2.85769E-17	Q8BSQ9
	LWTMPISSVR	0.01	2.85769E-17	Q8BSQ9
	MPISLQQIR	0.01	2.85769E-17	Q8BSQ9
	MPISLQQIR	0.01	2.85769E-17	Q8BSQ9
	NGEILLSPALSYTTK	0.01	2.85769E-17	Q8BSQ9
	NHQGQLIAEPFFHLPSK	0.01	2.85769E-17	Q8BSQ9
	NQPDYYEVVSQPIDLMK	0.01	2.85769E-17	Q8BSQ9
	NTDNSDDNRAEDNFNLEK	0.083	0.141600198	Q8BSQ9
	RDDIEDGDSMISSATSDTGSAK	0.01	2.85769E-17	Q8BSQ9
	SEDSSGTTGLSGLHR	0.076	0.165174928	Q8BSQ9
	SSLGEERNPTSK	0.199	0.373473146	Q8BSQ9
	TYNEPGSQVFK	0.124	0.341529025	Q8BSQ9
	VASVFANADKGDDEK	0.01	2.85769E-17	Q8BSQ9
	VGDCVFIK	0.01	2.85769E-17	Q8BSQ9
	VLLETR	0.283	0.622301094	Q8BSQ9
	VQYPDYYAIIK	0.01	2.85769E-17	Q8BSQ9
	VVDDEIYYFR	0.01	2.85769E-17	Q8BSQ9
	WDQTLAAR	0.108	0.261575498	Q8BSQ9
	YIEGLSAESNSISK	0.133	0.501286853	Q8BSQ9
ARID2	AVVAQHAAPPPGIVEIDSEK	0.01	2.85769E-17	E9Q7E2
Accession number	DALLAGLK	0.01	2.85769E-17	E9Q7E2
E9Q7E2	DIVDDNEVRDLISDR	0.01	2.85769E-17	E9Q7E2
	ELDLHGLYTR	0.088	0.216310732	E9Q7E2
	FSFITHLQDK	0.01	2.85769E-17	E9Q7E2
	GGILTSTGFYK	0.01	2.85769E-17	E9Q7E2
	LGINDIEGQR	0.341	0.83464027	E9Q7E2
	LTAALILK	0.01	2.85769E-17	E9Q7E2
	NLSFEESNVK	1.933	0.191277908	E9Q7E2
	VLQIAVILR	0.01	2.85769E-17	E9Q7E2
BRD7	EAEITQIEPTGR	0.189	0.667544614	O88665
Accession number	ELTQQVTPGDVVSIHGVR	0.178	0.441256222	O88665
O88665	LESSSQDRLTALQAVTTFGAPAEVFDSEEAEVFQR	0.01	2.85769E-17	O88665
	LQSGVNTLQGFK	0.01	2.85769E-17	O88665
	LTALQAVTTFGAPAEVFDSEEAEVFQR	0.01	2.85769E-17	O88665
	NNDYQSIEELK	0.124	0.296418418	O88665
	QSIDFMSDLQK	0.01	2.85769E-17	O88665
	RKPDGTTTLGLLHPVDPIVGEPGYCPVR	0.01	2.85769E-17	O88665
	SLQDLDMSSPEDEGQTR	0.01	2.85769E-17	O88665
	VGGSEVTELSTGSSGHDSSLFEDR	0.166	0.435718058	O88665
	VGGSEVTELSTGSSGHDSSLFEDRSDHDK	0.01	2.85769E-17	O88665
PHF10	AAEFNSNLNR	0.217	0.70568805	Q9D8M7
Accession number	AYFDLQTHVIQVPQGK	0.01	2.85769E-17	Q9D8M7
Q9D8M7	HAEYSVILQEK	0.01	2.85769E-17	Q9D8M7
	RAYFDLQTHVIQVPQGK	0.01	2.85769E-17	Q9D8M7
	VSSYPVALIPGQFQEYYK	0.01	2.85769E-17	Q9D8M7
SMARCA4 (BRG1)	AIEEGTLEEIEEEVRQK	0.01	2.85769E-17	Q3TKT4
Accession number	ASGKFELLDR	0.01	2.85769E-17	Q3TKT4; Q6DIC0
Q3TKT4	DDAEVERLTCEEEEEK	0.01	2.85769E-17	Q3TKT4; Q6DIC0
	DTALETALNAK	0.01	2.85769E-17	Q3TKT4
	ELPEYYELIR	0.245	0.735373143	Q3TKT4
	EVDYSDSLTEK	0.15	0.470332013	Q3TKT4
	GLDPVEILQER	0.151	0.539957985	Q3TKT4
	HQEYLNSILQHAK	0.184	0.51057899	Q3TKT4; Q6DIC0
	KAENAEGQTPAIGPDGEPLDETSQMSDLPVK	0.01	2.85769E-17	Q3TKT4
	KIPDPDSDDVSEVDAR	0.01	2.85769E-17	Q3TKT4
	LLNFQR	0.445	0.999922489	Q3TKT4; Q6DIC0
	ILTGTDAPK	0.089	0.118200019	Q3TKT4
	LMEEDELPSWIIK	0.167	0.599067879	Q3TKT4; Q6DIC0
	IQELENLPGSLAGDLR	0.01	2.85769E-17	Q3TKT4
	LTQVLNTHYVAPR	0.01	2.85769E-17	Q3TKT4; Q6DIC0
	IVDAVIK	0.01	2.85769E-17	Q3TKT4
	QDVDDEYGVSQALAR	0.263	0.764518597	Q3TKT4
	QLSEVFIQLPSRK	0.01	2.85769E-17	Q3TKT4; Q6DIC0
	VDLNEEETILIIR	0.546	0.985811044	Q3TKT4; Q6DIC0
	VIQAGMFDQK	0.241	0.729503073	Q3TKT4; Q6DIC0
	WAPSVVK	0.01	2.85769E-17	Q3TKT4; Q6DIC0

SMARCB1	ASEVEEILDGNDEK	0.147	0.500516284	Q9Z0H3
Accession number	AVSISTEPPTYLR	0.141	0.583944869	Q9Z0H3
Q9Z0H3	DHGYTTLATSVTLLK	0.01	2.85769E-17	Q9Z0H3
	NSQWVPTLPNSSHHLDAVPCSTTINR	0.01	2.85769E-17	Q9Z0H3
	TYAFSENPLPTVEIAIR	0.01	2.85769E-17	Q9Z0H3
SMARCC1	ALPEFFNGK	0.01	2.85769E-17	P97496; Q6PDG5
Accession number	ASGKVDPTYGLESSCIAGTGPDEPEK	0.01	2.85769E-17	P97496
P97496	EKPIDLQNFGLR	0.183	0.627830505	P97496
	GGTVADLDEQDEEAVTTGGK	0.01	2.85769E-17	P97496
	GGTVADLDEQDEEAVTTGGKEDEDPSK	0.01	2.85769E-17	P97496
	HLAAVEERK	0.01	2.85769E-17	P97496; Q6PDG5
	LNPQEYLTSTACRR	0.01	2.85769E-17	P97496; Q6PDG5
	NFMIDTYR	0.277	0.699904856	P97496; Q6PDG5
	SLVALLVETQMK	0.01	2.85769E-17	P97496; Q6PDG5
	SLVALLVETQMK	0.01	2.85769E-17	P97496; Q6PDG5
	TPEIYLAYR	0.355	0.953866532	P97496; Q6PDG5
	VREEVPLELVEAHVK	0.234	0.51733371	P97496
SMARCC2	ADPAFGLESSGIAGTASDEPERIEESGTEEARPEGQAADEK	0.13	0.420612589	Q6PDG5
Accession number	ADPAFGLESSGIAGTASDEPERIEESGTEEARPEGQAADEKK	0.01	2.85769E-17	Q6PDG5
Q6PDG5	ALPEFFNGK	0.01	2.85769E-17	P97496; Q6PDG5
	DKEPTEGQEEVLK	0.184	0.699924481	Q6PDG5
	DIGEGNLSTAAAAALAAAAVK	0.141	0.519401089	Q6PDG5
	DMDEPSPVPNVEEVTLPK	0.01	2.85769E-17	Q6PDG5
	DMDEPSPVPNVEEVTLPK	0.229	0.772016944	Q6PDG5
	EEISEVPK	0.228	0.762214265	Q6PDG5
	EEVPTALVEAHVR	0.246	0.811368332	Q6PDG5
	EKPADMQNFGLR	0.094	0.207369241	Q6PDG5
	GGTMTDLDEQDDESMETTGK	0.01	2.85769E-17	Q6PDG5
	HLAAVEERK	0.01	2.85769E-17	P97496; Q6PDG5
	KGPSTPYTK	0.175	0.366885475	Q6PDG5
	LNPQEYLTSTACRR	0.01	2.85769E-17	P97496; Q6PDG5
	MKEEVPTALVEAHVR	0.086	0.216155355	Q6PDG5
	MKEEVPTALVEAHVR	0.267	0.775039684	Q6PDG5
	NFMIDTYR	0.277	0.699904856	P97496; Q6PDG5
	QAFHMEQLK	0.132	0.274317045	Q6PDG5
	QQLLADR	0.349	0.952217698	Q6PDG5
	RGHREEEQEDLTK	0.026	3.98651E-05	Q6PDG5
	SALEEFSK	0.135	0.444599652	Q6PDG5
	SDGDPIVDPEK	0.203	0.701211382	Q6PDG5
	SLVALLVETQMK	0.01	2.85769E-17	P97496; Q6PDG5
	SLVALLVETQMK	0.01	2.85769E-17	P97496; Q6PDG5
	SNASHVVYPVPGNLEEEEWVRPVMK	0.01	2.85769E-17	Q6PDG5
	TPEIYLAYR	0.355	0.953866532	P97496; Q6PDG5
	YYEAADTVTQFDNVR	0.01	2.85769E-17	Q6PDG5
SMARCD2	AAFYHQPWAQEAVGR	0.167	0.433240457	Q99JR8
Accession number	AQMSNFLASTTNQQEIASLDVK	0.01	2.85769E-17	Q99JR8
Q99JR8	ELYGPDNHLVEWHR	0.01	2.85769E-17	Q99JR8
	IHETIESINQLK	0.106	0.254419396	Q99JR8
	LLDDPSK	0.189	0.480054657	Q99JR8
	IITDVIGNPEEERR	0.155	0.514834585	Q99JR8
	IRELVPESQAYMDLLAFER	0.258	0.721574911	Q61466; Q99JR8
	IYISNTFSPSK	0.161	0.536561621	Q99JR8
	MPTTQETDGFQVK	0.346	0.908698918	Q99JR8
	RQELEQVLGIR	0.11	0.288693984	Q99JR8
	TACYDIDVEVDDPLK	0.01	2.85769E-17	Q99JR8
	VASWELRVEGK	0.01	2.85769E-17	Q99JR8
SMARCE1	AYHNSPAYLAYINAK	0.092	0.231428868	O54941
Accession number	FLESTDSFNNELK	0.235	0.771265298	O54941
O54941	KLEAELLQIEER	0.151	0.493349175	O54941
	IAAEIAQAEEQAR	0.179	0.623467787	O54941
	LISEILSESVVPDVR	0.01	2.85769E-17	O54941
	QEYLNEYEAEK	0.255	0.829204572	O54941
	SRAEAALEEESR	100	2.85769E-17	O54941
ACTL6A	ENMEAISPLK	0.286	0.877295705	Q9Z2N8
Accession number	ENMEAISPLK	0.421	0.916538138	Q9Z2N8
Q9Z2N8	LIANNTTVER	100	2.85769E-17	Q9Z2N8
	IPEGLFDPSNVK	0.263	0.811365434	Q9Z2N8
	MSGGVYGGDEVGALVFDIGSYTVR	0.226	0.483798444	Q9Z2N8
	QGGPTYYIDTNALR	0.086	0.388838869	Q9Z2N8
	SEASLHPVLMSEAPWNTR	0.01	2.85769E-17	Q9Z2N8
	SEASLHPVLMSEAPWNTR	0.01	2.85769E-17	Q9Z2N8
	STGLILDSGATHTTAIPVHDGYVLQQGIVK	0.119	0.478894534	Q9Z2N8
	TAVLTAFANGR	0.01	2.85769E-17	Q9Z2N8
	VDFPTAIGVVLER	0.781	0.747599165	Q9Z2N8
	VDFPTAIGVVLERDDGSTMMEIDGDK	0.01	2.85769E-17	Q9Z2N8
	VPRENMEAISPLK	0.01	2.85769E-17	Q9Z2N8
SMARCA2 (BRM)	AIEDGNLEEMEEEVR	0.01	2.85769E-17	Q6DIC0
Accession number	AQILAYK	0.148	0.340344772	Q6DIC0
Q6DIC0	ASGKFELLDR	0.01	2.85769E-17	Q3TKT4; Q6DIC0
	DDAEVERLTCEEEEEK	0.01	2.85769E-17	Q3TKT4; Q6DIC0
	DTTLETALNSK	0.196	0.489210875	Q6DIC0
	DVDYSDALTEK	0.134	0.41236107	Q6DIC0
	GPSPFSPVQLHQLR	0.01	2.85769E-17	Q6DIC0
	GQPLPETLQLAVQGK	0.01	2.85769E-17	Q6DIC0
	HQEYLNSILQHAK	0.184	0.51057899	Q3TKT4; Q6DIC0
	KAEENAEGGEPALGPDGEPIDESSQMSDLPVK	0.01	2.85769E-17	Q6DIC0
	ILLDPNSEEVSEK	0.172	0.591734929	Q6DIC0
	LLNFQR	0.445	0.999922489	Q3TKT4; Q6DIC0
	LMEEDELPSWIIK	0.167	0.599067879	Q3TKT4; Q6DIC0
	ISPIQKPQGLDPVEILQER	0.155	0.501679244	Q6DIC0
	LTQVLNTHYVAPR	0.01	2.85769E-17	Q3TKT4; Q6DIC0
	QLSEVFIQLPSRK	0.01	2.85769E-17	Q3TKT4; Q6DIC0
	VDLNEEETILIIR	0.546	0.985811044	Q3TKT4; Q6DIC0
	VLFGPEAPK	0.143	0.492184081	Q6DIC0
	VIQAGMFDQK	0.241	0.729503073	Q3TKT4; Q6DIC0
	WAPSVVK	0.01	2.85769E-17	Q3TKT4; Q6DIC0
ARID1A	AGPPVPASHIAPTPVQPPMIR	0.01	2.85769E-17	A2BH40
Accession number	FPFGISPAQSHR	0.01	2.85769E-17	A2BH40
A2BH40	NDPFVVDCSDK	0.292	0.645108354	A2BH40
DPF2	EGLISQDGSSLEALLR	0.01	2.85769E-17	Q61103
Accession number	MAAVVENVVK	0.191	0.688018051	Q61103
Q61103	VDDDSLGEFPVSNSR	0.01	2.85769E-17	Q61103

Biological replicate 2: highlighted in green are peptides that are significantly missing in H3.3A interactome in PerKO livers.

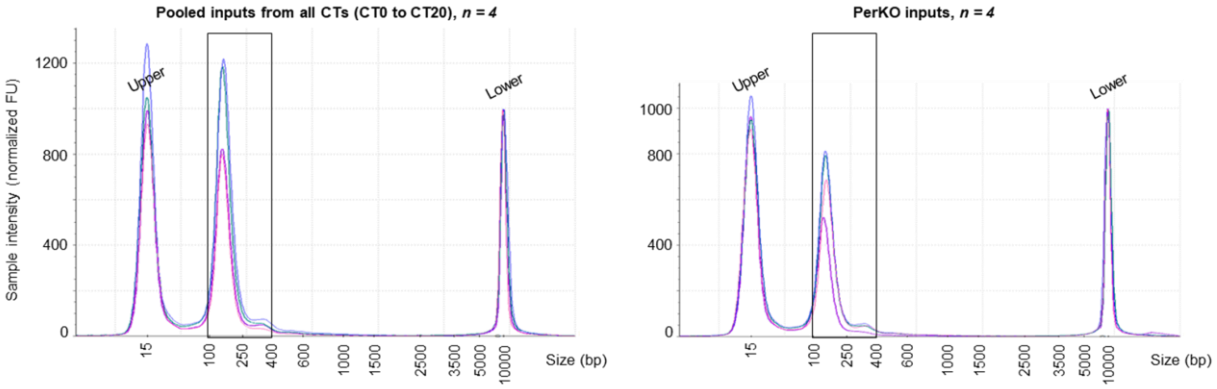
Protein name	Detected peptides (sequence)	Abundance ratio: (H3.3A PerKO Night) / (H3.3A Night)	Abundance Ratio Adj. P-Value: (H3.3A PerKO Night) / (H3.3A Night)	Master Protein Accessions
PBRM1	AQHPDYSFGELSR	0.34	0.217552826	Q8BSQ9
Accession number	ATSPSSSVSGDFDDGHHSVPTPGPSR	0.01	5.58805E-17	Q8BSQ9
Q8BSQ9	DALVLHK	0.01	5.58805E-17	Q8BSQ9
	DGAAYFYGPIFIHPEETEHEPTK	0.422	0.374684623	Q8BSQ9
	DIDLLAK	0.276	0.066630772	Q8BSQ9
	ELGPLPDDDDMASPK	0.403	0.336988839	Q8BSQ9
	GEADDEDDDEDGQDNQGTLADGSSPGYLK	0.01	5.58805E-17	Q8BSQ9
	HYNEEGSQVYNDAHILEK	0.347	0.235013516	Q8BSQ9
	KYPDYYQQIK	0.289	0.144223905	Q8BSQ9
	LCPENFRDEDVFVCESR	0.01	5.58805E-17	Q8BSQ9
	IIEHNIRNDK	0.302	0.151545873	Q8BSQ9
	ILFNVVLEAR	0.468	0.506214968	Q8BSQ9
	LLHSEAYLK	0.147	0.001212932	Q8BSQ9
	IILEPMDLK	0.474	0.521032035	Q8BSQ9
	LISELFQK	0.337	0.185990913	Q8BSQ9
	LNEVYEAVK	0.344	0.216199522	Q8BSQ9
	LPSHWLK	0.223	0.037493684	Q8BSQ9
	LPSRSELPDYYLTIK	0.319	0.147418617	Q8BSQ9
	LSAIFLR	0.394	0.310473803	Q8BSQ9
	LSAITMALQYGSESEEDAALAAAR	0.643	0.920743161	Q8BSQ9
	LWDLYLR	0.515	0.674475167	Q8BSQ9
	LWTMPISSVR	0.414	0.433132248	Q8BSQ9
	MPISLQQIR	0.492	0.563816862	Q8BSQ9
	MPISLQQIR	0.274	0.111827049	Q8BSQ9
	NGEILLSPALSYTTK	0.406	0.414723075	Q8BSQ9
	NHQGQLIAEPFFHLPSK	0.51	0.571813168	Q8BSQ9
	NQPDYYEVVSQPIDLMK	0.01	5.58805E-17	Q8BSQ9
	NTDNSDDNRAEDNFNLEK	0.01	5.58805E-17	Q8BSQ9
	RDDIEDGDSMISSATSDTGSAK	0.01	5.58805E-17	Q8BSQ9
	SEDSSGTTGLSGLHR	0.27	0.073960651	Q8BSQ9
	SELPDYYLTIK	0.347	0.216997807	Q8BSQ9
	TYNEPGSQVFK	0.23	0.029390794	Q8BSQ9
	VGDCVFIK	0.252	0.051107492	Q8BSQ9
	VLLETR	0.01	5.58805E-17	Q8BSQ9
	VQYPDYYAIIK	0.353	0.219162426	Q8BSQ9
	VVDDEIYYFR	0.336	0.183587321	Q8BSQ9
	WDQTLAAR	0.332	0.157789763	Q8BSQ9
	YIEGLSAESNSISK	0.36	0.244929989	Q8BSQ9
ARID2	ALPLPIQMYYQQQPISTPVVR	0.01	5.58805E-17	E9Q7E2
Accession number	AVVAQHAAPPPGIVEIDSEK	0.33	0.219351298	E9Q7E2
E9Q7E2	DALLAGLK	0.353	0.250137223	E9Q7E2
	DIVDDNEVRDLISDR	0.284	0.110081597	E9Q7E2
	ELDLHGLYTR	0.343	0.201555529	E9Q7E2
	FSFITHLQDK	0.15	0.002710081	E9Q7E2
	GGILTSTGFYK	0.328	0.149820257	E9Q7E2
	GLAFLDELR	1.394	0.846587824	E9Q7E2
	LGINDIEGQR	0.411	0.360014432	E9Q7E2
	LIEHPSSSHQVLSEIRPQAIEQVQTQTHIASGPASR	0.01	5.58805E-17	E9Q7E2
	LTAALILK	0.389	0.371959596	E9Q7E2
	NLSFEESNVK	0.01	5.58805E-17	E9Q7E2
	NLVFRDFTDEK	0.01	5.58805E-17	E9Q7E2
	SCSNAAFALK	0.296	0.15134286	E9Q7E2
BRD7	EAEITQIEPTGR	0.349	0.207337137	O88665
Accession number	ELTQQVTPGDVVSIHGVR	0.314	0.174557017	O88665
O88665	ELTQQVTPGDVVSIHGVRK	0.432	0.515164418	O88665
	LQSGVNTLQGFK	0.402	0.342018435	O88665
	LTALQAVTTFGAPAEVFDSEEAEVFQR	0.01	5.58805E-17	O88665
	NNDYQSIEELK	0.913	0.984522088	O88665
	RKPDGTTTLGLLHPVDPIVGEPGYCPVR	0.226	0.05138052	O88665
	SLQDLDMSSPEDEGQTR	0.01	5.58805E-17	O88665
	VGGSEVTELSTGSSGHDSSLFEDR	0.01	5.58805E-17	O88665
PHF10	AAEFNSNLNR	0.01	5.58805E-17	Q9D8M7
Accession number	AYFDLQTHVIQVPQGK	0.684	0.945083098	Q9D8M7
Q9D8M7	ELNVITETQCTLGLTALR	0.01	5.58805E-17	Q9D8M7
	RAYFDLQTHVIQVPQGK	0.497	0.642263476	Q9D8M7
	VSSYPVALIPGQFQEYYK	0.263	0.063223166	Q9D8M7
SMARCA4 (BRG1)	AIEEGTLEEIEEEVR	0.01	5.58805E-17	Q3TKT4
Accession number	AIEEGTLEEIEEEVRQK	0.01	5.58805E-17	Q3TKT4
Q3TKT4	ASGKFELLDR	0.415	0.387228764	Q3TKT4; Q6DIC0
	DDAEVERLTCEEEEEK	0.797	0.987980438	Q3TKT4; Q6DIC0
	DTALETALNAK	0.01	5.58805E-17	Q3TKT4
	ELPEYYELIR	0.456	0.489453612	Q3TKT4
	EVDYSDSLTEK	0.313	0.178634665	Q3TKT4
	FNVLLTTYEYIIK	1.176	0.868585255	Q3TKT4; Q6DIC0
	GLDPVEILQER	0.438	0.42580772	Q3TKT4
	GLQSYYAVAHAVTERVDK	0.277	0.133396504	Q3TKT4
	HQEYLNSILQHAK	0.456	0.470674435	Q3TKT4; Q6DIC0
	KAENAEGQTPAIGPDGEPLDETSQMSDLPVK	0.01	5.58805E-17	Q3TKT4
	KIPDPDSDDVSEVDAR	0.399	0.435552471	Q3TKT4
	ILTGTDAPK	0.01	5.58805E-17	Q3TKT4
	LMEEDELPSWIIK	0.728	0.970977193	Q3TKT4; Q6DIC0
	LMEEDELPSWIIKDDAEVER	0.01	5.58805E-17	Q3TKT4; Q6DIC0
	IQELENLPGSLAGDLR	0.01	5.58805E-17	Q3TKT4
	LTQVLNTHYVAPR	0.306	0.115860177	Q3TKT4; Q6DIC0
	IVDAVIK	0.01	5.58805E-17	Q3TKT4
	QDVDDEYGVSQALAR	0.216	0.034353821	Q3TKT4
	QLSEVFIQLPSRK	0.01	5.58805E-17	Q3TKT4; Q6DIC0
	TLMNTIMQLR	0.738	0.972448477	Q3TKT4; Q6DIC0
	VDLNEEETILIIR	0.01	5.58805E-17	Q3TKT4; Q6DIC0
	VIQAGMFDQK	0.511	0.687894857	Q3TKT4; Q6DIC0
	WAPSVVK	0.333	0.220159559	Q3TKT4; Q6DIC0

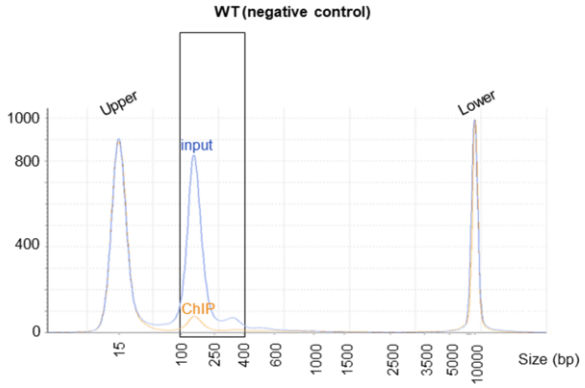
SMARCB1	ASEVEEILDGNDEK	0.434	0.445783839	Q9Z0H3
Accession number	AVSISTEPPTYLR	0.413	0.354211033	Q9Z0H3
Q9Z0H3	DHGYTTLATSVTLLK	0.01	5.58805E-17	Q9Z0H3
	NSQWVPTLPNSSHHLDAVPCSTTINR	0.01	5.58805E-17	Q9Z0H3
	RNSQWVPTLPNSSHHLDAVPCSTTINR	0.01	5.58805E-17	Q9Z0H3
	TYAFSENPLPTVEIAIR	0.472	0.500433167	Q9Z0H3
SMARCC1	ALPEFFNGK	0.57	0.807147795	P97496; Q6PDG5
Accession number	EKPIDLQNFGLR	0.311	0.176487835	P97496
P97496	GGTVADLDEQDEEAVTTGGKEDEDPSK	0.01	5.58805E-17	P97496
	SKTPEIYLAYR	0.412	0.474491282	P97496; Q6PDG5
	SLVALLVETQMK	0.639	0.800639155	P97496; Q6PDG5
	SLVALLVETQMK	0.01	5.58805E-17	P97496; Q6PDG5
	TPEIYLAYR	0.505	0.561565086	P97496; Q6PDG5
	TQDECILHFLR	0.398	0.345419575	P97496; Q6PDG5
	VREEVPLELVEAHVK	0.44	0.544251068	P97496
SMARCC2	ADPAFGLESSGIAGTASDEPERIEESGTEEARPEGQAADEK	0.447	0.432094523	Q6PDG5
Accession number	ADPAFGLESSGIAGTASDEPERIEESGTEEARPEGQAADEKK	0.01	5.58805E-17	Q6PDG5
Q6PDG5	AGGSLCHILAAAYK	0.431	0.5160911	Q6PDG5
	ALPEFFNGK	0.57	0.807147795	P97496; Q6PDG5
	DKEPTEGQEEVLK	0.01	5.58805E-17	Q6PDG5
	DIGEGNLSTAAAAALAAAAVK	0.193	0.01329889	Q6PDG5
	DMDEPSPVPNVEEVTLPK	0.608	0.82185269	Q6PDG5
	DMDEPSPVPNVEEVTLPK	0.967	0.970977193	Q6PDG5
	EALEYQR	0.01	5.58805E-17	Q6PDG5
	EEVPTALVEAHVR	0.414	0.464696289	Q6PDG5
	EGGGAVEEEAKEEISEVPK	0.01	5.58805E-17	Q6PDG5
	EKPADMQNFGLR	0.316	0.169439719	Q6PDG5
	KGPSTPYTK	0.01	5.58805E-17	Q6PDG5
	MKEEVPTALVEAHVR	0.458	0.506860442	Q6PDG5
	MKEEVPTALVEAHVR	0.389	0.417760847	Q6PDG5
	QQLLADR	0.356	0.219100706	Q6PDG5
	SALEEFSK	0.418	0.36657812	Q6PDG5
	SDGDPIVDPEK	0.282	0.079445528	Q6PDG5
	SKTPEIYLAYR	0.412	0.474491282	P97496; Q6PDG5
	SLVALLVETQMK	0.639	0.800639155	P97496; Q6PDG5
	SLVALLVETQMK	0.01	5.58805E-17	P97496; Q6PDG5
	SLVQNNCLSRPNIFLCPEIEPK	0.01	5.58805E-17	Q6PDG5
	SNASHVVYPVPGNLEEEEWVRPVMK	0.498	0.662166861	Q6PDG5
	TPEIYLAYR	0.505	0.561565086	P97496; Q6PDG5
	TQDECILHFLR	0.398	0.345419575	P97496; Q6PDG5
	YDFQNPSR	1.188	0.945083098	Q6PDG5
	YYEAADTVTQFDNVR	0.474	0.53443213	Q6PDG5
SMARCD2	AAFYHQPWAQEAVGR	0.491	0.621347829	Q99JR8
Accession number	AQMSNFLASTTNQQEIASLDVK	0.481	0.593806144	Q99JR8
Q99JR8	ELYGPDNHLVEWHR	0.565	0.819050288	Q99JR8
	FSSFFK	0.425	0.419479336	Q61466; Q99JR8
	IHETIESINQLK	0.348	0.231657475	Q99JR8
	LLDDPSK	0.01	5.58805E-17	Q99JR8
	IITDVIGNPEEERR	0.318	0.14828087	Q99JR8
	IRELVPESQAYMDLLAFER	100	5.58805E-17	Q61466; Q99JR8
	IYISNTFSPSK	0.366	0.255507602	Q99JR8
	MPTTQETDGFQVK	0.468	0.574941521	Q99JR8
	RQELEQVLGIR	0.53	0.659848136	Q99JR8
	TACYDIDVEVDDPLK	0.419	0.443824012	Q99JR8
	VASWELRVEGK	0.01	5.58805E-17	Q99JR8
SMARCE1	AYHNSPAYLAYINAK	0.447	0.468657381	O54941
Accession number	DLTDEEKQEYLNEYEAEK	0.01	5.58805E-17	O54941
O54941	FLESTDSFNNELK	0.582	0.76239478	O54941
	KLEAELLQIEER	0.351	0.237950613	O54941
	IAAEIAQAEEQAR	0.371	0.249707626	O54941
	IAAEIAQAEEQARK	0.01	5.58805E-17	O54941
	LISEILSESVVPDVR	0.421	0.417760847	O54941
	QEYLNEYEAEK	0.652	0.908279544	O54941
	SQSSMAPEEEQVANKAEEK	0.01	5.58805E-17	O54941
ACTL6A	ENMEAISPLK	0.633	0.857415325	Q9Z2N8
Accession number	LIANNTTVER	0.01	5.58805E-17	Q9Z2N8
Q9Z2N8	IPEGLFDPSNVK	0.517	0.583774182	Q9Z2N8
	MSGGVYGGDEVGALVFDIGSYTVR	0.46	0.497345222	Q9Z2N8
	QGGPTYYIDTNALR	0.52	0.591896955	Q9Z2N8
	SEASLHPVLMSEAPWNTR	0.507	0.565276718	Q9Z2N8
	SEASLHPVLMSEAPWNTR	0.01	5.58805E-17	Q9Z2N8
	SPLAGDFITMQCR	0.01	5.58805E-17	Q9Z2N8
	SPLAGDFITMQCR	0.387	0.413430091	Q9Z2N8
	STGLILDSGATHTTAIPVHDGYVLQQGIVK	0.486	0.52196895	Q9Z2N8
	TAVLTAFANGR	0.594	0.858511127	Q9Z2N8
	VDFPTAIGVVLER	0.378	0.347182516	Q9Z2N8
	VDFPTAIGVVLERDDGSTMMEIDGDK	0.01	5.58805E-17	Q9Z2N8
	VPRENMEAISPLK	0.601	0.876316496	Q9Z2N8
SMARCA2 (BRM)	ASGKFELLDR	0.415	0.387228764	Q3TKT4; Q6DIC0
Accession number	DDAEVERLTCEEEEEK	0.797	0.987980438	Q3TKT4; Q6DIC0
Q6DIC0	DTTLETALNSK	0.366	0.308902702	Q6DIC0
	DVDYSDALTEK	0.438	0.445783839	Q6DIC0
	FNVLLTTYEYIIK	1.176	0.868585255	Q3TKT4; Q6DIC0
	GPSPFSPVQLHQLR	0.559	0.787463866	Q6DIC0
	GQPLPETLQLAVQGK	0.306	0.108426438	Q6DIC0
	GQPLPETLQLAVQGKR	0.01	5.58805E-17	Q6DIC0
	HQEYLNSILQHAK	0.456	0.470674435	Q3TKT4; Q6DIC0
	KAEENAEGGEPALGPDGEPIDESSQMSDLPVK	0.01	5.58805E-17	Q6DIC0
	ILLDPNSEEVSEK	0.444	0.456453101	Q6DIC0
	LMEEDELPSWIIK	0.728	0.970977193	Q3TKT4; Q6DIC0
	LMEEDELPSWIIKDDAEVER	0.01	5.58805E-17	Q3TKT4; Q6DIC0
	ISPIQKPQGLDPVEILQER	0.529	0.606861824	Q6DIC0
	LTQVLNTHYVAPR	0.306	0.115860177	Q3TKT4; Q6DIC0
	QLSEVFIQLPSRK	0.01	5.58805E-17	Q3TKT4; Q6DIC0
	SLGDLEK	0.01	5.58805E-17	Q6DIC0
	TLMNTIMQLR	0.738	0.972448477	Q3TKT4; Q6DIC0
	VDLNEEETILIIR	0.01	5.58805E-17	Q3TKT4; Q6DIC0
	VLFGPEAPK	0.396	0.349485855	Q6DIC0
	VIQAGMFDQK	0.511	0.687894857	Q3TKT4; Q6DIC0
	WAPSVVK	0.333	0.220159559	Q3TKT4; Q6DIC0
ARID1A	FPFGISPAQSHR	0.937	0.970199508	A2BH40
Accession number	LVLETLSK	0.782	0.990885155	A2BH40
A2BH40	NDPFVVDCSDK	0.01	5.58805E-17	A2BH40
DPF2	EGLISQDGSSLEALLR	0.519	0.642745788	Q61103
Accession number	MAAVVENVVK	0.563	0.738507496	Q61103
Q61103	VDDDSLGEFPVSNSR	0.01	5.58805E-17	Q61103

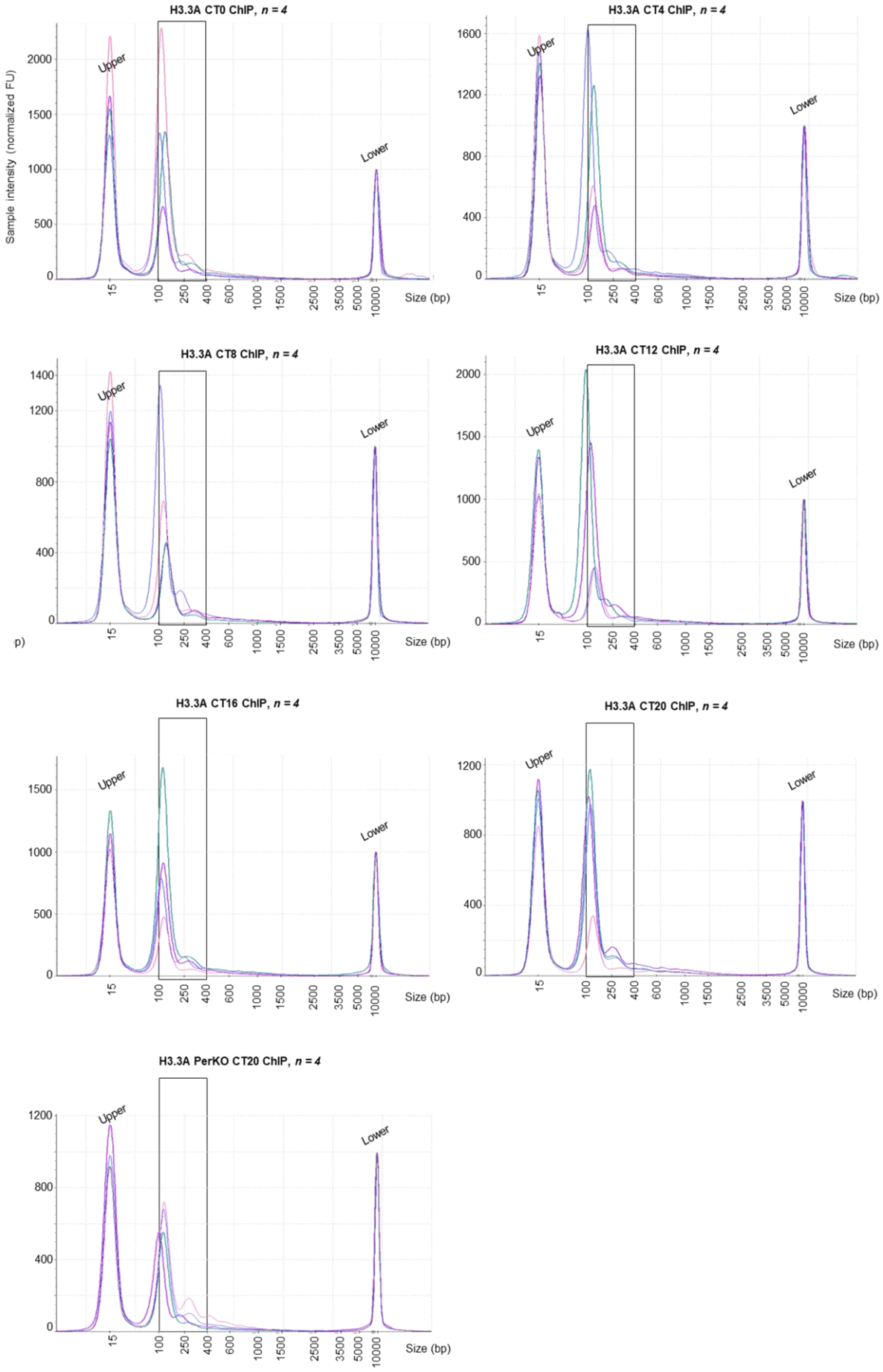
Table 15. ChIP fragment length and Tapestation profiles.

FH-H3.3A circadian ChIP. Table showing the individual and average fragment length for each replicate based on data from Tapestation analysis, followed with Tapestation profiles.

Replicates HA	Peak size (bp)	Average peak size (bp) at mononucleosomal level
input all CTs_1	**143**	**143**
input all CTs_2	**150**	
input all CTs_3	**144**	
input all CTs_4	**134**	
input PerKO CT20_1	**142**	**137**
input PerKO CT20_2	**140**	
input PerKO CT20_3	**141**	
input PerKO CT20_4	**124**	
HA CT0_1	109	**118**
HA CT0_2	108	
HA CT0_3	134	
HA CT0_4	121	
HA CT4_1	120	**121**
HA CT4_2	104	
HA CT4_3	129	
HA CT4_4	131	
HA CT8_1	117	**124**
HA CT8_2	109	
HA CT8_3	136	
HA CT8_4	135	
HA CT12_1	133	**120**
HA CT12_2	133	
HA CT12_3	98	
HA CT12_4	114	
HA CT16_1	121	**119**
HA CT16_2	113	
HA CT16_3	122	
HA CT16_4	119	
HA CT20_1	124	**118**
HA CT20_2	120	
HA CT20_3	118	
HA CT20_4	108	
HA PerKO CT20_1	118	**117**
HA PerKO CT20_2	125	
HA PerKO CT20_3	123	
HA PerKO CT20_4	101	

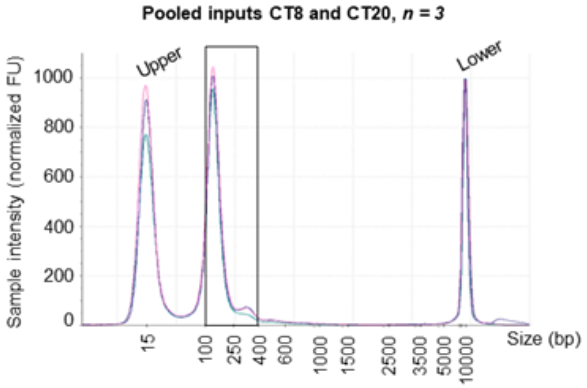


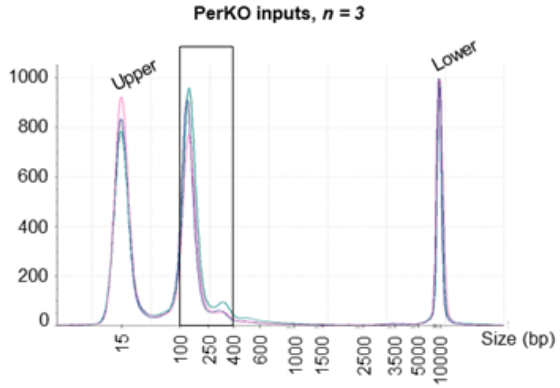


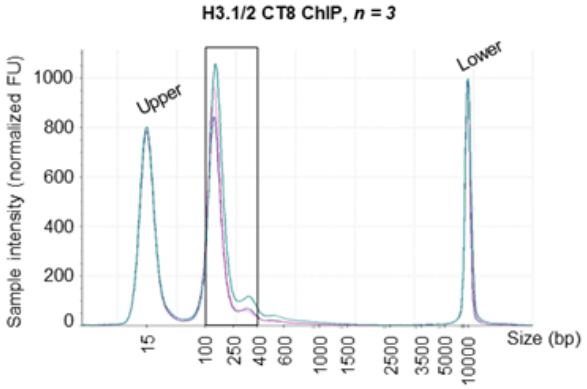

H3.3A CT0 ChIP, n = 4
H3.3A CT4 ChIP, n = 4
H3.3A CT8 ChIP, n = 4
H3.3A CT12 ChIP, n = 4
H3.3A CT16 ChIP, n = 4
H3.3A CT20 ChIP, n = 4
H3.3A PerKO CT20 ChIP, n = 4
Sample intensity (normalized FU)
Upper
Lower
Size (bp)
15
100
250
400
600
1000
1500
2500
3500
5000
10000

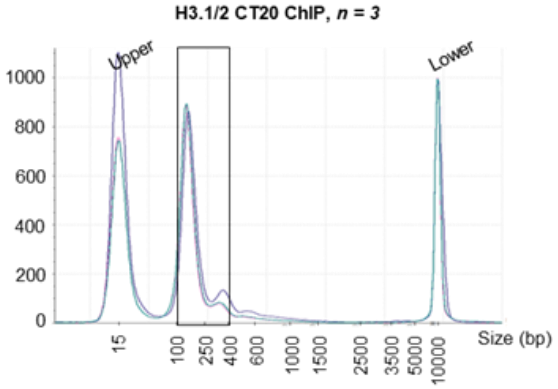
H3.31/2 ChIP. Table showing the individual and average fragment length for each replicate based on data from Tapestation analysis, followed with Tapestation profiles.

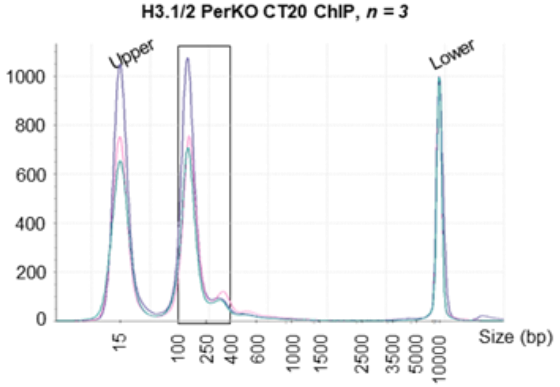
Replicates H3.1/2	Peak size (bp)	Average peak size (bp) at mononucleosomal level
input CT8/20_1	133	139
input CT8/20_2	131	
input CT8/20_3	152	
input PerKO CT20_1	135	141
input PerKO CT20_2	137	
input PerKO CT20_3	150	
H3.1/2 CT8_1	141	136
H3.1/2 CT8_2	130	
H3.1/2 CT8_3	138	
H3.1/2 CT20_1	140	142
H3.1/2 CT20_2	134	
H3.1/2 CT20_3	152	
H3.1/2 PerKO CT20_1	138	140
H3.1/2 PerKO CT20_2	141	
H3.1/2 PerKO CT20_3	140	





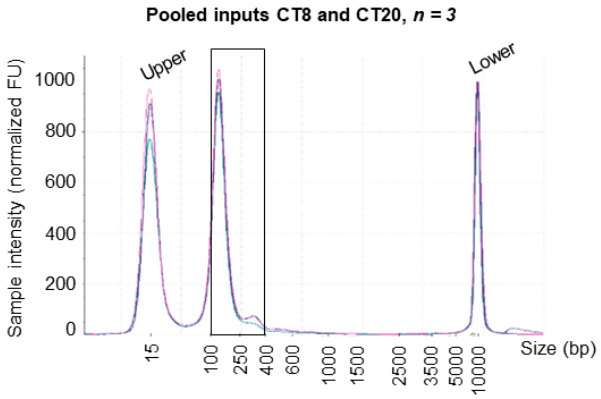


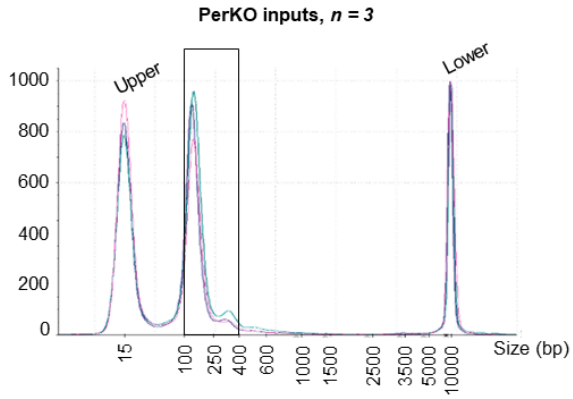


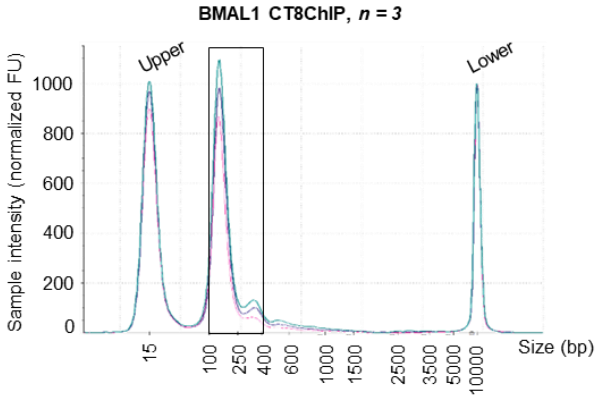


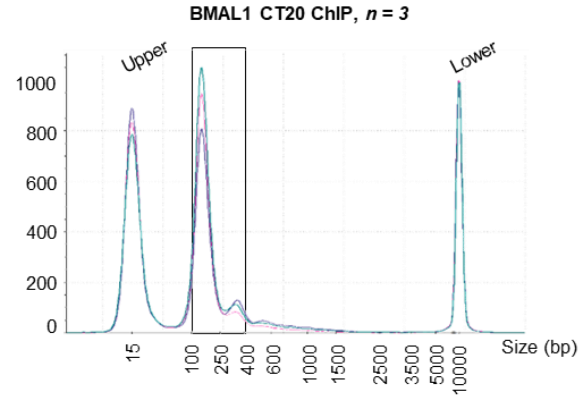
BMAL1 ChIP. Table showing the individual and average fragment length for each replicate based on data from Tapestation analysis, followed with Tapestation profiles.

Replicates BMAL1	Peak size (bp)	Average peak size (bp) at mononucleosomal level
same input as for H3.1/2		
BMAL1 CT8_1	140	139
BMAL1 CT8_2	133	
BMAL1 CT8_3	145	
BMAL1 CT20_1	139	140
BMAL1 CT20_2	136	
BMAL1 CT20_3	144	
BMAL1 PerKO CT20_1	134	125
BMAL1 PerKO CT20_2	121	
BMAL1 PerKO CT20_3	120	









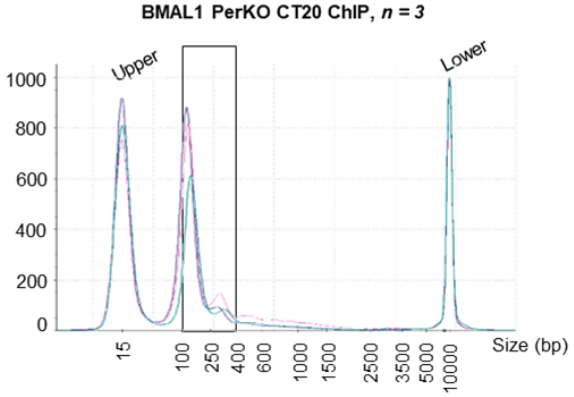


Table 16. Primer sequences.

Primers for mRNA relative expression analysis			
Gene name	Forward sequence (5' → 3')	Reverse sequence (5' → 3')	PrimerBank ID
Pbrm1	CTGTAGATCCTATTGCTGTGTGC	GCTTTGGAGCCCTAATGAACA	26326785a1
Arid2	TGGATCTTCACGGGCTCTACA	CGTTGGAACAACTTCTGGGAAA	12840712a1
Smarca4	GGTTCTGCCCACAGCATGAT	GGACTCCATAGGCTTGTGCAT	32449925a1
Phf10	ACAGCAACTTAAACCGGGAGC	GTCGGCAACACTTTGTACTTTC	31980708a1
Brd7	AAGCGACCATGACAAACACAA	ATCCTCCTTGACTCTTCTCCG	6755234a1
Per1	CTTATCGCCCAGTGGGTCTG	GCCAAGATCTCTGAAGCGGT	home-made
H3f3a	ACAAAAGCCGCTCGCAAGAG	ATTTCTCGCACCAGACGCTG	Goldberg *et al*. Cell 2010

Primers for promoter E-box analysis			
Gene name	Forward primer sequence (5' → 3')	Reverse primer sequence (5' → 3')	primers described in
Per1	ATCCTGATCGCATTGGCTGACTGA	TCTCTTCCTGGCATCTGATTGGCT	
Dbp	AAAACCAGTGCTGCACATTC	GCCTACAGCTTCCCCTTTC	Lande-Diner L *et al.*
Per2	ATGTGACAGCGGAGGGCGAC	CTCGGCCCGTCACTTGGTGC	Proc Natl Acad Sci USA
Rev-erbα	AGGCACACTCCACCTACATTGTCA	TGGAGCAGGTACCATGTGATTCCA	2013
Cry2	GCAGCACAGGGAGAACAAA	CACTGGAGAGGAGGGTTCAC	
Rorc	GCTGGGAGCGAAGGGACAGC	TCGCCCACTCCCTCCACCTG	

Primers for genotyping			
Primer type	Forward primer sequence (5' → 3')	Reverse primer sequence (5' → 3')	primers described in
FH-H3.3A	TTTGCAGACGTTTCTAATTTCTACT	ATATCGGATTCAACTAAAACATAAC	Fontaine *et al.* NAR 2022
Per1 Brdm1 WT	GTCTTGGTCTCATTCTAGGACACC	AACATGAGAGCTTCCAGTCCTCTC	
Per1 Brdm1 KO*	ACAAACTCACAGAGCCCATCC	ACTTCCATTTGTCACGTCCTGCAC	Zheng *et al.* Nature 1999
Per2 Brdm1 WT	AGTAGGTCGTCTTCTTTATGCCCC	CTCTGCTTTCAACTCCTGTGTCTG	Zheng *et al.* Cell 2001
Per2 Brdm1 KO*	TTTGTTCTGTGAGCTCCTGAACGC	ACTTCCATTTGTCACGTCCTGCAC	

*same reverse primer for Per1 and Per2 Brdm1 KO

Quantification of immunoprecipitation experiments

Figures 13, 21 (and 19A for the HA-tag)

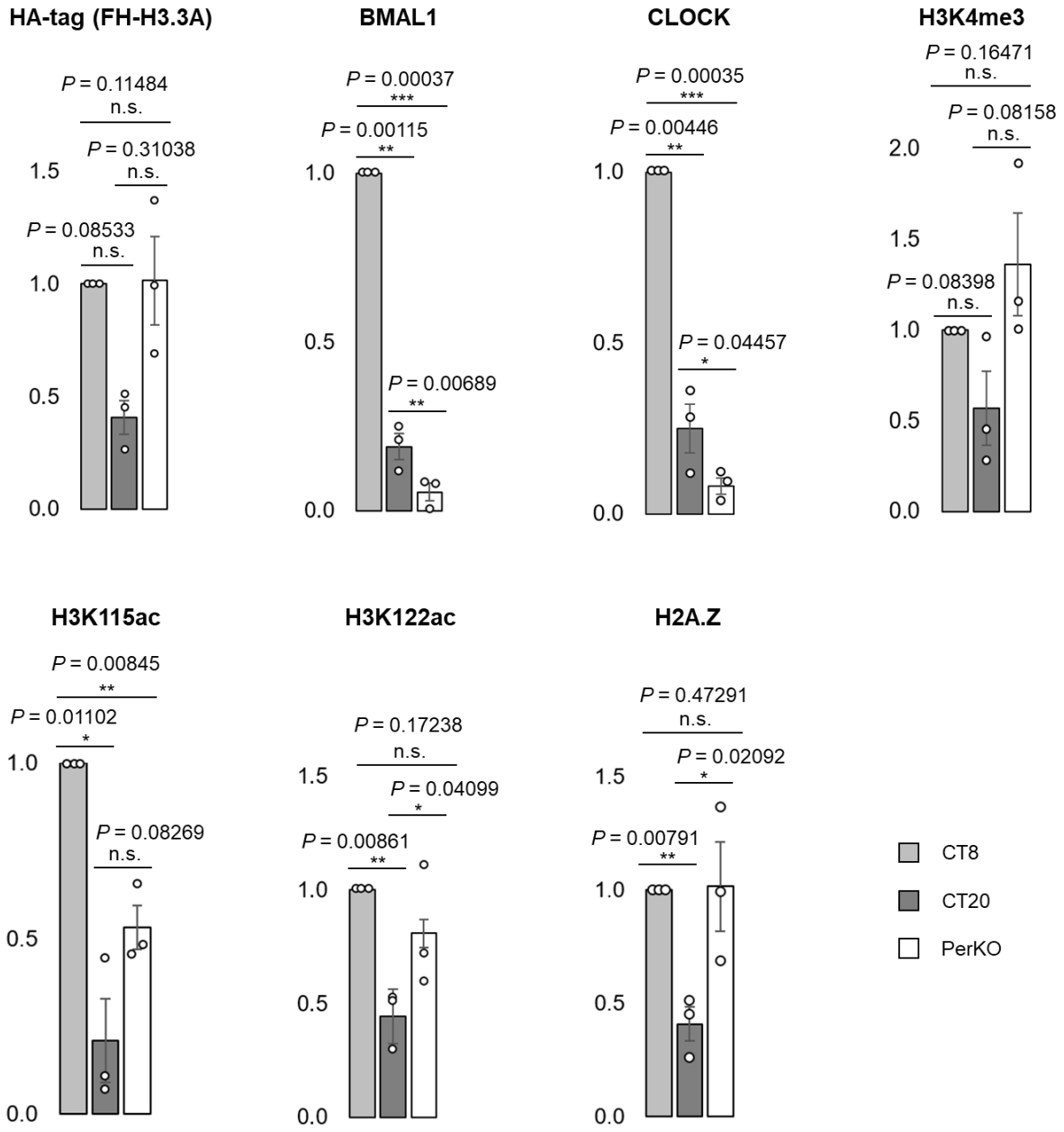


Figure 19A

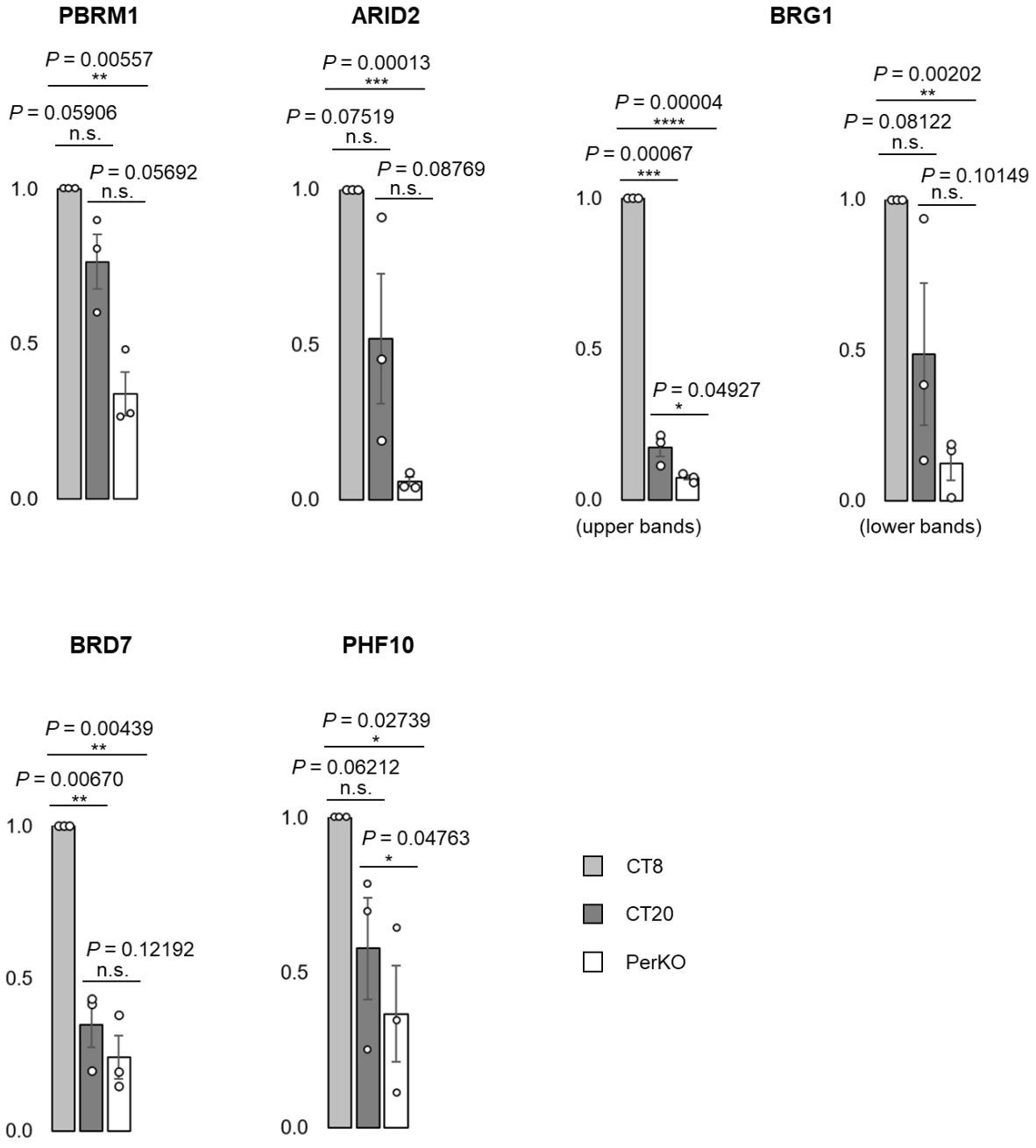

PBRM1
P = 0.00557
**
P = 0.05906
n.s.
P = 0.05692
n.s.
1.0
0.5
0.0
ARID2
P = 0.00013
***
P = 0.07519
n.s.
P = 0.08769
n.s.
1.0
0.5
0.0
BRG1
P = 0.00004
****
P = 0.00067
***
P = 0.04927
*
1.0
0.5
0.0
(upper bands)
P = 0.00202
**
P = 0.08122
n.s.
P = 0.10149
n.s.
1.0
0.5
0.0
(lower bands)
BRD7
P = 0.00439
**
P = 0.00670
**
P = 0.12192
n.s.
1.0
0.5
0.0
PHF10
P = 0.02739
*
P = 0.06212
n.s.
P = 0.04763
*
1.0
0.5
0.0
CT8
CT20
PerKO

Figure 19B (part 1)

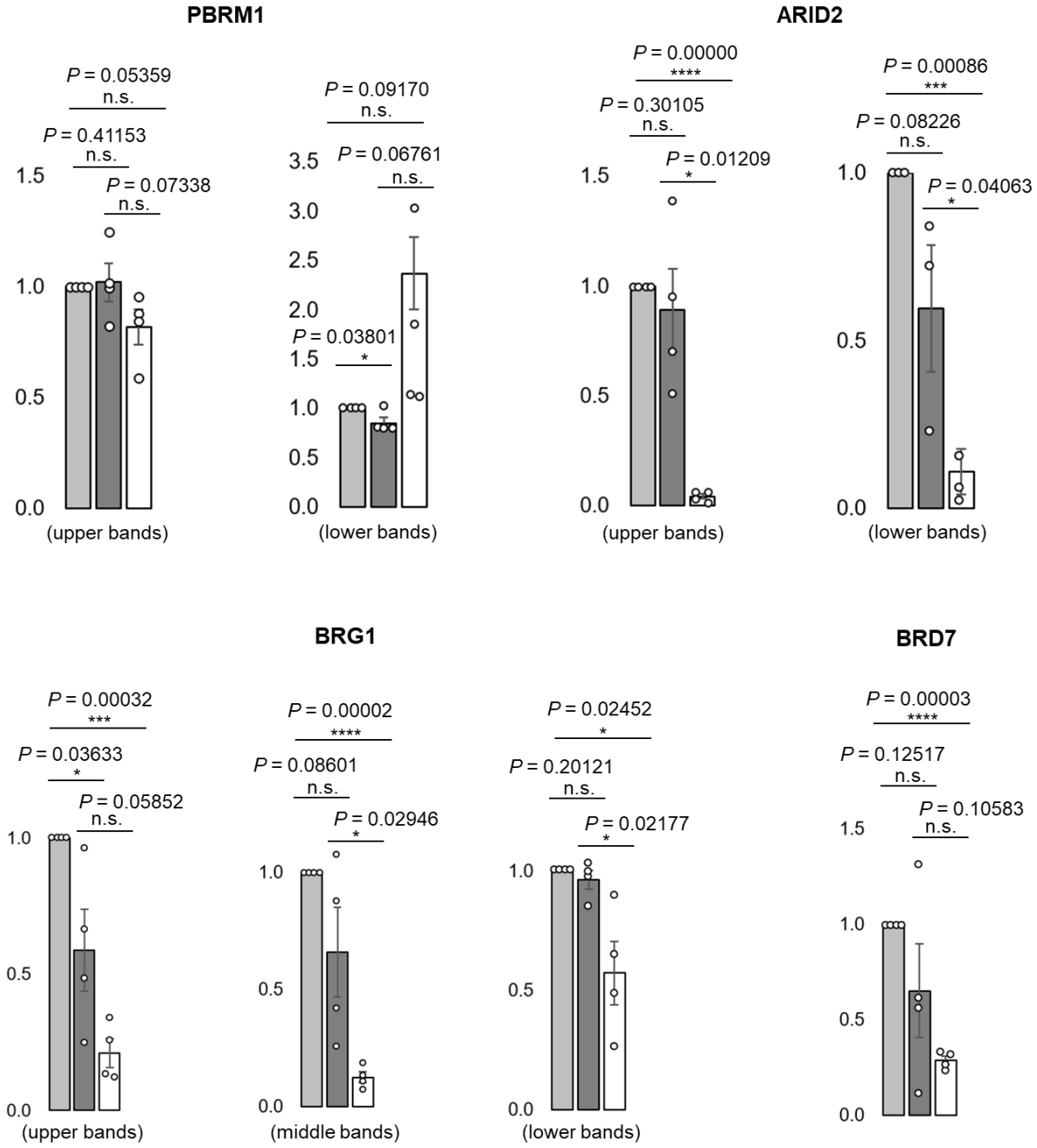


Figure 19B (part 2)

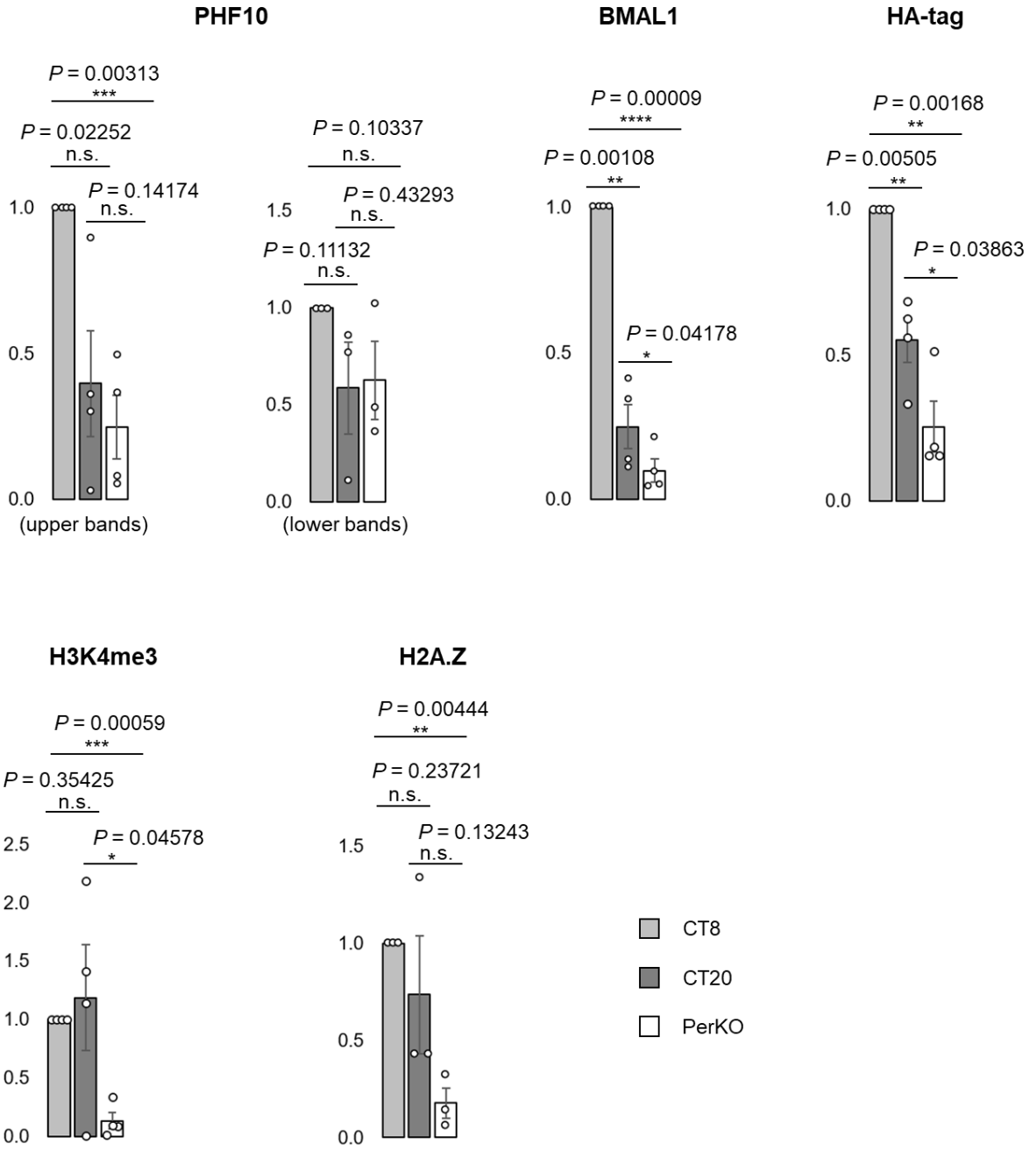


Figure 20A

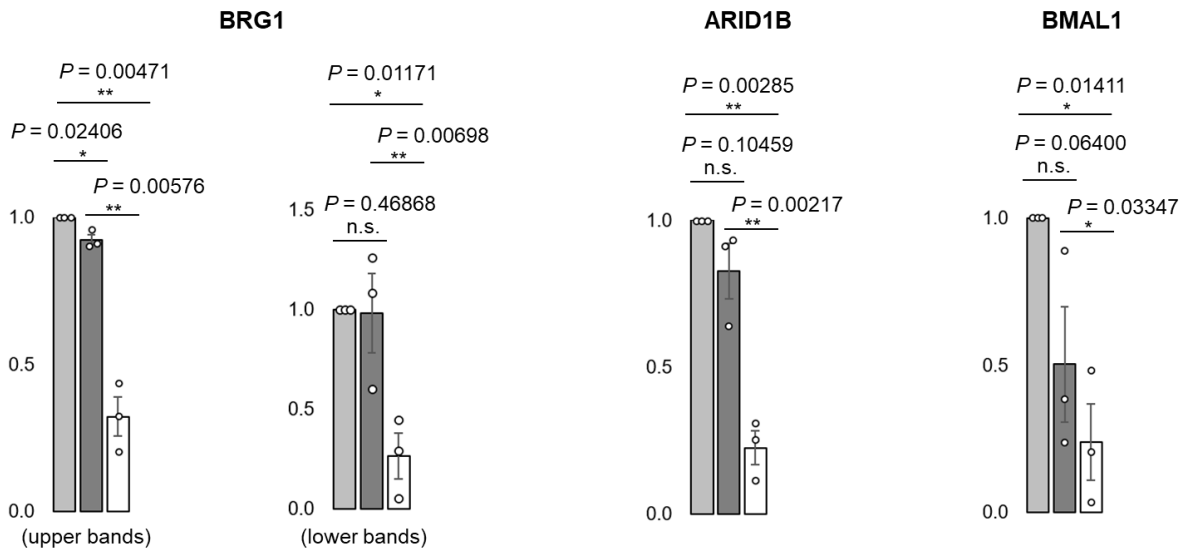


Figure 20B

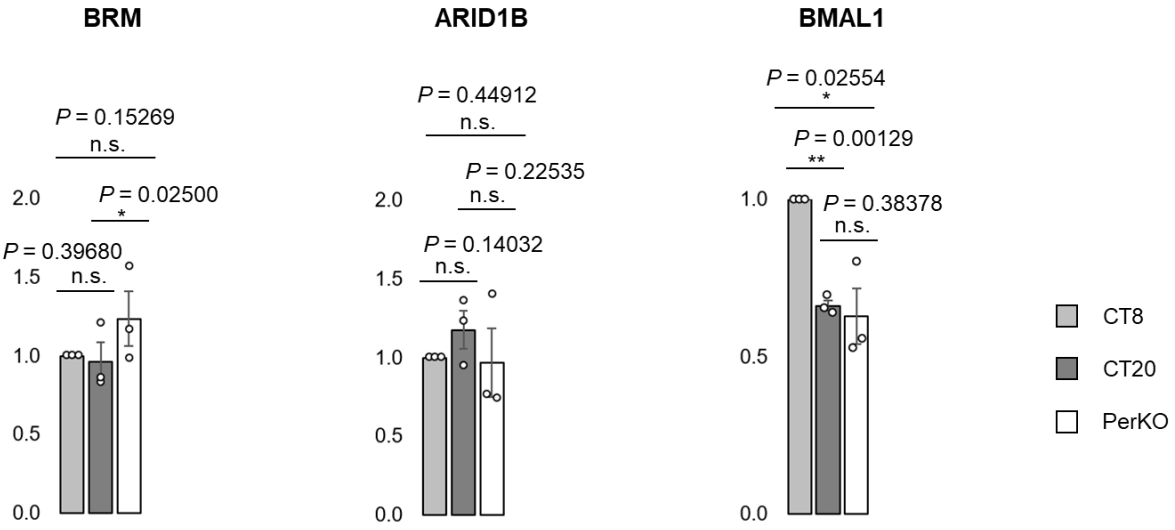


Figure 22B

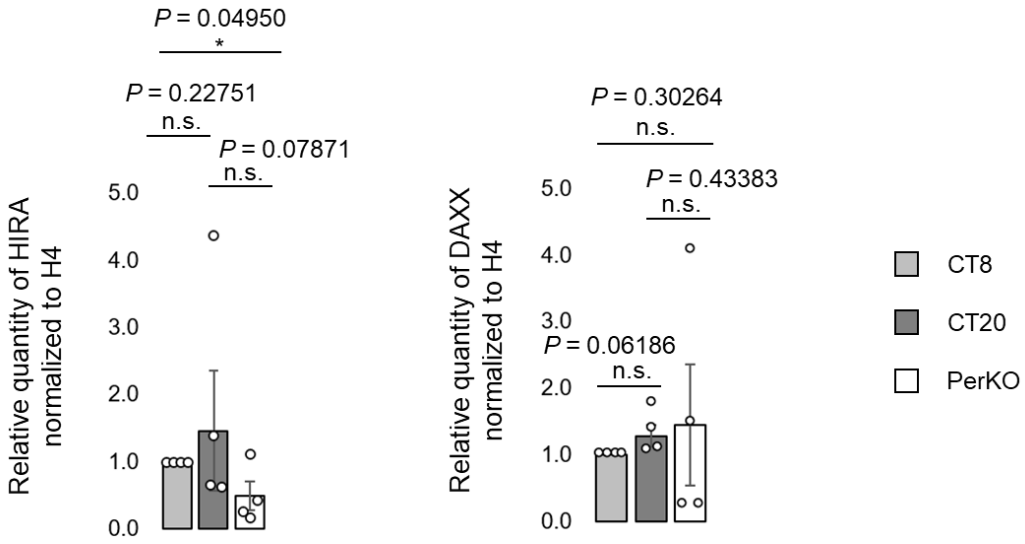

P = 0.04950
*
P = 0.22751
n.s.
P = 0.07871
n.s.
Relative quantity of HIRA normalized to H4
5.0
4.0
3.0
2.0
1.0
0.0
P = 0.30264
n.s.
P = 0.43383
n.s.
P = 0.06186
n.s.
Relative quantity of DAXX normalized to H4
CT8
CT20
PerKO

Figure 23 (part 1)

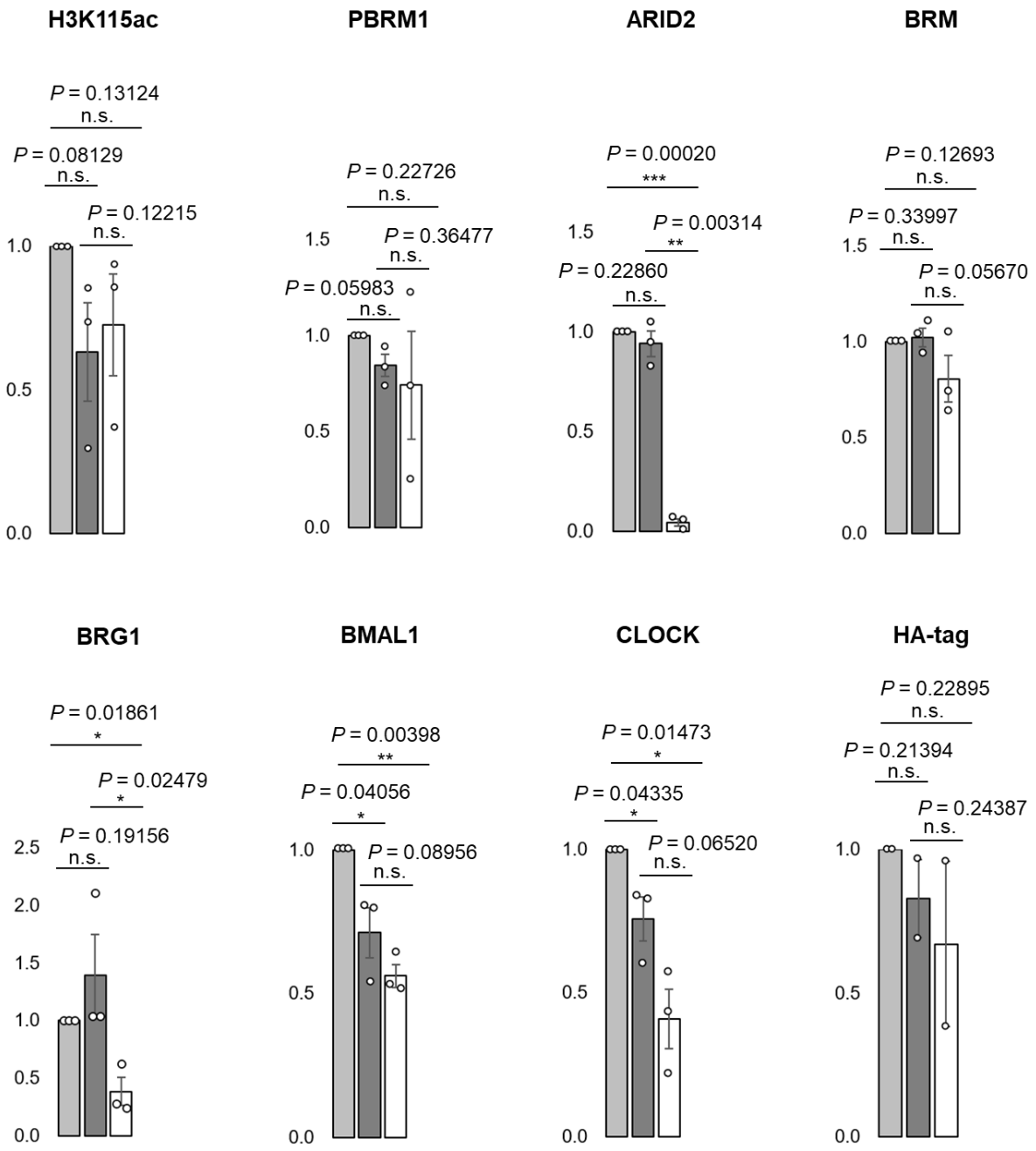


Figure 23 (part 2)

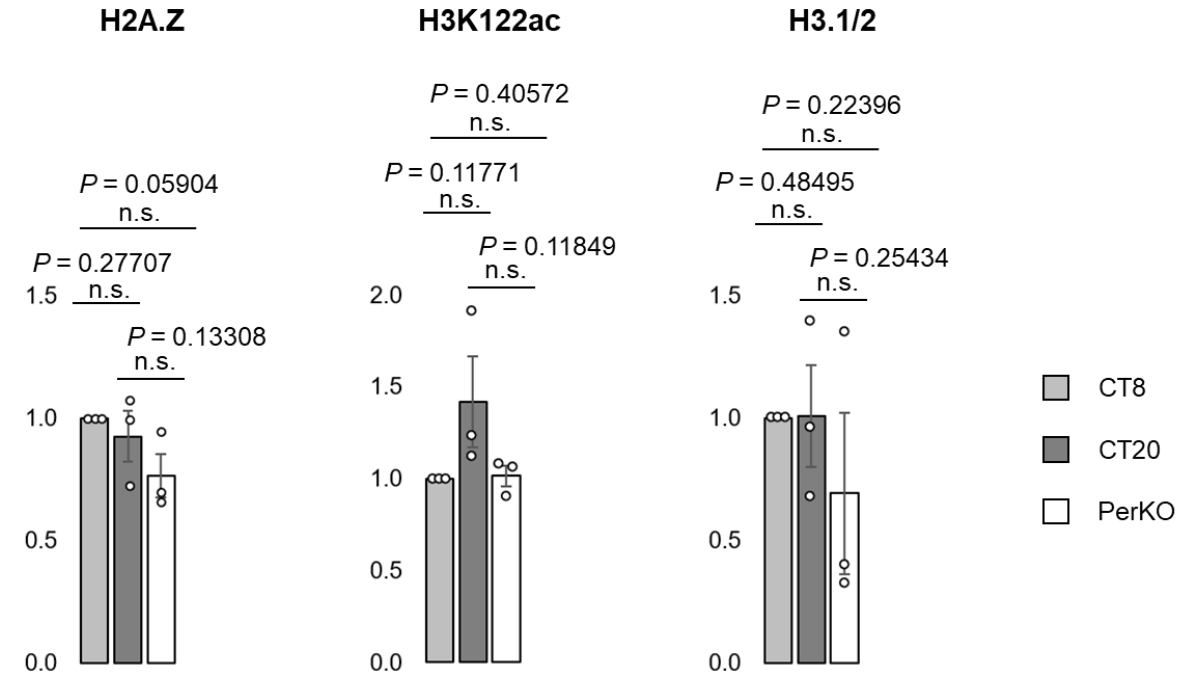
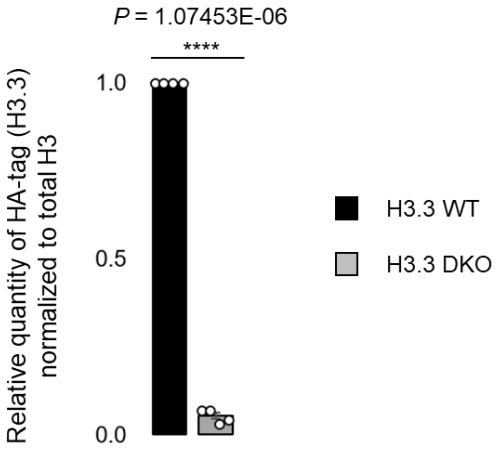


Figure 26



Chapitres et résumés des chapitres en français

Chapters and summary of chapters in French

1. Table des matières (Sommaire)

2. Introduction

3. Résumé des sections (Matériel et Méthodes, Résultats)

4. Discussion/ Conclusion

Sommaire

Traduction de la table des matières originale à la page 2.

Remerciements 5

Résumé (en anglais) 7

Résumé (en français) 9

Liste des figures 11

Liste des tableaux 13

Liste des abréviations 14

Introduction 17

1. Rythmes circadiens : du mécanisme moléculaire à la physiologie 17

1.1 Horloges circadiennes : l'élément important pour l'aptitude à la survie et l'homéostasie de l'organisme 17

1.1.1 Découverte des rythmes circadiens : des plantes aux mammifères 17

1.1.2 Propriétés universelles des oscillateurs circadiens 19

1.2 Niveaux d'organisation des horloges circadiennes chez les mammifères 21

1.2.1 Noyaux suprachiasmatiques : l'horloge maîtresse 21

1.2.2 Oscillateurs périphériques 22

1.2.3 Exemple de l'horloge périphérique chez les mammifères : le foie au centre de l'interaction entre l'horloge circadienne et le métabolisme 22

1.3 Mécanismes moléculaires des horloges circadiennes chez les mammifères 25

1.4 Altérations des horloges circadiennes dans les pathologies 27

2. Dynamique de la chromatine et signatures épigénétiques 29

2.1 Organisation de la chromatine : vue générale 29

2.2 Mécanismes épigénétiques établissant des changements dynamiques de la chromatine 31

2.2.1 Exemple des signatures épigénétiques : modifications post-traductionnelles des histones 31

2.2.2 Remodeleurs de la chromatine de la famille SWI/SNF 32

2.2.3 Variants d'histones : vue générale 36

3. Interaction entre la dynamique de la chromatine et les horloges circadiennes 40

3.1 Dialogue entre les horloges circadiennes et l'épigénome 40

3.1.1 Dynamique des marques d'histones et l'accessibilité de la chromatine 40

3.1.2 Dynamique de la chromatine marquée par le variant d'histone H2A.Z aux *loci* régulés par l'horloge 41

3.1.3 Remodelage circadien de la chromatine ……42

4. Variant d'histone H3.3 ……..44

4.1 Famille des histones H3 : les modulateurs clés des états chromatiniens ……...44

4.2 Le variant d'histone H3.3 ……..44

4.2.1 Voies spécifiques de déposition du variant H3.3 ……45

4.2.2 H3.3, le régulateur transcriptionnel clé et au-delà ……45

4.2.3 Nucléosomes fragiles, double-variants H3.3/H2A.Z ……46

5. Hypothèses de recherche et objectifs ……48

5.1 Contexte scientifique et hypothèses ……48

5.2 Modèles murins et objectifs de l'étude ……48

Matériel et méthodes ……..……..50

Matériel ……..……..50

1. Réactifs, produits chimiques et autres produits utilisés dans cette étude ……..50

Méthodes ...……53

1. Modèles murins, génotypage et prélèvement de tissus ……..…..53

2. Isolation des noyaux à partir des foies murins ……54

3. Purification native des complexes protéiques de H3.3A pour l'analyse par spectrométrie de masse ...……56

4. Analyse LC-MS/MS ……59

5. Immunoprécipitation native et western-blotting ……60

6. Immunoprécipitation native de la chromatine suivie par le séquençage ……..63

7. Filtrage des données, analyse ChIP-Seq et représentation graphique ……...64

8. Cross-linked ChIP-qPCR ……...65

9. Niveaux d'expression des ARNm et RT-qPCR ……...68

10. Monitoring des oscillations circadiennes de cellules en culture par bioluminescence en temps réel ……68

11. Fractionnement subcellulaire de protéines des tissus ……69

12. Traitement MG132 et fractionnement subcellulaire de protéines ……..70

13. Réanalyse des données publiques de criblage par ARN interférence ……..70

Résultats ……71

1. Caractérisation des complexes protéiques de H3.3A spécifiques du foie au cours du temps …...……71

1.1 Etablissement de la méthode de purification et défis rencontrés ……..71

1.2 Assemblage de H3.3A avec les facteurs de transcription BMAL1-CLOCK en fonction du temps ……..72

1.3 Identification des remodeleurs chromatiniens PBAF de la famille SWI/SNF comme interacteurs principaux de H3.3A ……74

1.4 Complexe circadien PBAF-BMAL1 s'assemble sur la chromatine dynamique marquée par H3.3 ……...74

2. Rythmicité au sein de l'occupation des nucléosomes contenant le variant H3.3A ……76

2.1 Le variant H3.3A génère la dynamique chromatinienne de 24h au niveau des *loci* circadiens ……76

2.2 Impact de la perturbation des horloges circadiennes sur les paysages chromatiniens de H3.3A ……..76

3. Réorganisation des remodeleurs chromatiniens lors de la perturbation circadienne ……80

3.1 Perte de ARID2 conduit au désassemblage du complexe PBAF en absence de PER ……...80

3.2 Favorisation des complexes remodeleurs cBAF/BRM caractérise l'état perturbé de l'horloge circadienne dans les foies PerKO ……..……..81

4. Altérations des états chromatiniens marqués par les nucléosomes H3.3A fragiles et de la liaison de BMAL1 ……85

4.1 BMAL1-CLOCK sont recrutés aux nucléosomes H3.3 fragiles lors de la phase activatrice ……...…85

4.2 Identification de deux sous-types différents de nucléosomes fragiles marqués par H3K115ac ……87

4.3 Chromatine marquée par les nucléosomes H3.3 fragiles dans les foies PerKO promeut l'accessibilité des E-box spécifiques de BMAL1 ……..……87

4.4 Turnover de BMAL1 en absence de feedback circadien ……..89

5. Impact sur la fonction des horloges circadiennes ……...91

5.1 Rôle de H3.3 dans la fonction des horloges circadiennes ……91

5.2 Impact des composantes spécifiques des complexes PBAF/cBAF sur les rythmes circadiens ……91

Discussion ……..94

Proposition du modèle, questions ouvertes et perspectives ……94

Références ……...103

Matériel supplémentaire ……117

Liste de matériel supplémentaire ……117

Figure S1. Axe temporel des découvertes majeures initiales dans le domaine de la recherche sur les horloges circadiennes chez les mammifères ……..118

Figure S2. Modèle détaillé du mécanisme moléculaire de l'horloge circadienne chez les mammifères ..……119

Figure S3. Enrichissement différentiel des composantes de PBAF/cBAF au sein des complexes H3.3A dans les foies de souris sauvages vs. PerKO ……120

Table S1. Analyse par spectrométrie de masse des peptides détectés des composantes de PBAF/cBAF au sein des complexes H3.3A dans les foies sauvages vs. PerKO ……121

Table S2. Longueur des fragments de ChIP et les profils de Tapestation ……125

Table S3. Séquences des amorces ……129

Quantification des expériences d'immunoprécipitation……130

Chapitres et résumés des chapitres en français ..……138

Articles ……..183

Liste des articles ……183

Article 1. Mammalian PERIOD2 regulates H2A.Z incorporation in chromatin to orchestrate circadian negative feedback. ……..183

Article 2. PBAF/cBAF reorganization on H3.3 chromatin regulates BMAL1 activity in the absence of circadian negative feedback. ……..183

Introduction

1. Rythmes circadiens : du mécanisme moléculaire à la physiologie

1.1 Horloges circadiennes : l'élément important pour l'aptitude à la survie et l'homéostasie de l'organisme

Quasiment tous les organismes vivants sur Terre, des cyanobactéries aux mammifères, ont développé des oscillateurs biologiques, parmi lesquels les horloges circadiennes (*circa diem*, environ un jour) déterminent les rythmes d'environ de 24 heures dans l'expression des gènes, la physiologie et le comportement. Ces oscillations autonomes et robustes permettent aux organismes de s'adapter et d'anticiper les changements journaliers dans leur environnement [1, 2]. L'anticipation des signaux environnementaux externes (*Zeitgebers*, « donneurs de temps »), tels que l'alternance des cycles de la lumière et de l'obscurité, l'heure de la prise alimentaire, ainsi que les variations de température par les oscillateurs circadiens, est essentielle pour l'homéostasie interne de l'organisme [1, 2].

1.1.1 Découverte des rythmes circadiens : des plantes aux mammifères

La toute première observation scientifique d'un comportement rythmique a été faite par l'astronome français Jean Jacques d'Ortous de Mairan en 1729, lors de ses études sur le mouvement des feuilles de la plante *Mimosa pudica* [3]. En imitant des conditions physiologiques (12 heures de lumière : 12 heures d'obscurité), il a observé que les feuilles de Mimosa se dépliaient dans la journée et se repliaient lors de la tombée de nuit. Ce mouvement s'était systématiquement reproduit au cours du temps, en suivant l'alternance jour/nuit. De manière intéressante, lorsque la plante de Mimosa a été placée dans une chambre noire, étanche à la lumière (conditions de l'obscurité constante), il a observé que les feuilles continuaient à se déplier rythmiquement pendant le « jour » et à se replier pendant la « nuit », même en absence de lumière. Dans sa publication *Observation botanique - Histoire de l'Académie Royale des Sciences* [4], Mairan décrit pour la première fois qu'un facteur externe, tel que la lumière, n'est pas nécessaire pour les oscillations du mouvement des feuilles de Mimosa. Ces observations soulignent que le comportement rythmique persiste en absence des facteurs environnementaux externes et donc que telles oscillations sont très probablement endogènes [3, 4]. De plus, de Mairan a émis l'hypothèse que les variations de température pourraient potentiellement influencer la capacité des plantes à percevoir le temps, contribuant ainsi à leur comportement rythmique. En 1832, le botaniste suisse Augustin Pyramus de Candolle a remarqué que les feuilles de Mimosa se dépliaient un peu plus tôt chaque jour et a mesuré une période de ces mouvements légèrement inférieure à 24 heures. Le repliage rythmique des

feuilles présentait une période de 22.5 heures, ce qui suggérait que ces rythmes étaient bien endogènes [5].

Suite à ces observations, il a fallu presque 200 ans afin de reconnaître que les rythmes circadiens observés dans le comportement, comme par exemple le photopériodisme chez les plantes, sont en effet régulés par une horloge endogène qui répond à et qui peut être synchronisée par des stimuli externes. C'était Erwin Bünning, un biologiste allemand, qui dans les années 1930 a mené l'étude sur le mouvement des feuilles d'haricots et a noté que le fait de placer la plante dans des conditions de lumière constante entraîne un mouvement rythmique des feuilles, dit de libre-cours. Un rythme de libre-cours dont la période était légèrement supérieure à 24 heures (24.4 heures) [3]. Il a ainsi fallu peu de temps pour caractériser les premiers gènes impliqués dans le comportement de l'organisme [6, 7]. Dans les années 1960, alors qu'ils effectuaient des criblages par mutagenèse pour étudier des gènes impliqués dans l'éclosion de la pupe et dans les rythmes d'activité locomotrice de la mouche *Drosophila melanogaster*, Ronald J. Konopka et Seymour Benzer ont identifié trois mutants monogéniques, cartographiés sur le même locus du chromosome X [6]. Ces mutants présentaient des altérations importantes des rythmes d'éclosion et d'activité locomotrice, telles que le raccourcissement ou l'allongement de la période de 24 heures, aboutissant respectivement à des rythmes d'environ de 19 ou 28 heures, ainsi que des mutants présentant un comportement arythmique dans les phénomènes décrits. Ils ont ainsi nommé ce gène *Period*. Cependant, la communauté scientifique à l'époque était restreinte à l'idée qu'un seul gène puisse contrôler le comportement complexe d'un organisme [6, 7].

Néanmoins, leurs découvertes ont conduit à une nouvelle ère d'études sur les mécanismes moléculaires à l'origine des rythmes circadiens [3, 8]. Dans les années 1980, trois scientifiques - Jeffrey C. Hall, Michael Rosbash et Michael W. Young avec leurs collègues, ont indépendamment cloné et identifié *Period* (*Per*) comme le premier gène de l'horloge chez la drosophile [9, 10]. Leurs études ultérieures ont fourni des informations importantes sur les mécanismes moléculaires des horloges circadiennes. Ils ont découvert que dans les têtes de drosophile, les niveaux d'ARNm *Per* présentent des rythmes circadiens de libre-cours, avec un pic d'expression en début de nuit, suivis par les oscillations et un pic d'expression de la protéine PER 4 à 6 heures plus tard [11, 12]. De plus, une mutation antisens au sein du gène *Per* a aboli les oscillations des niveaux de ses ARNm correspondants et a conduit aux altérations des rythmes comportementaux des drosophiles affectées. Ces altérations ont pu ainsi être résolues par l'approche de transfert de gène *Per*, issu des drosophiles de type sauvage [13]. D'autre part, ils ont caractérisé PER comme étant une protéine nucléaire, faisant la navette entre le cytoplasme et le noyau de manière rythmique au cours du temps [14]. Par ailleurs, la surexpression de la protéine PER a inhibé les oscillations des niveaux d'ARNm *Per*, ce qui a

conduit à l'établissement d'un modèle de régulation dans lequel, la protéine PER module directement l'expression de son propre gène [11, 12]. Dix ans plus tard, l'identification du deuxième gène de l'horloge *Timeless* (*Tim*) a révélé un lien étroit avec le mécanisme de régulation de PER [15, 16]. En effet, TIM a été identifié comme essentiel pour la translocation et l'entrée nucléaire de PER, les oscillations de ses niveaux protéiques, ainsi que dans l'établissement des rythmes d'éclosion des pupes et d'activité locomotrice des mouches adultes [17, 18, 19]. Un modèle de boucle de rétroaction transcriptionnelle-traductionnelle permettant d'établir des oscillations d' ~ 24 heures dans l'expression des gènes, les niveaux de protéines et le comportement a ainsi été proposé. En parallèle, la branche positive de la boucle de rétroaction a été caractérisée grâce à la découverte du gène *Clock* chez la souris par Joseph Takahashi et ses collègues [20, 21, 22], suivie par l'identification de son partenaire BMAL1 [23]. Les deux se sont montrés essentiels pour le comportement circadien des souris. BMAL1-CLOCK ont ensuite été identifiés comme des activateurs des oscillations transcriptionnelles, et leurs orthologues CYCLE [24] et CLOCK [25], comme des facteurs de transcription activateurs de l'expression de *Per* et *Tim* chez la drosophile. Toutes ces découvertes initiales ont progressivement conduit à l'identification de l'ensemble du réseau moléculaire régulateur de l'horloge circadienne chez la drosophile et les mammifères (Figure S1), et parallèlement également chez d'autres organismes. Le mécanisme de la boucle de rétroaction transcriptionnelle-traductionnelle principale de l'horloge circadienne a été caractérisé et élargi davantage par la suite, lors de la découverte de régulateurs post-transcriptionnels et post-traductionnels auxiliaires des facteurs principaux de l'horloge. Comme par exemple le gène *Doubletime* chez la drosophile, codant pour la caséine kinase CK1 et ses orthologues chez les mammifères qui participent à la stabilité de la protéine PERIOD [26, 27, 28]. Ces régulateurs « auxiliaires » sont impliqués dans le maintien des rythmes de 24 heures dans les processus transcriptionnels-traductionnels qui, en général, se déroulent en quelques minutes voir maximum en quelques heures seulement au sein des cellules eucaryotes [29].

En 2017, le prix Nobel de physiologie ou de médecine a été co-attribué à Jeffrey C. Hall, Michael Rosbash and Michael W. Young pour *leurs découvertes des mécanismes moléculaires régulant le rythme circadien* [30]. Néanmoins, la question principale dans ce domaine, à savoir comprendre comment la machinerie moléculaire de l'horloge circadienne génère et maintient le retard de 24 heures dans les processus biochimiques « rapides » tels que la transcription et la traduction, reste un domaine de recherche active.

1.1.2 Propriétés universelles des oscillateurs circadiens

Les propriétés des oscillateurs circadiens ont été décrites pour la première fois dans leur globalité en 1960 par Colin Stephenson Pittendrigh, en se basant principalement sur les découvertes initiales, y compris les observations des rythmes comportementaux chez la drosophile [31]. Les horloges circadiennes sont caractérisées comme des pacemakers endogènes, qui s'auto-entretiennent et qui sont autonomes au niveau cellulaire (voir Boîte 1 pour les définitions et la terminologie). Ce sont des oscillateurs de libre-cours, extrêmement robustes avec une erreur physiologique temporelle de quelques minutes seulement toutes les 24 heures. De plus, ils sont innés et ubiquitaires (par exemple, présents au sein de chaque cellule). Malgré leurs propriétés endogènes, les horloges circadiennes répondent à des signaux environnementaux externes (les *Zeitgebers*) pour synchroniser les organismes avec leur environnement [31, 32]. Par conséquent, ces oscillateurs peuvent donc être entraînés par des *Zeitgebers*. Néanmoins, ces rythmes biologiques journaliers sont compensés par la température (Boîte 1) [2, 31, 33].

Boîte 1. Définitions des propriétés clés des rythmes circadiens et terminologie.

- Rythmes circadiens. Les rythmes circadiens (*Circa diem* - environ un jour) sont des rythmes biologiques dont la période de libre-cours (τ_{FR}) reflète approximativement la période de rotation de la Terre.
- Période. Désigne le temps nécessaire d'un oscillateur biologique pour accomplir un cycle. Pour les oscillations circadiennes, la période est environ de 24 heures.
- Période de libre-cours (τ_{FR}). Durée nécessaire à la répétition d'un rythme endogène de l'organisme, en absence des facteurs environnementaux temporels. τ_{FR} peut être mesurée dans les conditions expérimentales constantes (par exemple, l'obscurité constante). Il ne s'agit pas d'une caractéristique fixe, mais plutôt d'une caractéristique flexible d'un organisme donné, qui s'adapte aux changements spontanés et induits (par exemple, voyager à travers des différents fuseaux horaires), dans une certaine gamme de valeurs. Cette propriété de libre-cours des rythmes circadiens est liée avec leur caractéristique endogène et d'auto-entretien.
- Endogènes, auto-entretenus. Les oscillateurs circadiens sont intrinsèques à un organisme (c'est-à-dire, « fonctionnent de l'intérieur »). Ils sont capables d'« auto-générer » des variations rythmiques et répétitives dans les phénomènes physiologiques en absence de facteurs environnementaux externes.

- Autonomes au niveau cellulaire. Les rythmes circadiens sont autonomes aux niveaux cellulaire et tissulaire, ce qui signifie qu'ils sont capables de se produire indépendamment des cellules ou des tissus environnants. Des enregistrements des rythmes de cellules individuelles et même des tissus ont été réalisés dans des systèmes de culture *in vitro**.
- Robustes. La robustesse des horloges circadiennes fait référence à leur remarquable précision. Comme décrit précédemment par CS Pittendrigh, l'erreur physiologique temporelle observée de la période circadienne pourrait être inférieure à 2 minutes dans un cycle de 24 heures.
- Innés. Les rythmes circadiens sont innés d'un organisme.
- Ubiquitaires. Cette propriété fait référence non seulement au fait que presque tous les organismes vivants sur Terre ont développé des oscillateurs circadiens, mais aussi à leur niveau d'organisation (c'est-à-dire qu'ils sont présents dans tous les tissus et virtuellement dans chaque cellule), ainsi qu'à leur rôle dans les divers processus biologiques - allant des rythmes de synthèse d'ADN au comportement rhythmique des organismes.
- Entraînables. Les horloges circadiennes perçoivent et sont sensibles à divers facteurs environnementaux externes, tels que les altérations lumière/obscurité, les variations de température, ainsi que les cycles de jeûne/ prise alimentaire. Ces facteurs ont été nommés *Zeitgebers* (« donneurs de temps » ou synchroniseurs) par le biologiste allemand Jürgen Aschoff**. La propriété d'entraînement des oscillateurs circadiens fait référence au couplage d'un rythme observable dans un organisme à un *Zeitgeber* donné. C'est-à-dire, l'horloge endogène qui répond à un facteur environnemental perçu (stimulus) ajuste le rythme interne d'un organisme à son environnement, ce qui donne lieu à une période synchronisée entre l'environnement interne et externe de l'organisme.
- Compensés par la température. Cette propriété reflète la capacité des horloges circadiennes à maintenir une période de libre-cours relativement constante, n'étant pas affectée par les variations de température environnementale externe.

* 34, 35, 36, 37; ** 32

Néanmoins, ces propriétés clés restent caractéristiques des oscillateurs circadiens de n'importe quelle espèce donnée.

Étant donné que les horloges circadiennes sont à la fois endogènes et entraînables, deux concepts différents de perception et de définition du temps, liés aux conditions expérimentales, ont été établis dans le domaine (Boîte 2).

Boîte 2. Concepts de temps liés aux conditions expérimentales.

- Temps Zeitgeber (ZT). Il est défini comme un temps référant aux facteurs environnementaux externes, tels que l'alternance de lumière/obscurité. Par conséquent, les études sur l'entraînement circadien sont réalisées dans des conditions expérimentales imitant l'environnement externe d'un organisme. Par exemple, des conditions 12h de lumière/ 12h d'obscurité, où le premier point temporel ZT0 correspond au début de l'exposition à la lumière (le jour) et 12h plus tard, le point temporel ZT12, au début de l'obscurité (la nuit).
- Temps circadien (CT). Au contraire, le temps circadien est défini par les horloges endogènes d'un organisme placé dans les conditions constantes (par exemple, obscurité constante), sans faisant référence à des facteurs environnementaux externes. Par conséquent, afin de faire une expérience circadienne et d'étudier les rôles intrinsèques des horloges d'un organisme dans les processus biologiques, les animaux sont entraînés pendant deux semaines par les cycles 12h de lumière : 12h d'obscurité et sont ensuite placés dans l'obscurité constante juste avant la manipulation (par exemple, prélèvements de tissus). Ainsi, CT0 fait référence au premier moment dans l'obscurité constante - début de la journée subjective, et 12 heures plus tard, CT12 fait référence au début de la nuit subjective.

1.2 Niveaux d'organisation des horloges circadiennes chez les mammifères

Chez les mammifères, les horloges circadiennes sont présentes dans l'ensemble de l'organisme : dans chaque organe et virtuellement dans chaque cellule. Elles sont organisées hiérarchiquement en deux niveaux : le pacemaker central, appelé l'horloge maîtresse, situé dans le cerveau, et les oscillateurs périphériques, présents dans tous les autres tissus de l'organisme [1, 8].

1.2.1 Noyaux suprachiasmatiques : l'horloge maîtresse

Composés d'environ de 20 000 neurones, les noyaux suprachiasmatiques (SCN) résident dans une petite région du cerveau, appelée l'hypothalamus, située juste au-dessus du chiasma optique [1, 8]. L'importance de SCN dans les rythmes circadiens a été mise en évidence lors de l'étude sur les diverses structures cérébrales pour leur rôle potentiel en tant que pacemaker

endogène central au sein de l'organisme, en effectuant des expériences de lésion cérébrale chez les rats [38, 39]. Les lésions de SCN ont entraîné la perte de rythmes comportementaux chez ces rats, tels que les rythmes de l'activité locomotrice [39]. De manière intéressante, la transplantation de SCN intact chez des animaux ayant subi une lésion de SCN a permis de rétablir les rythmes comportementaux, avec une période caractéristique du donneur [40, 41]. De plus, chez les souris arythmiques génétiquement modifiées, la transplantation de SCN de souris sauvages a permis une restauration complète des rythmes circadiens au niveau comportemental [42], ce qui a montré le rôle principal de SCN en tant que pacemaker endogène central de l'organisme, localisé au niveau du cerveau. Par ailleurs, dans les cultures dispersées de neurones isolés, il a été montré que les neurones individuels de SCN sont capables de générer des oscillations circadiennes dans l'expression des gènes de l'horloge, ainsi que dans l'activité neuronale. Ces oscillations sont générées indépendamment, à l'extérieur de l'organisme d'une manière autonome au niveau cellulaire [43, 44]. Cependant, pour que le SCN fonctionne correctement en tant que pacemaker circadien central, il est nécessaire de maintenir un réseau neuronal intact [45, 46, 47].

Afin de synchroniser les oscillateurs périphériques au sein d'autres organes, y compris les oscillateurs cérébraux secondaires, le SCN intègre les informations lumineuses reçues, étant initialement perçues par les cellules ganglionnaires photosensibles de la rétine (pRGC) [48]. Les signaux photiques sont ensuite transmis de la rétine directement au SCN [49], qui convertit à son tour les informations reçues en une multitude de signaux neuronaux et hormonaux. Ces derniers synchronisent les horloges des tissus périphériques [1, 8, 50]. En parallèle, l'horloge maîtresse intègre les signaux provenant de la périphérie. Cette interaction entre les horloges circadiennes à différents niveaux au sein de l'organisme permet d'établir une synchronisation, un équilibre globale entre les environnements externes et internes de l'organisme (l'homéostasie) [1, 8].

1.2.2 Oscillateurs périphériques

On trouve des oscillateurs périphériques dans tous les organes, ainsi que dans chaque cellule. Synchronisées par le pacemaker central au niveau de SCN, les horloges périphériques entraînent des rythmes d'environ de 24 heures dans les programmes d'expression génique locaux [50, 51, 52]. Bien que les gènes spécifiques d'un organe, impliqués dans la régulation de processus métaboliques clés de ce tissu donné oscillent à leur propre rythme, les gènes de l'horloge restent synchronisés entre plusieurs tissus [53]. Cette coordination entre différents organes se traduit par une rythmicité d'environ de 10 à 15 % du transcriptome, dont la phase des oscillations est spécifique à chaque tissu donné [51, 52, 53]. En outre, comme pour le SCN, les oscillateurs des tissus périphériques continuent à maintenir les rythmes circadiens

indépendamment des signaux de synchronisation externes et internes, lorsqu'ils sont cultivés *in vitro* [34, 35, 36, 37, 50].

1.2.3 Exemple de l'horloge périphérique chez les mammifères : le foie au centre de l'interaction entre l'horloge circadienne et le métabolisme

Le foie est l'un des oscillateurs périphériques les mieux étudiés et caractérisés, très probablement en raison de son rôle central dans le métabolisme, ainsi que par le lien étroit entre les horloges circadiennes et les voies métaboliques [54].

Chez les mammifères, le foie est constitué de quatre lobes principaux, de centaines de milliers de lobules hépatiques et il est également hautement vascularisé [55]. Le réseau veineux hépatique est principalement composé des veines portales et centrale. Ce réseau veineux génère des gradients dans les concentrations d'oxygène et de nutriments, les voies de signalisation, ainsi que des gradients dans les programmes d'expression génique, tout le long de l'axe portal-central [55]. Cette polarisation des lobules hépatiques conduit à une zonation du foie, ce qui entraîne une compartimentation spatiale des voies métaboliques clés [56]. De plus, le foie héberge différents types cellulaires. Alors que les cellules post-mitotiques du foie dans l'état quiescent, les hépatocytes, représentent environ 80-90% du tissu, le foie contient également des cellules non parenchymateuses, des cellules de Kupffer (les macrophages hépatiques), des cellules endothéliales sinusoïdales du foie, des cellules d'Ito (cellules stellaires hépatiques), des cholangiocytes intrahépatiques et des cellules épithéliales de l'arbre biliaire, ce qui entraîne une hétérogénéité importante au sein du foie [57].

Le foie, carrefour métabolique central de l'organisme, est impliqué dans la régulation de plusieurs processus métaboliques tels que le métabolisme des glucides et des lipides, la synthèse des acides biliaires et des hormones, le transport des nutriments, la transformation des acides aminés et la détoxification. Tous ces processus sont hautement rythmiques et étroitement liés à la régulation médiée par l'horloge circadienne [54, 58, 59]. Le foie est synchronisé par plusieurs signaux systémiques, tels que l'alternance de la prise d'alimentation et de jeûne, les oscillations de température corporelle, les niveaux d'oxygène, d'hormones et des métabolites, et à son tour, la rythmicité au sein du foie peut également être coordonnée par l'horloge hépatique elle-même (Figure 1) [58, 60, 61, 62]. En conséquence, environ 15 à 20 % du transcriptome hépatique cycle. Ces oscillations sont suivies par des oscillations du protéome hépatique, y compris des modifications post-traductionnelles telles que la phosphorylation et l'acétylation, ainsi que par les oscillations du métabolome [63, 64, 65]. Par exemple, l'activité enzymatique de l'histone désacétylase SIRT1 (Sirtuin 1) dépend du métabolite nicotinamide adénine dinucléotide (NAD+), qui agit comme un cofacteur. Les niveaux de NAD+ oscillent, ainsi que les niveaux de son enzyme régulatrice NAMPT (Nicotinamide phosphoribosyl-transferase). À son tour, la désacétylation médiée par SIRT1 répond aux changements

rythmiques du ratio NAD+/NADH [66]. En effet, l'activité de SIRT1 s'est avérée concomitante avec l'état d'acétylation du facteur de transcription de l'horloge centrale BMAL1 et de l'histone H3 au niveau des promoteurs circadiens dans les foies murins [67]. De plus, la désacétylation de PER2 par SIRT1 s'est avérée importante pour sa dégradation/stabilité, jouant un rôle important dans le mécanisme moléculaire de l'horloge circadienne [68]. Enfin, l'élimination de *Sirt1* dans le foie a entraîné une altération des rythmes circadiens *in vivo* [67]. Par ailleurs, il a été montré que les mutations dans les gènes de l'horloge centrale, tels que *Bmal1*, entraînent des altérations des fonctions métaboliques clés, telles que l'altération de l'homéostasie du glucose, soulignant ainsi le rôle clé de la machinerie moléculaire de l'horloge circadienne dans la physiologie et l'homéostasie du foie [69].

L'importance du moment de la prise alimentaire (reflétée par la disponibilité de la nourriture et l'heure de repas) comme étant le facteur principal de synchronisation de l'horloge hépatique a été démontrée au début des années 2000 [70, 71]. Dans ces études, des rats et des souris ont été exposés à une alimentation restreinte dans le temps, soit dans les conditions d'alternance de lumière/obscurité, ou dans l'obscurité constante. La restriction alimentaire imposée par rapport à la disponibilité de nourriture à un moment donnée de la journée a entraîné un déphasage d'environ 10-12 heures dans l'expression des gènes circadiens au sein des oscillateurs périphériques chez ces animaux (principalement observés dans le foie). Cependant, la phase de l'expression cyclique des gènes au sein de l'horloge maîtresse au niveau de SCN n'a pas été affectée [70, 71]. Au contraire, les rythmes hépatiques ont été décalés très rapidement, en l'espace de 2 jours. Bien que le rétablissement de la phase s'est effectué plus rapidement dans le foie que dans d'autres tissus périphériques, tels que les reins, le pancréas ou le cœur, les phases de l'expression cyclique des gènes se sont avérées similaires dans tous ces tissus après une semaine de cette restriction alimentaire imposée [70, 71]. Ces études ont donc fourni des indications importantes pour comprendre la relation entre le pacemaker central et les tissus périphériques. En effet, le lien (couplage) entre l'horloge maîtresse au niveau de SCN et les oscillateurs périphériques dépend principalement du moment de la prise et de la disponibilité de la nourriture [72]. Les changements métaboliques dus à une alimentation restreinte dans le temps entraînent ainsi un découplage des oscillateurs périphériques par rapport à l'horloge de SCN. Ce déphasage de l'expression des gènes circadiens se produit progressivement et graduellement dans les oscillateurs périphériques, affectant principalement le foie [70, 71]. Cela indique que les oscillateurs périphériques sont capables de fonctionner indépendamment du pacemaker central, ce qui a été confirmé par d'autres études dans lesquelles les lésions de SCN n'ont pas aboli les rythmes circadiens dans les tissus périphériques, mais ont plutôt conduit à une désynchronisation entre les différents organes [73].

Malgré un découplage important parmi les oscillateurs au cours des premiers jours suite au déphasage (ce qui peut être ressenti comme un décalage horaire - 'jet lag'), les oscillateurs sont capables de s'adapter au *Zeitgeber* imposé dans les jours qui suivent et de fonctionner à nouveau de manière synchronisée. Ces ajustements mettent en évidence la plasticité et l'adaptabilité remarquables des horloges circadiennes.

1.3 Mécanismes moléculaires des horloges circadiennes chez les mammifères

Les rythmes circadiens s'établissent *via* des boucles de rétroaction transcriptionnelle-traductionnelle (TTFL) d'environ 24 heures qui sont subdivisées en boucles centrale et auxiliaires (Figure 2), étant très conservées d'une espèce à l'autre [8, 75, 76].

Chez les mammifères, l'horloge moléculaire centrale comprend principalement quatre acteurs clés. Deux activateurs transcriptionnels : les facteurs de transcription (TF) bHLH - PER-ARNT-SIM (PAS) BMAL1 (Brain and Muscle ARNT-Like 1) et CLOCK (Circadian Locomotor Output Cycles Kaput), ainsi que son paralogue NPAS2 (Neuronal PAS domain protein 2), et deux familles de protéines répressives : PERIOD (PER, codé par *Per1*, *Per2* et *Per3*) et CRYPTOCHROME (CRY, codé par *Cry1* et *Cry2*) [75].

Au début de la journée, lors de l'initiation de la phase activatrice de l'horloge, l'hétérodimère des facteurs de transcription BMAL1-CLOCK se lie à ses séquences E-box spécifiques (CACGTG) sur l'ADN, ce qui conduit à l'ouverture de la chromatine et à l'activation transcriptionnelle des milliers de gènes contrôlés par l'horloge (CCGs). Parmi ces gènes se trouvent également leurs propres répresseurs, *Per* et *Cry*. Par conséquent, au début de la nuit, lorsque l'accumulation des protéines PER et CRY dans le cytoplasme atteint le niveau suffisant, PER-CRY forment des complexes hétérodimériques qui transloquent dans le noyau pour réprimer l'activité de BMAL1-CLOCK, afin de bloquer leur propre synthèse. Le nouveau cycle circadien commence le jour suivant, après la phosphorylation et la dégradation médiée par le protéasome des complexes répressifs PER-CRY, où BMAL1-CLOCK redevient actif de nouveau, établissant ainsi une boucle de rétroaction négative d'environ de 24h [75, 76, 77].

En parallèle, une boucle de rétroaction secondaire « auxiliaire » est générée par les récepteurs nucléaires REV-ERBα et REV-ERBβ (codés respectivement par les gènes *Nr1d1* et *Nr1d2*) et ROR (RAR-related orphan receptors) α, β et γ, dont l'activation transcriptionnelle est contrôlée par BMAL1-CLOCK. En retour, les REV-ERBs et les RORs régulent l'activité de BMAL1-CLOCK, en agissant respectivement comme des répresseurs et activateurs de l'expression du gène *Arntl* (*Bmal1*) [75, 78]. Un niveau supplémentaire de régulation de la boucle de rétroaction principale est assuré par des caséines kinases telles que CK1δ (Casein Kinase 1 delta) et CK1ε (Casein Kinase 1 epsilon). Ces caséines kinases phosphorylent PER et donc jouent un rôle important dans sa stabilité, étant impliquées dans les voies de dégradation

médiées par E3 ubiquitine ligase - protéasome [77]. En outre, une autre boucle auxiliaire contribue aux régulations rythmiques des processus transcriptionnels-traductionnels au sein de la cellule (Figure S2). L'expression de *Nfil3* (Nuclear factor, interleukin-3 regulated) est également régulée négativement par les REV-ERBs et, au contraire, positivement par les RORs. À son tour, NFIL3 réprime le facteur PAR-bZip DBP (D-box binding protein) qui régule l'expression rythmique des récepteurs nucléaires RORs [75].

Dans l'ensemble, les boucles de rétroaction circadiennes principale et auxiliaires établissent des changements dynamiques d'environ 24 heures dans l'architecture de la chromatine et donc dans les états chromatiniens - en générant des régions transcriptionnellement actives du génome (euchromatine) pendant le jour, suivies par la répression de l'expression des gènes et l'établissement de l'hétérochromatine facultative pendant la nuit.

1.4 Altérations des horloges circadiennes dans les pathologies

Les rythmes circadiens sont impliqués dans la régulation de divers processus biologiques et physiologiques, tels que le cycle veille-sommeil, la sécrétion d'hormones, l'équilibre redox, le métabolisme des xénobiotiques, ainsi que les processus immunitaires et inflammatoires. Ces rythmes sont donc essentiels à l'homéostasie de l'organisme [62, 79]. En outre, les horloges circadiennes sont également impliquées dans la régulation de la prolifération cellulaire et la réparation des dommages causés à l'ADN. La machinerie moléculaire de l'horloge guide les cellules en division en régulant de manière rythmique les principaux facteurs du cycle cellulaire impliqués dans les checkpoints mitotiques, tant au niveau transcriptionnel que post-traductionnel [80]. En parallèle, les voies de réponse aux dommages causés à l'ADN (DDR), telles que les lésions et la réparation de l'ADN, l'apoptose et la reprogrammation transcriptionnelle, sont également régulées par les horloges circadiennes. L'assemblage rythmique de la machinerie de réparation avec les complexes de l'horloge centrale, ainsi que l'expression rythmique des régulateurs clés de DDR, entraînent une coordination des oscillateurs circadiens avec les checkpoints de dommages/réparation de l'ADN, jouant ainsi un rôle clé dans la survie cellulaire [81, 82, 83].

Au vu de leur rôle crucial dans l'aptitude à la survie et la physiologie de l'organisme, la perturbation des rythmes circadiens par des altérations génétiques (par exemple, des mutations dans les gènes de l'horloge centrale) et épigénétiques dans ses régulateurs clés, voir même par le stress environnemental (par exemple, le travail de nuit entraînant un décalage horaire chronique) conduit au développement et à la progression de multiples troubles et maladies. Par exemple, des mutations du gène humain Per2 ont été décrites comme des perturbateurs de la période de libre-cours, entraînant des troubles circadiens du sommeil chez l'homme. Plus précisément, PER2 est impliqué dans le syndrome familial de

phase avancée du sommeil (FASPS), où la mutation S662G située dans le domaine de liaison de CK1ε entraîne une hypo-phosphorylation de PER2 [84, 85]. En conséquence, cette hypo-phosphorylation de PER2 accélèrerait son auto-répression en diminuant le temps de rétention nucléaire de PER2. Ceci résulterait en rythmes moléculaires à phase avancée, raccourcissant ainsi la période du cycle circadien et la phase de repos [86, 87]. Au contraire, des variations génétiques de Cry1 sont impliquées dans le trouble de phase de sommeil retardée (DSPD). Le variant de CRY1 à gain de fonction présente une affinité plus importante pour BMAL1 et CLOCK, ce qui entraîne une sous-expression des gènes cibles clés de l'horloge, allongeant ainsi la période du rythme circadien, caractérisée par un retard persistant dans l'endormissement et la mise en place de la phase de repos de l'individu [88].

De plus, des altérations des gènes de l'horloge centrale dues aux mutations ou à leur surexpression, sont impliquées dans l'apparition et le développement progressif de tumeurs dans des cancers divers. Par exemple, PER2 est également connu pour sa fonction de suppresseur de tumeur [89, 90], en étant impliqué dans la régulation des gènes liés au cycle cellulaire (par exemple *c-Myc*, *p53*, *p21*, *wee1*), des kinases dépendantes des cyclines (CDK), des checkpoints inhibiteurs des CDK, ainsi que de la transition épithélio-mésenchymateuse [91, 92, 93].

Par ailleurs, la perturbation de la coordination entre les oscillateurs au sein de l'organisme est due à la perte de synchronisation entre les horloges circadiennes internes et les facteurs environnementaux externes. Ce phénomène, appelé le désalignement circadien, est souvent caractéristique des travailleurs de nuit [94]. Il a été montré qu'en étant exposés à des conditions contrôlées de désalignement circadien imitant le travail de nuit (par exemple, une exposition prolongée à la lumière pendant la nuit), les sujets présentaient un déséquilibre au niveau de l'homéostasie du glucose, du contrôle de l'appétit et de la dépense énergétique [95, 96]. De plus, les études sur le désalignement circadien induit par un régime alimentaire riche en graisses accessible aux souris dans une fenêtre de temps donnée ont montré que tel régime alimentaire conduit à une augmentation significative du poids des animaux nourris pendant la journée par rapport à ceux nourris pendant leur horaire physiologique dans la nuit, favorisant ainsi l'obésité induite par l'alimentation imposée [97, 98].

Globalement, le désalignement circadien est associé à des perturbations de tolérance au glucose et de résistance à l'insuline, ce qui augmente le risque d'obésité et de diabète [69, 97, 98, 99]. En raison de l'exposition à la lumière et de l'alimentation au « mauvais moment de la journée », les travailleurs de nuit sont également plus à risque à développer des tumeurs [100, 101].

Dans l'ensemble, la perturbation des rythmes circadiens est directement impliquée dans les troubles du sommeil, le syndrome métabolique, l'obésité, le diabète, les maladies

cardiovasculaires, les maladies neurodégénératives et des cancers multiples, ainsi que dans le vieillissement pathologique [102, 103, 104, 105, 106]. Tous ces éléments ouvrent des voies vers le développement des nouvelles approches thérapeutiques, telles que la chronothérapie. La chronothérapie consiste à optimiser le succès du traitement en administrant le « bon médicament au bon moment » de la journée aux patients, en fonction de leurs rythmes internes. Le moment optimal d'administration de tout traitement thérapeutique ou médical (par exemple, médicament, radiation, chirurgie) favorise la réduction des effets secondaires et donc, améliore le pronostic des patients [62, 108, 109].

2. Dynamique de la chromatine et signatures épigénétiques

2.1 Organisation de la chromatine : vue générale

Dans les cellules eucaryotes, l'unité structurelle et fonctionnelle fondamentale de la chromatine est le nucléosome, qui consiste en environ 147 paires de bases d'ADN enroulées autour d'un octamère de protéines histones, dont deux copies de chacune des histones canoniques H2A, H2B, H3 et H4 constituent la partie cœur [110, 111, 112].

L'assemblage des nucléosomes est un processus très dynamique qui commence par l'incorporation d'un tétramère H3-H4 au sein de la chromatine, suivie par la déposition de deux hétérodimères H2A-H2B, ainsi que par l'enroulement de l'ADN autour de l'octamère d'histones nouvellement formé. L'assemblage et l'incorporation des nucléosomes *de novo* sur la chromatine a lieu pendant la phase S réplicative du cycle cellulaire [112]. Ce processus est médié par des protéines chaperones spécifiques : CAF-1 (Chromatin assembly factor 1) [113, 114] et ASF-1 (Anti-silencing function 1) [115, 116] impliquées dans l'incorporation du tétramère H3-H4 et par les chaperones FACT (Facilitates chromatin transcription) [117, 118] et NAP1 (Nucleosome assembly protein 1) [119], spécifiques de l'hétérodimère H2A-H2B. Les nucléosomes, ainsi que l'histone de liaison H1, sont impliqués dans la compaction de l'ADN au sein du noyau et les multiples couches de compaction de la chromatine médiées par les protéines histones aboutissent à une organisation chromatinienne ordonnée de l'ordre supérieur (Figure 3) [120].

Des niveaux supplémentaires d'organisation de la chromatine existent dans le noyau (Figure 4) [123, 124]. Dans les cellules eucaryotes, le noyau est en outre organisé en territoires chromosomiques distincts, subdivisés en compartiments A (actif) et B (inactif) contenant respectivement des gènes activement transcrits et des gènes silencieux [125, 126]. Le compartiment inter-chromatinien représente un « espace dépourvu de chromatine » séparant les différents territoires chromosomiques [124]. Au sein de ces territoires, on peut trouver d'autres niveaux de régulation, tels que les corps nucléaires - environnements locaux distincts avec leurs fonctions spécifiques (par exemple, “usine de transcription”, réponse au stress) [127, 128],

les domaines associés à la lamina (LAD) - zones dans lesquelles la chromatine entre en contact avec la lamina nucléaire, abritant principalement des gènes silencieux, ainsi que les domaines topologiquement associés (TAD) qui sont impliqués dans la médiation des interactions entre les séquences cis-régulatrices distales des gènes (enhancers) et leurs gènes cibles [124, 129]. Cette organisation tridimensionnelle de la chromatine nucléaire joue un rôle clé dans la régulation des gènes [123, 124, 129].

2.2 Mécanismes épigénétiques établissant des changements dynamiques de la chromatine

Les transitions dynamiques dans les états de la chromatine et son architecture sont modulées par plusieurs acteurs épigénétiques clés : les enzymes de modification de la chromatine, connues sous les noms d'« *écrivains*, *lecteurs*, *effaceurs* », les signatures épigénétiques telles que la méthylation de l'ADN et les modifications post-traductionnelles (PTMs) des histones (par exemple, acétylation, méthylation, phosphorylation, ubiquitination, sumoylation, *etc.*), les remodeleurs de la chromatine, ainsi que l'incorporation des variants d'histones au sein des nucléosomes. Tous ces éléments jouent un rôle important dans la régulation de la transcription, à la fois en tant qu'activateurs et répresseurs en fonction du contexte [130, 131, 132].

2.2.1 Exemple des signatures épigénétiques : modifications post-traductionnelles des histones

Les histones sont marquées par une multitude de PTMs, dont la combinaison servirait de *code épigénétique*. Ces marques jouent un rôle dans les processus biologiques clés, tels que la régulation de la transcription, la réplication et la réparation de l'ADN, le cycle cellulaire et la différenciation, ainsi que dans l'activation du génome zygotique et le développement [133, 134, 135]. Ces PTMs sont présentes sur les queues des histones (par exemple H3K4me3, H3K27ac), ainsi qu'au niveau des domaines globulaires cœur des histones, situés au sein de la dyade des nucléosomes, étant également connues sous le nom de PTMs de surface latérale (par exemple H3K115ac, H3K122ac). Impliquées dans la modulation de l'architecture de la chromatine, elles peuvent agir soit directement en affectant les interactions nucléosome-nucléosome, induisant des altérations locales de la chromatine pour entraîner l'activation ou la répression de la transcription, soit indirectement, nécessitant le recrutement de leurs « *lecteurs* » et/ou « *effaceurs* » pour avoir un effet à une plus grande échelle génomique [133]. D'un point de vue conceptuel, l'acétylation des histones est liée à l'activité transcriptionnelle, tandis que la méthylation des histones est liée aux gènes silencieux. Néanmoins, on sait que les marques de méthylation peuvent aussi être impliquées dans la régulation transcriptionnelle en tant qu'activateurs selon le contexte. Par exemple, la tri-méthylation de la lysine 4 de l'histone 3 (H3K4me3) marque le génome avant l'activation transcriptionnelle [136, 137], tandis que

la di-méthylation de la lysine 9 de l'histone 3 (H3K9me2) marque les régions génomiques avant leur répression/silencing [133, 134].

Parmi les histones canoniques, l'histone H3 est l'une des plus marquées. Des multiples combinaisons des PTMs d'histones (Figure 5) résultent du recrutement spatio-temporel de modificateurs de la chromatine impliqués dans leur incorporation ou leur éviction, tels que les histones acétyltransférases (HATs) (par exemple, p300 et CBP de la famille EP300 ; Tip60 de la famille MYST) et les histones méthyltransférases (HMTs) (par exemple, les enzymes SUV39H1/2 et SETD2, les familles MLL et PRC) [134]- les *écrivains*. Et parmi les *effaceurs*, les histones désacétylases (HDACs) (par exemple HDAC1-11, SIRT1-7) et les histones déméthylases (HDMs) (par exemple les familles JARID et JMJD) [138].

2.2.2 Remodeleurs de la chromatine de la famille SWI/SNF

Les complexes de remodelage de la chromatine jouent un rôle essentiel dans la modulation de l'architecture chromatinienne, la régulation de l'accessibilité d'ADN aux facteurs de transcription et, par conséquent, les programmes d'expression génique. Chez les mammifères, quatre familles différentes de remodeleurs dépendant de l'ATP ont été caractérisées : la famille SWI/SNF (mSWI/SNF), la famille INO80/SWR (comprenant les complexes INO80, p400/TIP60 et SRCAP), la famille ISWI et la famille du complexe CHD/NuRD [139].

Les remodeleurs de la famille SWI/SNF (SWItch/Sucrose non-fermentable) ont été identifiés pour la première fois lors de deux criblages indépendants chez la levure *Saccharomyces cerevisiae*, dans lesquels les mutations ont entraîné à la fois des altérations dans le changement du type d'accouplement des levures, ainsi que dans leur capacité à fermenter le saccharose [140, 141]. Ces complexes multiprotéiques d'environ 1 à 2 méga-daltons sont très conservés de la levure aux mammifères [142, 143]. Aussitôt, les premières purifications des complexes SWI/SNF chez les mammifères ont révélé l'hétérogénéité biochimique de leur composition et ont identifié les rôles clés de leurs différentes sous-unités dans le recrutement de ces complexes sur l'ADN, étant impliqués dans la régulation transcriptionnelle [144, 145, 146, 147]. Globalement, l'activité de remodelage des complexes SWI/SNF est impliquée dans les processus biologiques clés multiples, tels que l'expression des gènes, la croissance cellulaire et la progression mitotique, le développement et la neurogenèse, la réponse aux dommages de l'ADN et leur réparation. Dans ces processus, ils peuvent agir à la fois en tant qu' activateurs ou répresseurs, en fonction du contexte [142, 148, 149, 150, 151, 152].

Les complexes remodeleurs dépendants de l'ATP de la famille SWI/SNF sont impliqués dans le remodelage physique de l'architecture de la chromatine par trois modes différents : le repositionnement des nucléosomes, l'éjection des nucléosomes et l'éviction des dimères

d'histones de la chromatine [139]. En utilisant l'énergie issue de l'hydrolyse de l'ATP, ils font glisser l'ADN autour des nucléosomes et le remodelage s'effectue en quatre ou cinq étapes clés (Figure 6) [153, 154]. Le domaine translocase du remodeleur (composé des sous-domaines de torsion et de « tracking ») se lie à l'ADN nucléosomique, situé à environ deux tours de la dyade du nucléosome. À la suite de la liaison du remodeleur et de l'hydrolyse de l'ATP, le sous-domaine de torsion effectue une translocation directionnelle de l'ADN, en rompant les contacts entre les histones et l'ADN. Cette action entraîne la création d'une boucle d'ADN intra-nucléosomale transitoire qui se propage autour du nucléosome (Figure 6A) [154]. La résolution de la boucle se produit lorsque l'ADN déroulé atteint le site de sortie, ce qui entraîne le repositionnement ou l'éjection du nucléosome, suite à quoi le remodeleur se remet à sa position d'origine pour assurer un nouveau cycle de remodelage. De plus, pendant la phase de translocation, une translocation inverse ou un glissement de l'ADN peut se produire, suivi d'un repositionnement immédiat du nucléosome sans la formation de boucles d'ADN intra-nucléosomales (Figure 6B) [153].

Les complexes mSWI/SNF comprennent les remodeleurs PBAF (Polybromo-associated BAF), cBAF (canonical BRG1/BRM associated factor) et ncBAF (non-canonical BRG1/BRM associated factor) [155, 156]. Ces complexes possèdent un large nombre de sous-unités partagées, y compris les sous-unités catalytiques ATPasiques mutuellement exclusives BRG1 (Brahma-related gene 1) et BRM (Brahma). L'identité de ces complexes est déterminée par leurs sous-unités spécifiques (Table 1). Les complexes PBAF sont caractérisés par les sous-unités PBRM1 (Polybromo-1), ARID2 (AT-rich interactive domain-containing protein 2), BRD7 (Bromodomain-Containing Protein 7) et PHF10 (PHD Finger Protein 10). Les complexes cBAF sont caractérisés par les sous-unités ARID1A/B (AT-rich interactive domain-containing protein 1A/ 1B), DPF1/2/3 (Double PHD Fingers 1/2/3) et SS18/L1 (Synovial Sarcoma Translocated To X Chromosome Protein).

Les complexes PBAF et cBAF sont assemblés lors d'un processus multi- étapes, dans lequel les ARIDs jouent un rôle essentiel pour la détermination de leur identité (Figure 7) [155]. Une fois les sous-unités cœur assemblées, l'intégration de l'une des sous-unités ARID devient critique, donnant ainsi la naissance aux complexes PBAF (lors de l'intégration d'ARID2) ou cBAF (lors de l'intégration d'ARID1A ou ARID1B), suivie par l'assemblage de leurs sous-unités spécifiques restantes. L'intégration de deux copies de PBRM1 termine ainsi l'assemblage du complexe PBAF [155].

Alors que les sous-unités ARIDs, BRDs et PHF10/DPFs sont homologues entre ces complexes, PBRM1 est unique au complexe PBAF [142, 155]. PBRM1 est un *lecteur* des lysines acétylées et méthylées qui amène le complexe PBAF sur la chromatine, rentrant directement

en contact avec les nucléosomes par l'intermédiaire de ses bromodomaines multiples [157, 158]. Les bromodomaines BD2 et BD4 sont essentiels, car ils sont directement impliqués dans le remodelage des nucléosomes, en reconnaissant les marques d'acétylation. Les bromodomaines BD1 et BD5 renforcent respectivement l'activité des BD2 et BD4. Au contraire, BD3 atténue l'activité de PBRM1 [157]. Le rôle de BD6 reste inconnu. De plus, PBRM1 contient deux domaines BAH (Bromo-adjacent homology) qui sont directement impliqués dans la reconnaissance des marques d'histones méthylées [159, 160]. Le contact direct de PBRM1 avec l'ADN est médié par son domaine HMG (High mobility group) [157]. En parallèle de PBRM1, d'autres sous-unités spécifiques sont également impliquées dans le recrutement du complexe sur l'ADN. Néanmoins, leur rôle précis au cours du remodelage de la chromatine n'est toujours pas clair. En outre, les sous-unités SWI/SNF sont également caractérisées comme des suppresseurs de tumeurs clés et leurs altérations sont présentes dans plus de 20 % des cancers différents [161].

2.2.3 Variants d'histones : vue générale

Un niveau supplémentaire de régulation épigénétique dans les changements dynamiques d'états chromatiniens est médié par l'incorporation des variants d'histones au sein des nucléosomes [132]. Chez les mammifères, chaque histone canonique possède des variants correspondants (Table 2) qui modulent la stabilité des nucléosomes et donc, les propriétés et l'architecture de la chromatine [132, 162]. Par exemple, une seule copie de H2A.Z au sein du nucléosome génère des nucléosomes extrêmement stables, impliqués dans la compaction de la chromatine. Au contraire, l'incorporation de variant d'histone H3.3 crée des nucléosomes plus instables [132, 163]. De plus, les nucléosomes contenant des variants peuvent être soit hétérotypiques, c'est-à-dire que l'histone canonique et son variant sont tous les deux présents au sein du nucléosome, ou alors homotypiques, c'est-à-dire qu'un variant d'histone spécifique remplace les deux copies de l'histone canonique correspondante [164, 165, 166].

Les variants d'histones sont très conservés d'une espèce à l'autre et diffèrent principalement de leurs histones canoniques correspondantes dans leur domaine globulaire, soit de manière très importante (par exemple, H2A.Z partage 60% d'homologie avec H2A canonique), soit seulement par quelques acides aminés (par exemple, H3.3 diffère de 4 à 5 acides aminés de H3.2 et H3.1 canoniques respectivement) [167, 168]. Les gènes codant pour les variants d'histones diffèrent sur plusieurs points essentiels des gènes codant pour les histones canoniques. En termes d'organisation génomique, les gènes d'histones canoniques sont organisés en cluster, ils sont dépourvus d'introns et de queues polyA. En revanche, les gènes de variants d'histones sont des gènes à copie unique, situés dans des emplacements génomiques distincts, ils contiennent des exons et des introns et leurs ARNm sont polyadénylés [169]. En outre, la principale différence réside dans leurs voies de déposition, y

compris leurs chaperones spécifiques (Figure 8) [132]. Alors que les histones canoniques sont déposées sur la chromatine d'une manière dépendante de la réplication (couplée à la synthèse d'ADN), les variants d'histones sont principalement incorporés au sein des nucléosomes d'une manière indépendante de la réplication, tout au long du cycle cellulaire [132, 168].

Étant donné que le même variant d'histone peut être incorporé par différents complexes de chaperones au sein des emplacements génomiques distincts, les variants d'histone peuvent agir à la fois comme des régulateurs positifs et négatifs de programmes spécifiques d'expression génique [132, 162, 168]. De plus, ils agissent souvent en combinaison avec des PTMs d'histones et/ou d'autres variants d'histones [162]. Les variants d'histones jouent un rôle essentiel dans l'activation transcriptionnelle, due à leur localisation au niveau des enhancers, promoteurs et des sites de début de transcription (TSS), ainsi que dans la répression des gènes et la formation de l'hétérochromatine, lorsqu'ils sont situés au sein des régions centromériques et télomériques [132, 162]. Ils sont également impliqués dans la progression du cycle cellulaire, la réplication d'ADN, la ségrégation et l'intégrité des chromosomes. Ils jouent également un rôle dans la réponse et la réparation des dommages de l'ADN, au cours du développement embryonnaire, de la différenciation cellulaire et du vieillissement [162, 170]. En raison de leurs rôles polyvalents dans des nombreux processus biologiques, les altérations au sein de leur structure, de leur expression et/ou leurs voies d'incorporation conduisent au développement et à la progression des nombreuses maladies, y compris des cancers [162]. Des exemples spécifiques d'altérations des variants d'histones H2A et H3 liés à leurs maladies respectives sont illustrés dans la Figure 9 [162].

3. Interaction entre la dynamique de la chromatine et les horloges circadiennes

3.1 Dialogue entre les horloges circadiennes et l'épigénome

Comment l'architecture de la chromatine est-elle réorganisée afin de permettre, et de favoriser, la liaison rythmique de BMAL1-CLOCK à un « moment et à un endroit spécifiques » du génome ? Les changements au sein de l'architecture de la chromatine médiés par les signatures épigénétiques et le remodelage des nucléosomes modulent l'accessibilité des facteurs régulateurs qui se lient à l'ADN [171, 172]. En retour, la liaison de la machinerie de l'horloge centrale établit une dynamique de 24 heures dans l'organisation de la chromatine. Par conséquent, cette régulation rythmique des états chromatiniens entraîne une coordination étroite entre l'établissement des paysages épigénétiques spécifiques et les programmes circadiens d'expression des gènes [51, 75, 76, 173].

3.1.1 Dynamique des marques d'histones et l'accessibilité de la chromatine

Au niveau des gènes régulés par l'horloge, les PTMs situées sur les queues d'histones subissent des oscillations rythmiques et, à leur tour, les PTMs dynamiques génèrent une rythmicité « jour vs. nuit » dans les paysages chromatiniens [51, 75, 76, 174, 175]. La déposition rythmique des marques d'acétylation des histones près des promoteurs et enhancers des gènes régulés par l'horloge (par exemple H3K27ac, H3K9ac) résulte du recrutement des HATs par la machinerie de l'horloge centrale. De plus, il a été montré que les rythmes au niveau de l'acétylation de l'histone H3 situés aux *loci* des gènes régulés par l'horloge et le recrutement de l'ARN polymérase II (Pol II) coïncident avec la dynamique de leurs niveaux d'ARNm dans les foies murins [176]. L'hétérodimère BMAL1-CLOCK interagit de manière rythmique avec les HATs p300 et CBP (CREB binding protein). Alors que l'HAT p300 a été trouvée dans les complexes spécifiques de CLOCK [176], il a été proposé que CBP soit directement recrutée par BMAL1 pour médier la transactivation des cibles spécifiques de BMAL1-CLOCK [177]. En outre, le facteur de transcription CLOCK possède une activité HAT intrinsèque. CLOCK partage une similarité de séquence, ainsi qu'une spécificité enzymatique de l'HAT pour les histones H3-H4 avec le coactivateur du récepteur nucléaire ACTR/SRC-1 (Steroid receptor co-activator- 1) [178]. Enfin, ACTR/SRC-1 est également connu pour interagir et former un complexe multimérique avec p300 et CBP [179, 180]. Il a été proposé que les HATs CLOCK, p300 et CBP puissent également posséder des activités redondantes, puisqu'elles partagent les mêmes cibles au sein des histones (par exemple H3K9, H3K14). Cependant, il est également supposé que CLOCK, p300 et CBP agissent en tandem aux différents moments de l'activation transcriptionnelle circadienne, et donc que leur fonction pourrait être coopérative en fonction du temps [75, 76]. Par exemple, BMAL1-CLOCK sont connus pour fonctionner comme des facteurs de transcription pionniers, et l'activité HAT intrinsèque de CLOCK pourrait donc jouer un rôle important dans l'acétylation des histones et l'éviction des nucléosomes pendant la phase d'activation initiale du cycle circadien[178, 181]. D'autre part, en interagissant directement avec l'hétérodimère BMAL1-CLOCK, les HATs p300 et CBP acétyleraient les nucléosomes flanquant des sites cibles de BMAL1-CLOCK pour relâcher davantage la chromatine et permettre ainsi l'activation transcriptionnelle lors de la phase d'activation plus tardive au cours du cycle circadien [176, 177].

A son tour, la désacétylation des histones est également régulée de manière rythmique par les HDACs (par exemple, SIRT1, HDAC3). Notamment, dans les foies murins, tandis que la désacétylation médiée par SIRT1 s'effectue rythmiquement au niveau des gènes de l'horloge et de leurs cibles [67], l'interaction de HDAC3 avec REV-ERBα et leur recrutement sur les sites de régulation des gènes impliqués dans le métabolisme des lipides est nécessaire à l'homéostasie hépatique des lipides [182]. Un autre exemple implique la répression des cibles de

l'horloge centrale médiée par les complexes PER-CRY. PER-CRY interagit dynamiquement avec le corépresseur SIN3A (SIN3 Transcription Regulator Family Member A), qui agit comme un échafaudage des complexes répressifs. En parallèle, PER-CRY interagit avec le complexe répressif NuRD (Nucleosome Remodeling Deacetylase), qui avec SIN3A contiennent tous les deux les désacétylases HDAC1 et HDAC2 [183, 184].

De plus, le recrutement rythmique des HMTs entraîne des changements dynamiques dans les niveaux de méthylation des histones au cours de 24 heures. La déposition de la marque H3K4me3 est régulée de manière dynamique au niveau des TSS et des enhancers de l'horloge et des gènes régulés par l'horloge pendant la phase activatrice du cycle circadien. La rythmicité de H3K4me3 est médiée par la famille MLL (Mixed Lineage Leukemia) des HMTs, notamment MLL1 et MLL3, qui sont dynamiquement recrutées par la machinerie de l'horloge centrale. Il a été montré qu'elles favorisent des oscillations transcriptionnelles robustes des promoteurs des gènes de l'horloge, tels que *Bmal1*, *Per2*, *Cry1* et *Rev-erbα* dans les foies murins [185, 186]. Au contraire, la déposition de la marque H3K9me2 à proximité des E-box circadiens entraîne la répression des gènes [187]. Médiée par la méthyltransférase SUV39H (Suppressor of variegation 3-9 homolog), la di-méthylation de H3K9 au niveau des E-box circadiens conduit au recrutement de HP1α (Heterochromatin protein 1 alpha), ce qui entraîne la répression des gènes de l'horloge, ainsi que de leurs cibles. De plus, l'hypothèse suivante que le silencing épigénétique des cibles de l'horloge médié par SUV39H/HP1α pourrait être maintenu jusqu'à ce que BMAL1-CLOCK initie un nouveau cycle circadien a été émise. Ce complexe SUV39H/HP1α contribuerait ainsi à la formation circadienne de l'hétérochromatine facultative pendant la phase répressive de l'horloge [187].

3.1.2 Dynamique de la chromatine marquée par le variant d'histone H2A.Z aux *loci* régulés par l'horloge

Chez *Neurospora crassa*, le recrutement rythmique de la chaperone FACT au niveau du promoteur du gène *frq* (*Frequency*, équivalent de *Period* chez les mammifères) génère une dynamique d'occupation au cours de 24 heures des nucléosomes contenant le variant H2A.Z [188]. Les niveaux de H2A.Z ont un impact sur la liaison du complexe White Collar (WCC, équivalent de BMAL1-CLOCK chez les mammifères), en corrélant avec la régulation transcriptionnelle du gène *frq*. Ce mécanisme est hautement conservé à travers les espèces, y compris la plante *Arabidopsis thaliana* et au niveau des neurones de l'horloge chez la drosophile [188, 189, 190].

Chez les mammifères, l'incorporation de H2A.Z qui s'effectue indépendamment de la réplication est médiée par les complexes de remodelage p400-Tip60 et SRCAP (SWI2-SNF2-related CBP activator protein) qui sont distincts de la chaperonne FACT. Les TSS

transcriptionnellement actifs sont enrichis en nucléosomes contenant H2A.Z, dont le turnover est rapide [191]. En effet, le déplacement du nucléosome acétylé H2A.Z en position +1 par le complexe de l'ARN polymérase II engagé dans l'élongation coïncide avec la transcription des gènes actifs. Les nucléosomes enrichis en H2A.Z se trouvent également au niveau des régions insulatrices, flanquant les sites de liaison de CTCF (CCCTC-binding factor) qui assurent la médiation des interactions chromosomiques à longue distance, en facilitant les contacts entre les régions distales des promoteurs-enhancers [192]. De plus, les expériences d'immunoprécipitation de la chromatine suivie par le séquençage (ChIP-seq) effectuées dans les foies murins à l'échelle du génome entier ont révélé que les changements rythmiques dans l'occupation des nucléosomes H2A.Z s'effectuent au niveau des gènes de l'horloge et ceux régulés par l'horloge, lors de la liaison de BMAL1-CLOCK à l'ADN. Ceci suggère que BMAL1-CLOCK régulent dynamiquement l'accessibilité de l'ADN aux facteurs de transcription adjacents, directement par le remodelage des nucléosomes contenant le variant H2A.Z, en agissant donc comme des facteurs de transcription pionniers [181].

Nous avons récemment montré (voir Article 1) que la déposition de H2A.Z près des TSS et des enhancers de l'horloge se produit pendant la phase répressive du cycle circadien, et que cette déposition est médiée par les complexes PER-YL1. De plus, dans cette étude, j'ai contribué à la mise en évidence du lien entre CTCF et la machinerie moléculaire de l'horloge centrale (voir la figure 6h de l'Article 1). La purification des complexes endogènes de PER2 à partir de la chromatine soluble des foies murins a révélé une interaction spécifique au cours du temps avec CTCF, pendant les dernières étapes de la phase répressive du cycle circadien. Cela suggère que la déposition de H2A.Z médiée par PER2 pourrait s'effectuer au niveau des régions insulatrices afin d'établir l'hétérochromatine facultative rythmique [193].

Par ailleurs, le double knock-out de H2A.Z (*H2afz*$^{-/-}$, *H2afv*$^{-/-}$) entraîne une perte complète des rythmes circadiens cellulaires, ce qui indique que les composantes épigénétiques, telles que le variant d'histone H2A.Z, jouent un rôle essentiel dans l'établissement de la boucle de rétroaction transcriptionnelle-traductionnelle d' ~ 24 heures [193]. Cependant, si d'autres variants d'histones jouent un rôle dans la dynamique chromatinienne circadienne, ainsi que leur lien avec la liaison de BMAL1-CLOCK, reste à explorer.

3.1.3 Remodelage circadien de la chromatine

Chez *Neurospora crassa*, le remodelage dynamique des nucléosomes s'effectue lors de la liaison de WCC aux séquences C-box (équivalentes aux E-box chez les mammifères) situés près du promoteur *frq*. Il a été montré que WC-1, qui forme le complexe WCC avec WC-2 (équivalent de l'hétérodimère BMAL1-CLOCK chez les mammifères), recrute les remodeleurs SWI/SNF sur les sites de régulation de *frq*. Ce recrutement entraîne le remodelage des nucléosomes et looping (formation des boucles) de la chromatine afin de favoriser les

interactions entre les enhancers et les promoteurs, ce qui conduit à l'activation transcriptionnelle du gène *frq*. Les auteurs proposent un modèle dans lequel les complexes WC-1 -SWI/SNF activent l'expression du gène *frq*, initiant ainsi l'activation du cycle circadien [194].

Comme mentionné précédemment, il est connu que la déposition/éviction de H2A.Z est rythmiquement régulée près des TSS de *frq* chez *Neurospora crassa* [188] et chez les levures, il a été montré que les nucléosomes H2A.Z situés au niveau des TSS sont remodelés par le complexe de remodelage de type PBAF de la famille SWI/SNF, appelé RSC (Remodeling the Structure of Chromatin) [195]. Par ailleurs, chez la levure, le remodelage des nucléosomes médié par les complexes BAF agit en synergie avec ARN Pol II afin de rendre la chromatine accessible aux facteurs de transcription adjacents [196]. Cependant, si la dynamique observée au cours de 24 heures des nucléosomes contenant H2A.Z chez *Neurospora crassa* pourrait être liée au remodelage circadien, et si le remodelage des nucléosomes H2A.Z par le complexe RSC chez la levure se produit de manière dynamique au cours du temps, reste encore inconnu.

Chez les mammifères, il a été proposé que l'activité de RORα et BMAL1 favorise le relâchement de la chromatine au sein des fois murins afin de faciliter la liaison de REV-ERBα au niveau de la chromatine par la suite, pendant la phase répressive du cycle circadien. En effet, il a été montré que la liaison de REV-ERBα sur la chromatine est facilitée par le recrutement rythmique des complexes remodeleurs SWI/SNF SRC-2/PBAF pendant la phase activatrice de l'horloge. Ainsi, la perte de SRC-2 ou de PBAF a entraîné une altération de la liaison de REV-ERBα, ce qui a conduit à la génération des rythmes de faible amplitude [197].

Néanmoins, très peu est connu par rapport au mécanisme de coopération entre les remodeleurs chromatiniens SWI/SNF et la machinerie de l'horloge centrale pour établir la dynamique de la chromatine au cours de 24 heures.

4. Variant d'histone H3.3

4.1 Famille des histones H3 : les modulateurs clés des états chromatiniens

Chez les mammifères, la famille des histones H3 comprend les deux histones canoniques H3.1/H3.2 et six variants (Table 2), comme par exemple H3.3 (H3.3A et H3.3B), CenH3/CENP-A et H3T spécifique de testicules. Les variants H3 sont impliqués dans la modulation de la stabilité des nucléosomes et le maintien de l'intégrité du génome, jouant ainsi un rôle dans des processus biologiques multiples (Figure 9), comme allant de la régulation transcriptionnelle à la division cellulaire, l'activation du génome zygotique et le développement embryonnaire [132, 162].

4.2 Le variant d'histone H3.3

De point de vue de l'évolution, le variant H3.3 de l'histone canonique H3 est l'une des protéines les plus conservées chez tous les eucaryotes. Chez les mammifères, H3.3 est principalement codé par les gènes *H3f3a* et *H3f3b*, donnant lieu respectivement aux protéines H3.3A et H3.3B [169]. Chez la souris, les gènes *H3f3a* et *H3f3b* sont situés à des endroits distincts du génome, respectivement au niveau des chromosomes 1 et 11. Bien qu'ils diffèrent dans leurs séquences nucléotidiques et leurs ARNm dans les régions 5' et 3' UTR, ils codent pour des protéines identiques en termes de séquence d'acides aminés et de structure [169]. En outre, treize autres gènes similaires à H3.3 ont été identifiés chez la souris, étant exclusifs au génome de la souris puisqu'aucun orthologue n'a été retrouvé chez les espèces de rats et l'homme [198].

Les variants H3.3 ne diffèrent que de 4 à 5 acides aminés de leurs homologues canoniques H3.2 et H3.1 respectivement. Les principales différences résident dans leur domaine de repliement (le domaine globulaire) sur les résidus 87, 89 et 90 (Figure 10), qui jouent un rôle important dans la reconnaissance de H3.3 par ses chaperones spécifiques. De plus, H3.3 diffère au niveau du résidu 31, où l'alanine des histones canoniques H3.1/2 est remplacée par une sérine, dont la phosphorylation joue un rôle important dans la progression mitotique et la régulation du cycle cellulaire [169, 199].

4.2.1 Voies spécifiques de déposition du variant H3.3

La déposition du variant H3.3 est médiée par deux complexes de chaperones spécifiques, HIRA (Histone cell cycle Regulation defective homolog A) et DAXX (Death domain-associated protein), qui incorporent H3.3 au sein des régions génomiques distinctes (Figure 8) [201, 202, 203].

Le complexe de la chaperone HIRA s'assemble avec les sous-unités UBN1/2 (Ubinuclein 1/2), étant impliquées dans la reconnaissance directe et la liaison au variant H3.3, ainsi que son incorporation au sein de la chromatine, et également avec la sous-unité CABIN1 (Calcineurin-binding protein 1) qui est impliquée dans la stabilité du complexe de la chaperone [201, 204, 205]. La déposition médiée par HIRA entraîne un enrichissement des nucléosomes H3.3 à proximité des promoteurs et des enhancers des gènes transcriptionnellement actifs et inactifs, établissant l'état de la chromatine caractéristique de l'état juste avant l'activation transcriptionnelle [169, 201, 202]. Dans les cellules en division, le complexe de la chaperone HIRA est impliqué dans la régulation de la présence de l'ARN Pol II au niveau des TSS et des éléments régulateurs, jouant un rôle crucial dans l'expression des gènes. Ce complexe a également été associé à la déposition temporaire de H3.3 au niveau des centromères avant l'incorporation de CENP-A, où H3.3 sert d'emplacement pour ce variant centromérique à la fin de la métaphase/au début de la phase G1 du cycle cellulaire [206, 207]. Par ailleurs, l'incorporation de H3.3 médiée par HIRA s'est avérée essentielle pour le développement embryonnaire

précoce et la pluripotence cellulaire. De plus, il a été montré que HIRA est impliquée dans la formation des foyers d'hétérochromatine associés à la sénescence (SAHF), ce qui renforce le rôle du variant H3.3 dans les processus liés au vieillissement [207, 208, 209].

La deuxième chaperone spécifique de H3.3, DAXX, est associée à la sous-unité ATRX (alpha-thalassemia/mental retardation syndrome X-linked protein), un membre des remodeleurs de la chromatine dépendant de l'ATP. L'incorporation de H3.3 médiée par DAXX s'effectue au sein des régions télomériques et de l'hétérochromatine péricentrique (Figure 8) [169, 201, 210]. Bien qu'au sein de ce complexe, l'activité chaperone soit exclusivement liée à DAXX, sa coopération avec ATRX s'est avérée essentielle pour l'accumulation de H3.3 dans les régions télomériques [169]. En outre, comme pour HIRA, DAXX a été montrée essentielle au cours du développement de la souris, puisque sa perte entraîne de l'apoptose massive, conduisant à une létalité embryonnaire chez la souris [210, 211].

4.2.2 H3.3, le régulateur transcriptionnel clé et au-delà

Impliqué dans la modulation d'états chromatiniens, H3.3 joue un rôle important dans la régulation de l'expression des gènes [202, 207]. Positionnés au niveau des enhancers et promoteurs des gènes activement transcrits, les nucléosomes H3.3 marqués par des PTMs activatrices (par exemple H3K4me3) favorisent l'activation transcriptionnelle et possèdent un turnover rapide, indépendant de la réplication. Il a été montré que ce renouvellement indépendant de la réplication des nucléosomes H3.3 au niveau des enhancers des gènes actifs est en corrélation avec la dynamique de l'ARN Pol II [212, 213]. Au contraire, lorsque marqués par des PTMs répressives (par exemple H3K9me3), ces nucléosomes H3.3 se situent au niveau des régions transcriptionnellement inactives du génome, ayant un turnover lent [213].

Outre leur rôle régulateur dans l'expression des gènes, les variants H3.3A et H3.3B sont également impliqués dans la régulation et le maintien de l'intégrité du génome au cours du développement chez les mammifères [214, 215]. Chez la souris, la perte complète du variant H3.3 entraîne des défauts mitotiques et un retard de développement qui se traduit par une létalité embryonnaire précoce. Dans les cellules, la déplétion de H3.3 entraîne la mort cellulaire, ce qui indique le rôle essentiel du variant H3.3 dans la survie cellulaire [215]. Par ailleurs, la régulation de la longévité par H3.3 et son accumulation liée à l'âge dans les cellules post-mitotiques indiquent que l'incorporation et le renouvellement de H3.3 joueraient également un rôle régulateur important dans la formation des paysages chromatiniens au cours du vieillissement physiologique [208, 207].

4.2.3 Nucléosomes fragiles, double-variants H3.3/H2A.Z

La déposition du variant H3.3 sur la chromatine module la stabilité des nucléosomes et la combinaison des variants d'histones H3.3/H2A.Z au sein d'un même nucléosome entraîne la formation des nucléosomes fragiles, dits double-variants qui sont très mobiles et instables [163, 191, 212].

In vitro, les nucléosomes double-variants H3.3/H2A.Z sont très sensibles aux concentrations en sel et il est ainsi très probable qu'ils soient beaucoup moins stables que les nucléosomes couplés à la réplication contenant des histones canoniques *in vivo* [212]. Par ailleurs, les nucléosomes H2A.Z positionnés au niveau des promoteurs des gènes inactifs sont enlevés de la chromatine lors de l'activation transcriptionnelle et leur éviction a été montrée concomitante à la déposition de H3.3 sur ces sites [212, 216]. Le knockdown de H3.3 entraîne l'inhibition du recrutement de Tip60 et de SRCAP dans les régions promotrices des gènes inductibles par l'acide rétinoïque, ce qui indique que H3.3 est impliqué dans le recrutement des chaperones spécifiques de H2A.Z sur ces sites [212].

Les nucléosomes double-variants empêcheraient la déposition des nucléosomes canoniques stables autour de ces sites régulatrices afin de faciliter l'accessibilité de l'ADN à la machinerie transcriptionnelle de l'ARN Pol II, aux facteurs de transcription adjacents et à d'autres complexes régulateurs (Figure 11) [212]. Récemment, il a été montré dans les cellules souches embryonnaires de souris (mESc) que le complexe de la chaperone HIRA médie la co-déposition des variants H3.3 et H2A.Z au sein des nucléosomes au niveau des promoteurs et TSS des gènes « en attente », tout juste avant l'activation transcriptionnelle, en corégulant le recrutement de SRCAP à ces sites [217]. Cependant, si l'établissement de l'architecture de la chromatine marquée par H3.3 et H3.3/H2A.Z pourrait s'effectuer au niveau des promoteurs et TSS de gènes de l'horloge et des gènes régulés par l'horloge afin de générer une dynamique de 24 heures dans les paysages chromatiniens, reste inconnu.

5. Hypothèses de recherche et objectifs

5.1 Contexte scientifique et hypothèses

Au vu de l'implication du variant d'histone H2A.Z dans le fonctionnement de l'horloge circadienne chez des nombreuses espèces [181, 188, 193], nous nous sommes demandés si d'autres variants d'histones, tels que H3.3, pouvaient jouer un rôle dans la dynamique des états chromatiniens au niveau des *loci* circadiens. Nous avons donc eu pour but d'étudier le lien entre le variant d'histone H3.3 et la machinerie moléculaire des horloges circadiennes chez les mammifères. Autrement dit, comment les nucléosomes H3.3 pourraient-ils moduler l'architecture de la chromatine afin de contribuer à la dynamique transcriptionnelle au cours de

24 heures en lien étroit avec les régulateurs de l'horloge circadienne dans les tissus murins, tels que le foie.

L'expression des gènes *H3f3a* et *H3f3b* oscille au cours du temps dans des nombreux tissus murins, tels que le foie, les reins et le cœur (les données sont disponibles sur CircaDB, la base de données des profils d'expression des gènes circadiens). Cependant, si les variants H3.3 jouent un rôle dans l'établissement des rythmes chromatiniens de 24 heures chez les mammifères est inconnu. Nous avons donc émis l'hypothèse que H3.3 pourrait contribuer au fonctionnement de l'horloge circadienne, en générant la dynamique de la chromatine au cours de 24 heures. Pour ce faire, i) les nucléosomes H3.3 seraient enrichis au niveau des *loci* de l'horloge et leur déposition et/ou éviction suivrait une dynamique de 24 heures, et ii) H3.3 s'assemblerait avec les principaux facteurs de l'horloge centrale dans des complexes dynamiques au cours du temps.

Comme la famille de variants H3.3 comprend deux variants principaux, H3.3A et H3.3B, dont l'expression est différentiellement cyclique dans les foies murins, nous avons d'abord eu pour but d'étudier les différences potentielles dans leur implication dans l'établissement des rythmes circadiens chez les mammifères, en étudiant leurs rôles de manière indépendante. Cependant, en étudiant le rôle des deux variants H3.3 en parallèle, nous avons rencontré des difficultés techniques inattendues et nous nous sommes donc concentrés sur le variant d'histone H3.3A.

5.2 Modèles murins et objectifs de l'étude

Afin d'étudier le rôle de H3.3A dans les rythmes circadiens, et puisque H3.3A ne diffère des histones H3 canoniques que par 4-5 acides aminés, nous avons utilisé un modèle de souris knock-in conditionnel, dans lequel la séquence FLAG-FLAG-HA-tag (FH) a été insérée dans le cadre de l'extrémité N-terminale au sein d'un seul allèle de H3.3A, comme décrit dans [218]. Ce modèle de souris hétérozygote FH-H3.3A$^{+/-}$ permet de mener des études biochimiques spécifiques, ciblant exclusivement H3.3A et les complexes protéiques associés. Ce modèle de souris nous a été aimablement fourni par Dr. Stefan Dimitrov. De plus, le laboratoire de Dr. Padmanabhan a généré une lignée de souris FH-H3.3A$^{+/-}$ *Per1*$^{-/-}$, *Per2*$^{-/-}$ knockout afin d'évaluer les changements potentiels au sein des paysages chromatiniens de H3.3A lors de la perturbation de l'horloge circadienne, en absence de PER. Les souris *Per1*$^{-/-}$, *Per2* $^{Brdm-/-}$ nous ont été aimablement fournies par Prof. Marie-Paule Felder Schmittbuhl et Prof. Urs Albrecht.

Ayant ces modèles de souris à notre disposition, nous avons eu pour objectifs de 1) caractériser les complexes protéiques spécifiques de H3.3A au cours du temps, tout en recherchant les interactions avec des facteurs de l'horloge centrale et des facteurs épigénétiques impliqués dans la dynamique chromatinienne - en effectuant des purifications

des complexes H3.3A, suivies d'une analyse par spectrométrie de masse et d'expériences d'immunoprécipitation ; 2) évaluer l'occupation des nucléosomes contenant H3.3A au cours du temps, à l'échelle du génome entier et en s'intéressant particulièrement aux sites de liaison de BMAL1-CLOCK, les TSS des gènes cibles de BMAL1-CLOCK et les sites CTCF - en réalisant des expériences de ChIP-seq ; ainsi que 3) étudier l'impact de la perturbation de l'horloge circadienne sur les paysages chromatiniens marqués par H3.3A et ses complexes d'interaction dans les foies murins FH-H3.3A$^{+/-}$ *Per1*$^{-/-}$, *Per2*$^{-/-}$.

Résumé des sections

Dans mes travaux de thèse, nous nous sommes intéressés à étudier le rôle de variant d'histone H3.3A dans l'établissement des rythmes circadiens chez les mammifères.

Afin d'étudier son rôle dans l'établissement des paysages chromatiniens dynamiques au cours du temps dans les tissus murins, tels que le foie, nous avons utilisé les modèles de souris spécifiques où un allèle de H3.3A a été étiquetée par l'épitope FLAG-FLAG-HA (FH) au niveau N-terminal, dans un contexte de souris « sauvages » hétérozygotes C57Bl/6J FH-H3.3A$^{+/-}$, et également dans un contexte de souris C57Bl/6J FH-H3.3A$^{+/-}$ *Per1*$^{-/-}$, *Per2*$^{-/-}$ knockout (PerKO).

Nous avons émis l'hypothèse que si le variant d'histone H3.3A joue un rôle dans l'établissement des rythmes circadiens dans le foie, alors son incorporation sur la chromatine et/ou son éviction serait dynamique au cours du temps. Par ailleurs, nous avons également émis l'hypothèse que le variant H3.3A s'assemblerait avec les facteurs clés de l'horloge circadienne au sein des complexes dynamiques en fonction du temps. Ainsi, la dynamique des nucléosomes contenant le variant H3.3A et de ses complexes associés serait altérée lors de la perturbation de l'horloge circadienne, en absence de PER, s'il y a un lien. Nous avons donc procédé aux prélèvements des foies murins toutes les 4 heures au cours de 24 heures, aux temps circadiens (CT) 0, 4, 8, 12, 16 et 20, afin de pouvoir étudier la dynamique du variant H3.3A. Les CT 0, 4 et 8 correspondent au jour subjectif (phase activatrice de l'horloge circadienne) et inversement, les CT 12, 16 et 20 à la nuit subjective (phase répressive).

Afin de vérifier ces hypothèses, il a fallu avant tout établir la méthode de purification des complexes spécifiques associés à H3.3A dans les foies murins. Cette tâche s'est avérée initialement assez complexe, dû au manque d'études et de méthodes de purification spécifiques des variants d'histones à partir des tissus murins. En effet, le peu de protocoles de purification disponibles étaient établis pour les études des histones et leurs variants à partir des systèmes de culture de cellules en division. Ainsi, j'ai adapté des protocoles de purification publiés pour les systèmes de culture cellulaire aux tissus murins, tels que le foie. Cette méthode de purification établie dans mes travaux consiste en isolation des noyaux intacts à partir des foies murins, suite à quoi les extraits nucléaires sont préparés, en enrichissant la chromatine en mononucléosomes. En effet, la chromatine est digérée par la MNase, qui est une nucléase qui coupe préférentiellement les sites « nus » de l'ADN, dépourvus de nucléosomes, afin de libérer les nucléosomes et leurs complexes associés dans la partie soluble de la fraction nucléaire. Une fois la fraction enrichie en mononucléosomes, on procède à la purification des complexes spécifiques de FH-H3.3A, en effectuant l'immunoprécipitation de H3.3A en utilisant les anticorps spécifiques anti-FLAG ou anti-HA. Cette méthode possède

un enjeu double, permettant à la fois i) de purifier les interacteurs spécifiques de H3.3A et définir ainsi son interactome, en effectuant une analyse par spectrométrie de masse, ainsi que ii) d'identifier les régions de la chromatine enrichies en nucléosomes contenant le variant H3.3A, en poursuivant la purification des complexes protéiques enrichis en H3.3A par la purification de l'ADN co-immunoprécipité, suivie par des analyses de ChIP-seq.

Dans le contexte physiologique des souris FH-H3.3A$^{+/-}$ sauvages, la purification des complexes spécifiques de H3.3A a permis d'identifier un lien important avec la machinerie moléculaire de l'horloge circadienne, précédemment inconnu. Nous avons montré que les facteurs de transcription BMAL1-CLOCK s'assemblent de manière dynamique au cours de la phase activatrice de l'horloge sur les nucléosomes contenant le variant H3.3A, avec un pic au temps circadien CT8. Par la suite, grâce à l'analyse par spectrométrie de masse et les études de validation, nous avons également pu mettre en évidence l'assemblage des complexes remodeleurs PBAF et cBAF/BRG1 de la famille SWI/SNF sur les nucléosomes contenant le variant H3.3A. Ainsi, on a montré que les complexes PBAF et cBAF/BRG1 s'assemblent avec le facteur de transcription BMAL1, de manière spécifique lors de la phase activatrice de l'horloge, à CT4 et CT8. De manière surprenante, la purification des complexes H3.3A a révélé la présence des nucléosomes homotypiques, contenant le variant FH-H3.3A avec les variants H3.3 non-étiquetés, suite à l'absence de l'histone canonique H3.1/2 au sein de ces complexes. De plus, ces nucléosomes homotypiques H3.3 sont marqués spécifiquement par les modifications post-traductionnelles H3K115ac et H3K122ac, exclusivement pendant la phase de la journée subjective. Ces modifications rendent ainsi ces nucléosomes H3.3 plus instables et plus mobiles (fragiles).

Ensuite, les analyses de ChIP-seq ont permis d'identifier que les nucléosomes H3.3 sont incorporés à la chromatine de manière dynamique au cours du temps dans les foies murins, étant majoritairement enrichis lors de la phase activatrice de l'horloge, entre CT0 et CT8. Ainsi, cet enrichissement important de H3.3 s'est montré spécifique aux *loci* circadiens (*loci* de l'horloge et ceux régulés par l'horloge présents au niveau des TSS, des sites de liaison de BMAL1-CLOCK, ainsi que les sites CTCF), comme telle dynamique d'incorporation n'a été détectée à aucun autre endroit du génome (par exemple, les éléments SINE ou encore des régions intergéniques). Le variant H3.3 a été notamment spécifiquement enrichis au niveau des TSS de manière générale, par rapport aux histones canoniques H3.1/2.

Globalement, ces résultats ont mis en évidence que la dynamique de variant H3.3 génère des paysages épigénétiques spécifiques au cours du temps, promouvant le recrutement des facteurs de transcription BMAL1-CLOCK avec les remodeleurs de la chromatine PBAF-cBAF/BRG1 de la famille SWI/SNF.

Par la suite, nous nous sommes donc intéressés à caractériser les paysages chromatiniens impliquant le variant d'histone H3.3A, en absence de l'horloge circadienne fonctionnelle chez les animaux PerKO. Cette caractérisation nous a permis de mettre en évidence plusieurs éléments nouveaux - clés.

L'absence de PER conduit à l'augmentation de l'incorporation de H3.3 sur la chromatine, cet enrichissement plus important étant présent au niveau des TSS cibles et des sites de liaison de BMAL1-CLOCK, mais aussi au niveau des sites CTCF. De plus, de manière surprenante, les nucléosomes H3.3 sont marqués par les modifications post-traductionnelles H3K115ac et H3K122ac, caractéristiques de la phase de la journée subjective/ la phase activatrice de l'horloge dans les conditions physiologiques. Ces résultats nous ont donc amené à penser que lors de la perturbation de l'horloge circadienne chez les animaux PerKO, la chromatine est plus ouverte, étant enrichie davantage par des marques rendant les nucléosomes H3.3 fragiles.

Nous nous sommes donc interrogés si l'absence de PER conduit à un changement structurel des complexes remodeleurs de la famille SWI/SNF associés à H3.3. Nous avons mis en évidence que les remodeleurs chromatiniens subissent une réorganisation structurelle. En effet, en absence de l'horloge fonctionnelle (suite à la délétion de *Per*), on observe une perte presque totale au niveau protéique de la sous-unité ARID2, spécifique des complexes PBAF. Cette sous-unité étant clé lors du processus d'assemblage de ces remodeleurs, on constante donc le désassemblage de PBAF causé par l'absence d'ARID2. Ensuite, nous observons également une réduction de la sous-unité ATPasique BRG1 (partagée par les complexes PBAF/cBAF) et de la sous-unité ARID1B, spécifique des complexes cBAF, conduisant ainsi également à la perturbation des complexes cBAF/BRG1 en absence de PER. De plus, cette perturbation conduit à l'absence d'interaction de ces complexes avec BMAL1.

De manière surprenante, la réduction importante de la sous-unité ARID1B chez les souris PerKO n'affecte pas l'assemblage des complexes cBAF/BRM, ni leur interaction avec BMAL1. En effet, les remodeleurs cBAF/BRM interagissent avec BMAL1 à la fois au cours de la phase activatrice et répressive de l'horloge, à CT8 et CT20 respectivement, mais aussi lors de la perturbation de l'horloge circadienne. Tandis que l'effet général de l'absence de PER impacte de manière importante l'assemblage des remodeleurs PBAF-cBAF/BRG1, les remodeleurs cBAF/BRM restent maintenus, probablement afin de compenser la perte observée des autres remodeleurs de la famille SWI/SNF. Ainsi, il est très probable que les complexes cBAF/BRM régulent la présence de BMAL1 sur chromatine en absence de feedback négatif.

Enfin, nous nous sommes donc intéressés à l'impact de la perturbation circadienne sur l'activité de BMAL1. Les expériences de ChIP-seq natives de BMAL1 nous ont permis de

mettre en évidence de manière surprenante, une augmentation de la liaison de ce facteur de transcription sur ses sites cibles. Ainsi, les sites de liaison de BMAL1-CLOCK pourraient être rendus plus accessibles par l'augmentation de l'enrichissement de H3.3 au niveau de ces sites.

En conclusion, dans ces travaux, nous montrons pour la première fois que la présence de variant H3.3 sur la chromatine est dynamique au cours de 24 heures dans les tissus murins, tels que le foie, enrichi essentiellement en cellules post-mitotiques. Cette dynamique d'incorporation de H3.3 au sein de la chromatine établit des paysages épigénétiques spécifiques, promouvant le recrutement des facteurs de transcription de la machinerie moléculaire circadienne BMAL1-CLOCK au cours de la phase activatrice de l'horloge. De plus, BMAL1 s'assemble de manière dynamique avec des remodeleurs PBAF-cBAF/BRG1 sur les nucléosomes H3.3 fragiles, marqués par H3K115ac et H3K122ac. Suite à la perturbation de l'horloge circadienne en absence de PER, plusieurs éléments conduisent aux réarrangements de l'architecture chromatinienne. Tels que l'augmentation de l'enrichissement de variant H3.3 au sein de la chromatine. La présence des nucléosomes H3.3 fragiles. La réorganisation structurelle des remodeleurs chromatiniens, conduisant au maintien des complexes cBAF/BRM, suite au désassemblage des remodeleurs PBAF-cBAF/BRG1. Le maintien de l'interaction de BMAL1 avec les complexes cBAF/BRM et ainsi une augmentation de liaison et d'activité de BMAL1 chez les animaux PerKO. Tous ces éléments montrent que la chromatine est « piégée » dans un état transcriptionnellement actif en permanence lors de l'absence de feedback négatif. Etant donné que les altérations des sous-unités des complexes SWI/SNF, ainsi que des altérations de H3.3 et de l'horloge circadienne sont fortement présentes dans les contextes pathologiques, tels que les cancers, nos données permettraient ainsi de mieux caractériser le lien entre les composantes épigénétiques et l'horloge circadienne dans le but d'amélioration des stratégies thérapeutiques actuellement proposées.

Discussion

Proposition du modèle, questions ouvertes et perspectives

Dans l'ensemble, nous décrivons et proposons un modèle dans lequel les nucléosomes fragiles contenant le variant H3.3 établissent des paysages chromatiniens dynamiques qui favorisent l'assemblage des complexes BMAL1-CLOCK et des remodeleurs PBAF-cBAF/BRG1 au cours du temps (Figure 28A). Nous constatons que la déposition/éviction de H3.3 est dynamique au cours du temps, avec un pic lors de la phase activatrice du cycle circadien, entre CT0 et CT8. Ces nucléosomes H3.3 sont enrichis en marques d'histones de surface latérale, telles que H3K115ac et H3K122ac, ce qui les rend très mobiles et instables (fragiles) [237, 238]. Ces nucléosomes sont également marqués par la marque activatrice H3K4me3 lors de la phase de la journée subjective, à CT8. La rythmicité observée dans la déposition de H3.3 et ses PTMs associées est concomitante avec la phase active de transcription au sein des foies murins [51]. Les nucléosomes H3.3 fragiles facilitent la liaison de BMAL1-CLOCK et contribuent donc à l'activation transcriptionnelle circadienne. En outre, les complexes PBAF s'assemblent de manière rythmique avec le facteur de transcription BMAL1 sur la chromatine marquée par H3.3 pendant la phase activatrice de l'horloge, à CT4 et CT8 (Figure 14). La diminution ultérieure des nucléosomes contenant H3.3, observée aux *loci* de l'horloge à CT12 (Figure 15A, B), suggère un remodelage actif de ces nucléosomes par le complexe PBAF. D'autres complexes de remodelage de la famille SWI/SNF BAF s'assemblent dynamiquement avec BMAL1. Tandis que l'association de BMAL1 avec le remodeleur cBAF/BRG1 se fait spécifiquement lors de la phase de la journée subjective, avec un pic sur la chromatine à CT8, l'assemblage des complexes cBAF/BRM-BMAL1 s'effectue à la fois pendant les phases subjectives journalière et nocturne.

La perturbation de l'horloge circadienne entraîne une augmentation globale de l'incorporation de H3.3 au sein de la chromatine dans les foies PerKO, y compris au niveau des *loci* de l'horloge. Ces nucléosomes conservent leur fragilité, établissant des paysages chromatiniens similaires à ceux établis au cours de la journée chez les souris sauvages. Malgré les états chromatiniens « journaliers » favorisés dans les foies PerKO, nous avons constaté que la perturbation de l'horloge circadienne s'accompagne d'une réorganisation structurelle des complexes de remodelage (Figure 28B). En absence de PER, nous observons une déplétion quasi-totale de la sous-unité ARID2 et de l'ATPase partagée BRG1 dans le noyau, ce qui conduit au désassemblage des complexes PBAF. Tandis qu'aucun changement ne s'effectue au niveau des ARNm pour les composantes spécifiques du complexe PBAF en absence de PER, la perte quasi-totale d'ARID2 observée au niveau protéique indique que

l'incapacité d'assembler les complexes PBAF, en absence de la boucle de rétroaction négative, résulte très probablement de modifications post-traductionnelles de la protéine ARID2 et/ou suite aux altérations de sa stabilité.

La perte de fonction du complexe PBAF pourrait-elle être compensée par les autres remodeleurs BAF de la famille SWI/SNF ? La réduction observée de l'ATPase partagée BRG1 et de la sous-unité ARID1B spécifique du complexe cBAF conduit à une perturbation des complexes de remodelage cBAF/BRG1 ainsi que de leur interaction avec BMAL1. De manière surprenante, l'assemblage des remodeleurs cBAF/BRM ainsi que leur association avec BMAL1 ne sont pas affectés en absence de PER, ce qui suggère que le maintien des remodeleurs cBAF/BRM favorise les états chromatiniens ON (fixé à la chromatine) / OFF (non-fixé à la chromatine) de BMAL1 en cas de perturbation de l'horloge circadienne. En outre, nous avons constaté que l'absence de rétroaction négative circadienne entraîne une augmentation de la liaison de BMAL1 sur la chromatine, très probablement en raison de l'accessibilité augmentée des sites de liaison de BMAL1-CLOCK. Ainsi, ces sites seraient rendus plus accessibles très probablement par l'incorporation plus élevée des nucléosomes H3.3 fragiles. De plus, l'absence de phase répressive médiée par PER entraine elle-même, une activité plus élevée de BMAL1, comme montré par des études précédentes [240, 241].

Tous ces événements caractérisent ainsi l'établissement d'états chromatiniens transcriptionnellement actifs en permanence, lors de la perturbation de l'horloge circadienne, impliquant le variant H3.3 et l'interaction entre le facteur de transcription de l'horloge centrale BMAL1 et les remodeleurs de la chromatine de la famille SWI/SNF. De plus, ces réarrangements de l'architecture chromatinienne reflètent l'effet général de la perte de PER et donc, l'absence de feedback négatif circadien dans sa globalité. Néanmoins, quelques questions subsistent concernant le rôle de H3.3 et des remodeleurs chromatiniens dans le fonctionnement de l'horloge circadienne.

Chez *Neurospora crassa*, l'assemblage dynamique de WCC avec des complexes SWI/SNF de type BAF sur les sites régulatrices de *frq* (C-box) est suivi d'un remodelage rythmique de la chromatine et de l'activation de l'expression du gène *frq* [194]. En outre, les auteurs montrent qu'un tel remodelage est accompagné par la perte de nucléosomes contenant H3 en quelques heures sur ces sites régulatrices [194]. Ces résultats pourraient suggérer les hypothèses suivantes : i) soit le complexe SWI/SNF éjecte rythmiquement les nucléosomes H3 au niveau des C-box, générant directement des régions déplétées en nucléosomes (NDR) pendant la phase d'initiation de la transcription, soit ii) très probablement, les nucléosomes éjectés contenant H3 pourraient être remplacés par les nucléosomes fragiles contenant H3.3 (éviction du dimère ou du tétramère H3-H4, remplacé ensuite par H3.3-H4) afin de rendre la chromatine plus accessible pendant la phase initiale de la phase activatrice

de l'horloge. Dans ce cas, le variant d'histone H3.3 servirait de « marque-page » pour le recrutement des remodeleurs chromatiniens SWI/SNF.

Au début de nos recherches, nous nous sommes interrogés si un mécanisme similaire au recrutement des remodeleurs SWI/SNF par WCC, décrit chez *Neurospora*, avait lieu dans les foies murins, impliquant H3.3. En étudiant le lien entre les remodeleurs PBAF/cBAF et le variant H3.3A, ainsi que les complexes de l'horloge centrale, nous avons découvert un mécanisme sous-jacent à la régulation transcriptionnelle circadienne par BMAL1-CLOCK.

Dans notre étude, nous avons découvert que contrairement aux nucléosomes canoniques H3, les nucléosomes contenant H3.3A sont dynamiquement enrichis au cours de 24 heures au niveau des sites régulatrices de l'horloge. En outre, l'augmentation globale des nucléosomes H3.3A au niveau des TSS des gènes, observée à CT8 et CT20 par rapport aux histones H3.1/2 canoniques chez les souris sauvages (Figure 15E), reflète très probablement les résultats des études précédentes, dans lesquelles les auteurs ont montré que dans les hépatocytes sains (non-cancéreux), la proportion globale des variants H3.3 est plus élevée que la proportion de l'histone H3.1/2 [208]. Par conséquent, la dynamique de recrutement de BMAL1-CLOCK aux nucléosomes H3.3A qui a lieu spécifiquement au cours de la journée, est très probablement médiée par les marques d'acétylation de H3K115 et H3K122 spécifiques au variant H3.3, comme notre purification des complexes protéiques de FH-H3.3A le montre, en révélant la formation des nucléosomes homotypiques H3.3 au sein de ces complexes (Figure 14A et Figure 21). Ainsi, pour déterminer et confirmer si les nucléosomes H3.3A fragiles marqués par H3K115ac occupent les TSS des gènes cibles de l'horloge, il serait très informatif de réaliser une expérience de ChIP-reChIP, en utilisant un anticorps anti-HA-tag (ChIP initial), suivi par l'utilisation d'un anticorps anti-H3K115ac (reChIP). De plus, afin de mieux comprendre la dynamique des nucléosomes homotypiques H3.3 par rapport aux nucléosomes hétérotypiques H3.3-H3.1/2, au lieu de « cartographier bioinformatiquement » les régions du génome qui se chevauchent entre les expériences de ChIP-seq FH-H3.3A et H3.1/2 que nous avons réalisées indépendamment, ChIP-reChIP de variant H3.3-H3 canonique pourrait également apporter des réponses plus précises. Initialement, j'ai essayé d'étudier la dynamique des nucléosomes hétérotypiques H3.3A-H3.1/2 en réalisant des expériences d'IP séquentielles et en évaluant le résultat par western-blotting. Tandis que l'IP FH-H3.3A suivie de l'IP H3.1/2 a systématiquement échoué de détecter les histones H3.1/2 canoniques dans les complexes H3.3A, les expériences inverses préliminaires commençant par l'IP H3.1/2 suivie de l'IP FH-H3.3A ont indiqué la présence d'une bande de FH-H3.3A modifié, migrant à une taille différente et inférieure à celle de la forme principale, qui migre à ~28kDa sur les gels de polyacrylamide. Bien que nous n'ayons aucun indice sur cette forme de FH-H3.3A modifiée, ces données préliminaires suggèrent l'existence d'un sous-ensemble de nucléosomes hétérotypiques H3.3A-H3.1/2 modifiés, formés de manière constante au

cours du temps (données non montrées). Ces résultats préliminaires renforceraient ainsi notre modèle, dans lequel nous proposons que le recrutement dynamique de BMAL1-CLOCK aux nucléosomes H3.3A est médié par les marques d'acétylation H3K115 et H3K122 spécifiques au H3.3.

Par ailleurs, les découvertes sur la dynamique circadienne de la déposition du variant H2A.Z aux *loci* de l'horloge et aux sites CTCF établie dans des nombreuses espèces [188, 189, 190], ainsi que le remodelage dynamique des nucléosomes contenant H2A.Z par le complexe RSC de type PBAF chez la levure [195], mènent aux questions suivantes, en lien avec notre étude sur la dynamique des nucléosomes H3.3 fragiles au niveau de ces sites régulatrices. Les nucléosomes fragiles double-variants H3.3/H2A.Z, serviraient-ils de « marque-pages » épigénomiques au niveau des *loci* circadiens pour la machinerie de l'horloge centrale, en suivant une dynamique de 24 heures lors de leur formation et/ou éviction ? Par exemple, l'incorporation nocturne du variant H2A.Z médiée par PER, établissant l'hétérochromatine facultative lors de la phase répressive au niveau des *loci* de l'horloge [193] pourrait être éventuellement suivie par la déposition co-régulée de H3.3 à ces sites lors de la phase activatrice de l'horloge pour initier la transcription, comme observé dans les cellules souches embryonnaires de souris (mESc), au niveau des enhancers et promoteurs des gènes [217], résultant ainsi en formation des nucléosomes fragiles double-variants. De plus, les nucléosomes H3.3/H2A.Z pourraient être remodelés de façon rythmique par les complexes SWI/SNF sur ces sites. Des expériences classiques de ChIP-seq pour des composantes spécifiques des complexes remodeleurs PBAF/cBAF permettraient d'identifier des régions génomiques où le remodelage dynamique des nucléosomes H3.3 et potentiellement des nucléosomes double-variants H3.3/H2A.Z pourrait avoir lieu. Tandis que les expériences de ChIP-seq natives pour les composantes spécifiques du complexe PBAF que nous avons réalisées ont échoué (données non montrées), les expériences de ChIP-seq avec cross-linking qui n'ont pas pu être réalisées en raison du nombre limité d'échantillons et du manque de temps, pourraient apporter des réponses - à ce stade, au moins, en ce qui concerne le remodelage des régions spécifiques marquées par le variant H3.3A, en évaluant le chevauchement entre les régions respectivement immunoprécipitées, à l'échelle du génome entier.

En outre, la présence des nucléosomes H3.3A détectés aux sites CTCF, comme décrit précédemment pour H2A.Z [192, 233], suggère une co-déposition potentielle de ces deux variants avant l'activation transcriptionnelle. Du point de vue circadien, l'interaction temporelle de PER2 avec CTCF pendant la phase répressive de l'horloge suggère que l'incorporation du variant H2A.Z médiée par PER2 s'effectue sur les régions insulatrices pendant la nuit afin d'établir l'hétérochromatine facultative [193]. Par conséquent, l'enrichissement dynamique du variant

H3.3A observé aux sites CTCF dans notre étude, suggère fortement une co-déposition de ce variant au sein des nucléosomes contenant H2A.Z, conduisant très probablement à l'ouverture des frontières chromatiniennes médiées par le CTCF et établies par l'incorporation de H2A.Z au cours de la nuit précédente. Si cela est vrai, alors les nucléosomes H3.3/H2A.Z se formeraient dynamiquement au cours des 24 heures sur ces sites, juste avant l'activation transcriptionnelle lors de la phase activatrice de l'horloge.

Bien que tous ces événements puissent très probablement avoir lieu, le manque de données expérimentales maintient actuellement ces suggestions à un niveau hypothétique. Les expériences de ChIP-reChIP de H3.3-H2A.Z pourraient apporter des réponses potentielles à ces questions. Dans l'ensemble, ce type d'expérience reste cependant extrêmement difficile à réaliser. Principalement, en raison du manque d'informations dans les protocoles actuellement publiés sur la façon dont les expériences de reChIP ont été effectuées et réalisées. Par exemple, des informations manquantes sur la quantité de la chromatine utilisée lors des deux étapes de ChIP, ainsi qu'une description insuffisante des méthodes d'élution et d'immunoprécipitation, et le manque d'informations sur la composition optimale des solutions utilisées pour chaque étape [243, 244, 245]. De plus, une grande quantité initiale de la chromatine serait nécessaire, étant donné que la fraction des nucléosomes double-variants H3.3/H2A.Z pourrait très probablement être minoritaire, si la formation de ces nucléosomes se produisait uniquement sur des sites régulatrices de gènes spécifiques, par exemple, plutôt qu'au niveau du génome entier.

Néanmoins, en approchant la fin de ma thèse, j'ai essayé d'établir une méthode qui permettrait de faire le reChIP spécifique des variants H2A.Z associés aux nucléosomes contenant H3.3, sans aucun bruit de fond aspécifique. Malgré les tous premiers résultats préliminaires très prometteurs, montrant l'enrichissement de l'ADN mononucléosomal post-reChIP, ainsi que la co-immunoprécipitation spécifique de H2A.Z avec H3.3 lors des deux étapes de ChIP et reChIP, évaluée par western-blotting, les deux essais suivants n'étaient pas réussis. Les résultats prometteurs initiaux n'étaient pas reproductibles et des variations importantes ont été observées lors des deux essais suivants. Dans un essai, seulement des niveaux caractéristiques de bruit de fond d'ADN mononucléosomal ont été détectés, ou encore des préoccupations sérieuses concernant la non-spécificité de l'enrichissement de H2A.Z ont été soulevées dû au bruit de fond non-spécifique important et l'enrichissement de H2A.Z présent dans le contrôle négatif dans un autre essai. Malheureusement, par manque de temps, je n'étais pas en mesure d'essayer d'améliorer cette méthode, et donc toutes les questions et hypothèses discutées au-dessus reste ouvertes.

Lors de la perturbation de l'horloge circadienne, nous avons observé des changements importants dans l'architecture de la chromatine marquée par H3.3. L'incorporation augmentée

des nucléosomes H3.3A fragiles au niveau de la chromatine en absence de PER suggère que l'activité et le turnover et/ou les niveaux de protéines des chaperones spécifiques de H3.3 pourraient être également plus élevés. Cependant, des changements inconsistants observés dans les niveaux protéiques des chaperones connues de H3.3, HIRA et DAXX, dans les foies PerKO (Figure 22B) indiquent que d'autres chaperones spécifiques des variants H3.3 pourraient être impliquées dans le foie. La dégradation totale de l'ADN suivie par la purification des complexes protéiques spécifiques du foie qui s'assemblent avec H3.3A indépendamment de la chromatine, et ensuite suivie par l'analyse par spectrométrie de masse, a mis en évidence la présence d'autres chaperones d'histones connues au sein des complexes formés avec H3.3A (données non montrées). Ces chaperones mériteraient d'être explorées davantage afin d'évaluer si leurs niveaux protéiques augmentent et si elles peuvent jouer un rôle dans la déposition plus élevée de H3.3 au niveau de la chromatine dans le foie PerKO, en absence de la rétroaction négative. De plus, l'augmentation observée des nucléosomes H3.3A fragiles sur les sites de liaison de BMAL1-CLOCK au niveau de la chromatine hépatique des souris PerKO rend ces sites de liaison plus accessibles, ce qui est accompagné par une augmentation de l'activité de BMAL1. Tous ces événements indiquent que la chromatine est « piégée » dans un état transcriptionnel actif, chez les souris PerKO dépourvues d'oscillateurs circadiens fonctionnels. En outre, l'augmentation globale observée de l'incorporation de H3.3 au niveau de la chromatine des foies PerKO suggère une accélération du vieillissement hépatique, puisqu'une accumulation importante de H3.3 a été observée avec l'âge dans plusieurs tissus murins [208].

Par ailleurs, la réorganisation structurelle des remodeleurs chromatiniens, due à la perte d'ARID2 et à la réduction des niveaux de protéines BRG1 et ARID1B, pourrait également expliquer et entraîner les changements observés au sein de l'architecture de la chromatine marquée par H3.3 dans les foies PerKO. Il a été récemment montré que la perte de la sous-unité ARID1A spécifique du complexe cBAF conduit à la dérégulation de l'expression des gènes liés au sexe, ce qui s'accompagne par des modifications de l'occupation et de la distribution de H3.3 [246]. Les auteurs ont également noté que le knockout de ARID1A entraîne une augmentation et un déplacement de l'accumulation de H3.3 des régions intergéniques vers les régions proximales des promoteurs sur les chromosomes X et Y. Ceci résulte ainsi en un enrichissement du variant H3.3 au niveau des TSS des gènes liés au sexe et, parallèlement, sa déplétion au sein des régions intergéniques [246].

Il a été proposé que la régulation dynamique des programmes d'expression génique médiés par la machinerie de l'horloge circadienne et les remodeleurs de la chromatine soit étroitement liée [76]. En effet, l'horloge circadienne entraîne l'expression rythmique des gènes et favorise le recrutement spécifique en fonction du temps des remodeleurs de la chromatine.

Parallèlement à ce recrutement, l'activation rythmique des remodeleurs de la chromatine par la machinerie de l'horloge centrale pourrait également avoir lieu. À leur tour, les complexes de remodelage réguleraient l'accessibilité de l'ADN aux facteurs de transcription de l'horloge centrale [76]. Néanmoins, la manière dont l'horloge circadienne et les remodeleurs de la chromatine coopèrent afin d'établir une dynamique de 24 heures dans les états chromatiniens, n'est pas encore totalement compris. Notre étude apporte des éléments clés afin de mieux comprendre ces mécanismes de régulation et la manière dont les remodeleurs coopèrent avec les facteurs de transcription BMAL1-CLOCK et les nucléosomes H3.3 fragiles, afin d'établir des paysages chromatiniens dynamiques. Par ailleurs, nous avons également découvert comment ces mécanismes sont altérés lors de la perturbation de l'horloge circadienne, qui est accompagnée par une réorganisation structurelle des remodeleurs de la chromatine, en raison de la perturbation des complexes PBAF/cBAF-BRG1. Par conséquent, il est très probable que le désassemblage des complexes PBAF chez les souris PerKO perturbe la boucle de rétroaction auxiliaire précédemment décrite, médiée par SRC-2 - PBAF - REV-ERBα [197]. Ceci entraîne très probablement des altérations du métabolisme et de la physiologie hépatiques. Cependant, la réanalyse des données publiées [229] (Figure 27) a montré que la perte des sous-unités individuelles des complexes SWI/SNF n'a que des effets limités sur la fonction de l'horloge circadienne dans les systèmes de culture cellulaire. Cela suggère que très probablement, la perte d'une des composantes de ces complexes n'a pas d'effet immédiat sur la transcription des gènes de l'horloge, dû à leur redondance fonctionnelle. Cette hypothèse pourrait être confirmée par le knockdown des composantes individuelles de ces complexes, suivi d'une analyse RT-qPCR de l'expression de plusieurs gènes de l'horloge centrale dans les cellules déplétées. Notamment, des effets plus visibles pourraient probablement être observés lors de l'atténuation combinée de plusieurs sous-unités de PBAF/cBAF en parallèle, affectant cependant très probablement la viabilité cellulaire.

Une étude récente réalisée chez la drosophile a montré que, malgré l'expression constante de la protéine BRM au cours du temps, la liaison du remodeleur BRM aux *loci* de l'horloge s'effectue de manière rythmique, avec un pic pendant la phase répressive [247]. Cette étude renforce les découvertes précédentes concernant le rôle répressif du remodeleur BRM dans l'expression des gènes circadiens, où il a été montré que son activité catalytique augmente la densité des nucléosomes au niveau des *loci* circadiens pour limiter la transcription pendant les derniers stades de la phase activatrice de l'horloge. D'autre part, l'activité non catalytique de BRM limite la liaison des facteurs de transcription de l'horloge centrale aux promoteurs de leurs gènes cibles pendant la phase répressive [248]. Ces données suggèrent que l'interaction observée entre le remodeleur cBAF/BRM et BMAL1, ayant lieu à la fois à CT8 et CT20 dans notre modèle, pourrait refléter la présence des complexes BMAL1-BRM

distincts. Le complexe BRM-BMAL1 catalytiquement actif pendant la phase active à CT8, limitant l'activité transcriptionnelle des cibles de l'horloge, et le complexe BRM-BMAL1 catalytiquement inactif pendant la phase répressive à CT20, promouvant l'état de BMAL1 non-fixé à la chromatine.

En outre, il est important de noter que la réorganisation structurelle des remodeleurs de la chromatine observée, résultant d'un « échange » (switch) des complexes PBAF/cBAF-BRG1 aux complexes cBAF-BRM dans les foies PerKO, reflète très probablement un maintien des complexes cBAF-BRM lors de la perturbation de l'horloge circadienne plutôt qu'un vrai échange. En effet, l'absence de PER favorise le maintien des complexes de remodelage associés à BRM en tant que principaux remodeleurs SWI/SNF. Ces complexes pourraient ainsi à leur tour moduler l'activité de BMAL1 en réponse à l'augmentation de sa liaison à la chromatine dans les foies avec l'horloge perturbée, conformément a ce qui a été proposé pour le double rôle de la fonction catalytique et non-catalytique des complexes BRM au niveau des gènes de l'horloge chez la drosophile [248]. Bien que nous ne disposions pas d'informations mécanistiques détaillées sur ce qui déclenche exactement ce « switch » du remodeleur, nous avons constaté que la perte de PER est suffisante pour favoriser le désassemblage du complexe PBAF en raison de la perte d'ARID2, ainsi que la perturbation du complexe cBAF-BRG1 en raison de la réduction de BRG1, suivies par la redistribution ultérieure des sous-unités disponibles. Des phénomènes similaires ont été observés dans les lignées cellulaires de mélanome déficientes en ARID2, où la perte d'ARID2 entraîne le désassemblage des complexes PBAF, qui est suivi d'une redistribution des sous-unités restantes et d'une orientation préférentielle vers les remodeleurs de la chromatine cBAF [236]. Par ailleurs, une étude récente sur ces lignées cellulaires de mélanome déficientes en ARID2 a montré que la perturbation du complexe PBAF entraîne une surexpression des gènes neuronaux en altérant la capacité du facteur de transcription REST (RE1 silencing transcription factor) à inactiver ses cibles [249]. La perte d'ARID2 dans ces lignées cellulaires dérivées de patients atteints de mélanome entraînerait-elle des altérations de la période des rythmes circadiens, et/ou ces lignées cellulaires seraient-elles naturellement dépourvues d'horloges fonctionnelles ? La perturbation des complexes PBAF pourrait-elle entraîner des modifications similaires de l'architecture chromatinienne de H3.3 dans ces lignées cellulaires déficientes en ARID2, ainsi qu'une surexpression des cibles de BMAL1, comme cela a été observé dans les foies PerKO ? Bien que les réponses à ces questions restent inconnues pour l'instant, tous ces résultats indiquent le lien fort entre la perturbation de l'horloge circadienne et les altérations épigénétiques liées au cancer. En outre, les sous-unités des complexes de remodelage SWI/SNF sont mutées dans plus de 20 % des différents cancers, principalement avec des altérations se produisant au sein des sous-unités PBRM1, ARID2 et BRG1 [142, 161]. De plus, des

mutations dans les variants H3.3 (par exemple H3.3G34R/V) ont été montrées impliquées dans plusieurs cancers, tels que les glioblastomes pédiatriques [250], ainsi que les altérations des paysages chromatiniens de H3.3 sont impliquées dans le développement du carcinome hépatocellulaire (HCC) [251]. Dans l'ensemble, les réarrangements observés dans l'architecture chromatinienne de H3.3, ainsi que la réorganisation structurelle des remodeleurs de la chromatine lors de la perturbation de l'horloge circadienne dans notre étude, mettent en évidence des états chromatiniens caractéristiques des altérations épigénétiques impliquées dans l'apparition et la progression de cancer.

Enfin, des nombreuses études sur le rôle de H3.3 dans la régulation transcriptionnelle et les interacteurs spécifiques de H3.3 ont été menées dans des systèmes de culture des cellules en division, telles que les fibroblastes embryonnaires de souris (MEFs) ou les cellules HeLa, où H3.3 a été exprimé de manière stable, en tant que protéine de fusion avec l'étiquette 2X FLAG-2X HA du côté C-terminal [210, 252, 253]. Dans notre étude, nous avons eu pour objectif d'établir des conditions dans lesquelles nous serions en mesure de purifier les complexes H3.3 natifs à partir de tissus des foies murins, afin d'étudier l'implication des variants d'histones H3.3 dans l'établissement d'états chromatiniens dynamiques au niveau des *loci* de l'horloge au cours de 24 heures. Contrairement aux études précédentes, réalisées dans des systèmes de culture cellulaire, nous avons utilisé des modèles de souris exprimant le variant H3.3A étiqueté du côté N-terminal avec l'épitope FLAG-FLAG-HA à des niveaux endogènes [218]. Nous avons montré pour la première fois que l'incorporation de H3.3A sur la chromatine est dynamique dans les tissus murins, tels que le foie, et que H3.3A est impliqué dans l'établissement de la dynamique circadienne au sein des paysages chromatiniens, avec BMAL1 et les remodeleurs SWI/SNF. De plus, il serait intéressant d'évaluer par la suite, l'impact de la délétion de H3.3 sur les niveaux d'expression des gènes de l'horloge, ainsi que ceux des composantes spécifiques des complexes PBAF/cBAF. Cependant, la réalisation de knockout fiable des principaux variants H3.3A et H3.3B dans les modèles murins, ainsi que des treize autres gènes similaires à H3.3 identifiés chez la souris [198], et les knockouts de ses chaperones spécifiques, reste une tâche assez laborieuse, qui pourrait néanmoins être très instructive afin de comprendre davantage le rôle de H3.3 dans le fonctionnement de l'horloge circadienne et les réarrangements des paysages chromatiniens en absence de H3.3.

Articles

List of articles

Article 1. Mammalian PERIOD2 regulates H2A.Z incorporation in chromatin to orchestrate circadian negative feedback.

Tartour K, Andriani F, Folco EG, Letkova D, Schneider R, Saidi I, Sato T, Welz PS, Benitah SA, Allier C, Padmanabhan K. Nat Struct Mol Biol. 2022, doi: 10.1038/s41594-022-00777-9

Article 2. PBAF/cBAF reorganization on H3.3 chromatin regulates BMAL1 activity in the absence of circadian negative feedback.

Dominika Letkova, Aurelie Peticca, Damien Sery, Masahide Seki, Yutaka Suzuki and Kiran Padmanabhan. Nat Commun 2025, doi: https://doi.org/10.1038/s41467-025-64045-2

49 Spadina Ave. Suite 200
Toronto ON M5V 2J1 Canada
www.biorender.com

Confirmation of Publication and Licensing Rights - Open Access

September 9th, 2025

Subscription Type:	*Student Plan - Academic*
Agreement number:	*AV28QF6BZY*
Publisher Name:	*BIBLIOTHÈQUE DIDEROT DE LYON*
Figure Title:	*Native purification of H3.3A liver protein complexes*
Citation to Use:	*Created in BioRender. Letkova, D. (2025) https://BioRender.com/vjtqp5b*

To whom this may concern,

This document ("Confirmation") hereby confirms that Science Suite Inc. dba BioRender ("BioRender") has granted the following BioRender user: Dominika Letkova ("User") a BioRender Academic Publication License in accordance with BioRender's Terms of Service and Academic License Terms ("License Terms") to permit such User to do the following on the condition that all requirements in this Confirmation are met:

1) publish their Completed Graphics created in the BioRender Services containing both User Content and BioRender Content (as both are defined in the License Terms) in publications (journals, textbooks, websites, etc.); and
2) sublicense such Completed Graphics under "open access" publication sublicensing models such as CC-BY 4.0 and more restrictive models, so long as the conditions set forth herein are fully met.

Requirements of User:

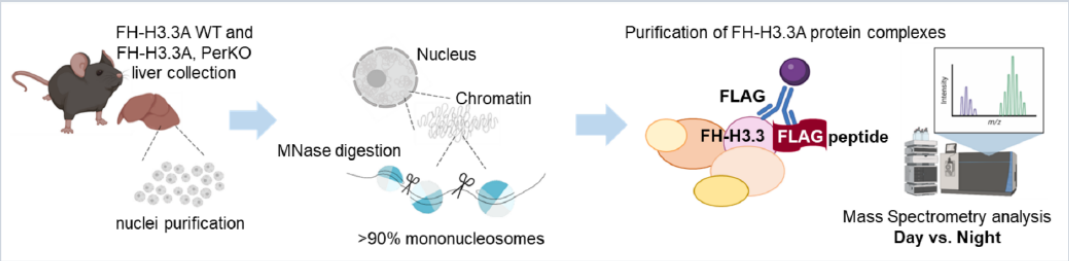
1) All Completed Graphics to be published in any publication (journals, textbooks, websites, etc.) must be accompanied by the following citation either as a caption, footnote or reference for each figure that includes a Completed Graphic:
"Created in BioRender. Letkova, D. (2025) https://BioRender.com/vjtqp5b ".
2) All terms of the License Terms including all Prohibited Uses are fully complied with. E.g. For Academic License Users, no commercial uses (beyond publication in journals, textbooks or websites) are permitted without obtaining or switching to a BioRender Industry Plan.
3) A Reader (defined below) may request that the User allow their figure to be a public template for Readers to view, copy, and modify the figure. It is up to the User to determine what level of access to grant.

Open-Access Journal Readers:

Open-Access journal readers ("Reader") who wish to view and/or re-use a particular Completed Graphic in an Open-Access journal subject to CC-BY sublicensing may do so by clicking on the URL link in the applicable citation for the subject Completed Graphic.

The re-use/modification options below are available after the Reader requests the User to adapt their figure as a BioRender template and the User has granted such access.

1) View-Only/Free Plan Use: A Reader who wishes to only view the Completed Graphic may do so in the BioRender Services as either a BioRender Free Plan user or simply as a viewer. By becoming a BioRender Free Plan user, the Reader may view, modify and re-use the Completed Graphic as permitted under BioRender's Basic License Terms (e.g. personal use only, no publishing or commercial use permitted).
2) Re-Use/Publish with No Modifications: For any re-use and re-publication of a Completed Graphic with no modification(s) to the Completed Graphic made by the Reader, a Reader may do so by citing the original author using the citation noted above with the Completed Graphic. The Reader must also comply with the underlying License Terms which apply to the Completed Graphic as noted above (e.g. no commercial use for Academic License).
3) Re-Use/Publish with Modifications: For any re-use and re-publication of a Completed Graphic with a modification(s) made by the Reader, the Reader may do so by becoming a BioRender user themselves under either an Academic or Industry Plan, citing the original author using the citation noted above with the Completed Graphic and complying with the applicable License Terms.



For any questions regarding this document, or other questions about publishing with BioRender, please refer to our BioRender Publication Guide, or contact BioRender Support at support@biorender.com.